STATUS OF THESIS

Title of thesis	STRENGTHENING OF REINFORCED CONCRETE BEAMS WITH OPENINGS USING CFRP LAMINATES

I CHIN SIEW CHOO

hereby allow my thesis to be placed at the Information Resource Center (IRC) of Universiti Teknologi PETRONAS (UTP) with the following conditions:

1. The thesis becomes the property of UTP
2. The IRC of UTP may make copies of the thesis for academic purposes only.
3. This thesis is classified as

☐ Confidential

☑ Non-confidential

If the thesis is confidential, please state the reason:

The contents of the thesis will remain confidential for ____________ years.

Remarks on disclosure:

Signature of Author

Permanent address:
PT 1126, Jln Teratai 4,
Tmn Marida, Senawang
70450 Seremban
Negeri Sembilan

Date: 27-2-2013

Endorsed by

Signature of Supervisor

Name of Supervisor:
Assoc. Prof. Dr. Nasir Shafiq

Assoc Prof Dr Nasir Shafiq
Associate Professor
Civil Engineering Department
Universiti Teknologi PETRONAS
Bandar Seri Iskandar, 31750 Tronoh
Perak Darul Ridzuan MALAYSIA

Date: 27-2-2013

UNIVERSITI TEKNOLOGI PETRONAS

STRENGTHENING OF REINFORCED CONCRETE BEAMS
WITH OPENINGS USING
CFRP LAMINATES

by

CHIN SIEW CHOO

The undersigned certify that they have read, and recommend to the Postgraduate Studies Programme for acceptance this thesis for the fulfillment of the requirements for the degree stated.

Signature: ______________________ Assoc Prof Dr Nasir Shafiq
Associate Professor
Civil Engineering Department
Universiti Teknologi PETRONAS
Bandar Seri Iskandar, 31750 Tronoh
Perak Darul Ridzuan MALAYSIA

Main Supervisor: Assoc. Prof. Dr. Nasir Shafiq

Signature: ______________________ Prof. Ir. Dr Muhd Fadhil Nuruddin
Dean, Faculty of Engineering
Universiti Teknologi PETRONAS
Bandar Seri Iskandar
31750 Tronoh, Perak, MALAYSIA

Co-Supervisor: Prof. Ir. Dr. Muhd Fadhil Nuruddin

Signature: ______________________ Assoc. Prof. Ir. Dr Mohd Shahir Liew
Head
Civil Engineering Department
Universiti Teknologi PETRONAS
Bandar Seri Iksandar, 31750 Tronoh
Perak Darul Ridzuan, MALAYSIA

Head of Department: Assoc. Prof. Dr. Mohd Shahir Liew

Date: 28-2-2013

STRENGTHENING OF REINFORCED CONCRETE BEAMS WITH OPENINGS USING CFRP LAMINATES

by

CHIN SIEW CHOO

A Thesis

Submitted to the Postgraduate Studies Programme
as a Requirement for the Degree of

DOCTOR OF PHILOSOPHY

CIVIL ENGINEERING DEPARTMENT

UNIVERSITI TEKNOLOGI PETRONAS

BANDAR SERI ISKANDAR,

PERAK

FEBRUARY 2013

DECLARATION OF THESIS

Title of thesis: STRENGTHENING OF REINFORCED CONCRETE BEAMS WITH OPENINGS USING CFRP LAMINATES

I CHIN SIEW CHOO

hereby declare that the thesis is based on my original work except for quotations and citations which have been duly acknowledged. I also declare that it has not been previously or concurrently submitted for any other degree at UTP or other institutions.

Signature of Author

Permanent address:

PT 1126, Jln Teratai 4,

Tmn Marida, Senawang

70450 Seremban

Negeri Sembilan

Date: 27-2-2013

Witnessed by

Assoc Prof Dr Nasir Shafiq
Associate Professor
Civil Engineering Department
Universiti Teknologi PETRONAS
Bandar Seri Iskandar, 31750 Tronoh
Perak Darul Ridzuan MALAYSIA

Signature of Supervisor

Name of Supervisor:

Assoc. Prof. Dr. Nasir Shafiq

Date: 27-2-2013

ACKNOWLEDGEMENTS

First of all, I would like to acknowledge the Universiti Teknologi PETRONAS for giving me the opportunity of Graduate Assistantship Scheme to further my study on full time basis. I would like to express my deepest gratitude to my supervisor Assoc. Prof. Dr. Nasir Shafiq for his guidance, continuous encouragement, motivation and support throughout the research program. Without his guidance and comments, the process of accomplishing the research would have never been possible. I am also indebted to Prof. Ir. Dr. Muhd. Fadhil Nuruddin who co-supervised my PhD study as well as provided many constructive advices during the research period.

Grateful acknowledgement is given to all academic staffs in Civil Engineering Department for their moral support and assistance as well as the facilities that the department has provided at the concrete laboratory.

Heartfelt thanks are also given to the technical staff of Civil Engineering Department, Universiti Teknologi PETRONAS, especially the help of Mr. Johan Ariff and Mr. Hafiz Baharun during the experimental program in the concrete laboratory.

I would like to thank my fellow postgraduate colleagues of Civil Engineering Department especially Ervina Ariatedja, Siti Nur Hanani Sulong and Dr. Andri Kusbiantoro, for their research spirit, continual motivation and support.

Finally but most importantly, I would like to express my gratefulness to my parents and siblings for their patience, continuous moral support and encouragement throughout this research study.

ABSTRACT

Holes or openings are required to be provided through beams to facilitate services in buildings, i.e. commercial and residential. Such services are usually electrical cables, water supplies, air-conditioning, network cables and ventilation system accommodated in utility pipes and ducts. However, the provisions of openings in reinforced concrete (RC) beams have caused many problems to the beam behaviour. The change in the beam cross-sectional area changes the beam engineering behaviour. The change in the mechanical properties also causes cracking and deflection as well as reduction of the beam stiffness and capacity.

In the first part of the research study, the effects of openings on the structural behaviour of RC beams with openings of various sizes and shapes located in the critical shear and bending zones were investigated. The openings including circular, square, large elliptical and rectangular in shape provided in simply-supported beams were studied. The methodologies of this research cover the use of finite element (FE) analysis and comparison with the experimental testing. A two-dimensional (2D) plane stress modelling using a non-linear FE program, ATENA, was performed on the RC beams and validated with the experimental program. All the beam specimens were of cross-section of 120 x 300 mm and length of 2000 mm. The beams were tested to failure under four-points loading. The load-deflections and crack patterns of beams were recorded up to failure. In the second part of the research, the most effective strengthening of openings using carbon fiber reinforced polymer (CFRP) laminates was studied to restore the losses of beam capacity due to the openings.

To study the behaviour of the beams with openings located in bending, results of FE analysis show that circular and square openings provided in the beam mid-span did not cause a significant reduction in beam capacity; about 2% reduction. The provision of large rectangular and elliptical openings had caused about 50% reduction in the beam capacity. Significant loss of the beam capacity was observed in rectangular

opening due to the stress concentration effects at the opening corners. To study the behaviour of the beams with openings in the shear zone, circular and square openings were located at both ends (at distances 0, 0.5d and d from the support) and at one end only (at distance 0.5d, d and 1.5d from the support). The results of the FE analysis show that the beam capacity was reduced about 70%. Openings provided at various locations in the shear zone were not significant, with a difference of 5%. The results of both experimental and FE analysis were found to be similar. Crack patterns of these beams were observed and recorded up to failure in both FE and experimental testing. The results are compared and showed a good agreement.

To study the most effective strengthening of openings using CFRP laminates, various strengthening configurations were conducted in FE modelling and the most effective strengthening option was chosen for experimental validation. The provision of elliptical and rectangular openings in the mid-span caused about 50% loss in beam capacity. Strengthening of such beams could restore about 75% of the loss capacity.

Similarly, to strengthen beams with openings at both ends and at one end only which suffer about 70% loss in capacity, a restoration of 40 – 50% of beam capacity was obtained using CFRP. The validation in the experimental testing showed almost similar results as obtained in the FE analysis. The FE analysis is a complementary to study the behaviour of beams with openings at various locations as well as the strengthening of openings.

ABSTRAK

Lubang atau bukaan pada rasuk konkrit diperlukan untuk laluan servis di dalam bangunan, seperti bangunan komersil dan kediaman. Penyediaan servis ini biasanya untuk kabel elektrik, bekalan air, penghawa dingin, kabel rangkaian dan sistem pengudaraan yang ditempatkan dalam paip utiliti dan saluran. Walau bagaimanapun, penyediaan bukaan dalam rasuk konkrit bertetulang (RC) telah menyebabkan banyak masalah kepada kelakuan rasuk. Perubahan dalam keratan rentas rasuk telah mengubah sifat kejuruteraan rasuk. Perubahan dalam sifat-sifat mekanikal juga menyebabkan keretakan dan pesongan serta pengurangan kekukuhan rasuk dan kapasiti.

Dalam bahagian pertama penyelidikan kajian ini, kesan daripada bukaan ke atas bentuk struktur rasuk RC dengan pembukaan pelbagai jenis bentuk dan saiz yang terletak di dalam kawasan lengkokan dan zon ricih kritikal telah dikaji selidik. Bukaan berbentuk bulat, segiempat sama, dan bentuk elips dan segiempat tepat yang besar telah disediakan dalam rasuk dan telah dikaji. Metodologi untuk kajian ini merangkumi penggunaan analisis unsur terhingga dan pengesahan dengan ujian eksperimen. Model dua dimensi yang menggunakan program unsur terhingga bukan linear, ATENA, telah dilakukan pada rasuk RC dan disahkan dengan program eksperimen. Kesemua spesimen rasuk RC adalah berukuran panjang 2000 mm dengan ukuran keratan rentas 120 x 300 mm. Ujian eksperimen telah dilakukan ke atas rasuk sehingga kegagalan berdasarkan pemuatan empat titik. Beban-pesongan dan corak keretakan rasuk sehingga kegagalan telah direkodkan. Dalam bahagian kedua kajian penyelidikan ini, pengukuhan paling effektif pembukaan menggunakan polimer bertetulang gentian karbon (CFRP) telah dikaji selidik untuk memulihkan kerugian kapasiti rasuk yang disebabkan oleh bukaan.

Bagi mengkaji sifat-sifat rasuk dengan bukaan yang terletak di dalam lengkokan, hasil analisis unsur terhingga menunjukkan bahawa bukaan berbentuk bulat dan segiempat sama yang diletakkan di bahagian pertengahan rentang rasuk tidak menyebabkan pengurangan kapasiti yang ketara iaitu pengurangan sebanyak 2%. Penyediaan bukaan berbentuk segiempat tepat dan elips yang besar telah menyebabkan pengurangan kapasiti rasuk sebanyak 50%. Kerugian kapasiti rasuk yang ketara telah diperhatikan dalam bukaan berbentuk segiempat tepat dan ini adalah disebabkan oleh kesan kepekatan tekanan di sudut-sudut pembukaan. Bagi mengkaji sifat rasuk dengan bukaan dalam zon ricih, bukaan berbentuk bulat dan segiempat sama telah diletakkan di kedua-dua hujung (pada jarak 0, 0.5d dan d daripada sokongan) dan pada satu hujung sahaja (pada jarak 0.5d, d dan 1.5d dari sokongan). Keputusan analisis unsur terhingga menunjukkan bahawa kapasiti rasuk telah dikurangkan kira-kira 70%. Pembukaan yang disediakan di pelbagai lokasi di zon ricih tidak menunjukkan perbezaan yang ketara, sebanyak 5%. Hasil keputusan daripada kedua-dua eksperimen dan analisis unsur terhingga telah menunjukkan persamaan. Corak keretakan rasuk-rasuk telah diperhatikan dan direkodkan sehingga kegagalan dalam analisis unsur terhingga dan ujian eksperimen. Keputusan dibandingkan dan menunjukkan satu keputusan gabungan yang baik.

Bagi mengkaji pengukuhan paling effektif pembukaan menggunakan CFRP, pelbagai konfigurasi pengukuhan telah dilakukan dalam analisis unsur terhingga dan pengukuhan yang paling berkesan telah dipilih untuk pengesahan eksperimen. Penyediaan bukaan berbentuk elips dan segiempat tepat yang terletak di jarak pertengahan rasuk telah menyebabkan kehilangan kapasiti rasuk sebanyak 50%. Pengukuhan rasuk tersebut dapat memulihkan kira-kira 75% daripada kapasiti kehilangan.

Begitu juga, untuk mengukuhkan rasuk dengan bukaan pada kedua-dua penghujung dan satu penghujung sahaja yang mengalami kehilangan kapasiti sebanyak 70%, pemulihan kapasiti rasuk sebanyak 40 - 50% telah diperolehi menggunakan CFRP. Pengesahan dalam ujian eksperimen menunjukkan hasil yang hampir sama seperti yang diperolehi dalam analisis unsur terhingga. Analisis unsur terhingga adalah pelengkap untuk mengkaji kelakuan rasuk dengan bukaan di pelbagai lokasi serta pengukuhan bukaan.

TABLE OF CONTENTS

LIST OF TABLES

LIST OF FIGURES

LIST OF ABBREVIATIONS

AFRP	Aramid Fiber Reinforced Polymer
CFRP	Carbon Fiber Reinforced Polymer
FE	Finite Element
FEM	Finite Element Modelling
FEM	Finite Element Method
FRP	Fiber Reinforced Plastic/Polymer
GFRP	Glass Fiber Reinforced Polymer
M & E	Mechanical & Electrical
NLFEA	Non-Linear Finite Element Analysis
RC	Reinforced Concrete
2D	Two-dimensional
3D	Three-dimensional

LIST OF NOMENCLATURE

A_s = area of tensile reinforcement

A_v = area of vertical legs of stirrups per spacing

a = depth of rectangular compressive stress block

b = width of the section

b_w = width of the web

b_f = CFRP laminate width

b_c = width of the beam

β_w = width ratio parameter

σ = normal stress in the crack (crack cohesion)

σ_c^{ef} = concrete compressive stress

σ_c^{ef} = effective stress

σ_c^{ef} = concrete compressive stress

d = the effective depth of beam

d_o = diameter of opening

E_c = elastic modulus of concrete

E_c = secant elastic modulus at the peak stress

E_o = initial elastic modulus

E_{sh} = hardening modulus

E_s = elastic modulus of steel

ε^{eq} = equivalent uniaxial strain

ε_c = strain at the peak stress, $f_c'^{ef}$

ε_d = limit compressive strain

ε_{cr} = crack opening strain

f'_c = cylinder compressive strength of concrete

$f_c^{`ef}$ = concrete effective compressive strength

f_t = tensile strength of the concrete

f'^{ef}_t = effective tensile strength

f_y = yield strength of tensile reinforcement

f_{yv} = yield strength of stirrups

G_f = the fracture energy needed to create a unit area of stress-free crack

G_t = tangent shear modulus

k = shape perimeter

L'_d = band size

L'_t = band size of the element in tension

r_{ec} = reduction factor of the compressive strength

s_o = corresponding slip

s = relative displacement

τ_{max} = maximum shear stress

τ = local shear stress

V_u = the ultimate shear strength of the beam

V_c = the shear strength

V_s = shear reinforcement

ν = Poisson's ratio

w = crack opening displacement

w_c = crack width at the complete release of stress

w_d = the plastic displacement at the end point of the softening curve

x = normalized strain

CHAPTER 1

INTRODUCTION

1.1 Background

Commercial and residential buildings either in high rise or low rise structures need to be installed with building services such as conduits, electrical cables, air-conditioning, ventilation system and network system access. To accommodate such services, services can be provided through pipes and ducts which run horizontally or vertically. The routes of the pipes and ducts are usually under the ceiling which will penetrate through the beams or suspended under the soffit of the beam. When suspending under the beam soffit, the storey-height may be higher to meet the headroom requirement. On the other hand, in order to reduce the storey-height and to maintain the headroom requirement, the pipes and ducts are usually penetrated through the beam structures.

The provision of openings in the web of RC beams causes many issues concerning to the beam behaviour such as the reduction in structural stiffness, excessive cracking, deflection and reduction in beam capacity. In addition, such openings may cause stress concentration depending on the shape and size of the openings. The reduction of the total cross-sectional area changes the beam mechanical behaviour. Strengthening of beams containing openings primarily depends on the condition of the building services. When openings in the beams are designed before construction, the effects of opening size, shape and location can easily be addressed. Hence, adequate strength and serviceability can be ensured before construction. To restore the lost structural capacity of beams, researchers (Mansur et al. 1985; Tan et al. 2001) investigated the role of diagonal bars as corner reinforcement and inclined reinforcement for strengthening around openings (Yang & Ashour, 2007).

Openings to be provided in constructed beams are typically known as post-planned openings which are made by drilling and/or hacking. In this case, Mechanical & Electrical (M & E) engineers normally identify the location and tentative size of openings that may fall in the critical region from a structural point of view. In order to make an appropriate decision, structural engineers have to analyze the effects of proposed openings on the shear and bending capacity of the beams and need to design an effective external strengthening system. In the last few years, fiber reinforced plastic (FRP) laminates have become popular in the repair and strengthening of concrete structure. Such FRP laminates may be beneficial to strengthen the openings.

The most common types of FRP laminates being used in the concrete industry are derived from carbon (CFRP), aramid (AFRP) or glass fibers (GFRP). Among these fibers, CFRP possess the highest strength properties and stiffness as compared to AFRP and GFRP (Tuakta, 2004; GangaRao et al., 2006, Rai & Indolia, 2011). The FRP sheets are bonded to the external surfaces of beams using various configurations and layouts. The attraction of FRP sheets in repair and rehabilitation activities is due to its outstanding characteristics such as good mechanical properties, high strength to weight ratio, low weight, corrosion resistance, reduced maintenance costs and faster installation time compared to conventional materials, such as steel plates. Many experimental studies have reported that externally bonded FRP laminates could significantly increase the stiffness and load carrying capacity of members, enhance flexural and shear capacities, provide confinement and ductility to compression structural members and also control the propagation of cracks (Ferrier et al., 2003; Madkour, 2009).

Although FRP materials have plentiful applications in repair and retrofitting activities, the literature reviews show that very few studies are focused on FRP applications to strengthen the openings in RC beams. Mansur et. al. (1999) investigated the use of FRP plates to strengthen RC T-beams with small circular openings. Abdalla et al. (2003) and Allam (2005) studied shear strengthening of RC beams with rectangular openings using FRP sheets. El Maaddawy and Sherif (2009) investigated the use of FRP sheets for shear strengthening of RC deep beams with square openings while Pimanmas (2010) studied the strengthening of RC beams with circular and square openings by externally installing FRP rods.

Most of the available researches on the study of the effects of openings are experimental based. The experimental studies are always very tedious and time consuming. Through literature review, it is identified that only two researchers (Madkour, 2009; Pimanmas, 2010) used FE based numerical analysis to estimate the beam strength incorporating the effects of openings. If such methodology is validated through experimental studies, the effects of the openings could be accurately determined and mitigated.

Therefore, there is a need that further research should be conducted to investigate the effects of openings using numerical modelling and develop the validated systems for strengthening of openings of different sizes, shapes and locations.

1.2 Problem Statement and Need for this Research

Providing openings in RC beams to accommodate the passage of utility pipes and ducts have been a challenging issue. Therefore, many research interests in this area have been dedicated since 1960s. Numerous literatures addressed the problems including the behaviour of beams containing large rectangular, small circular and multiple openings in simply supported beams, continuous two spans and three spans beams and T-beams; various models and equations were used for predictions of beams' torsional and ultimate strength; and investigation of beams with openings subjected to torsion, bending, shear and combined loading. Despite the intensive efforts that have been made to deal with the openings in RC beams, many issues are still pending and need to be resolved. Those issues are:

1. The provision of small and/or large openings (circular, square, elliptical and rectangular) placed at critical locations in the shear and bending zones of simply supported RC beams.
2. The structural behaviour of beams due to the effects of openings of different sizes and shapes located in the shear and bending zones i.e. crack patterns and load-deflection behaviour.
3. The use of numerical approach (FE analysis) rather than the often used experimental based study.

4. The effects of external strengthening of openings using CFRP laminates in both numerical analysis and experimental testing.
5. An effective strengthening system around the openings by CFRP laminates using numerical analysis and experimental testing.

1.3 Aim and Objectives of the Research

The principal aim of this research is to understand the structural behaviour of beams containing openings using experimental and numerical analysis as well as to develop an effective external strengthening system using FE analysis software, ATENA. This aim is supported by the following objectives:

1. The first main objective of this research study is to investigate the effects of openings on the structural behaviour of RC beams using FE analysis and experimental testing. In order to achieve the first main objective, the following sub-objectives were designed.

    i. To determine the capacity (load-deflection behaviour and crack patterns) of beams by placing openings (small and/or large) in the critical shear and bending zones.

    ii. To determine the opening shapes (circular, square, elliptical and rectangular) and sizes effects.

    iii. To compare the FE analysis with the experimental results.

2. The second main objective of this research is to determine the most effective strengthening of openings using CFRP laminates and conduct numerical analysis and experimental testing.

1.4 Scope and Methodology

The scope of this research study consists of two major methodologies as described below:

1. A 2D FE modelling and analysis using ATENA to model RC beams containing small and/or large openings with the shapes of circular, square, elliptical and rectangular located in the bending (opening at mid-span) and critical shear zones (opening at both ends and at one end only).
2. An experimental program was performed on simply-supported beams under four-point loading subjected to static loads.
3. Comparison of FE and experimental results in terms of load-deflection behaviour and crack patterns.

1.4.1 Numerical Analysis

The FE modelling and analysis were conducted using ATENA to determine the behaviour of beams containing openings. To restore and re-gain the losses of beam capacity due to openings, various strengthening configurations were designed in ATENA to determine the most effective strengthening systems. Element types in two-dimensional plane stress models and material models to predict the actual behaviour of the beams are presented in Chapter 4. The results of the FE analysis are presented and discussed in Chapter 5.

1.4.2 Experimental Study

The experimental methodology consists of testing of specified number of RC beams with openings to determine the beam behaviour. Strengthening using CFRP laminates around the openings was performed based on the effective strengthening systems obtained from the results of FE analysis in order to reinstate the beam capacity as of the control beams (without opening). Experimental results of the tested beams including load-deflection behaviour, failure modes and crack patterns are obtained and discussed in details in Chapter 6.

1.5 Significance of the Research

This research study can contribute to develop an understanding on the provision of small and/or large opening within the critical locations in constructed beams to accommodate essential services as required by the M & E engineers. To facilitate the structural engineers in making appropriate decision; sufficient analysis and the effects of openings need to be investigated. Application of FE tools have proved their effectiveness in terms of accuracy and time saving in many disciplines. Therefore, detailed analysis of beams with openings using FE tools such as ATENA can increase the confidence of the designers.

In order to restore and re-gain the losses of beam capacity due to the openings, various external strengthening configurations around the openings can be designed using ATENA to determine the most effective strengthening systems. Problems and uncertainties faced by the structural engineers can be solved when the FE analysis can accurately predict the effects and behaviour of beams with various types of openings and also to produce an effective strengthening system for the respective types of openings. Hence, structural engineers would be able to predict suitable type of openings to be provided in the constructed beams and at the same time the strengthening systems could restore the beam capacity as of the original state ensuring the serviceability of the structure.

FE analysis is very useful to analyze the behaviour of beams containing openings as well as the strengthening effects accurately, saving time and money by reducing the number of prototypes required as compared to the experimental work which is time consuming, need numerous prototypes, accurate equipments and testing machines and high cost of labor and materials.

1.6 Thesis Outlines

Chapter 1 provides the background, problem statement and the need of the research, objectives, scope and methodology and significance of the research.

Chapter 2 of this dissertation gives a brief review of the effects of openings for various sizes, shapes and locations in RC beams, traditional design approach for small and large openings, traditional and current strengthening methods for solid RC beams and RC beams with openings. Also, a review of computer simulation and FE analysis of RC structures is provided in this chapter.

Chapter 3 outlines the methodologies that were used in this research. The methodologies of this research are divided into two parts which is comprised of FE analysis and experimental testing.

Chapter 4 presents the material models that were used in this research to simulate the structural behaviour of concrete, steel reinforcements and CFRP under static loading. The boundary conditions, meshing, monitoring points and non-linear solutions are discussed in detail in this chapter.

Chapters 5 provides the results of FE analysis pertaining the simulation of beams with openings of various sizes and shapes in bending and shear zones. In the later part of this chapter, the strengthening results of beams with openings using CFRP laminates in the FE analysis were reported and discussed. The results presented are in terms of load-deflection behaviour, crack patterns, stress and strain distributions.

Chapter 6 provides the results obtained from the experimental testing. The study of the behaviour of beams with openings of various sizes, shapes and locations were presented and discussed. Strengthening of beams with openings using CFRP laminates by effective strengthening systems obtained from FE analysis were presented. The results are discussed in terms of load-deflection behaviour, failure modes and crack patterns.

Chapter 7 presents the comparative analysis of the results of experimental testing and numerical analysis. The comparisons were made in terms of load-deflection behaviour and crack patterns. In the later part of this chapter, the relationship between the experimental and numerical results are presented and discussed.

Chapter 8 summarizes the main output from this research investigation and provided general recommendations for further work.

CHAPTER 2

LITERATURE REVIEW

2.1 Introduction

The purpose of this literature review is to understand the purpose of providing openings in structural members particularly in RC beams, to find out the effects and consequences to the structural members due to the presence of openings. Various ways to re-gain the structural capacities of beams were reported by researchers and to find out the possible gaps for this investigation.

Generally, holes or openings are usually found in floors due to staircase, elevators, ducts and pipes. Openings are provided through the floor beams to facilitate the passage of utility pipes and service ducts. These service ducts are to accommodate essential services such as conduits, power supplies, water and drainage pipes, ventilation system, air-conditioning and network system access or even for inspection purposes in beam structures. These arrangements of building services resulted in a significant reduction in headroom, minimize the storey height and results in major savings in material and construction cost especially in multi-storey buildings and tall buildings construction. Openings are required after construction due to the changes in services, rehabilitation and other reasons.

In order to understand the behaviour of beams with openings, the structural behaviour of solid beams need to be reviewed in the first place.

2.2 Behaviour of a Solid Beam (Without Opening)

A solid beam when subjected to pure bending will exhibit a well-developed pattern of crack at ultimate condition, as shown in Figure 2.1(a). The cracks initiated at the tensile face when the extreme fiber stress exceeds the flexural tensile strength capacity of the concrete. The tensile cracks of the beam would propagate vertically upward and extend up to the neutral axis. Based on the usual flexural strength theory, the strain and stress distributions across a section at failure are shown in Figure 2.1(b). The tensile stress resultant, T and the compressive stress resultant, C, form a couple exactly equal to the applied moment at failure (Mansur & Tan, 1999).

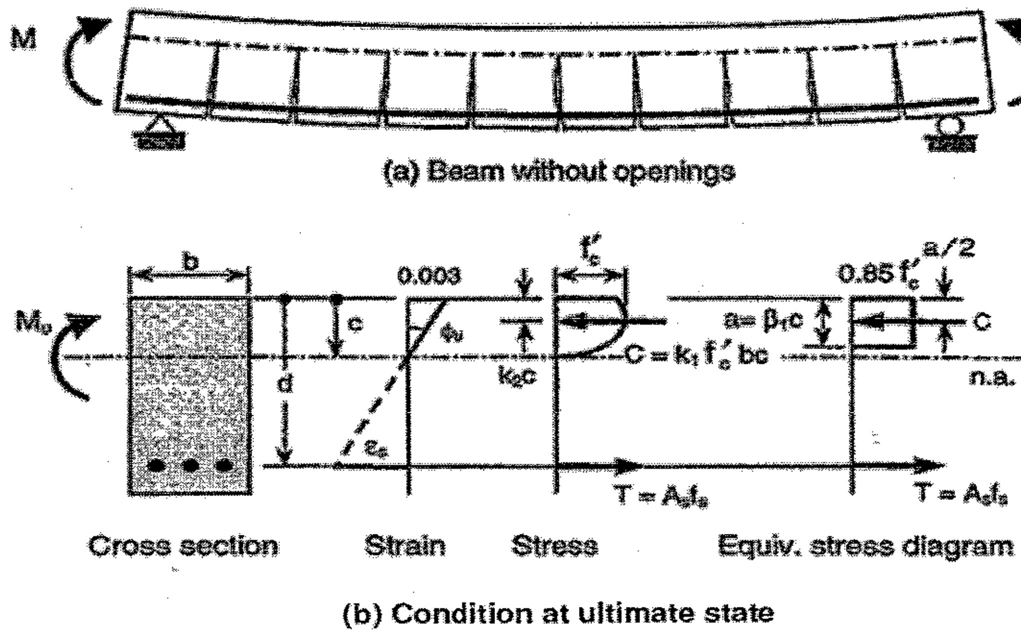

Figure 2.1 Beam under pure bending (Mansur & Tan, 1999)

When the beam section in Figure 2.1(b) is in under-reinforced condition, it causes yielding of steel reinforcement at failure. Replacing Whitney's equivalent rectangular stress block into the actual compressive stress block at nominal bending strength, T and C may be obtained as shown in Eq. (2.1) as follows (Mansur & Tan, 1999):

$$T= A_s f_y \tag{2.1}$$

$$C=0.85f'_c ba \tag{2.2}$$

where:

A_s = area of tensile reinforcement

f_y = yield strength of tensile reinforcement

f'_c = cylinder compressive strength of concrete

b = width of the section

a = depth of rectangular compressive stress block

The horizontal equilibrium, which is C = T gives:

$$a=\frac{A_s f_y}{0.85f'_c b} \tag{2.3}$$

The nominal flexural strength, M_n is then obtained from moment equilibrium as:-

$$M_n= A_s f_y\left(d - \frac{a}{2}\right) \tag{2.4}$$

Which, or substituting from Eq.(2.3), reduces to:

$$M_n= A_s f_y\left(d - 0.59\frac{A_s f_y}{f'_c b}\right) \tag{2.5}$$

2.3 Behaviour of Beams with Small Openings

In this section, the behaviour of beams due to the effects of small openings provided in bending and shear zones are being considered.

2.3.1.1 Pure Bending

When holes or openings of any shape are created in a solid beam, as illustrated in Figure 2.2(a) the provision of opening would not change the load carrying mechanism unless the opening remains within the tension zone of the beam as concrete at the location would have crack in flexure at ultimate state. Therefore, the ultimate strength of the beam will not be affected by the presence of opening. Also, openings with depth (or diameter) less than 40% of overall beam depth does not change the beam behaviour (Mansur & Tan, 1999). Other researchers in the past (Salam, 1977; Tan et al., 1996) also confirmed and noted that the strength of a beam with openings will remain the same as that of the respective solid beam as long as the openings do not reduce the concrete area which is important for the development of the compressive stress block at ultimate. Because of reduction in moment of inertia at a section through the opening, cracks will initiate at an earlier stage of loading. However, the early initiation of cracking has only marginal effect on crack widths and deflection (Mansur & Tan, 1999).

It is also found (Mansur & Tan, 1999) that the reduction in the ultimate moment capacity of the beam will not occur if the minimum depth of the compression chord, h_c is greater than or equal to the depth of compressive stress block, a, which is shown in Eq. (2.6):

$$h_c \geq \frac{A_s f_y}{0.85 f'_c b} \tag{2.6}$$

in which A_s = area of tensile reinforcement; f_y = yield strength of tensile reinforcement; f'_c = cylinder compressive strength of concrete; b = width of the compression zone.

However, if the opening is located at a section that cuts material from the compression zone, it reduces the concrete area needed for the development of the full compression stress block at ultimate. This occurs when the depth of the compression chord, $h_c < a$, the reduced area of concrete in compression should be considered in design. Fig. 2.2(b) illustrates a beam with opening at ultimate state.

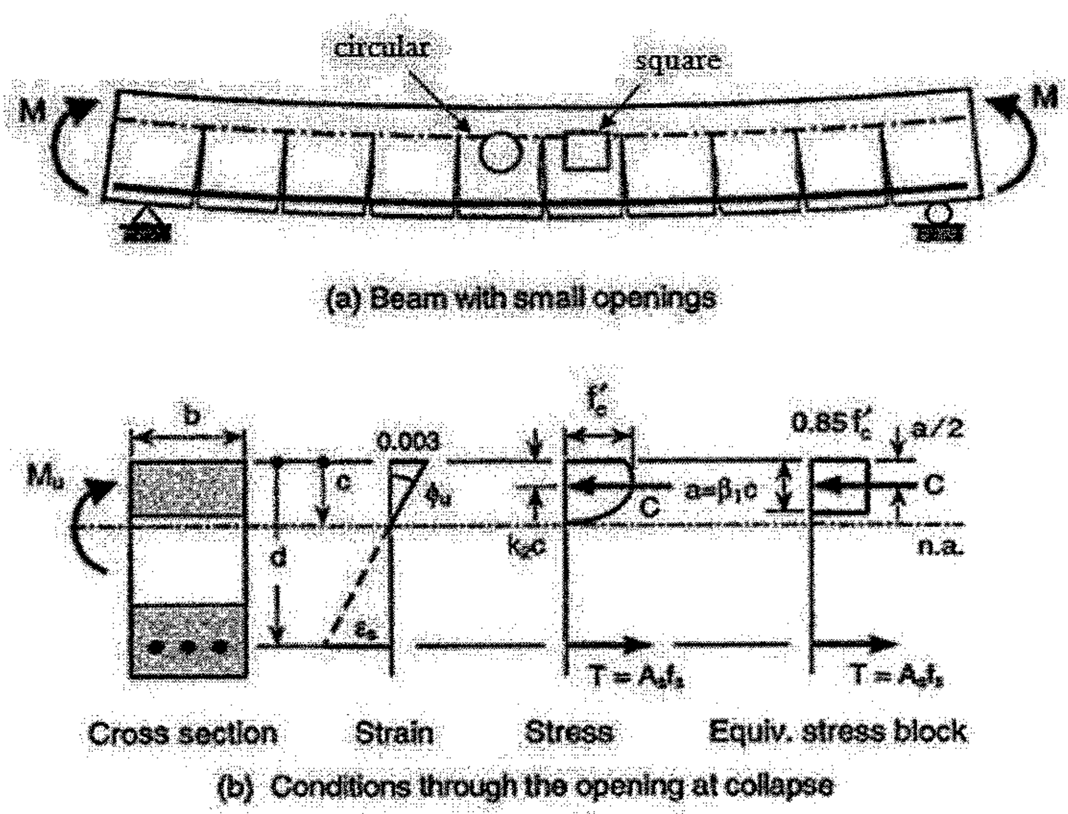

Figure 2.2 Beam with small openings under pure bending (Mansur & Tan, 1999)

2.3.1.2 Shear

The placement of a small opening in the web of a beam under-reinforced in shear has the same failure mode as that of a solid beam, as proven by the researchers (Hanson 1969; Somes & Corley 1974; Salam 1977). Opening is a source of weakness which eventually causes the failure plane to always pass through the center of the opening unless when the opening is located very close to the support that avoided the potential inclined failure plane. Some typical shear failures of beams containing square and circular openings reported by the researchers (Hanson,1969; Somes & Corley, 1974) is shown in Figure 2.3.

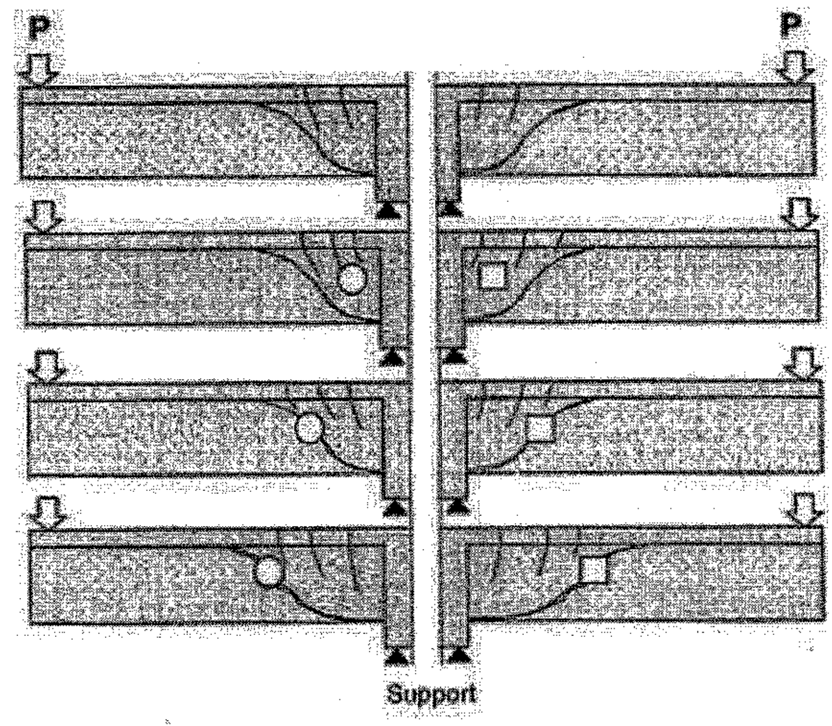

Figure 2.3 Typical shear failure of a beam without shear reinforcement (Mansur & Tan, 1999)

On the other hand, a series of longitudinal reinforced T-beams representing a typical joist-floor contained square openings were tested in an inverted position under a central point load to simulate the joists on either side of a continuous support (Hanson, 1969). In the study, the major parameters included the size, d_o and horizontal (from the edge of the central stub) and vertical (from the compression face of the beam) locations, X and Y respectively, of the opening. Similarly, the same case with specimens contained circular openings was studied (Somes & Corley 1974). Figure 2.4(a) summarized the effect of horizontal location, X of an opening on nominal shear strength, $V_u / (\sqrt{f'_c} b_w d)$ of the beam in which V_u is the ultimate shear strength of the beam in kN, f'_c is the concrete cylinder strength in MPa, b_w is the width of the web in mm and d is the effective depth in mm.

The results show that placing an opening adjacent to the simulated continuous support produced no reduction in strength. When the opening is moved away from the support, the strength reduced gradually until it reaches a constant value. Summarizing the results, it is found that vertical position of opening gives no significant effect while an increase in the size of opening causes an almost linear reduction in strength as shown in Figure 2.4(b). However, there are some opening sizes that cause no reduction in shear strength; such opening size corresponds to about 20% and 30% of the beam depth for square and circular openings, respectively. The strength of such beams may be fully restored by providing stirrups on either side of the opening (Mansur & Tan, 1999).

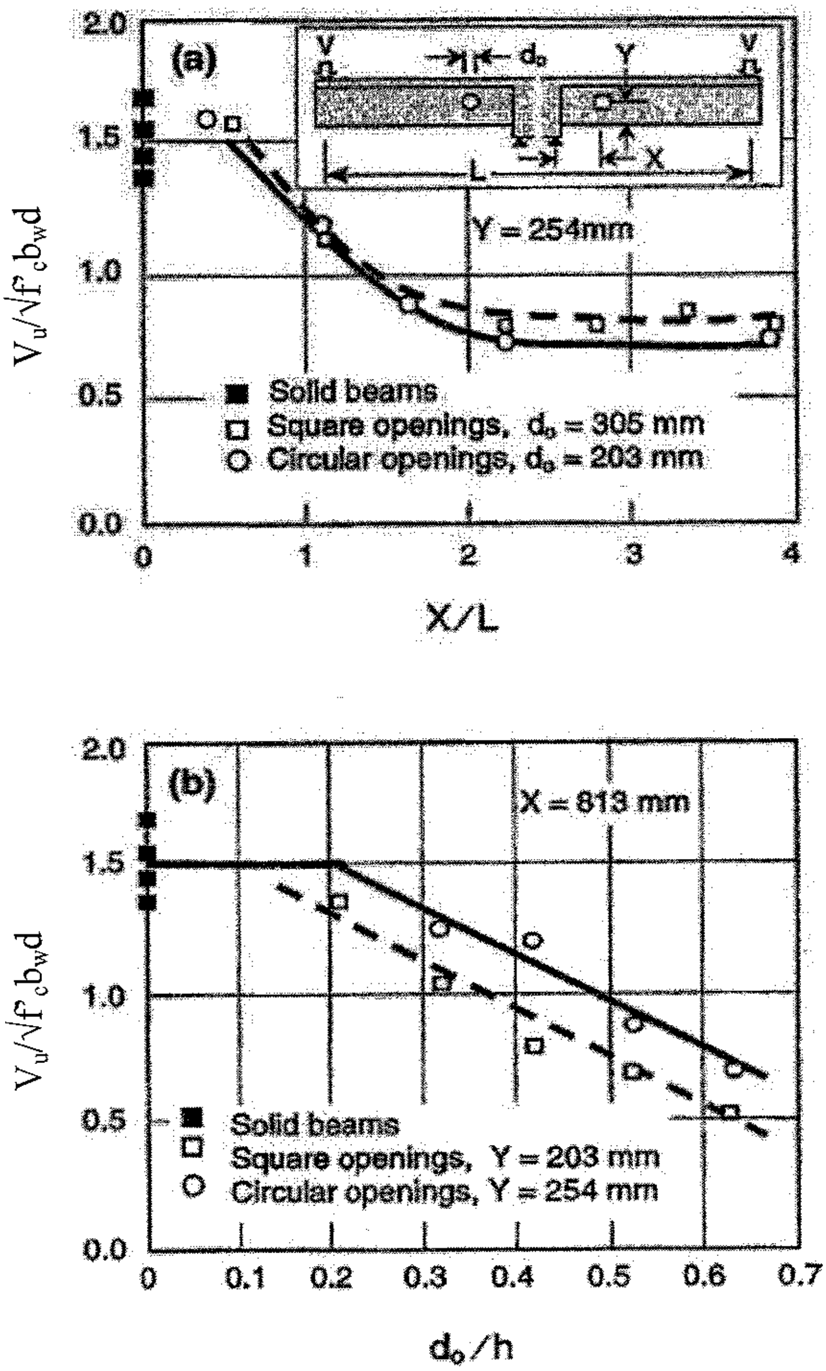

Figure 2.4 Effects of (a) horizontal location and (b) size of opening on shear strength of a beam without shear reinforcement (Mansur & Tan, 1999)

2.4 Behaviour of Beams with Large Openings

In the following sub-sections, the provision of large openings in bending and shear zones of RC beams is discussed.

2.4.1.1 Pure Bending

Similarly as to that of a beam with small openings, the placement of a large opening in the pure bending zone of a beam will not affect its moment capacity except that the depth of the compression chord is greater than or equal to the depth of the compressive stress block. In addition, by limiting the length of the opening the instability failure of the compression chord is prevented (Mansur & Tan, 1999).

2.4.1.2 Shear

Large opening provided near to the support where shear region is predominant has been the subject of many investigations conducted in the past (Nasser et al., 1967; Ragan & Warwaruk, 1967; Barney et al., 1977; Mansur et al., 1985). Figure 2.5 shows a beam with a large rectangular shape of opening provided at the major shear zone. Researchers conducted a test on beam with no additional reinforcement is provided in the members above and below the opening (Siao & Yap 1990), and found that the beams fail prematurely by sudden formation of a diagonal crack in the compression chord (Mansur, 1998).

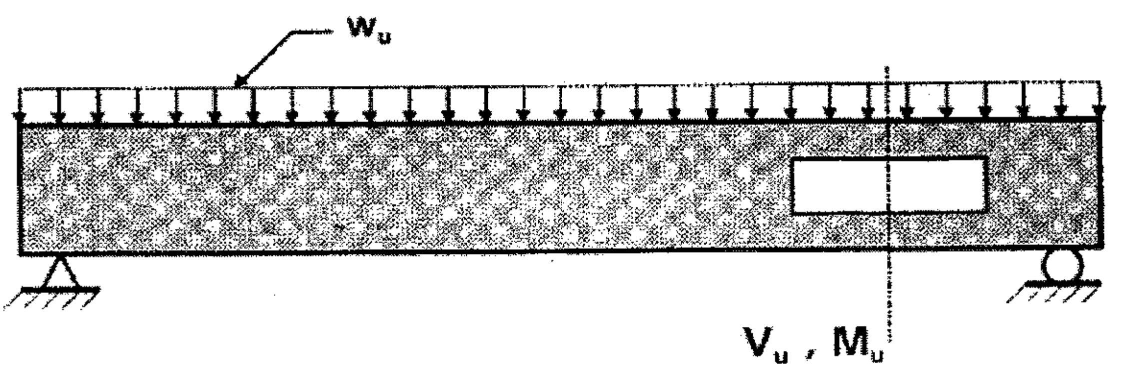

Figure 2.5 Beam with a large opening in the major shear zone (Mansur, 1998)

The introduction of a suitable scheme consisting of additional longitudinal bars near the top and bottom faces of the bottom and top chords as well as short stirrups in both the chords is provided as shown in Figure 2.6, the failure eventually occurs in a gradual manner (Mansur,1998; Mansur 2006). The design of reinforcement around large opening is according to the ACI Code (ACI, 1983; Mansur et al., 1985).

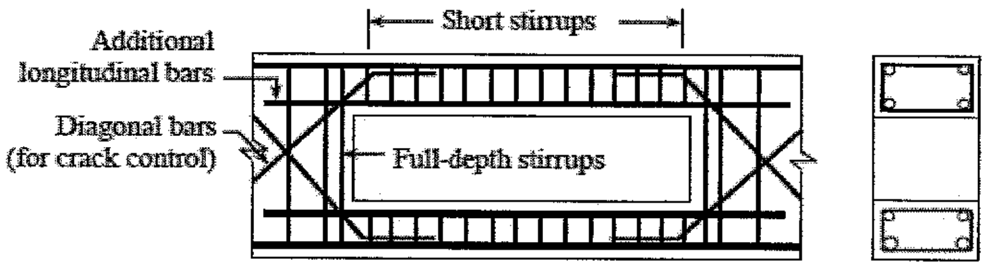

Figure 2.6 A suitable reinforcement scheme around the large opening (Mansur, 2006)

Numerous experimental investigations were conducted to observe the effects of introducing a large rectangular opening on the overall response of a beam as found in the literatures (Nasser et al., 1967; Ragan & Warwaruk, 1967; Prentzas, 1968; Barney et al., 1977; Mansur et al., 1984; Mansur et al., 1991; Tan et al., 1996; Mansur 1998):

- Introducing an opening in the web of a beam leads to early diagonal cracking, and the load at first crack decreases with an increase in either the length or the depth of the opening.

- Sufficient reinforcement is required to restrict the growth of cracks; otherwise the opening corners are subjected to wide cracking.

- Using the same amount and scheme of reinforcement, the opening size can be increased either by increasing the length or the depth of opening reduces the strength and stiffness of the beam. However, the eccentricity of the opening gives very little influence on the strength and stiffness.

- The chord members of the opening (top and bottom) behave similar to a Vierendeel panel with contraflexure points located about at the midspan of the chords (strictly valid when the chord members are symmetrically reinforced).

Formation of a mechanism with four hinges in the chord members, one at each corner of the opening as shown in Figure 2.7 happens during the final failure of the beam.

Figure 2.7 Final failure of a beam with the formation of four hinges at each corners (Mansur, 2006)

Observations of the final mode of failure during the experimental testing have led to further investigations to predict the ultimate strength of a beam with large rectangular opening (Mansur et al., 1984) and several design proposals (Ragan & Warwaruk, 1967; Nasser et al., 1967; Barney et al, 1977; Mansur et al., 1985; Mansur, 1988).

On the other hand, the local forces and moments acting in the chord members are described in the free body diagram as shown in Figure. 2.8. It was observed that the global moment, M_u at the center of the opening is resisted by the normal stress resultants in the two chords. Also, the global shear, V_u is shared by the shear stresses developed in the two chords. With the known amount of shear carried by each chord, the forces and moments acting at the critical end sections of the chord members may be determined using statics, and the chords can be designed independently as eccentrically loaded tension and compression members with significant shear by following any of the current codes of practice (Mansur, 1998).

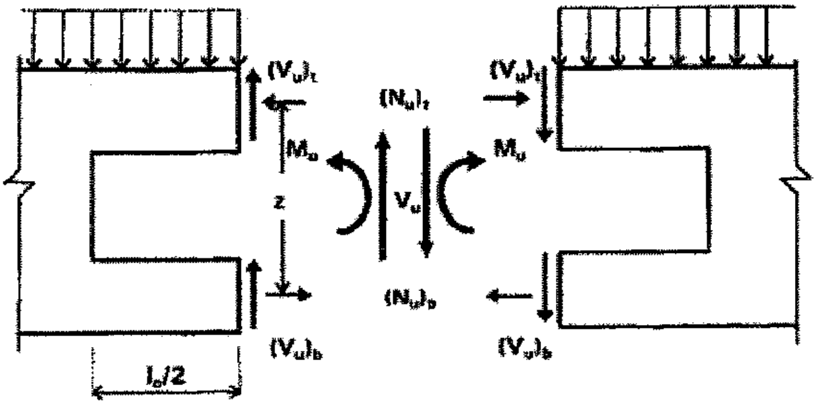

Figure 2.8 Forces acting in the chord members. (Mansur, 1998)

2.5 Summary

The following remarks are drawn from the previous studies related to the solid beam, beams with small (circular, square) and large openings (rectangular) that may lead to the research gaps:

- In a solid beam, openings with depth (or diameter) less than 40% of overall beam depth does not change the beam behaviour. The analysis and design of a beam with small openings (circular, square or nearly square in shape) may have the same beam behaviour as the solid beam.

- In general, the literatures available focus on the presence of small openings (circular, square or nearly square in shape) in T-beams, RC continuous beams and less investigation in simply supported beams.

- Large rectangular opening subjected to pure bending and shear zones (near to the support) were investigated in the past literatures.

2.6 Openings

Openings provided through RC beams are subjected to the shape, size and location. The effects of openings due to the shape, size and location are explained in details.

2.6.1 Size

Openings are divided into two categories based on their sizes, either small or large. They are grouped based on the investigations reported in the past literatures. Circular, square or nearly square in shape was defined as small opening (Mansur & Hasnat, 1979). Meanwhile, a circular opening may be considered as large when its diameter exceeds 0.25 times the depth of the web, as the introduction of such openings reduces the strength of the beam (Somes & Corley, 1974). Another researcher found that the classification of the opening to either small or large depends on the effect of such opening in the structural response of the beam. An opening may be considered small when the presence of such opening does not change the beam type behaviour. However, if the presence of opening causes the change from beam type behaviour to a frame type behavior, then such opening will be considered as large (Mansur, 1998).

Figure 2.9 shows the two modes of shear failure at small opening. Beam-type failure is a typical type of failure commonly observed in solid beams except that the failure plane passes through the center of the opening. While frame-type failure is a type of failure with the formation of two independent diagonal cracks, one in each member, bridging the two solid beam segments, which eventually leads to failure (Mansur & Tan, 1999).

Based on the above criterion, the definition of an opening being either small or large depends on the type of loading (Mansur & Tan 1999). For instance, if the opening segment is subjected to pure bending, then beam theory may be assumed to be applicable up to a length of the compression chord beyond which instability failure takes place. Similarly, for a beam subject to combined bending and shear, experimental reports from literatures (Nasser et al., 1967; Prentzas, 1968; Mansur et al., 1985) have shown that the beam-type behaviour transforms into a Vierendeel truss action as the size of opening is increased.

Mansur (2006) eventually classified openings of circular, square or nearly square in shape as small openings provided that the depth (or diameter) of the opening is in a realistic proportion to the beam size, e.g. about less than 40% of the overall beam depth. The behaviour of a beam depends on the size of opening, thus, small and large openings need separate treatment.

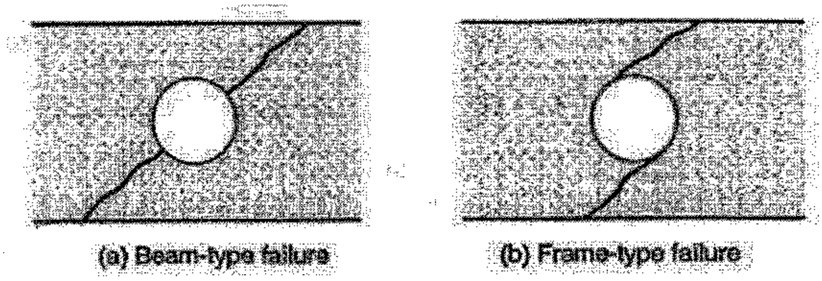

Figure 2.9 Two typical failure modes at small opening (Mansur & Tan, 1999)

2.6.2 Shape

An extensive experimental study was conducted with openings of various shapes including circular, rectangular, diamond, triangular, trapezoidal and even irregular shapes. However, circular and rectangular openings are the most common type in practice. Figure 2.10 shows the various types of opening considered by (Pretzas, 1968).

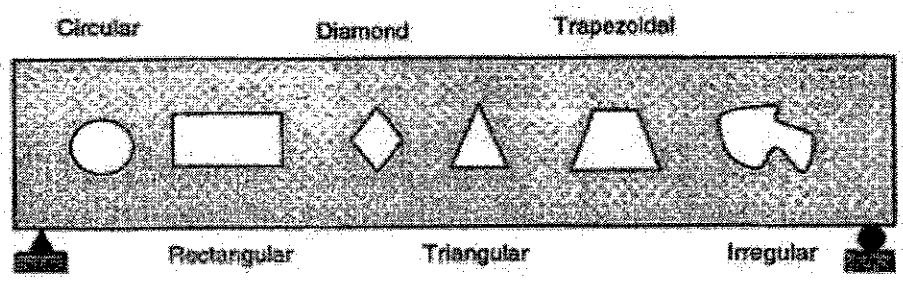

Figure 2.10 Various opening shapes considered (Prentzas, 1968; Mansur & Tan, 1999)

2.6.2.1 Elliptical and Circular Openings (Round Edges)

Provision of openings produces discontinuity in the normal flow of stresses and results in stress concentration. However, elliptical and circular types of openings have less stress concentration due to the rounded radii (Moreno, 2011). A larger radius in the notch tip will lower the stress concentration as shown in Figure 2.11 (Kokcharov, N/A).

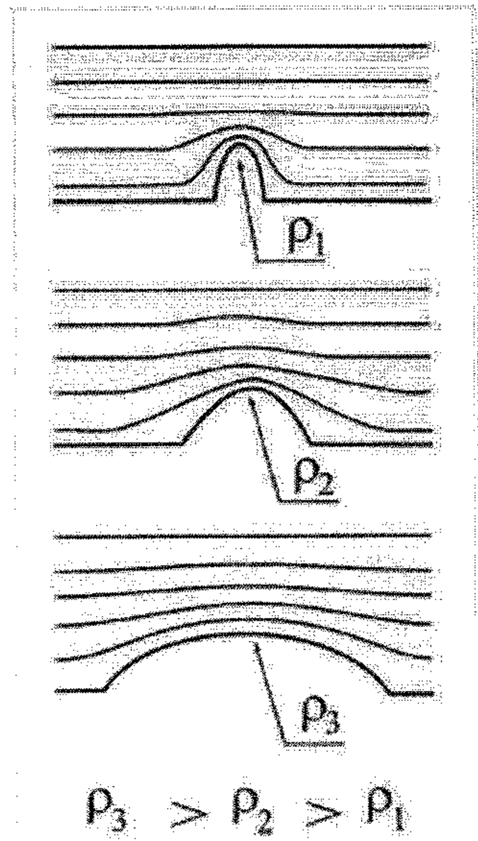

ρ = radius in the notch tip

Figure 2.11 Stress profile of small to large radius in the notch tip (Kokcharov, N/A)

2.6.2.2 Rectangular and Square Openings (With Sharp Corners)

The presence of rectangular and square shape of openings leads to high stress concentration at the sharp corners (Allam, 2005). Such openings which consist of four sharp corners are subjected to the early formation of diagonal crack around the corner of the opening due to stress concentration (Pimanmas, 2010). In general, stress concentration arises due to the various local changes in shape; i.e. sharp corners. This happened when the inner forces go around openings or notches; these forces will concentrate near such "obstacle". Areas that tend to magnify the stress level within a part are known as stress concentrators. Such stress that is higher in one area than it is in surrounding regions can cause the part to fail. Furthermore, the stress level is very high if the radius of curvature in the notch tip is very small or if there is no radius (crack), in which the sharp corners are especially critical (Kokcharov, N/A). Figure 2.12 shows that stresses are at maximum at the sharp corner. According to the theory of elasticity, the tensile stress near an opening is three times higher than nominal stress, as shown in Figure 2.13 (Kokcharov, N/A).

Also, high local stresses lower the resistance of the material to impact and fatigue loadings and cause the beam to fail more quickly (Huston & Josephs, 2008). The severity of the shape of openings also subjected to size and location in a beam. Occasionally, the corners of opening, i.e. square and rectangular are rounded off with the intention of reducing possible stress concentration at sharp corners, thus improving the cracking behaviour of the beam in service (Mansur & Tan, 1999).

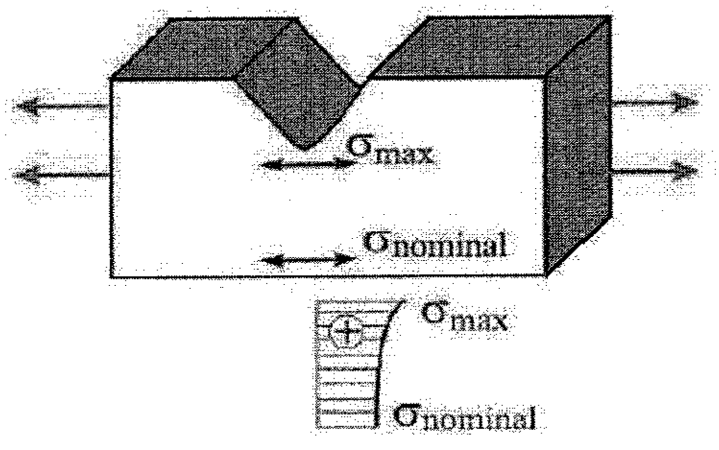

Figure 2.12 Maximum stress at sharp corner (Kokcharov, N/A)

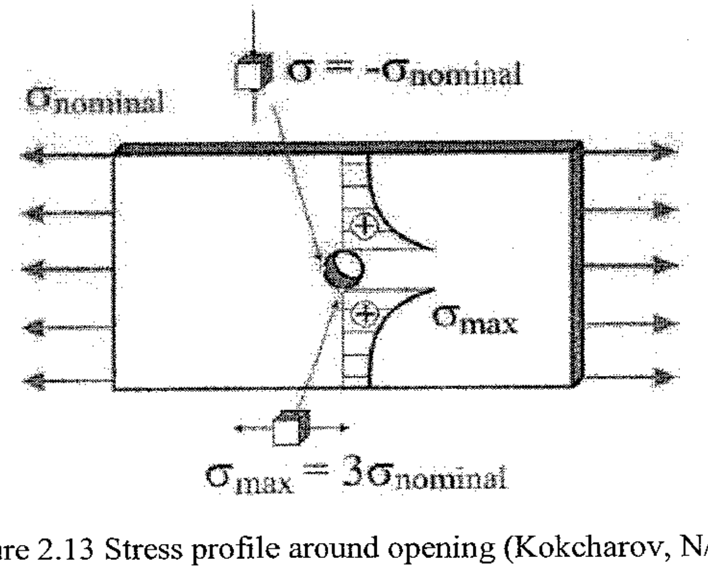

Figure 2.13 Stress profile around opening (Kokcharov, N/A)

2.6.3 Traditional Design Approach for Small Opening

According to the traditional design approach proposed by Mansur (1998), the total nominal shear strength, V_n is the sum of the two components in Eq. (2.7);

$$V_n = V_c + V_s \tag{2.7}$$

In which V_c represents the shear strength of the beam that attribute the concrete and V_s represents the shear reinforcement. By taking into consideration a 45° failure plane, the expression for V_s can be easily derived for a beam without opening. However, there are two types of diagonal tension failure that are possible to occur with the presence of small opening in a beam. The first type is commonly observed in solid beam, except that the failure plane passes through the centre of the opening. While for the second type, formation of two independent diagonal cracks, one in each member bridging the two solid beam segments leads to the failure. Such types of failure may be termed as "beam-type" and "frame-type" failure, respectively which require separate treatment for the whole design.

2.6.3.1 Beam-Type Failure

According to (Mansur, 1998), this type of failure is designed based on assumption of a 45° inclined failure plan similar to a solid beam, the plane being traversed through the center of the opening, as shown in Figure 2.14. The simplified approach of the ACI Code (ACI Committee 318, 1995) is adopted, in which the shear resistance V_c provided by the concrete may be estimated by considering the net concrete area available as in Eq. (2.8):-

$$V_c = \frac{1}{6}\sqrt{f'_c}\, b_w (d - d_o) \tag{2.8}$$

In which b_w represents the web width, d is the effective depth and d_o denotes diameter of opening.

Figure 2.14 shows the contribution of the shear reinforcement, V_S. The stirrups located by the sides of the opening within a distance (d_v - d_o) are available to resist shear across the failure plane. The term d_v is the distance between the top and bottom longitudinal rebars while d_o is the diameter (or depth) of opening. Hence, forming the Eq. (2.9):

$$V_S = \frac{A_v f_{yv}}{s}(d_v - d_0) \tag{2.9}$$

Whereby A_v is the area of vertical legs of stirrups per spacing, s; f_{yv} is the yield strength of stirrups.

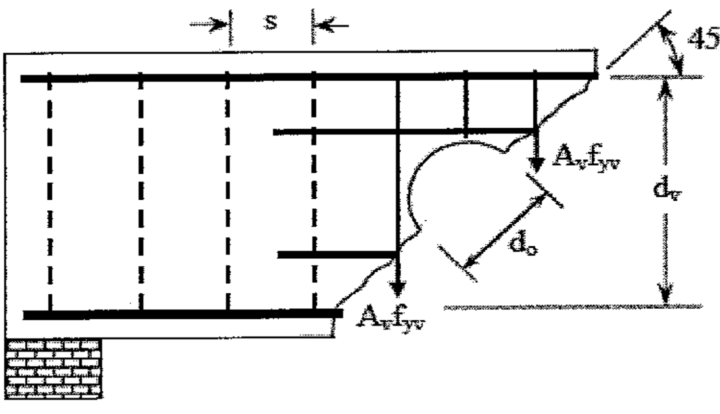

Figure 2.14 Shear resistance, V_S provided by shear reinforcement at an opening (Mansur, 2006)

When the values of V_c and V_s are known, the required amount of web reinforcement to carry the factored shear through the centre of the opening may be calculated in the normal method. This amount may be obtained within a distance $(d_v - d_0)/2$, or preferably be lumped together on either side of the opening. Other restrictions applicable to the usual shear design procedure of solid beams must also be strictly adhered to (Mansur, 1998; Mansur 2006).

2.6.3.2 Frame-Type Failure

For this mode of failure, the reinforcement is designed by considering the free body diagram at beam opening, as illustrated in Figure 2.15. As shown, the applied factored moment, M_u at the center of the opening from the global action is resisted by the usual bending mechanism, which is, by the couple formed due to the compressive and tensile stress resultants, N_u in the members above and below the opening. These stress resultants may be obtained by:-

$$(N_u)_t = \frac{M_u}{\left(d - \frac{a}{2}\right)} = -(N_u)_b \qquad (2.10)$$

according to the restrictions imposed by Eq. (2.6). Hence, in this equation, d represents the effective depth of the beam, a represents the depth of equivalent rectangular stress block while the subscripts t and b are the top and bottom cross members of the opening, respectively (Mansur, 2006).

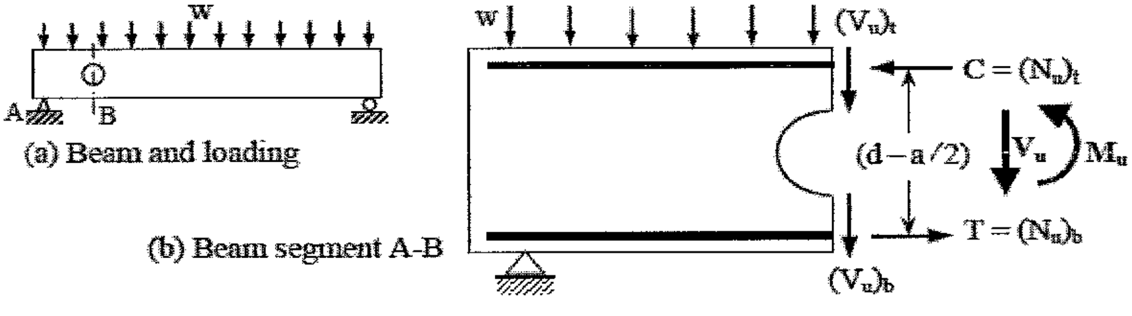

Figure 2.15 Free body diagram at beam opening (Mansur, 2006)

In addition, the applied shear V_u may be distributed between the two members in proportion to their cross-sectional areas (Nasser et al., 1967, Mansur, 2006). Therefore,

$$(V_u)_t = V_u \left[\frac{A_t}{A_t + A_b}\right] \qquad (2.11)$$

and,

$$(V_u)_b = V_u - (V_u)_t \qquad (2.12)$$

When the factored shear and axial forces are known, the shear can be designed independently for each member by following the same method as for solid beam with axial compression for the top chord and axial tension for the bottom chord (Mansur, 1998; Mansur 2006).

2.6.3.3 Reinforcing

From the two types of failure as discussed in sections 2.6.3.1 and 2.6.3.2, beam-type failure will need long stirrups to be located on either side of the opening; meanwhile the frame-type failure will require short stirrups above and below the opening. To ensure adequate strength, for anchorage of short stirrups, nominal bars must be placed at each corner if none is available from the design of solid segments. On the other hand, nominal bars should also be positioned diagonally on either side for effective crack control. As a result, the arrangement of reinforcement around the opening is shown in Figure 2.16. Under usual conditions, the placement of a small opening in a beam with proper detailing of reinforcement does not seriously affect the service load deflection (Mansur, 2006). In designing the steel reinforcement around a small opening, the Australian Code (SAA, 1974) and ACI Code (ACI, 1999) were referred (Mansur, 1999).

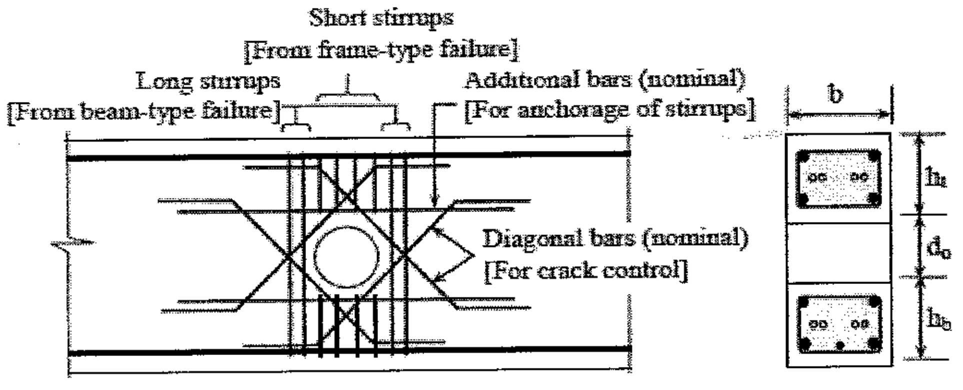

Figure 2.16 Details of reinforcement around a small opening (Mansur, 2006)

Furthermore, shear design of RC beams with circular openings using modified ACI Code approach was also studied. T-beams with circular web openings which designed for moderate to high shear force were tested in an inverted position to simulate the conditions that exist in the negative moment region of a continuous beam. The authors reported that adequate crack control and preservation of ultimate strength may be achieved by providing reinforcement around the opening. The diagonal bars were found to reduce the high stress in the compression chord, hence premature crushing of the concrete may be avoided (Tan et al., 2001).

2.6.4 Traditional Design Approach for Large Opening

RC beams with the presence of large openings must be checked for its strength or the region near the opening should be designed adequately to eliminate the weakness which caused by stress concentration that occurs due to a sudden reduction in beam cross section. Insufficient reinforcement or improper detailing causes wide cracking and premature failure of the beam (Mansur et al., 1985).

To solve problems which caused by stress concentration, several researchers had proposed their respective design methods. Nasser et al., (1967) suggested the use of diagonal bars at each corner of the opening and recommended to provide sufficient quantity in order to carry double the amount of external shear. On the other hand, Lorensten (1962) and Barney et al. (1968) proposed the method of using stirrups in the solid section adjacent to each side of the opening. The stirrups should be designed to sustain the entire shear force, nevertheless without any magnification.

Eventually, Mansur et al. (1985) proposed a rational design method for RC beams with large rectangular openings that are subjected to bending and shear. A total of twelve rectangular beams designed by the proposed method were tested under a point load. The major variables included the length, depth, eccentricity and location of openings, and the amount and arrangement of corner reinforcement. The authors noticed that diagonal bars as corner reinforcement were found to be more effective in controlling crack width and reducing beam deflection than vertical stirrups. It was found that the serviceability criterion of maximum crack width can be satisfied with the usage of a suitable combination of diagonal bars and full depth vertical stirrups as corner reinforcement. The diagonal bars also contribute to the increase of ultimate strength of the beams. Figure 2.17 shows the proposed reinforcement details around a large opening.

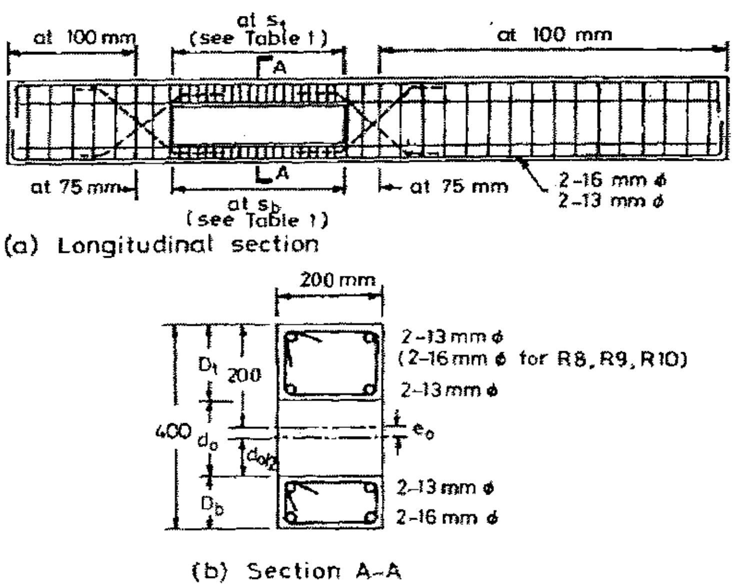

Figure 2.17 Reinforcement details around a large opening (Mansur et al., 1985)

2.6.5 Openings in Existing Beams

It is very clear that the presence of openings may contribute to the weakness of a beam. This situation can be avoided if the plan of the service systems is known in advance, so that the sizes and locations of openings required to fulfil the layout of the pipes and ducts system are well decided in advance. Thus, sufficient strength and serviceability of beams with opening may be ensured during the design stage by following the design methods and guidelines from the literatures before the construction process.

However, there are several issues which usually arise during the construction stage. In the process of ducts laying in a newly constructed building, M & E contractors will usually request to drill an opening to simplify the arrangement of pipes as this could significantly cause a huge savings in terms of cost. It is usually a difficult decision to make for the structural engineers to facilitate such request. As from the owner's point of view, the placement of an opening may reduce the cost. Hence, the structural engineers need to compromise with the M & E contractors as well as the owner by providing a solution that would not endanger the safety and serviceability of the structure (Mansur, 2006).

For existing building, problem arises in which concrete cores are taken for structural assessment of the building (Mansur, 2006). When the concrete cores are removed, the holes/openings are usually filled in by non-shrink grout in which such repair is remained uncertain whether it could adequately restore the original level of safety and serviceability of the structure (Mansur, 2006).

Due to many queries, an attempt was made to study the effect of drilling holes in an existing beam in which the openings were provided near the support region. This research involved testing a total of nine prototype T-beams simulating the conditions that exist in the negative moment region of a continuous beam. The beams were 2.9 m long and contained a central stub to indicate the continuous support. The cross section consisted of a 400 mm deep and 200 mm wide web, a 100 mm thick and 700 mm wide flange. The openings provided were circular in shape as it is easily created in an existing beam without affecting the integrity of the surrounding concrete by using a coring machine. For symmetry, an identical opening was created on each side of the central stub, and all beams contained the same amount and arrangement of reinforcement as illustrated in Figure 2.18. The parameters considered in the study were the size and location of openings and method of repair or strengthening (Mansur et al., 1999).

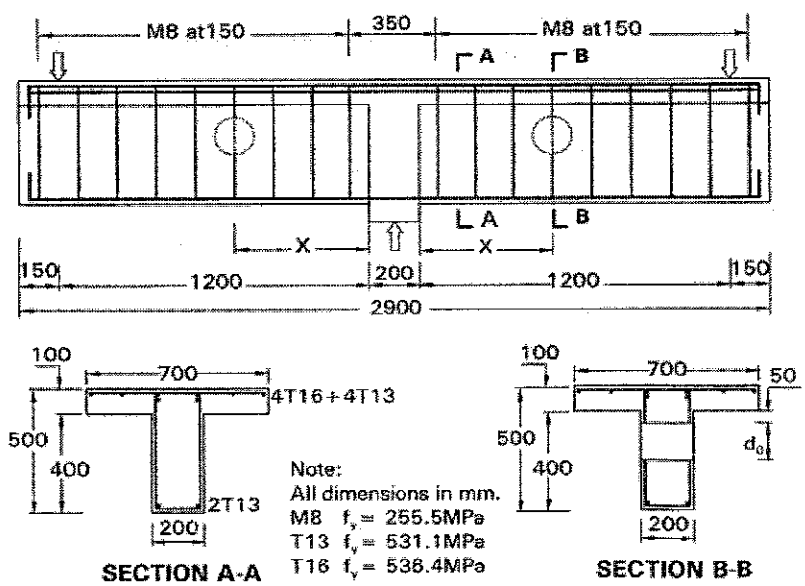

Figure 2.18 Reinforcement details of beam (Mansur et al., 1999)

To simulate the condition of coring the opening, the stirrups intercepting the opening were cut during fabrication of the reinforcement cage and the openings were provided during the casting process. The first method of beam repair was filling the beams with non-shrink construction grout to simulate the field condition of a hole/opening created for finding the in place concrete strength. The results of the beams clearly show that creating an opening near the support region of an existing beam can seriously impair the safety and serviceability of the structure. The authors have discovered that filling the opening by non-shrink grout is inadequate to restore the beam original response. Hence, if such opening is unavoidable, sufficient measures should be undertaken to strengthen the beam in order to maintain the safety and serviceability considered in the original design (Mansur et al., 1999).

2.6.6 Summary

The following remarks are drawn from the previous studies related to the size and shape of openings, traditional design approach for small and large openings and openings in existing beams:

- The investigations conducted are basically with small openings, i.e. circular, square or nearly square in shape. Large openings in the shape of circular and square dimensions have not being fully investigated.

- The traditional design approach can be applied if the location of the opening is known before or during the construction process. Various design methods and procedures proposed by researchers to solve problems due to the stress concentration in small and large openings such as the provision of diagonal bars as corner reinforcement around the opening and vertical stirrups. However, this approach can be applied provided that the opening location is known in advance. More research is needed when openings are to be provided in constructed beams.

- For openings provided in existing beams, it was found that filling the opening by non-shrink grout is inadequate to restore the beam original response. Drilling an opening near the support region of an existing beam may seriously affect the safety and serviceability of the structure. Hence, when such opening is unavoidable, sufficient measures should be undertaken to strengthen the beam in order to maintain the safety and serviceability considered in the original design. Hence, for this opening condition, other strengthening options are needed in order to reinstate the original structural capacity.

2.7 Rehabilitation and Strengthening

Over the years, deterioration of buildings and civil infrastructure has become a critical issue to many developed and industrialized countries especially Europe, United States and Japan. The degradation of RC structures for example decks, superstructure elements and columns are mainly due to condition of the concrete materials. The concrete may have become structurally inadequate due to deterioration of materials, poor initial design and/or construction, lack of maintenance, upgrading of design loads or because of environmentally induced disasters such as earthquakes. In terms of deterioration of materials, concrete and/or reinforcement can be attacked by the fluids and/or ions entrance from environment such as chloride attack, sulfate attack, carbonation (Badea et al., 2008). Steel bars in RC are protected from corrosion by the high pH environment of the surrounding concrete. This alkaline environment is destroyed by the reaction of atmospheric carbon dioxide CO_2 with the calcium hydroxide $Ca(OH)_2$ of the concrete mass. When this process, known as carbonation of concrete reaches the reinforcing bars, corrosion may occur (Papadakis et al., 1989).

Other issues related to problems of deterioration that requires an increased in loadings and number of lanes to accommodate the ever-increasing traffic flow and changes in their use which gives a significant impact to the current infrastructure to be structurally or functionally deficient. In terms of sustainability, the deterioration of buildings and civil infrastructures becomes a critical issue. Thus, practical and cost effective of external strengthening is required compared to other traditional repair methods.

2.7.1 Traditional Strengthening Method

One of the most active areas in civil engineering recently is the need to increase the capacity of the existing structures. There are several strengthening methods which have been used in the past with varying degree of success. These include (1) enlargement of the cross section, (2) addition of new steel members, (3) steel plate bonding, (4) external post-tensioning and (5) reduction of span length (Hollaway & Leeming, 1999; Supaviriyakit et al., 2004).

2.7.1.1 Steel Plates

Traditionally, the rehabilitation or repair of RC structures has been achieved by using steel plates, which is the first generation of external strengthening methods being bonded to the tension surface of the structure. Steel plates were naturally the original choice for rehabilitation and repairing work because of the compatibility of their properties with concrete and partly because of their ability to maintain ductility and structural integrity when exposed to hostile environments, even though they are susceptible to atmospheric corrosion (Spadea et al., 2001).

The amount of materials added to the structure for strengthening should be ideally minimized to avoid increasing of dead load or decreasing of clearance requirements. Also, the strengthening technique should minimize disruption to the structure and its usage. For strengthening of indoor beams, the bonding of steel plates might be considered as the most suitable method for strengthening. As for outdoor applications, the main disadvantage of using steel plates is corrosion of steel. The corrosion tends to destroy the bonding between the plates and the epoxy (Grace et al., 1999).

Although the strengthening effectiveness of using the steel plates was acceptable, there are several disadvantages. These disadvantages include (1) susceptibility of the steel plates to corrosion or debonding; (2) the weight of the steel plate may be excessive for long-span beams; (3) difficult to handle on site; (4) undesirable formation of welds; and (5) partial composite action with the concrete surface and debonding.

Due to the mentioned disadvantages, thus there was a need for alternative materials. In recent years, FRP plates have shown promising results as an alternative to steel plates for concrete beam repair and rehabilitation (Ross et al., 1999).

2.7.2 Current Strengthening Method

To date, FRP has received overwhelming attention from the research community as external reinforcing materials due to its outstanding characteristics such as low weight, non-corrosive and easy to handle, apply and install on construction sites. The following sub-sections present the background, advantages and benefits of the FRP materials.

2.7.2.1 Fiber Reinforced Polymer (FRP)

Recently, the use of FRP plates for strengthening and repairing of RC structures has become an interesting alternative to steel plates. Over the years, many research efforts have been conducted with the use of FRP composite plates in strengthening applications by researchers (Meier et al., 1992; Meier, 1996; Emmons et al., 1998; Fanning & Kelly, 2000). It is found that the plate bonding techniques and the strengthening solutions related with FRP composite materials are greatly acknowledged, in such cases achieved better results compared to using steel (Fanning & Kelly, 2000;White et al., 2001).

2.7.2.2 History of FRP

Other than the use of FRP materials in the area of civil engineering, the successful use of FRP in aerospace, sports, recreation, and automobile industries helped in decreasing FRP cost. This decrease in cost together with the savings due to the elimination of future maintenance and repair costs causes the application of FRP to be economical and effective as compared to steel (Grace et al., 1999; Duthinh & Starnes, 2001; Buyle-Bodin et al. 2002).

2.7.2.3 Definition of FRP

FRP is a composite material consisting of numerous high-strength fibers embedded in a matrix material. The main function of the matrix material is to spread the load between the individual fibers and to protect the fibers against environmental influences, such as moisture, corrosion and wear. The fibers are the major load-carrying element and contain extensive range of strengths and stiffness with a linear stress-strain relationship up to failure. Typical fiber types that are used in the fabrication of FRP composites for construction include CFRP, AFRP and GFRP where such fibers are available commercially as continuous filaments. The matrix material is usually in two categories; thermosetting polymers (e.g. epoxy and polyester) and thermoplastic polymers (e.g. nylon).

2.7.2.4 Advantages of FRP Materials

The use of FRP materials offers many advantages such as:

- **High strength and stiffness:** The ultimate strength is 8 to 10 times greater than the mild steel plate.
- **Better resistance to electrochemical factor:** FRP systems are corrosive resistant, non-magnetic, a good resistant to chemical attack i.e. chloride attack, unlike steel plates which is susceptible to corrosion especially if the concrete to which they are fixed is cracked or contaminated by chloride.
- **Reduction in construction period:** The time taken for preparing and installing FRP system is very short period compare with the time taken for installing steel plates.
- **Ease of handling and installation:** Man-access platforms are sufficient for handling and installing in FRP system rather than using full scaffolding platforms in steel plates system. Installation of FRP system does not need extensive jacking and support system to move and hold in place.

- **Low weight:** Density of FRP materials is approximately 1/5 to 1/4 of the density of steel; hence it can be transported easily without the need of crane facilities.

- **Availability in any length or shape:** FRP are available in the form of rolls in very long lengths whereas steel plates are generally limited to 6 m lengths. FRP usually in the form of very thin layers, i.e. 1.2 -1.4 mm that can easily follow a curved profile without the need of pre-shaping compared to steel plates which have their own shape and if to be applied to curved surfaces, the material need to be bent in advance.

- **Savings of labour cost:** Low weight, easy installation and short construction period of the FRP system leads to a decrease in cost of labour.

- **Durability:** FRP system does not require maintenance unlike the steel plate system that needs regular maintenance that may cause traffic disruption and extra cost. Both the fiber and matrix of the CFRP composite material are inert, unlike steel plates bonded to concrete which are prone to corrosion does not affect the long term durability of the strengthened system.

The main disadvantages of FRP materials are the risks of fire and accidental damage. Another major concern for bridges over roads is the risk of soffit reinforcement being ripped off by over-height vehicles. Although the materials are rather expensive, however, generally the extra cost of the material is balanced by the reduction in labour cost. Furthermore, it is difficult to find specialist contractors with the appropriate expertise for the application of FRP.

2.7.2.5 Benefits and Contribution of FRP

The main benefits of FRP system are:

- **Earthquake and seismic retrofit:** FRP have been used extensively in seismic zones to confine concrete matrices in concrete columns and walls, i.e. bridge columns by wrapping method.

- **Strengthening:** FRP can be applied to strengthen structural members which have been severely damaged due to loading conditions, changes of structural purpose, etc.

- **Repair damaged concrete structures:** FRP is used to retrofit, and upgrade deteriorated bridges, poorly designed or constructed structures, concrete structures that exceeded their design life and showing signs of deteriorating.

2.7.3 Types of Fibers

Suitable types of fibers have to be chosen for the use of a particular application dependent on several factors which include the type of structure, the expected loading, and the environmental conditions. The following fibers are commonly used for strengthening and upgrading:

- CFRP
- AFRP
- GFRP

2.7.3.1 Carbon Fibers (CFRP)

Carbon fiber is defined as a fiber containing at least 90% carbon by weight obtained by the controlled pyrolysis of appropriate fibers (Rashid Khan & Barron, 2008). Carbon fibers are manufactured from synthetic fibers through heating and stretching treatments. The most commonly used precursors are polyacrylonitrile (PAN) and pitch fibers. PAN is a synthetic fiber that is premanufactured and wound onto spools, while pitch is a by-product of petroleum distillation or coal coaking that is melted, spun, and stretched into fibers. The fibers have to undergo three stages of treatment. Firstly, the carbon chains in the fiber are made cross-links in the thermoset treatment, and then through the carbonization process, the non-carbon impurities are eliminated. The process is completed with graphitization which produces fiber with crystalline orientation, similar to graphite. Carbon fibers are distinct from other fibers due to their properties and influenced by the processing conditions such as tension and temperature during the process. Carbon fiber composites are ideally suited for applications where strength, stiffness, lower weight, and outstanding fatigue characteristics to fulfil the critical requirements (GangaRao et al., 2006).

2.7.3.2 Aramid Fibers (AFRP)

Aramid fibers known as 'aromatic polyamide' are long-chain synthetic polyamides where at least 85% of the amide bonds are attached to the aromatic rings (Feldman & Barbalata, 1996). It is manufactured by extruding a solution of aromatic polyamide at a temperature between -50°C and -80°C into a hot cylinder at 200°C. Remaining fibers from evaporation are then stretched and drawn to increase their strength and stiffness. During the process, aramid molecules become highly oriented in the longitudinal direction. Aramid fibers are extremely high in tensile strength and toughness in which they are frequently used in advanced composite products. However, their strength and stiffness usually fall in between of glass and carbon fibers. These fibers have high static, dynamic fatigue, and impact strengths. One of the drawbacks of aramid fibers is that they are difficult for cutting and machining (Tuakta, 2004).

2.7.3.3 Glass Fibers (GFRP)

Glass fibers are processed form of glass, which is consisting of a number of oxides, such as silica oxide from silica sand, together with other raw materials, i.e. limestone, fluorspar, boric acid, and clay. They are manufactured by drawing those melt oxides into very fine filaments, ranging from 3 to 24 μm (Hollaway & Head, 2000; Tuakta, 2004). GFRP composites are widely used in variety of applications from aircraft to machine tools due to their light weight, high modulus, and specific strength (Hull & Clyne 1996). Although the strength properties are lower and less stiff than carbon and aramid fiber, it is much cheaper and significantly less brittle. E-glass is the most commonly used glass fibers available in the construction industry. Figure 2.19 shows the comparison in terms of stress strain relationship between carbon, aramid and glass fibers.

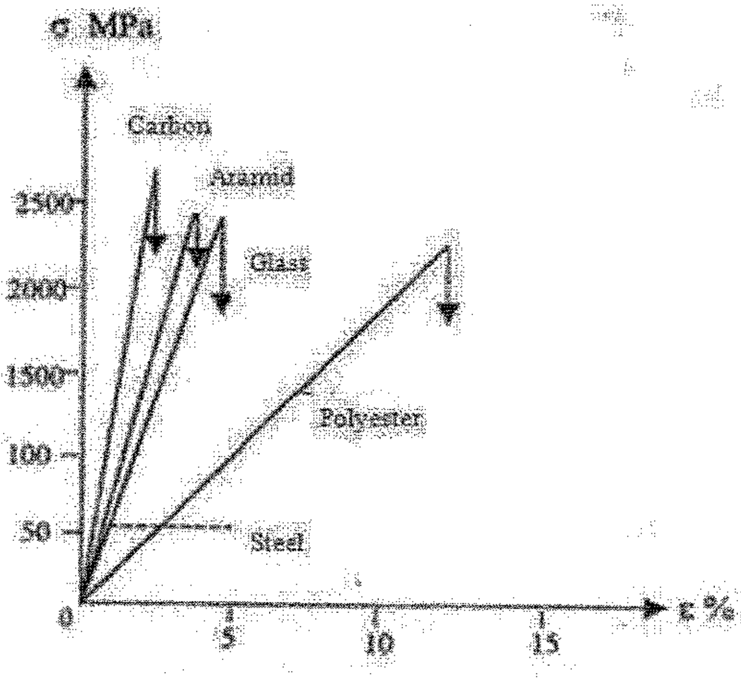

Figure 2.19 Stress strain comparison of different materials (Rai & Indolia, 2011)

2.7.4 Summary

The following remarks are drawn from previous studies:

- In the past, many investigations were conducted to study the rehabilitation and repair of RC structures using steel plates. To date, various investigations are performed using FRP materials due to its advantages and benefits.
- Among the three types of fibers, carbon fibers are used in this research study due to its outstanding characteristics and strength.

2.8 Strengthening of Structural Members

FRP reinforcement provides many advantages to the structural members. The use of externally bonded FRP reinforcement could significantly increase a member's stiffness and load carrying capacity, enhance flexural and shear capacities, providing confinement and ductility to compression structural members and also controls the propagation of cracks. Strengthening with externally bonded FRP sheets has been shown to be applicable to many forms of RC structures. Currently, this method has been implemented to strengthen structures such as columns, beams, slabs, walls, chimneys, tunnels and silos. Among these, numerous experimental studies have been conducted mainly on RC beams, slabs and columns.

2.8.1 Beam

The use of FRP composites for the rehabilitation of beams started about 25 years ago with the pioneering research performed at the Swiss Federal Laboratories for Materials Testing and Research (EMPA). These FRP composites increase the flexural capacity of beams by adding fiber composite materials to the tensile face.

Shear strengthening is essential when an RC beam is found deficient in shear or the shear capacity obtains a low flexural capacity after flexural strengthening. It is found that the shear strengthening studies have been rather limited compared to flexural strengthening of RC beams. Thus, one of the major strengthening applications of FRP composites is as additional web reinforcement of various forms for the enhancement of shear resistance of RC beams. (Elyasian et al., 2006).

Meanwhile, to increase the shear capacity of beams, fiber composite materials are added to the sides in the shear tensile zone. A report by (Esfahani et al., 2007) stated that the bonding of FRP on either the side faces, or the side faces and soffit will contribute to the shear strengthening for RC beams. The authors recommended that the FRP to be placed with the principal fiber orientation ß, is either 45° or 90° to the longitudinal axis of the member. It is verified that the shear resistance of beams can be further upgraded by bonding additional sheets with their fibers orientated at right angles to the principal fiber direction. Figure 2.20 shows the FRP shear strengthening configurations at (a) 90° and (b) 45°.

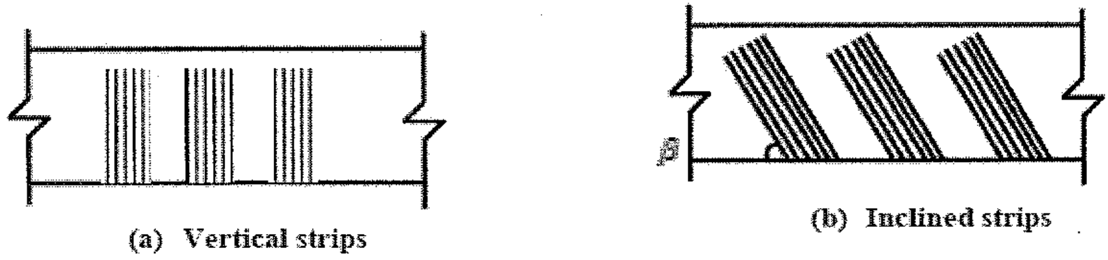

Figure 2.20 FRP shear strengthening configuration (Ibrahim & Mahmood, 2009)

2.8.2 Slab

Researches on reinforced slab have shown that two types of failure which generally encountered with non-strengthened RC slab are (1) failure by flexure and (2) by punching, which also apply in the cases of reinforced and strengthened concrete. The effectiveness of strengthening slabs using FRP has been demonstrated by numerous experimental investigations.

An experimental investigation and a limit analysis approach were conducted to study the strengthening of RC two-way slabs with CFRP strips bonded to the tensile face. The results of the experimental study show that externally bonded CFRP plates can efficiently used to strengthen two-way RC slabs (Limam et al., 2003).

On the other hand, an experimental and analytical investigation were performed for evaluating the ultimate response of unreinforced and reinforced two-way concrete slabs repaired and retrofitted with FRP composite strips. Based on the tested results, it is proven that FRP systems have succeeded in upgrading the structural capacity of both two-way unreinforced and RC slabs by 200% (Mosallam & Mossalam, 2003).

A series of one-way spanning simply supported RC slabs strengthened in flexure with tension face bonded FRP composites and anchored with different arrangements of FRP anchors tested by (Smith et al., 2011). The authors found that the increase in load and deflection of the slabs strengthened with FRP plates and anchored with FRP anchors was 30% and 110%, respectively over the unanchored FRP strengthened control slab. In general, FRP anchors are greatly effective in increasing the strength and deflection of FRP flexurally strengthened RC slabs.

2.8.3 Column

Deterioration of steel RC columns has been a topic of concerns for years in the infrastructure community due to corrosion of reinforcing steel and cracking and spalling of concrete. Numerous studies on the strengthening of RC columns with FRP materials were reported in the literatures. It is noticed an increase in the axial and shear capacity of columns by wrapping fiber composite materials around the perimeter.

The application of FRP composite wraps to repair earthquake-damaged RC columns was investigated (Saadatmanesh et al., 1997). The results proven that FRP wraps could effectively restore flexural strength and ductility in columns.

The behaviour of high strength concrete columns wrapped with FRP composites were studied (Hadi, 2007). The FRP composites were wrapped circumferentially around the columns. The columns were tested to failure by applying axial concentric or eccentric loads. The test results of the tested columns indicated that FRP is effective in producing columns with higher capacity and durability compared to RC columns.

Eight RC short columns retrofitted using CFRP or GFRP materials were tested by (Colomb et al., 2008) to study the effect of external bonded FRP reinforcement on the shear behaviour of strengthened short columns. The authors found that continuous FRP reinforcement column wrapping increase both the ductility and resistance of the columns. And recently, externally bonded FRP laminates and fabrics can be used to increase the shear strength of RC columns. The shear strength of columns can be easily improved by wrapping with a continuous sheet of FRP to form a complete ring around the member.

2.8.4 Summary

The following remarks are drawn from the previous section:

- FRP materials have been used for strengthening and retrofitting of RC structures including beams, slabs and columns. In this research topic, RC beams are selected for further investigations in the particular area.

2.9 Strengthening of Solid RC Beams by CFRP Composites

Strengthening and retrofitting using CFRP has received wider attention from the research community. Various studies have been conducted using CFRP materials to increase the flexural strength of RC beams in both analytical and numerical investigations.

2.9.1 Analytical Studies

An analytical model developed for the design of shear strengthening of concrete with composite beams within the framework of modern code formats, based on ultimate limit states. The model developed was to assess the contribution of FRP to shear capacity similar to steel stirrups, with an effective FRP strain which decreases when FRP axial rigidity increases. The contribution of the model was useful especially in designing FRP reinforcements and to determine the optimum material quantities. As for the fiber orientation, analysis and experimental results showed that the performance of FRP increases when the fibre's direction moved closer to the perpendicular diagonal crack (Triantafillou, 1998).

A non-linear model was developed (Ferretti & Savoia, 2003) for the analysis of RC tensile members strengthened with FRP plates applying non-linear laws by using cohesive stresses in concrete across cracks and non-linear bond-slip law between steel bars and concrete were adopted. These non-linear equations were resolved through finite difference method. The validity of the model was confirmed when compared with the experimental results and a good correlation was obtained. The authors found that a small-thickness of external FRP-plating was very effective in reducing crack width and increasing axial stiffness of tensile members under serviceability loads.

Gorji (2009) developed an analytical method to predict the deflection of rectangular RC beams strengthened using FRP composites placed at the bottom of the beams. A single span simply supported beam strengthened with FRP composite was considered in the analysis. The analytical method was based on energy variation method. Several assumptions were made in this study: (1) plane sections remain plane throughout and strain distribution of elements in cross section are linearly on height;

(2) no slip between the steel or FRP reinforcement concrete; (3) concrete only works in the compression zone and (4) stress-strain relationship is linear. The analytical results were compared with FE modeling results. The predicted results were found in well agreement with the FE model.

Meanwhile, the effect of transverse steel studied on the importance of FRP shear contribution, however was disregarded by the existing codes and guidelines. Thus, the authors proposed a new design method to calculate the shear contribution of FRP by considering the effect of transverse steel on the externally bonded FRP contribution in shear. The design equations for U-wrap and side bonded FRP configurations were proposed separately. The proposed model was validated with the experimental results and achieved a better correlation than the current guidelines (Mofidi & Chaallal, 2011).

A new mechanical model to predict the failure loads and failure modes of RC beams strengthened by externally bonded FRP plates/sheets to flexure and shear was presented (Colotti & Swamy, 2011). The model was developed according to truss analogy approach which refined to accommodate several critical aspects of the structural behaviour of FRP strengthened RC beams. The critical aspects included variable angle crack, non-uniform FRP stress distribution over the shear crack and shear/span depth ratio. This model was able of describing the main possible failure mechanisms of strengthened RC beams. This included flexural-shear interaction, shear-web crushing and pure flexural mechanisms. Validation of this model was conducted against seventy three (73) tested experimental beams collected from literatures whereby varieties of test geometries, structural variables and shear strengthening configurations were included. The numerical study exhibited a good agreement between predicted and experimental results, with a mean experimental/theoretical failure load ratio of 1.05 and an acceptable coefficient of correlation about 17% (Colotti & Swamy, 2011).

2.9.2 Experimental Studies

The following section is mainly about the study of CFRP laminates externally bonded to the tensile face of the concrete beams. This strengthening technique has been received overwhelming attention particularly in the repairing of damaged bridges. Numerous investigations were conducted to study the effect of CFRP laminates on the flexural performance of RC beam was discussed.

2.9.2.1 Flexural Strengthening

Thirteen (13) concrete beams cast for flexural tests to study the behaviour of damaged or under-strength concrete beams retrofitted with thin CFRP sheets. The CFRP sheets were epoxy bonded to the tension face of concrete beams to enhance the flexural strength. The beam specimens were fabricated, loaded beyond concrete cracking strength and retrofitted with three different CFRP systems. The beams were then loaded to failure. The dimension of the beams was 127 mm x 203 mm x2440 mm. The beams were over-designed against shear. The variables in this study including the use of three different fiber/epoxy systems and several fiber orientations on to the beam specimens. Two types of FRP systems were tested with respect to three fiber orientations (0°, 90°, and ±45 °) and the third fiber was used with orientations of 0°/90° and ±45°. The same fiber weight was applied to each of the beam. The results showed little difference between the types of fibers used and there was no difference in behaviour between the precracked and uncracked beams, but different fiber orientations provided significant results. Beam with fiber orientation 0° showed greater ultimate strength and stiffness and decrease in deflection compared to the control beam. The beams failed abruptly due to peeling of CFRP laminate from the concrete. Beam with 0°/90° fibers exhibited a lower ultimate strength with a higher ductility and deflection compared to beam with 0°. In this case, the beams failed less explosively than beams with 0° fiber orientation. The beam with ±45° fiber orientation demonstrated a lower strength and stiffness compared to 0° orientation. Unlike the first two beams, the behaviour of this beam was more ductile whereby the failure mode of the beam occurred in slow ductile manner. The authors concluded that off-axis CFRP laminates need to be further investigated. Different fiber orientations of CFRP laminates could increase the strength and stiffness of beams without causing catastrophic brittle failures related with unidirectional laminates (Norris et al., 1997).

Research of (Grace et al., 1999) was based on different pattern of FRP systems in strengthening RC beams and ductility of FRP strengthened beams. Fourteen (14) beams with a dimension of 152 mm x 292mm x 2743 mm were tested. Each beam was precracked and then strengthened with FRP material. The beams were tested to failure with a concentrated point load applied at mid-span. A total of five FRP strengthening systems were used which consisted of two types of CFRP sheets, two types of GFRP sheets and CFRP plates. Four types of epoxies were used in this study. Results showed that the use of FRP strengthening materials significantly reduced deflections compared at yield load. The decreased was mainly due to the type of strengthening material, type of epoxy and strengthening configuration. Grace et al concluded that the use of FRP laminates in strengthening concrete beams reduces deflection and increases load carrying capacity in the beams. The cracks appeared were smaller and more evenly distributed. Vertical orientation of FRP laminates could further reduced deflections and increased ultimate load capacity. This vertical layer also prevents rupture in the flexural (horizontal) fibers. Meanwhile, the ultimate load capacity of beams could be doubled by the use of suitable horizontal and vertical fibers combination together with a suitable type of epoxy. The use of CFRP plates on both bottom and sides of the beam exhibited a greater response compared to beam with CFRP plates only at the bottom of the beam.

An investigation conducted by (Alagusundaramoorthy et al., 2003) to study the flexural behaviour of RC beams strengthened with CFRP sheets or fabric. The main objective of this investigation was to study the effectiveness of externally bonded CFRP sheets or carbon fiber fabric in increasing the flexural strength of concrete beams. In order to achieve their objectives, several tasks were accomplished which include (1) flexural testing of concrete beams strengthened with different layouts of CFRP sheets or carbon fiber fabric; (2) calculating the effect of different layouts of CFRP sheets or carbon fiber fabric on the flexural strength; (3) evaluating the failure modes; (4) developing an analytical procedure to calculate the flexural strength of concrete beams strengthened with FRP composites; and (5) comparing the analytical calculations with experimental results. A total of nine (9) concrete beams strengthened with different layouts of CFRP sheets and carbon fiber fabric and another three beams with different layouts of anchored CFRP sheets were tested up to failure under four point loading.

The CFRP sheets or carbon fiber fabric were externally bonded to the tensile face of the beam. Two types of pultruded CFRP sheets were used which are (1) 76 mm width and 1.40 mm thick; and (2) 102 mm in width and 4.78 mm thick. As for the carbon fiber fabric, it was a stitched unidirectional cloth in the size of 203 mm width and 0.18 mm thick. The dimension of all beam specimens was kept constant with 230 mm x 380 mm with a length of 4880 mm. Also, an analytical investigation based on compatibility of deformations and equilibrium of forces was presented to predict the flexural behaviour of beams strengthened with CFRP sheets and carbon fiber fabric. The test results indicated that the flexural strength of the concrete beams strengthened with CFRP sheets was increased up to 49% while the flexural strength of concrete beams strengthened with anchored CFRP sheets and carbon fiber fabric was increased up to 58% and 40%, respectively. The authors recommended the prediction of the exact behaviour of beams bonded with CFRP sheets and carbon fiber fabric to be conducted using FE analysis.

Flexural strengthening of sixteen (16) RC continuous beams with different arrangements of internal steel bars and external CFRP laminates were assessed (Ashour et al., 2004). The beams were tested to failure. All the beam specimens had the same geometrical dimensions and were divided into three groups based on the amount of internal steel reinforcement. An un-strengthened control beam was located in each group designed to fail in flexure. The variable used in the experiment including the length, thickness, position, and form of the CFRP laminates. In addition, a simple method was developed to predict the flexural load capacity of the tested beams. It was found that all strengthened beams exhibited a higher beam loading capacity but showed lower in ductility compared with their respective un-strengthened control beams. Based on results obtained, three failure modes of beams with external CFRP laminates were identified namely laminate rupture, laminate separation and peeling failure of the concrete cover attached to the laminate. It was observed that the dominant failure mode of the strengthened beams was due to brittle peeling failure of the concrete cover adjacent to the CFRP sheets. Furthermore, the increase of CFRP sheet length to cover the whole negative or positive moment region did not prevent peeling failure of the CFRP laminate and the ineffectiveness was proven when the failure mode of the CFRP sheets was due to tensile rupture. In a continuous beam, it was found that the enhancement of bending moment capacity due to external strengthening was higher than the load capacity, unlike the simply supported beams.

The research by (Kotynia et al., 2008) was based on experimental and numerical investigations of RC beams strengthened in flexure with various externally bonded CFRP configurations. The purpose of the experimental study was to investigate the parameters that may delay the intermediate crack debonding of the bottom CFRP laminate, and increase the load carrying capacity and CFRP strength utilization ratio. A total of ten (10) rectangular RC specimens with a clear span of 4.2 m grouped in two series were tested to assess the effect of using the additional U-shaped CFRP systems on the intermediate crack debonding of the bottom laminate. In this study, two different strengthening configurations were used, namely continuous U-shaped wet layup sheets and spaced side-bonded CFRP L-shaped laminates. A numerical investigation was carried out using an incremental nonlinear displacement-controlled 3D FE model to investigate the flexural and CFRP/concrete interfacial responses of the tested beams. The authors found that the mode of failure of the tested beams was characterized by intermediate crack debonding of the bottom FRP flexural strengthening reinforcement. It was observed that the width of the flexural CFRP laminates portrayed a significant effect on the debonding mechanism. When using narrow laminates, the debonding plane occurred a few mm inside the thin concrete cover. While in the case of wide laminates, the debonding plane was observed inside the concrete cover, along the steel reinforcement. The results showed that an additional transverse FRP continuous U-wrap system with the fiber direction parallel to the beam axis increased the ultimate load carrying capacity. This was generally due to the flexural contribution of the additional CFRP reinforcement. In contrast, not extending the length of the U-shaped distance to cover the ends of the laminates causes limited effectiveness of the anchorage technique as well as the ultimate load capacity. The use of FE analysis is capable of predicting the experimentally observed CFRP debonding mode of failure i.e. intermediate crack debonding.

2.9.2.2 Shear Strengthening

Shear failure of concrete structures is catastrophic due to the brittle nature leading to failure without warning. Thus, existing RC structures that are found to be deficient in shear strength need to be repaired. Deficiencies may happen because of insufficient shear reinforcement, reduction in steel area due to corrosion, increased imposed load due to design or construction errors. Studies on the use of FRP materials to strengthen shear deficient structural members have been limited compared to the studies of flexural performance. This section contains some of the published research studies regarding the shear strengthening of RC structures with external bonded FRP reinforcement.

The work of (Chajes et al., 1995) dealt with shear strengthening of RC beams using externally applied composite fabric. Test was conducted on twelve (12) under-RC T-beams to study the effectiveness of using externally applied composite fabric to increase the shear capacity of a beam. The types of fiber used in the study were aramid, glass and carbon fiber. The fiber orientation used was 0°/90° and 45°/135°. The results showed that a substantial increase in ultimate load capacity was observed in all externally wrapped beams. The averaged increase in strength for beams with external reinforcement ranged from 83 to 125 percent was noted. In this investigation, the contribution of FRP to shear strength was modelled similar to steel stirrups contribution. An assumption was made in the analysis by limiting FRP strain, which was nearly 0.005 determined from the tests. Also, it was found that the orientation of fibers influences the shear strength contribution.

An experimental investigation was carried out to determine the response of RC beams strengthened in shear using unidirectional carbon fiber plastic strips (Chaallal et al., 1998). Eight (8) RC beams with the dimension of 150 mm x 250 mm x 1300 mm were categorized into three series. Two beams in the first series were designed at full strength in shear, two beams in the second series were under-reinforced in shear and the remaining four beams in the third series were strengthened in shear using externally bonded CFRP strips. Two beams were applied with CFRP strips being placed at 90° and 135° to the beam's longitudinal axis, respectively. The beams with a cleared span of 1200 mm were tested under a four point flexural bending test. Results showed that diagonal strips (135°) were slightly more efficient and exhibited a higher stiffness compared to vertical strips (90°). The author concluded that strengthening and upgrading of beam shear strength with CFRP side strips significantly increased the shear strength and stiffness by considerably reducing shear cracking. Although diagonal side strips demonstrated better performance than vertical side strips in terms of crack propagation, stiffness and shear strength, however they caused premature failure due to concrete peel-off at a strip curtailment especially in tension stressed zones.

Another research effort by Khalifa et al., 1999 presented the response of continuous RC beams with shear deficiencies, strengthened with externally bonded CFRP sheets. The experimental studies involved nine (9) full-scale, two (2) span continuous beams with rectangular cross section. The rectangular cross section of the beam was 150 mm x 305 mm x 4880 mm. The beams were categorized into three series. Three beams in each series contained a reference beam. The remaining beams were strengthened with CFRP sheets using different schemes. Each series had different longitudinal and transverse steel reinforcement ratios. The test parameters in this study included the amount of steel shear reinforcement, amount of CFRP, wrapping schemes, and 90°/0° ply combination. The results of various strengthening systems were discussed. Beam with CFRP at 90°/0° orientation and CFRP strips showed 22% and 83% increased in shear strength respectively, over the reference beam. Meanwhile, beam with CFRP continuous U-wrap failed by CFRP debonding but showed 135% increased in shear strength. Another strengthening system with continuous U-wrap oriented at 90° caused a changed in the final failure mode from shear to flexure. Khalifa et al concluded that externally bonded CFRP sheets can be utilized to enhance the shear capacity of the beams in positive and negative moment zones. The results of the tested beams showed an increased in shear strength from 22 to 135%. The test results signified that CFRP strengthening could improve beams without stirrups than beams with sufficient steel shear reinforcement.

An investigation to study the shear performance of RC beams with T-section was performed by Khalifa & Nanni, 2000. The externally bonded CFRP sheets were applied onto RC beams with different configurations to strengthen in shear. The experimental study included the test of six (6) full scale T-section RC beams with shear deficiencies. The test parameters in this investigation included wrapping schemes, amount of CFRP, 90°/0° ply combination and CFRP end anchorage. Two types of CFRP amount and distribution were compared, namely continuous sheets versus series of strips. In terms of bonded surface, two sides versus U-wrapped were compared whereas in fiber direction combination, 90°-0° versus 90° direction were compared. As for the end anchorage, U-wrap without end anchor versus with end anchor was compared. The beams were reinforced with longitudinal steel reinforcement without steel shear reinforcement in the test zone to ease shear failure. The results showed that strengthening of beam with CFRP U-wraps resulted in a 72% increase in the shear capacity. However, a significant increase in the shear capacity was observed when U-anchors were used. The failure mode at ultimate whereby the initial failure was CFRP debonding became failure in flexural. The load carrying capacity of CFRP anchored U-wrap was 442 kN with 145% and 42% increments over the reference beam and beam with CFRP U-wrap. Hence, this indicates that CFRP U-wrap end anchorage exhibited more stiffness and ductility than CFRP U-wrap without anchorage. Khalifa and Nanni concluded that externally bonded CFRP reinforcement can be used to restore and enhance the shear capacity of beams. The test results of all beams in the experimental study showed an increase in shear strength of 35-145%.

Eleven (11) RC beams were tested (Zhang & Hsu, 2005) to study the behaviour of shear strengthening with externally bonded CFRP laminates as external reinforcement. The external reinforcement was applied on both sides of the beam at various orientations. Two types of CFRP reinforcement were used including unidirectional CFRP strips and a CFRP fabric. In this study, no internal steel shear reinforcements were used in all beams. This is to evaluate the effectiveness of externally bonded CFRP in shear contribution. The test performed in the study shows the viability of using externally bonded CFRP systems to strengthen and increase the load carrying capacity in shear of RC beams. Due to the CFRP system, the serviceability, ductility and ultimate shear capacity of a beam are greatly increased provided that a suitable strengthening configuration is used. It was observed that the failure mode of the CFRP strips was caused by concrete delamination beneath the epoxy while the failure of CFRP fabrics was due to rupture of fiber. As a result, CFRP strips could significantly increase the shear strength of a beam compared to CFRP fabrics. Furthermore, CFRP diagonal side strips at 45°/135° orientation provides higher shear strength compared to vertical side strips.

2.9.3 Summary

The following remarks are drawn from this section:

- Various investigations (experimental and analytical) have been conducted in the area of flexural strengthening of RC solid beams using FRP materials by bonding it at the tensile face of the concrete; however the study of shear strengthening of solid beams with FRP materials is rather limited.
- Strengthening and upgrading of beam shear strength with CFRP side or diagonal strips significantly increased the shear strength and stiffness by considerably reducing shear cracking. In the case of CFRP wrapping, CFRP U-wraps resulted in a 72% increase in the shear capacity. Very little investigations on the effective strengthening configurations and/or effective strengthening systems are studied.

2.10 Strengthening of RC Beams with Openings by CFRP Composites

Numerous investigations were conducted to study the use of CFRP materials strengthening various types of structural members especially in solid beams. Recently, only a few literatures were found related to the study of beam strengthening with the presence of openings. Following an intensive literature review, a few publications on RC beams with openings strengthened using FRP materials have been found (Mansur et al., 1999; Abdalla et al., 2003; Allam, 2005; El Maaddawy & Sherif, 2009; Madkour, 2009; Pimanmas, 2010). The investigations were conducted by experiments supported by theoretical analysis and experiments validated with non-linear FE analysis. The authors have proved that FRPs are an effective strengthening material for strengthening RC beams with openings. CFRP shear strengthening around the openings increased the beam strength and stiffness and reduced the deflection.

2.10.1 Experimental Investigation

The literature reviews presented in this section are mainly experimental based studies.

2.10.1.1 Mansur et al. (1999)

This work involved testing a total of nine (9) prototype T-beams simulating the conditions that exist in the negative moment region of a continuous beam. The openings provided were circular in shape. The openings can be easily created in an existing beam without affecting the integrity of the surrounding concrete by using a coring machine. The major parameters considered in the study were the size and location of openings. One of the strengthening methods used in the study was external strengthening using FRP plates in the form of a truss around the position of the opening in an attempt to restore the original response. To prevent premature debonding, the three diagonal plates on each face were anchored by two horizontal plates with an expansion bolt at each intersection.

The results typically revealed that when an opening created near the support region of an existing beams leads to early diagonal cracking and significantly reduces the strength and stiffness of the beam. The results show that the weakness introduced in terms of cracking, deflection, and ultimate strength by creating an opening in existing beams can be completely eliminated by strengthening the opening region of the beam using FRP plates.

Another beam was strengthened by externally bonded FRP plates in order to restore the beam original response. The FRP plates used were with a thickness of 1.2 mm and a width of 50 mm bonded on both sides of the web using a recommended adhesive mortar. The arrangements of the FRP plates are shown Figure 2.21 in which the three diagonal plates on each face were anchored by two horizontal plates with an expansion bolt at each intersection to prevent premature debonding. The study reveals that strengthening by externally bonded FRP plates can completely eliminate the weakness introduced by creating an opening in an already constructed beam.

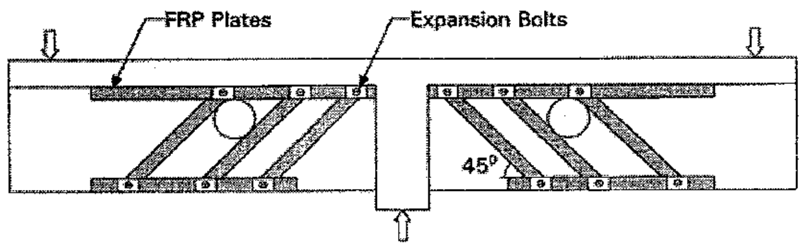

Figure 2.21 FRP arrangements in a T-beam (Mansur et. al., 1999)

2.10.2 Experimental and Theoretical Investigation

The following literatures are based on experimental study and theoretical analysis.

2.10.2.1 Abdalla et al. (2003)

This work involved an experimental program to study the usage of FRP sheets as a strengthening technique to substitute the expected reduction in beam strength due to the presence of opening. A total of ten (10) beams were tested and used to evaluate the efficiency of using CFRP sheets to strengthen the opening region as to control local cracks around openings and to resist excessive shear stresses in the opening chords. The tests were conducted on RC beams with openings in the shear zone. The design parameters are varied including opening width and depth, and the amount and configuration of the FRP sheets in the vicinity of the opening, as shown in Figure 2.22. The beams with 100 mm x 250 mm cross section and 2000 mm clear span were simply supported and subjected to two concentrated static loads. The beams were tested under two points loading to investigate their structural behaviour. Openings in all the tested beams were placed 200 mm away from support. The effect of the strengthening technique on deflection, strain, cracking and ultimate load was investigated.

Analytical procedures are developed to predict and design against the several types of cracking that are likely to occur in simply supported RC beams with rectangular openings. The effect of the amount and arrangement of the FRP reinforcement around the opening was studied. The ultimate shear capacities of the tested beams with strengthened openings were compared to those estimated using different models available for shear strengthening.

Results show that the presence of an un-strengthened opening in the shear zone of a RC beam significantly decreases its ultimate capacity. An un-strengthened opening with the height of 0.6 that of the beam depth may reduce the beam capacity by 75%. Meanwhile, the application of CFRP sheets according to the arrangement presented greatly decreases the beam deflection, controls cracks around opening, and increases the ultimate capacity of the beam. The usage of FRP sheets to strengthen the area around openings may retrieve the full capacity of the beam for relatively small openings. It is reported that the shear failure at the opening chords of strengthened openings occurs due to a combination of shear cracking of concrete and bond failure of the FRP sheets glued to the concrete. A conservative design method based on shear strengthening models available in the literature was presented in the research. The authors revealed that this method can be used to estimate the shear capacity of RC beams having CFRP strengthened the openings.

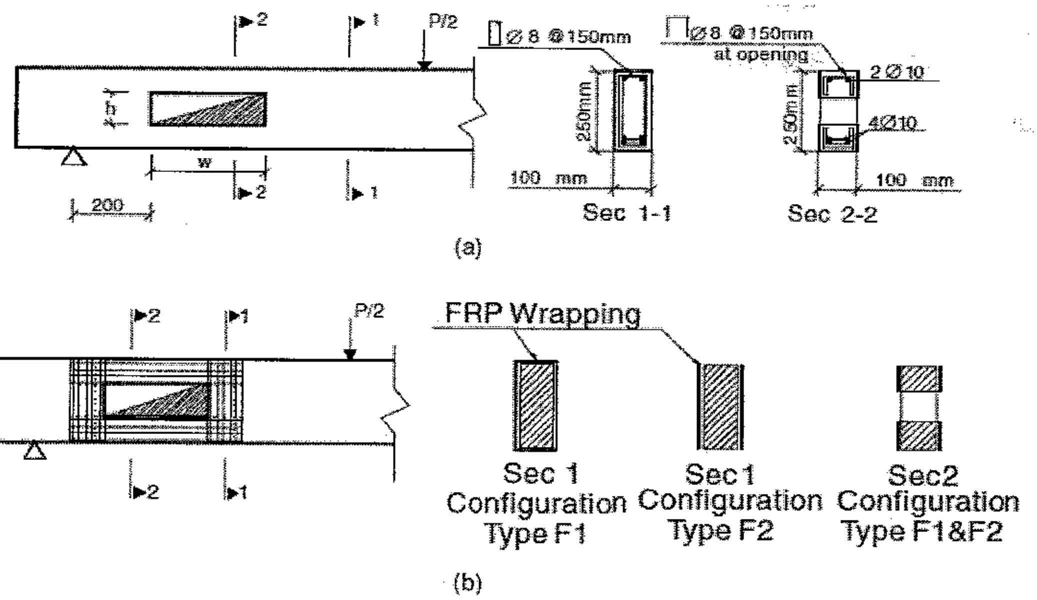

Figure 2.22 Details of the tested beams (a) internal steel reinforcement and (b) types of external CFRP strengthening (Abdalla et. al., 2003)

2.10.2.2 Allam (2005)

In this work, an experimental study was conducted on nine (9) RC simply-supported beams in order to investigate the efficiency of external strengthening of RC beams provided with large openings within the shear zone. All beams in the experimental study were tested to failure under two concentrated loads. The beams were provided with one rectangular opening with a cross section of 150 mm width and 400 mm height with a total length of 3200 mm and a clear span of 3000 mm. The length of the opening was 450 mm and its height was 150 mm. The openings were located within the shear zone of the beams starting at a distance of 300 mm from the support.

A total of six (6) beams were strengthened externally using steel plates or CFRP sheets along the opening edges. Both type of material used for strengthening and its configuration scheme significantly affects the efficiency of strengthening in terms of beam deflection, steel strain, cracking, ultimate capacity and failure mode of the beam. It was reported that the efficiency of external strengthening of beams with openings increased significantly when strengthening was applied to both inside and outside edges of the beam opening than that in the case of strengthening the outside edges only. External strengthening of beam opening using steel plates or CFRP sheets is more efficient than internal strengthening of the opening using internal steel reinforcement. Figures 2.23 and 2.24 show the strengthening schemes used for the tested beams.

Furthermore, theoretical analysis was performed for all tested beams with openings in order to calculate the ultimate shear force carried by such beams. The theoretical analysis was conducted using equations presented by Egyptian code in addition to empirical formulas found in the literature. The theoretical analysis of the tested beams was reliable since the theoretical results were in good agreement with the experimental results.

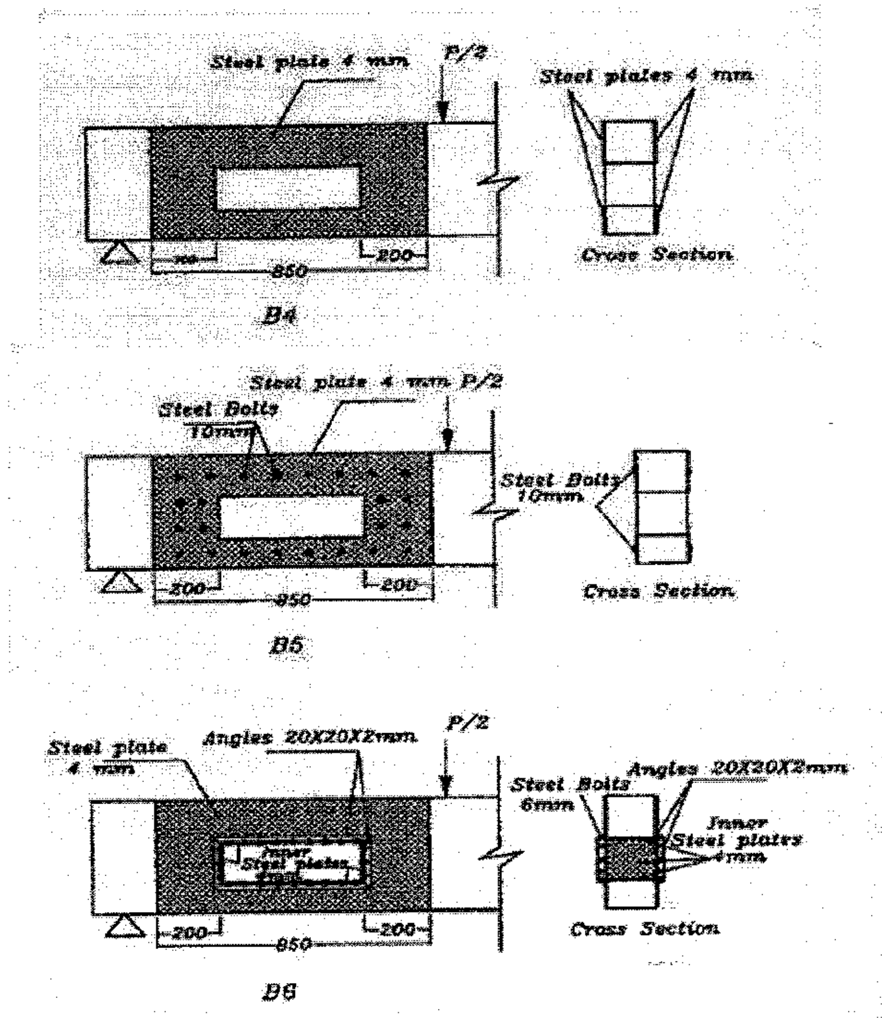

Figure 2.23 External strengthening schemes used for tested beams (Allam, 2005)

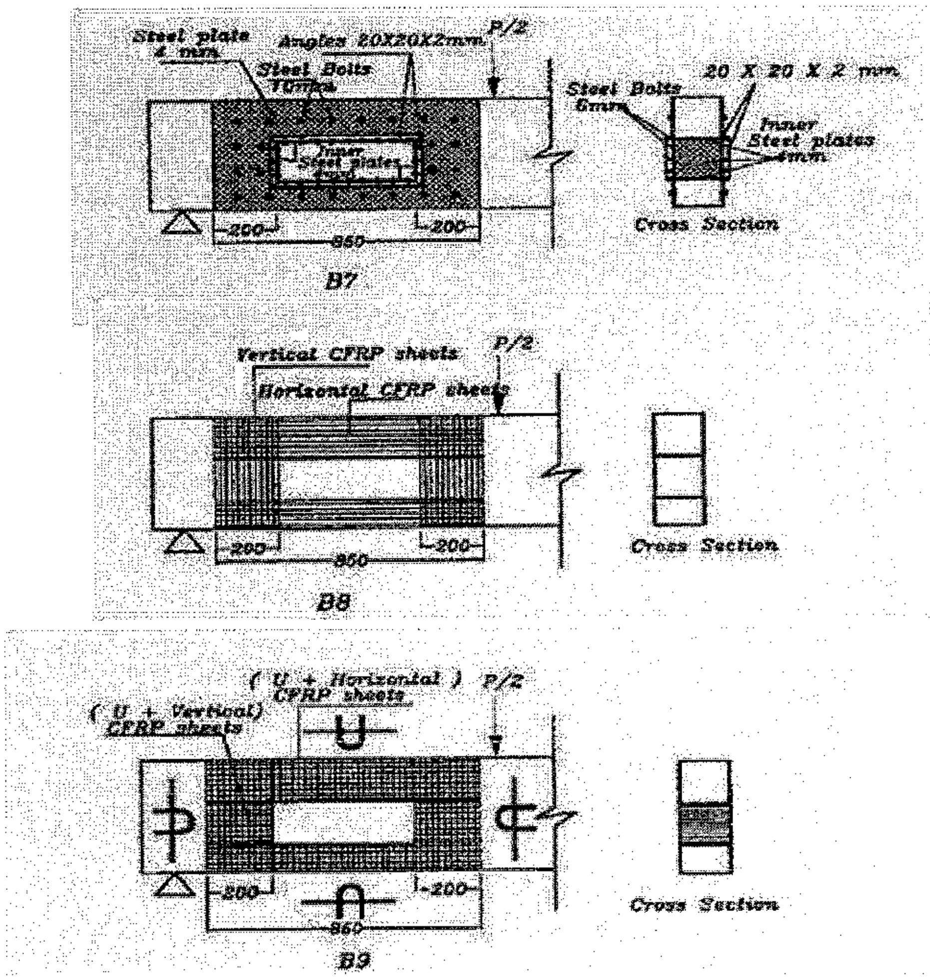

Figure 2.24 External strengthening schemes used for tested beams (Cont') (Allam, 2005)

2.10.2.3 El Maadawy and Sherif (2009)

This work involved examining the potential use of externally bonded CFRP composite sheets as a strengthening solution to upgrade RC deep beams with openings. The program involved testing a total of thirteen (13) deep beams with openings under four points loading. The deep beam was in the dimension of 80 x 500 x 1200 mm with an effective span of 1000 mm and a shear span of 400 mm. All specimens had two square openings, one in each shear span, placed symmetrically about the mid-point of the beam. The test parameters included the opening size, location and the presence of the CFRP sheets. The opening size was either 150 x 150 mm, 200 x 200 mm, or 250 x 250 mm which corresponded to opening height-to-depth (a/h) ratios of 0.3, 0.4 and 0.5, respectively.

CFRP shear strengthening around the opening of RC deep beams remarkably increased the beam strength and beam stiffness when the opening was located at the mid-point of the shear span. The strength gain due to the CFRP sheets was in the range of 35 - 73%. A method of analysis for shear strength prediction of RC deep beams containing openings strengthened with CFRP sheets was studied and examined against test results. The analytical results were compared with experimental results and showed that the analytical procedure can give reasonable prediction for the shear strength of RC deep beams with openings shear strengthened with CFRP sheets.

2.10.3 Experimental and Numerical Investigation

The studies presented herein were conducted for both experimental and numerical analysis i.e., FEM.

2.10.3.1 Pimanmas (2010)

The experimental program was conducted to study the strengthening of RC beams with opening using FRP rods. The study was performed on thirteen (13) RC beams with circular and square openings. The opening is provided to significantly reduce the shear capacity of the beam. Two pattern of strengthening were studied: (i) to place FRP rods enclosing the opening and (ii) to place FRP rods diagonally throughout the entire depth of the beam, as illustrated in Figure 2.25. The circular opening had the diameter of 150 mm and the square opening was 150 mm x 150 mm in size. The opening was located at 525 mm from the support position, which was exactly at the center of the shear span. The dimension of the beam was 160 mm x 400 mm with a clear span of 2100 mm. All the beams were monotonically loaded under three points loading. A nonlinear FE analysis based on smeared crack approach was applied. The FEM was to introduce an analytical modeling of the problem to serve as a numerical platform for performance check of strengthened specimens. It is also used to explore the behaviour of specimens that were neither tested nor obtained from the experiment.

It was revealed that openings fabricated in the beam may seriously decrease the shear capacity of the member and changes the failure mode from flexural yielding to brittle shear failure. Strengthening by placing FRP rods around the opening was not fully effective due to propagation of diagonal crack through the beam with the crack pattern diverted to avoid intersecting with the FRP rod. While FRP rods are placed throughout the entire beam's depth, a significant improvement in loading capacity and ductility was achieved. The beams behaviour of circular and square opening is the same, except that the square opening tends to yield lower performance compared with the circular one. The FE analysis with RC planar element is able to simulate all salient behaviours of the beams with opening and strengthened beams.

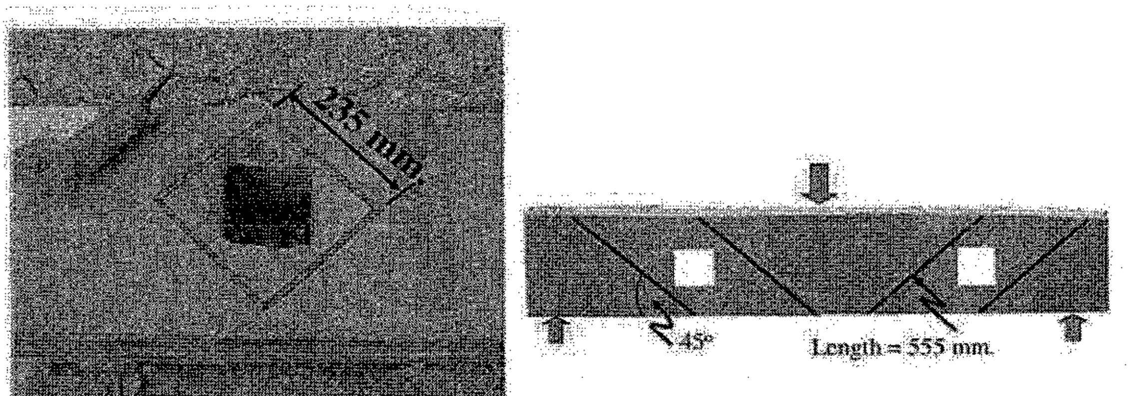

(a) Beam R-Rod1-s1 (b) Beam R-Rod2-s1

Figure 2.25 Strengthening patterns of FRP rods (Pimanmas, 2010)

2.10.4 Numerical Investigation

A study based on only numerical investigation using FEM is presented in the following sub-section.

2.10.4.1 Madkour (2009)

This literature intends to clarify the non-linear behaviour of strengthened RC beams with rectangular web openings. The non-linear behaviour was investigated by introducing a new numerical implementation of damage-non-linear elastic theory. The proposed theoretical approach analyzed the efficiency of applying CFRP laminates as an external strengthening technique in a 3D domain to determine the effective and economic strengthening configuration. The investigation was mainly focused on explaining the computational algorithm used in the non-linear analysis. The investigated parameters include the opening height and the strengthening configurations using CFRP in the vicinity of the web opening. The rectangular opening was located at each shear span near to the support. The numerical investigations have simulated 17 RC beams with web opening and the results were compared with the available experimental data in the literature.

It is reported that strengthening large web openings with CFRP laminates according to the configuration presented in this investigation controls cracks around opening, increases the ultimate capacity of the beam but shows slight influence on deflection. Utilizing CFRP laminates to strengthen the area around the openings for the investigated beams with large opening resulted in about 30% increase in the failure load which is in good agreement with the experimental results available in the literature. This increase is dependent on various factors including dimensions, reinforcement ratio, type, size, location and orientation of CFRP laminates.

The theoretical numerical approach can predict the failure mode, improve the design of external strengthening and predict strengths quite accurately. The modes of failure and strength predictions were compared with experimental measurements and the predictions are conservative and errors were acceptable. The strengthening systems applied in the current paper make the failure occur gradually and almost controls the sudden failure.

2.10.5 Summary

The following remarks are drawn from this section that may lead to the determination of gaps:

- The literatures presented herein revealed that very few investigations have dealt with the external strengthening of RC beams with large square and circular openings placed in the critical flexure and shear zones. Also, limited literatures available discussing on the various strengthening configurations and the effective use of CFRP materials.

- It is also found that the studies using numerical approach (FE analysis) are very limited to predict the behaviour of RC beams with openings in the experiment, as well as validating and comparing the results of the FE program to the experimental results.

2.11 Computer Simulation in Structural Analysis and Benefits

Computer simulation has become an important tool in the structure analysis and design with the development of mechanics and computer technology. Computer simulation also referred to as 'FEA'(FE Analysis), 'FEM' or computer analysis. It has been an important analysis tool since the development of FEM in 1960s (Zienkiewicz et al., 2005). Computer simulation now has evolved as a replacement of experimental research in some aspects, and helps to reduce the experimental work-load (Graybeal & Pooch, 1980).

Traditional testing usually involves the fabrication of costly prototypes, testing the specimens with expensive load frames, iterating the design according to the test results, and the process have to be repeated until acceptable results are achieved. Also, studying structures which are subjected to the effects of load disasters such as blast, penetration, impact of collapse or typhoon are difficult to be analyzed with the experimental testing. With computer simulation, the results of an experimental testing which are unable to be captured in the system can be analyzed on the computer with proper parameter and numerical model. Also, the results can be presented clearly with the computer graphic simulation.

The replacement of experimental works with computer simulation offers many advantages include safe, efficient and cheap. If possible, it is also wise to construct a minimum of one prototype and to conduct the testing work when an optimal design has been identified through the simulation process.

On the other hand, computer simulation is a relatively new and robust for checking the performance of concrete structures in design and development. This kind of simulation can be regarded as virtual testing and can be used to confirm and support the structural solutions with complex details or non-traditional problems.

Furthermore, it can serve to find and optimal and cost-effective design solution. Simulation is useful in cases where the code of practice provisions is not well covered. This application can also be used to assess the remaining structural capacity of existing structures and to investigate the causes of damage and failures. It can support the creativity of engineers and contribute to the safety and economy of designed structures (Cervenka, 1999).

In summary, computer simulation will benefit in the following ways:

- Time effectiveness;
- Lower prototyping and testing cost;
- Ability to quickly iterate on different design configurations;
- Simple acquisition of key data such as displacement and stresses;
- Safety.

2.11.1 General Methods of Simulation

There are three approaches to the simulation in structure analysis which include mechanics of material approach, the elasticity theory approach and the FE approach. The first two methods are based on analytical formulations which apply mostly to simple linear elastic models, lead to closed-form solutions which can be solved by hand. The FE approach is actually a numerical method for solving differential equations generated by theories of mechanics such as elasticity theory and strength of materials. The FE method needs the processing power of computer as it is applicable to structure of arbitrary size and complexity.

In the FE method, the mathematical problems can be solved by programming and software packages. In programming, the problems can be solved using programming languages which have strong ability in computation such as Fortran or C/C++ while the current structural analysis software such as common FEA software like ANSYS or SAP.

2.11.2 Finite Element Method (FEM)

The use of computer codes started in the late 1950s and early 1960s for solving structural analysis problems in an approach similar to the FEM started initially with the aircraft industry. The original researchers whom credited by many; Turner, Clough, Martin and Topp (Turner et al., 1956; Zienkiewicz et al., 2005) having established the method had published a paper in 1956. The researchers were mainly from the aircraft industry except Clough and yet he was the key person in the development of the method. Clough's contribution was more significant after his publication regarding 'FEM' in 1960.

Advancement in the modelling are constantly carried out as reported by (Zienkiewicz & Cheung, 1967; Ngo & Scordelis, 1967) and (Cervenka, 1970). The method has been develop to an advance level in the structural analysis with regards to concrete state, steel state, concrete-steel interactions and other important elemental components such as the representation of bond behaviour between concrete and steel.

2.11.2.1 Finite Element Analytical Models

The FE method is a general method of structural analysis in which the solution of a problem in continuum mechanics is approximated by the analysis of an assemblage of FEs which are interconnected at a finite number of nodal points and represent the solution domain of the problem. "The FE analysis of a problem is so systematic that it can be divided into a set of logical steps that can be implemented on a digital computer and can be utilized to solve a wide range of problems by merely changing the data input to the computer program." (Reddy, 1993). Some of the literatures presented herein are FE modelling of RC structures strengthened with FRP material.

RC beams strengthened externally with CFRP plates and sheets using a commercially available package (ABAQUS) based on a smeared cracking approach modelled by (Arduini et al., 1997). The beams strengthened with CFRP plates were analyzed using a two dimensional approach, while beams bonded with CFRP sheets were modelled in three dimensions. The FRP reinforcement was applied directly over the concrete elements with a perfect bond assumption. The authors reported that the results of the

FE analysis showed a good correlation with the experimental data. However, the FE analysis results were stiffer than the test results, as shown in Figure 2.26. This is due to the perfect bond assumption and the limited number of nodes that could be used. The FE analysis indicated that high stresses at the end of the FRP plate caused the delamination failure of the beam.

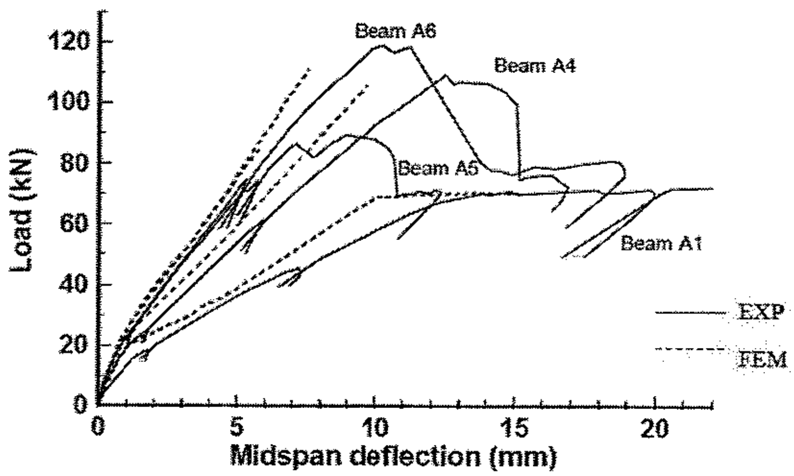

Figure 2.26 Comparison of experimental and FE results (Arduini et al., 1997)

A nonlinear 3D FEM program to model beams with short spans was performed by Zarnic et al., 1999. Each component of the beam consisting of concrete, steel reinforcement, epoxy and the CFRP plate were modelled, as illustrated in Figure 2.27. A fairly good agreement of numerical results with the measured response of the test beams for the ultimate loads was obtained, as shown in Figure 2.28. Beyond the former response, however, the post-cracking stiffness was higher than the test results.

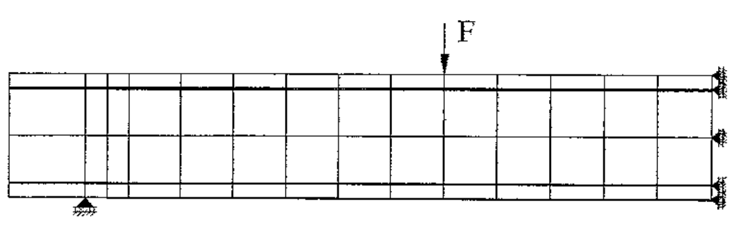

Figure 2.27 Finite element mesh of Zarnic et al. (1999)

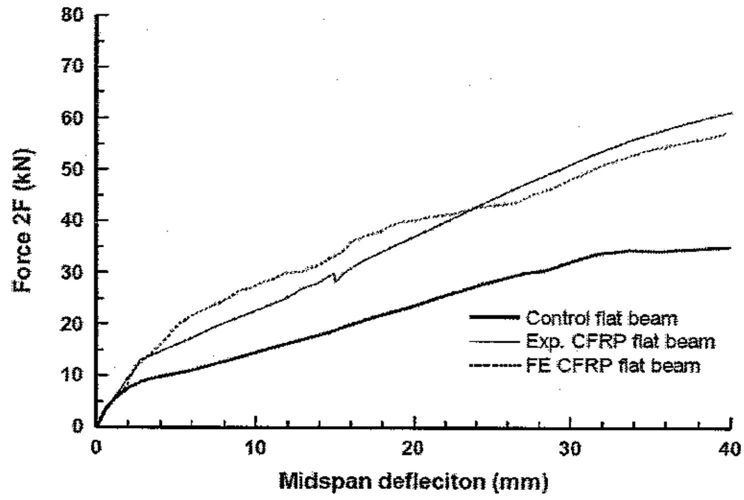

Figure 2.28 Finite element results of force versus midspan deflection (Zarnic et al.,1999)

LUSAS FE program was used to calculate the response of externally reinforced beams. A smeared crack model incorporating an isotropic damaged model to simulate the nonlinear behaviour of the concrete was adopted. To model the concrete, four-node or eight-node quadrilateral isoparametric elements were used, with the smeared reinforcement smeared onto concrete as two-or three-node bar elements. While for the strengthened beams, triangular elements were located in the transition zone to reduce the element size toward the bond region. The adhesive layer and FRP laminates were modelled with a row of four-or eight-node elements with the adhesive assumed to be elastic. It was found that the FE calculations were sensitive to concrete tensile strength with a value of 1.5 MPa that given the best agreement with the experimental load deflection response (for a concrete compressive strength between 54 and 69 MPa). Although the stiffness was slightly overestimated, but all calculated solutions for the beam strengths were within 20 percent of the test results (Rahimi & Hutchinson, 2001).

A nonlinear FE program, ADINA to model beams with or without FRP plates was investigated (Ross et al., 1999). Two dimensional, eight node plane stress elements were used to represent the concrete, and three node truss elements to represent the reinforcing steel and the FRP plates. A hypoelastic model was used for the concrete based on a uniaxial stress-strain relationship that accounts for biaxial and triaxial conditions. An elastic plastic response was used to represent the reinforcing steel and the CFRP was modelled as linear elastic until failure. The results of the FE analyses were compared to the experimental results and good agreement for the global behaviour was obtained. However, the failure mode was unable to be predicted due to the delamination of FRP plate. The results concluded that one of the most important factor affecting the beam behaviour was the bond strength between the concrete and FRP. To prevent debonding and to utilize the full capacity of the plate, the use of an anchorage system was suggested.

The response of RC beams with CFRP sheets bonded to the tensile face using a 2D nonlinear FE analysis was studied (Limam & Hamlin, 1998). To represent the concrete, eight-node membrane elements were used, while for the steel and CFRP reinforcement, two-node truss elements were adopted. A perfect bond condition was assumed between the steel reinforcement and the concrete. Bond slip was taken into account at the concrete –FRP interface through the use of two-node continuous contact elements, as illustrated in Figure 2.29. With a smeared crack approach, the concrete model was based on different yield surfaces in the tensile and compressive regions. The steel reinforcement was modelled using an elasto-plastic model with strain hardening. The results from experimental tests were utilized to define a constitutive law for the interface elements based on a Mohr-Coulomb failure criteria. Comparisons of numerical results with the experimental data showed that the ultimate load and deflections were within 10 percent of the measured values but were dependent on the modelling of the interface layer, as shown in Figure 2.30. The authors concluded that a non-realistic model for the interface leads to large discrepancies between the analytical and test results showing the importance of accurately modelling the concrete-CFRP interface.

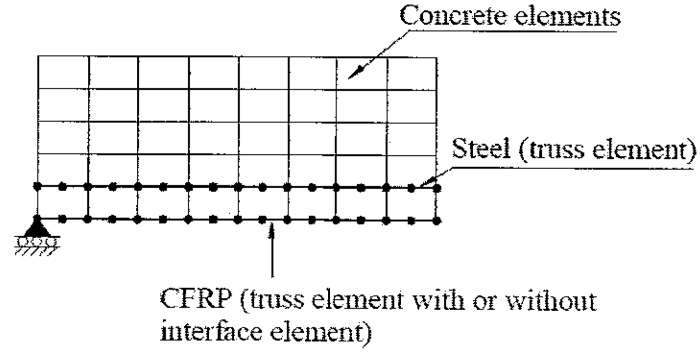

Figure 2.29 Finite element mesh of Limam and Hamelin (1998)

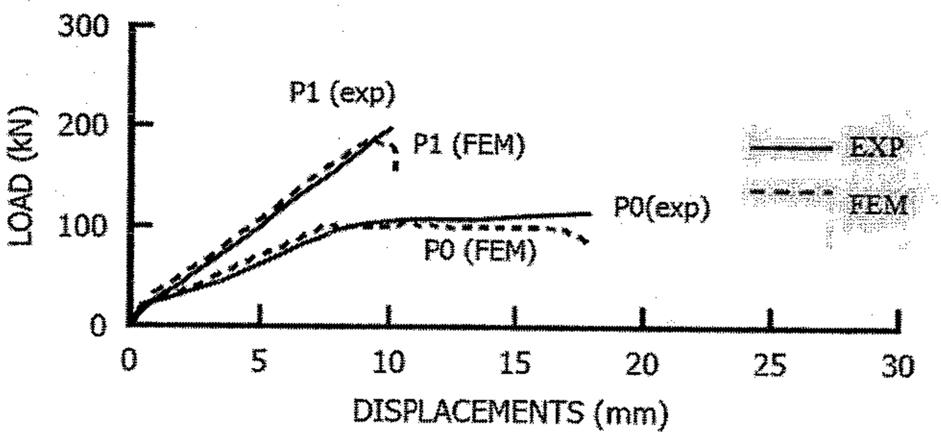

Figure 2.30 Comparison of FE results and experimental data (Limam and Hamelin, 1998)

2.11.3 Commercial Finite Element Program Packages

The first commercial FE software made its appearance in 1964 (Huebner et al., 2001). The general application of the FEM makes it a powerful and versatile tool for a wide range of problems. Due to this, a number of computer program packages have been developed for the solution of a variety of structural and solid mechanics problems.

Typical FE problems may consist of up to hundreds of thousands and even millions of elements and nodes and hence there are usually solved in practice using commercially available software packages. Currently, there is large number of commercial software packages available for solving various types of problems in structural analysis in which that the problems might be static, dynamic, linear and nonlinear. Most of the software packages use the FEM or are used in combining with other numerical methods (Liu & Quek, 2003). Table 2.1 lists some of the commercially available software packages that using the FEM.

Table 2.1 Commercially available software packages

Software packages	Method used	Application problems
ATENA	FEM	Structural analysis
ABAQUS	FEM	Structural analysis
I-deas	FEM	Structural analysis
LS-DYNA	FEM	Structural dynamics
NASTRAN	FEM	Structural analysis
MARC	FEM	Structural analysis
ANSYS	FEM	Structural analysis
ADINA DIANA	FEM	Structural analysis

The choice of selecting the suitable FE software involves a complex set of criteria which include analysis versatility, ease of use, efficiency, cost, technical support and training.

2.11.4 Summary

The following remarks are drawn from the previous section:

- As reported in the past literatures, mathematical problems in the FEM were solved initially by using programming languages and eventually the use of commercial available software packages are currently evolving in the research community.
- The investigations conducted using the software packages to study the strengthening of solid RC beams (without opening) with FRP materials are mainly in 2D and 3D approaches.
- From the available software packages, ATENA, a non-linear FE program is used in this research study to analyze the behaviour of RC structures with opening.

2.12 ATENA

ATENA is a commercial FE software package for nonlinear simulation of concrete and RC structures. Based on advanced material models, it can be used for realistic simulation of structural response and behaviour.

ATENA offers a user-friendly graphical interface which enables efficient solving of engineering problems including anchoring technology and reinforcing of concrete. Native ATENA GUI is available for 2D and rotationally symmetrical problems. It supports the user during pre-and post-processing, and enables real-time graphical tracing and control during the analysis. ATENA pre-processing includes an automatic meshing procedure, which generates Q10, isoparametric quadrilateral and triangular elements (Cervenka et al., 2002).

For the reinforcement in ATENA, it can be treated as smeared reinforcement, reinforcing bars or prestressing cables. The discrete reinforcement is independent on the FE mesh. Graphical post-processing can show cracks in concrete, with their thickness, shear and residual normal stresses. User defined crack filter is available for obtaining of realistic crack patterns. Other important values which include i.e. strains, stresses, deflection, forces, reactions, etc. can be represented graphically as rendered areas, isoareas, and isolines in the form of vector or tensor error fields. All values can be obtained in well-arranged numerical form.

ATENA enables loading of the structure with various actions which include body forces, nodal or linear forces, supports, prescribed deformations, temperature, shrinkage and pre-stressing. These loading cases are combined into load steps, which are solved using advanced solution methods: Newton-Raphson, Modified Newton-Raphson or Arc-Length. The material stiffness like secant, tangential or elastic material stiffness can be employed in particular models. Line search method with optional parameters accelerates the convergence of solution, which is controlled by residual-based and energy-based criteria. (Cervenka et al., 2002). All of the described features support the user by engineering analysis of connections between steel and concrete and computer simulation of its behaviour.

2.12.1 Concrete Constitutive model in ATENA

The following aspects of concrete behaviour are all included in the software and are discussed in more detail subsequently. The aspects include:

- Nonlinear behaviour in compression including hardening and softening
- Fracture of concrete in tension based on the nonlinear fracture mechanics
- Biaxial strength failure criterion
- Reduction of compressive strength after cracking
- Tension stiffening effect
- Reduction of the shear stiffness after cracking (variable shear retention)
- Involved two crack models: fixed crack direction and rotated crack direction

In detail, the non-linear fracture mechanics and a crack band method that utilizes the smeared crack concept are combined in the tensile concrete behaviour. The cracks in concrete occur when major principal stress exceeds the tensile strength; after the crack initiation (controlled by a bi-axial failure envelope), the isotropic material formulation changes to an orthotropic one. The stress on softening curve is determined by the crack opening displacement, calculated from the inelastic cracking strains (Cervenka et al., 2010).

2.12.2 Concrete Stress-Strain Relations

Details of the theories for concrete stress-strain relations in ATENA are presented in the followings.

2.12.2.1 Equivalent Uniaxial Law

The equivalent uniaxial law is used to describe the nonlinear behaviour of concrete in the biaxial state in terms of the equivalent uniaxial strain, ε^{eq} and the effective stress σ_c^{ef}. The complete equivalent uniaxial stress-strain diagram for concrete is shown in Figure 2.31 and this is built into the commercial software.

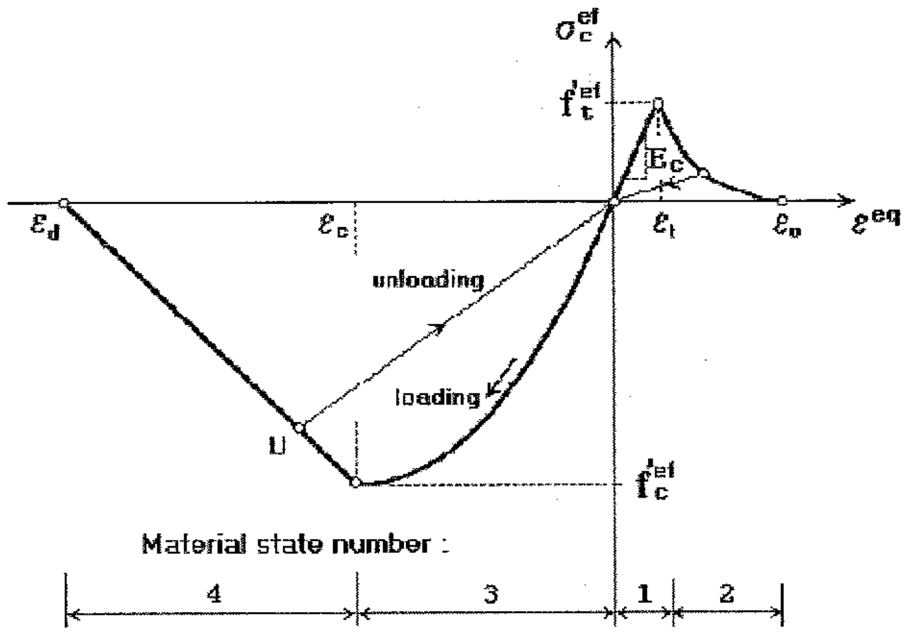

Figure 2.31 Uniaxial stress strain diagram for concrete (Cervenka et.al., 2010)

2.12.2.2 *Tension before Cracking*

Before cracking, the behaviour of concrete in tension is assumed linear elastic. The initial elastic modulus of concrete, E_c and the effective tensile strength, $f'_t{}^{ef}$ is derived from the biaxial failure function in Eq. (2.13) (Cervenka et al., 2010):

$$\sigma_c^{ef}=E_c\varepsilon^{eq},\ 0\leq\sigma_c\leq f'_t{}^{ef} \tag{2.13}$$

2.12.2.3 *Tension after Cracking*

After cracking, a fictitious model based on a crack opening law and fracture energy is used in combination with the crack band theory (Cervenka et al., 2010; Hordijk, 1991). There are a total of five softening laws in SBeta material model. In this study, exponential crack opening law is adopted and reported. The function of the crack opening law is given in Eq. (2.14):

1. Exponential crack opening law

Figure 2.32 shows the exponential crack opening law.

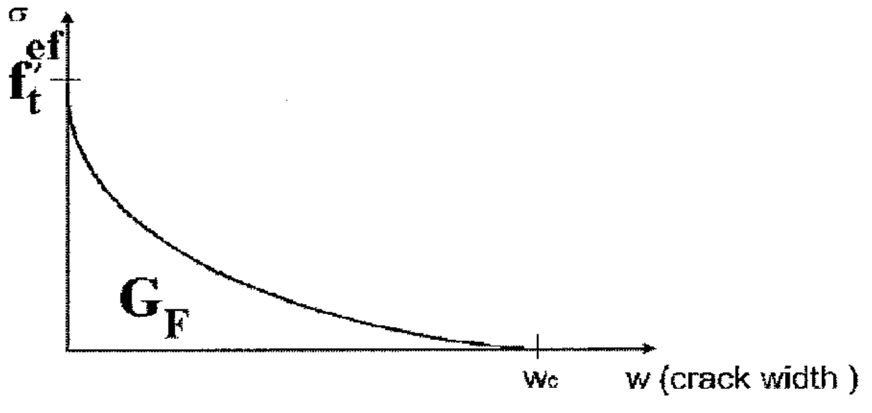

Figure 2.32 Exponential crack opening law (Cervenka et al., 2010)

$$\frac{\sigma}{f_t^{'ef}} = \left\{1 + \left(c_1 \frac{w}{w_c}\right)^3\right\} \exp\left(-c_2 \frac{w}{w_c}\right) - \frac{w}{w_c}(1+c_1^3)\exp(-c_2),$$

$$c_1 = 3;\ c_2 = 6.93;\ w_c = 5.14\left(\frac{G_f}{f_t^{'ef}}\right) \qquad (2.14)$$

Where w is the crack width; w_c is the crack width at the complete release of stress; σ is the normal stress in the crack (crack cohesion). G_f is the fracture energy needed to create a unit area of stress-free crack, $f_t^{'ef}$ is the effective tensile strength derived from the failure function. The crack opening displacement, w is derived from strains according to the crack band theory.

2.12.2.4 Compressive before Peak Stress

The compressive stress-strain curve for concrete is shown in Figure 2.33. The built-in model in ATENA, the CEB-FIP model is used for the ascending branch of the concrete stress-strain law in compression. Eq. (2.15) enables a wide range of curve forms, from linear to curved, which is appropriate for normal as well as high strength concrete in compression:

$$\sigma_c^{ef} = f_c^{'ef}\frac{kx - x^2}{1+(k-2)x};\ x = \frac{\varepsilon}{\varepsilon_c};\ k = \frac{E_o}{E_c} \qquad (2.15)$$

Where:

σ_c^{ef} = concrete compressive stress,

$f_c^{`ef}$ = concrete effective compressive strength

x = normalized strain,

ε = strain,

ε_c = strain at the peak stress, $f_c^{'ef}$,

k = shape perimeter (k = 1 linear, k = 2 parabola)

E_o = initial elastic modulus

E_c = secant elastic modulus at the peak stress, $E_c = f_c^{'ef} / \varepsilon_c$

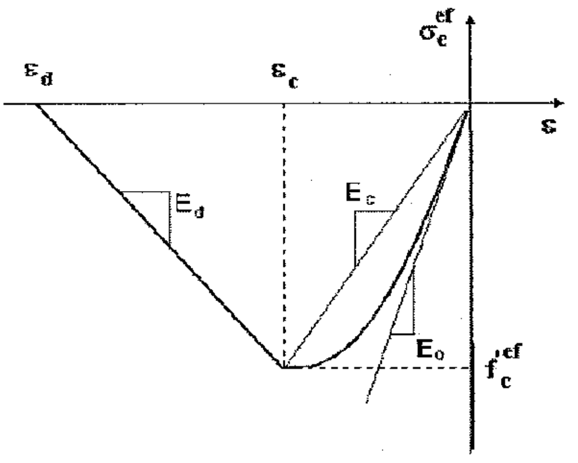

Figure 2.33 Stress strain diagram in compression (Cervenka et. al., 2010)

2.12.2.5 Compression after Peak Stress

A linear-descending model is utilized for the softening part of the stress-strain diagram in compression after the peak stress. Figure 2.34 shows the softening displacement in compression zone. One of the two models of strain softening in compression is adopted in which the model is based on dissipated energy.

1. **Fictitious compression plane model**

The fictitious compression plane model is based on dissipated energy. This model assumes that the compression failure is localized in a plane normal to the direction of comprehensive principal stress. All post-peak comprehensive displacements and energy dissipation are localized in this plane. This model is independent on the size of the structure in Eq. (2.16) (Vanmier, 1986; Cervenka et al., 2010):

$$\varepsilon = \varepsilon_c + \frac{w_d}{L'_d} \tag{2.16}$$

Where:

w_d = the plastic displacement at the end point of the softening curve

ε_d = limit compressive strain

L'_d = band size

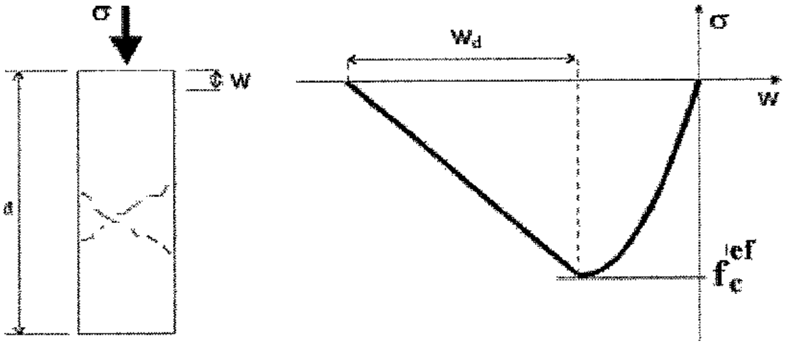

Figure 2.34 Softening displacement law in compression zone (Cervenka et. al. 2010)

2.12.3 Fracture Process

The crack formation process is divided into three stages. When the concrete is in the un-cracked stage, the principal tensile stress is less than the tensile strength $f_t^{'ef}$. The formation of crack starts in the process zone after reaching the tensile strength with a decrease in the tensile stress on the crack surface. The process zone is shown in Figure 2.35. In the last stage, cracks continue opening with no stresses after a complete release of stress.

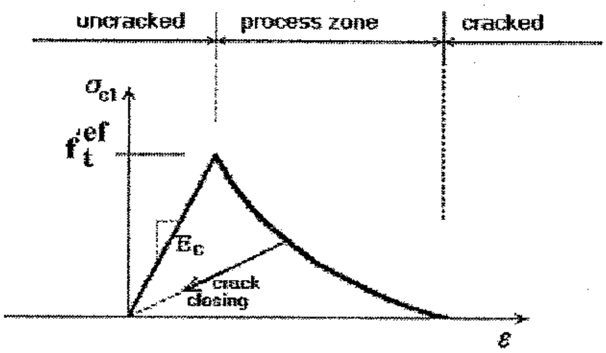

Figure 2.35 Stages of crack opening (Cervenka et. al., 2010)

2.12.4 Concrete Biaxial Stress

The biaxial stress of concrete is divided into compressive and tension failures as presented in the followings.

2.12.4.1 Compressive Failure

Figure 2.36 shows the concrete biaxial failure criterion according to (Kupfer et al., 1969). In the compression-compression zone, the state of stress failure is given in Eq. (2.17). In the tension-compression condition, the failure function is assumed to be linear, and stated in Eq. (2.18):

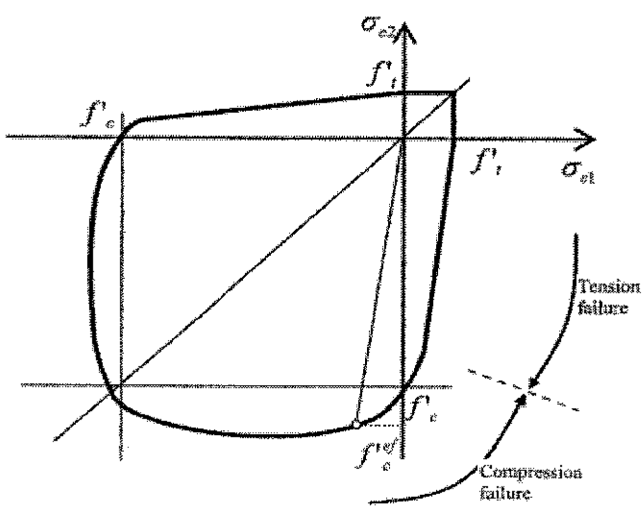

Figure 2.36 Biaxial failure criteria (Cervenka et. al., 2010)

$$f_c^{'ef} = \frac{1+3.65a}{(1+a)^2} f'_c, \; a = \frac{\sigma_{c1}}{\sigma_{c2}} \qquad (2.17)$$

$$f_c^{'ef} = f'_c \, r_{ec}, \; r_{ec} = \left(1+5.3278\frac{\sigma_{c1}}{f'_c}\right), \; 1.0 \geq r_{ec} \geq 0.9 \qquad (2.18)$$

Where σ_{c1}, σ_{c2} are the principal stresses in the concrete , f'_c is the uniaxial cylinder strength; r_{ec} is the reduction factor of the compressive strength in the principal direction 2 due to the tensile stress in the principal direction 1.

2.12.4.2 *Tension Failure*

In the tension-tension state, the tensile strength is constant and equal to the uniaxial tensile strength, f'_t. while in the tension-compression state, the tensile strength is reduced by the relation given in Eq. (2.19):

$$f_t^{'ef} = f'_t \, r_{et} \qquad (2.19)$$

Where r_{et} is the reduction factor of the tensile strength in the direction 1 due to the compressive stress in the direction 2.

2.12.5 Crack Model

Two smeared crack approaches for modeling of the cracks is available in ATENA, namely fixed crack model and rotated crack model (Cervenka et al., 2010). In both models, the crack is formed when the principal stress exceeds the tensile strength. It is assumed that the cracks are uniformly distributed within the material volume. This is reflected in the constitutive model by an introduction of orthotropy.

2.12.5.1 *Fixed Crack Model*

In the fixed crack model, (Cervenka, 1985; Darwin, 1974; Cervenka et al, 2010) the crack direction is given by the principal stress direction at the moment of the crack initiation. This direction is fixed during further loading and represents the material axis of the orthotropy.

The principal stress and strain directions coincide in the un-cracked concrete, because of the assumption of isotropy in the concrete component. After cracking, the orthotropy is introduced. The weak material axis m_1 is normal to the crack direction; the strong axis m_2 is parallel with the cracks. In a general case, the principal strain axes ε_1 and ε_2 rotate and need not to coincide with the axes of the orthotropy m_1 and m_2. This produces a shear stress on the crack face as shown in Figure 2.37. The stress components σc_1 and σc_2 denote respectively the stresses normal and parallel to the crack plane and due to shear stress, they are not the principal stresses.

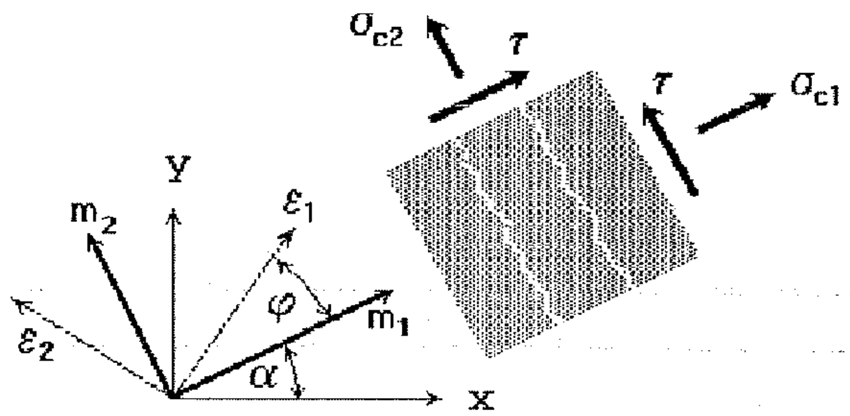

Figure 2.37 Fixed crack model (Stress and strain state)(Cervenka et.al. 2010)

2.12.5.2 Rotated Crack Model

For rotated crack model (Vecchio & Collins, 1986; Crisfield & Wills, 1989; Cervenka et al,. 2010), the direction of the principal stress coincides with the direction of the principal strain. Hence, no shear strain take place on the crack plane and only two normal stress components must be defined as shown in Figure 2.38. If the principal strain axes rotate during the loading, the direction of the cracks will also rotate. To ensure the co-axiality of the principal strain axes with the material axes, the tangent shear modulus G_t is calculated according to Crisfield (1989) as in Eq. (2.20):

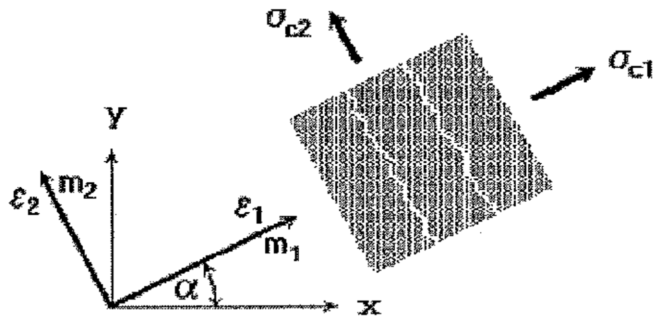

Figure 2.38 Rotated crack model. (Stress and strain state) (Cervenka et.al. 2010)

$$G_t = \frac{\sigma c_1 - \sigma c_2}{2(\varepsilon_1 - \varepsilon_2)} \tag{2.20}$$

2.12.6 Reinforcement Stress-Strain Laws

Reinforcement can be modelled in two different types, either discrete or smeared. Discrete reinforcement is in the form of reinforcing bars and is modeled by truss elements whereas smeared reinforcement is a component of composite material. It can be considered either as a single (only one constituent) material in the element under consideration or as one of the more such constituents.

2.12.6.1 Bilinear Law

The bilinear law, elastic-perfectly plastic, is assumed as shown in Figure 2.39. The initial elastic part has the elastic modulus of steel E_s. The second line represents the plasticity of the steel with hardening and its slope is the hardening modulus E_{sh}. In case of perfect plasticity, $E_{sh} = 0$. Limit strain ε_L represents limited ductility of the steel.

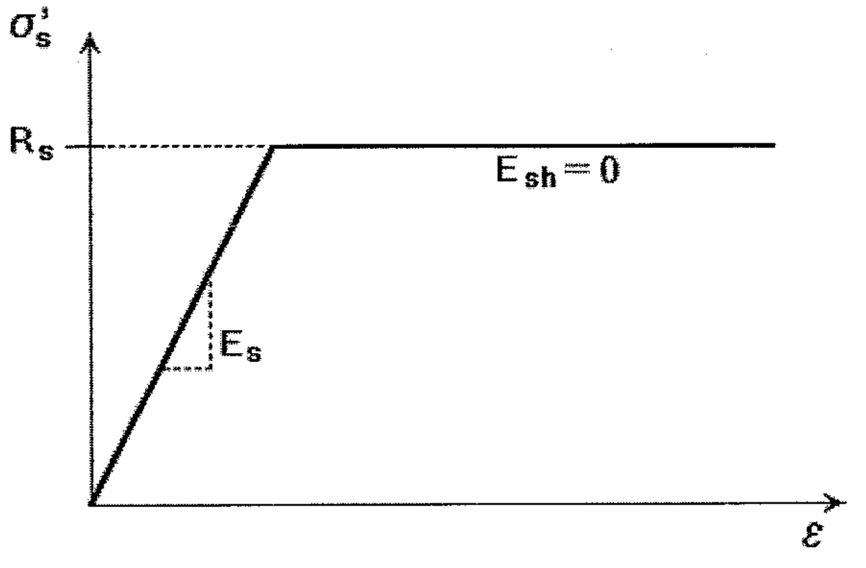

Figure 2.39 The bilinear stress-strain law for reinforcement (Cervenka et. al. 2010)

2.12.6.2 Multi-Linear Law

The multi-linear law is consisting of four lines as shown in Figure 2.40. This law allows to model all four stages of steel behaviour namely elastic state, yield plateau, hardening and fracture. This line is defined by four points, which can be specified by input. This stress-strain law can be used for the discrete and smeared reinforcement.

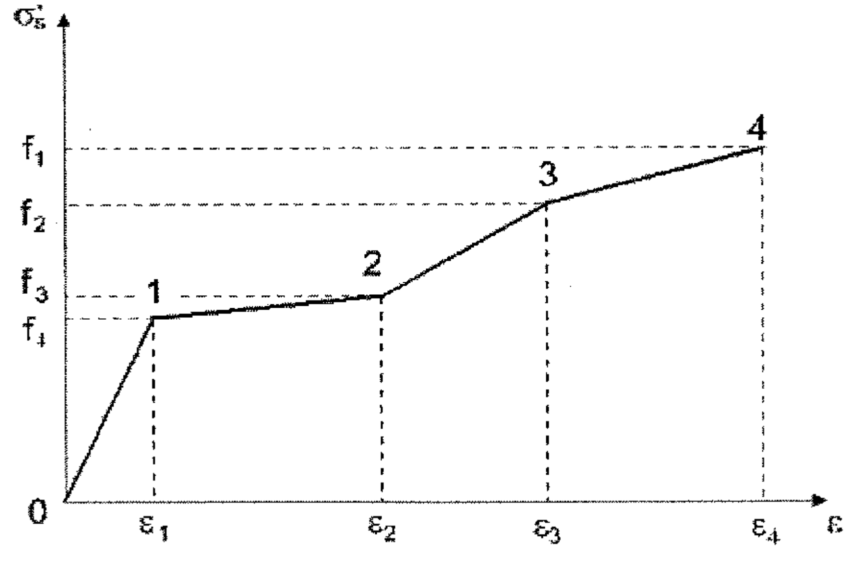

Figure 2.40 The multi-linear stress-strain law for reinforcement (Cervenka et. al., 2010)

2.12.7 CFRP Concrete Interface

A bond slip model between CFRP and concrete can be defined manually in ATENA. Several bond slip models used in literatures are presented.

A numerical analysis using an incremental nonlinear displacement control 3D FE model conducted (Kotynia et al., 2008) to investigate the flexural and CFRP/concrete interfacial responses of the tested beams. Orthotropic behaviour of the CFRP laminates was considered in the FE model. Interface elements between the CFRP and concrete which support a nonlinear bond stress-slip law were used to simulate the interface. The mechanical behaviour of the FRP/concrete interface is modelled as a relation between the local shear stress, τ and relative displacement, s between the CFRP laminate and the concrete as proposed by (Lu et al., 2005). The τ –s relationship is given by the following Eq. (2.21) – (2.27):

$$\tau = \tau_{max}\sqrt{s/s_o} \qquad \text{if } s \leq s_o \tag{2.21}$$

$$\tau = \tau_{max}\exp[-\alpha\,(s / s_o - 1)] \qquad \text{if } s \geq s_o \tag{2.22}$$

The maximum bond strength τ_{max} and the corresponding slip s_o are governed by the tensile strength of the concrete f_t and a width ratio parameter β_w as follows:

$$\tau_{max} = 1.5\beta_w f_t \tag{2.23}$$

$$s_o = 0.0195\beta_w f_t \tag{2.24}$$

The parameter β_w is defined in terms of the CFRP laminate width b_f and the width of the beam b_c as follows:

$$\beta_w = \sqrt{\frac{2.25 - b_f/b_c}{1.25 + b_f/b_c}} \tag{2.25}$$

The area under the τ –s curve represents the interfacial fracture energy G_f, which corresponds to the energy per unit bond area required for complete debonding; which is calculated as follows in Eq. (2.26):

$$G_f = 0.308\beta^2_w\sqrt{f_t} \qquad (2.26)$$

The factor α in Eq.(2.27) is related to G_f according to the following equation:

$$\sigma=1/[G_f/(\tau_{max}s_o)-2/3] \qquad (2.27)$$

The FE model predicted the ultimate load carrying capacities of the various FRP strengthened beams with an average numerical to experimental ratio and standard deviation of 0.998 and 0.0276, respectively. The FE analysis was capable of predicting the experimentally observed CFRP debonding mode of failure. The bond slip model for the interface is shown in Figure 2.41.

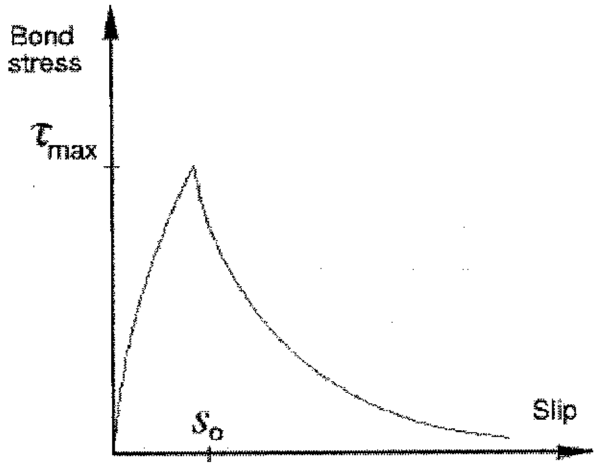

Figure 2.41 Bond slip model for the interface (Kotynia et.al. 2008)

A FE model developed to identify the parameters influencing the behaviour of FRP-shear strengthened beams. The constitutive law used to model the concrete is based on an elastic nonlinear stress-strain relationship to allow for weakening of the material under increasing compressive stresses. The steel was represented by an elastic-plastic constitutive relation with linear strain hardening while a linear elastic tensile model until failure is assumed to represent the CFRP strips. A rupture point on the stress-strain relationship defines the maximum stress of the CFRP strips. The authors considered the bond slip model developed by (Lu et al., 2005) as an accurate bond-slip model that can be incorporated into a FE analysis as the model has received wide acceptance. In this model, the behaviour of the FRP/concrete interface is simulated by a relationship between the bond stress, τ and the relative displacement, s. Figure 2.42 shows the typical bilinear bond slip model (Godat et al., 2012).

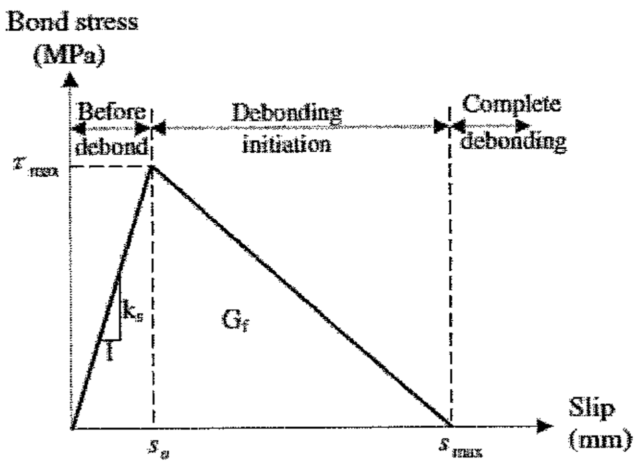

Figure 2.42 Typical bilinear bond slip model (Godat et al., 2012)

An investigation was performed to study the debonding failure modes of flexural FRP strengthened RC beams (Aram et al., 2008). The investigation involved experimental study of four point bending tests on FRP strengthened beams while the debonding failure mechanisms of strengthened beams were investigated using analytical and FE solutions. The nonlinear FE analysis was conducted using the commercial FE analysis, ATENA to predict the behaviour of the externally bonded FRP RC beams. The results from the experiments and calculations were compared with the existing international codes and guidelines from organizations such as ACI, *fib*, ISIS, JCEA, SIA and TR55. In one of the FE models, the nonlinear behaviour of the strengthened beams was examined by FE analysis using a smeared crack model for the concrete and a bond slip model for the FRP-concrete interface. The internal reinforcement and FRP plate were modelled with bar reinforcement elements. For the FRP, this assumption was indeed sufficiently accurate as the FRP plate externally strengthens the bottom face of the beam in the tensile direction.

For concrete, the SBeta material property of ATENA was used for the quadrilateral concrete elements and includes 20 material properties. The complete equivalent uniaxial stress-strain diagram and biaxial stress failure criterion according to (Kupfer et al., 1969) were used. In addition, from the cube strength of concrete, f_{cu}, the compressive strength, tensile strength, elastic modulus and fracture energy were determined by the program using the formulas from the CEB-FIP Model Code 90 and VOS 1983 (Cervenka et al., 2003). An appropriate bond model for the interface between the FRP plate and concrete must be incorporated in order to model the debonding behaviour accurately. The behaviour of the FRP-concrete interface was defined according to the bond-slip relationship given by (Ulaga et al., 2003). This behaviour is based on a bilinear relationship adopted as shown in Figure 2.43 where the variables are calculated in Eq, (2.28) – (2.30):

$$\tau_{f0}=\frac{4f_{ctm}}{3} \tag{2.28}$$

$$S_{f0}=\frac{G_a}{t_a}\tau_{f0} \tag{2.29}$$

$$S_{f1}=S_{f0}+0.225 \tag{2.30}$$

Where τ_{f0} is the bond shear stress; f_{ctm} is the mean value of concrete tensile strength; S_{f0} is the ultimate slip where debonding occurs; G_a is the shear modulus of adhesive; t_a is the thickness of adhesive.

Steel reinforcement was assumed to behave in an elastic plastic manner with strain hardening effects, while the FRP reinforcement was assumed to behave linear elastically with brittle failure in tension. The nonlinear analysis of flexural strengthened RC beams was conducted and compared to experimental results. The results show a discrepancy of up to 250% between predicted debonding failure loads using various codes and guidelines.

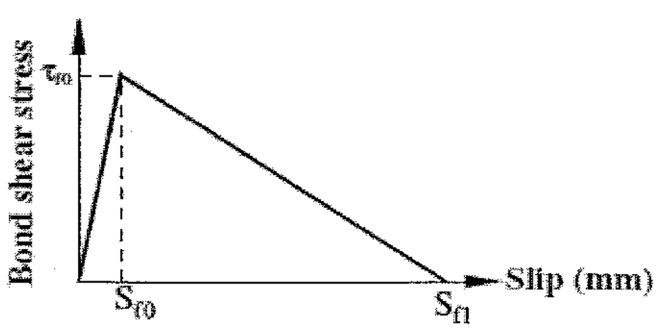

Figure 2.43 Bond slip relationship for FRP-concrete interface (Aram et al., 2008)

2.12.8 Two Dimensional Modelling of CFRP in ATENA

A nonlinear numerical model to simulate the behaviour of RC beams with prestressed CFRP laminates for flexural strengthening was conducted (Franca et al., 2007). The proposed model was implemented in the FE package ATENA, as shown in Figure 2.44. In the FE program, the tensile behaviour of concrete is modelled by non-linear fracture mechanics combined with the crack band method whereby the smeared crack concept is adopted. In this study, the rotated crack model is used instead of the fixed crack model as better results were obtained when compared with the behaviour of the tested beams with the numerical model. A two dimensional model was used for each beams. 2D macro elements was used to model the concrete beam, the stirrups was modelled by smeared reinforcement within the 2D macro elements while the reinforcement bars and CFRP laminates by bar reinforcement elements. Steel plates were modelled by 2D macro elements in the four loading points of the beams to avoid localized numerical errors due to point loads. A perfect connection between CFRP laminates and concrete surface was adopted since it is not possible to simulate the correct interface behaviour between the CFRP laminates and concrete. The numerical model predicted accurately the experimental behaviour of the reference beam as well as strengthened beam with prestressed CFRP laminates.

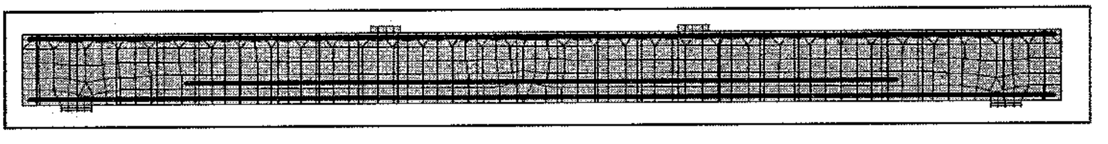

Figure 2.44 2D finite element model for the strengthened RC beam (Franca et.al., 2007)

2.12.9 Summary

The following remarks are drawn for this section:

- For the FRP concrete interface, researchers considered the bond model developed by Lu et al., 2005 as an accurate bond-slip model that can be incorporated into a FE analysis.

- The findings show that 2D modelling of RC beams with FRP in ATENA are rather limited. Hence, in this research, a 2D modelling of beams with openings and FRP are studied.

2.13 Failure Theory

Failure of a material represents either direct separation of particles from each other (brittle fracture) or slipping of particles (ductile fracture or yielding) accompanied by considerable plastic deformations. Due to the complex stress system of failure, various theories are developed in order to predict the failure of the material.

As discussed in the sections 2.6.2 to 2.6.4, the presence of openings in RC beams either small or large of various shapes and sizes cause stress concentration around them. Openings such as square and rectangular in shapes are subjected to high stress concentration especially at opening corners which lead to wide diagonal cracking. In an experimental testing of RC beams contained openings in the shear zone, the diagonal cracking from the opening usually penetrated towards the loading point and to the beam support respectively, which eventually cause the beam to fail in shear. This situation applies to most openings located in the shear zone.

Hence, in this research, it is assumed that the failure or yielding of the RC beams contained openings is according to the Maximum Shear Stress Theory, or known as Tresca's theory. According to this theory, yielding begins when the maximum shear stress at a point equals the maximum shear stress at yield in uniaxial tension (or compression). In the case of multi-axial stress state, the maximum shear stress is $\tau_{max} = (\sigma_{max} - \sigma_{min})/2$, where σ_{max} and σ_{min} denote the maximum and minimum ordered principal stress components, respectively. In uniaxial tension, ($\sigma_1 = \sigma$, $\sigma_2 = \sigma_3 = 0$), the maximum shear stress is $\tau_{max} = \sigma/2$. Since yield in uniaxial tension must begin when $\sigma = Y$, the shear stress associated with yielding is predicted to be $\tau_Y = Y/2$. Hence, the yield function for the maximum shear-stress criterion may be defined as in Eq. (2.31):

$$f = \sigma_e - \frac{Y}{2} \tag{2.31}$$

Where the effective stress is;

$$\sigma_e = \tau_{max} \tag{2.32}$$

The magnitude of the extreme values of the shear stresses is:

$$\tau_1 = \frac{|\sigma_2 - \sigma_3|}{2}$$

$$\tau_2 = \frac{|\sigma_3 - \sigma_1|}{2}$$

$$\tau_3 = \frac{|\sigma_1 - \sigma_2|}{2} \tag{2.33}$$

The maximum shear stress τ_{max} is the largest of (τ_1, τ_2, τ_3). If the principal stresses are unordered, yielding under a multi-axial stress state can occur for any of the following conditions:

$$\sigma_2 - \sigma_3 = \pm Y$$

$$\sigma_3 - \sigma_1 = \pm Y$$

$$\sigma_1 - \sigma_2 = \pm Y \tag{2.34}$$

By Eq. (2.34), the yield surface for the maximum shear-stress criterion is a regular hexagon in principal stress space, as shown in Figure 2.45. For a biaxial stress state, ($\sigma_3 = 0$), the yield surface takes the form of an elongated hexagon in the (σ_1, σ_2) plane as illustrated in Figure 2.46. The yielding occurs on planes oriented at 45° to the axis of the specimen, resulting in the smooth 45° failure surface at the outer portion of the specimen (Boresi & Schmidt, 2003). This clearly explains the formation of cracks around the openings in RC beams. In addition, a nonlinear FE analysis of RC structures using Tresca-type yield surface theory was performed by Nazem et al., 2009 to study the yield surface of concrete. The yield surface considers the behaviour of concrete in a three-dimensional stress state. Based on the yield surface, a non-linear FE formulation is provided to facilitate a three-dimensional analysis of RC structures and considerable results were obtained (Nazem et al., 2009).

On the other hand, according to (Boresi & Schmidt, 2003) another probable failure theory based on the distortional energy density criterion; often attributed to von Mises, states that yielding begins when distortional strain-energy density at a point equals the distortional strain-energy density at yield in uniaxial tension (or compression). The distortional strain-energy density is that energy associated with a change in the shape of a body. The total strain-energy density U_0 can be divided into two parts: (i) that causes volumetric change Uv (ii) that causes distortion U_D. The distortional strain-energy density equation is shown as follows:

$$U_D = \frac{(\sigma_1-\sigma_2)^2 + (\sigma_2-\sigma_3)^2 + (\sigma_3-\sigma_1)^2}{12G} \tag{2.35}$$

Where G is the shear modulus. At yield under a uniaxial stress state, ($\sigma_1 = \sigma$, $\sigma_2 = \sigma_3 = 0$), $U_D = U_{DY} = Y^2/6G$. Thus, for a multiaxial stress state, the distortional energy density criterion states that yielding is initiated when the distortional energy density U_D given by Eq. 2.35 equals $Y^2/6G$. In terms of the second deviatoric stress invariant J_2, the distortional energy density U_D can be expressed as;

$$U_D = \frac{1}{2G}|J_2| \tag{2.36}$$

Where;

$$J_2 = -\frac{1}{6}[(\sigma_1-\sigma_2)^2 + (\sigma_2-\sigma_3)^2 + (\sigma_3-\sigma_1)^2] \tag{2.37a}$$

Relative to the general (x, y and z) axes, J_2 can be expressed in terms of the stress invariants, I_1 and I_2 as

$$J_2 = I_2 - \frac{1}{3}I^2_1 \tag{2.37b}$$

At yield in uniaxial tension (or compression), $\sigma_1 = \pm Y$ and $\sigma_2 = \sigma_3 = 0$. Then,

$$|J_2| = \frac{1}{3}Y^2 \tag{2.38}$$

Therefore, by Eq. (2.37a) and (2.38), the yield function for the distortional energy (von Mises) can be written as;

$$f = \frac{1}{6}[(\sigma_1-\sigma_2)^2 + (\sigma_2-\sigma_3)^2 + (\sigma_3-\sigma_1)^2] - \frac{1}{3}Y^2 \qquad (2.39)$$

A more compact form for the yield function is;

$$f = \sigma_e^2 - Y^2 \qquad (2.40)$$

Where the effective stress is

$$\sigma_e = \sqrt{\frac{1}{2}[(\sigma_1-\sigma_2)^2 + (\sigma_2-\sigma_3)^2 + (\sigma_3-\sigma_1)^2]} = \sqrt{3|J_2|} \qquad (2.41a)$$

In terms of the rectangular components of stress, the effective stress for the von Mises criterion can be written as;

$$\sigma_e = \sqrt{\frac{1}{2}[(\sigma_{xx}-\sigma_{yy})^2 + (\sigma_{yy}-\sigma_{zz})^2 + (\sigma_{zz}-\sigma_{xx})^2] + 3(\sigma^2_{xy} + \sigma^2_{yz} + \sigma^2_{xz})} \qquad (2.41b)$$

J_2 and the octahedral are related by;

$$J_2 = -\frac{3}{2}\tau^2_{oct}$$

Hence, the yield function in Eq. (2.39) for the von Mises yield criterion can be expressed as;

$$f = \tau_{oct} - \frac{\sqrt{2}}{3}Y \qquad (2.42)$$

Thus, according to Eq. (2.42), when $f = 0$, the octahedral shear stress at a point reaches the value $(\sqrt{2}/3)Y = 0.471Y$, and cause yielding to occur. This result agrees with that obtained by Eq. (2.39). Hence, the distortional energy density (von Mises) criterion is also referred to as the octahedral shear-stress criterion. In terms of a three-dimensional stress state, the yield surface for the von Mises criterion forms a cylinder that circumscribes the Tresca hexagon, as shown in Figure 2.45. For a biaxial stress state ($\sigma_3 = 0$), the von Mises yield surface reduces to an ellipse in the $\sigma_1 - \sigma_2$ plane as illustrated in Figure 2.46.

Comparing to the Tresca criterion, the von Mises criterion is fairly accurate in predicting initiation of yield for certain ductile metals (Boresi & Schmidt, 2003). The von Mises criterion is more accurate for some materials than the Tresca criterion in predicting yield under pure shear. As shown in Figure 2.46, the von Mises criterion predicts that the pure-shear yield stress is approximately 15% greater than that predicted by the Tresca criterion.

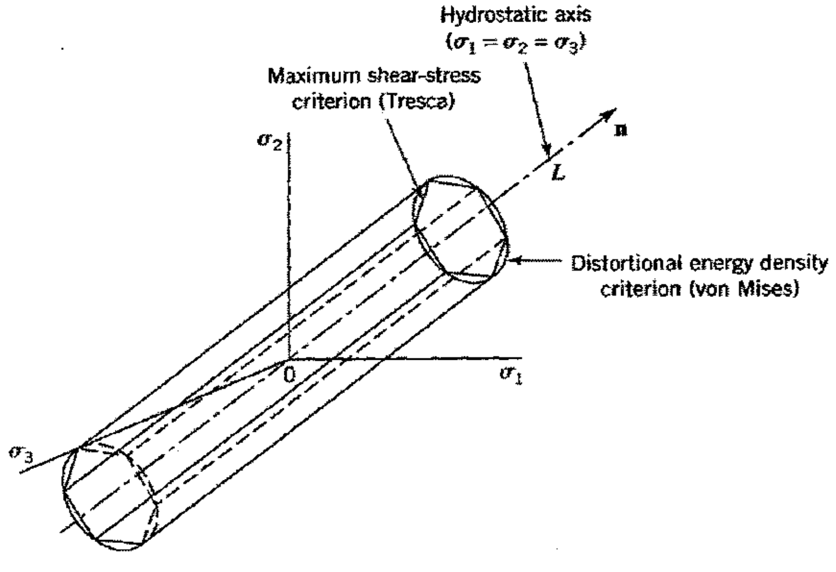

Figure 2.45 Yield surface in principal stress state (Boresi & Schmidt, 2003)

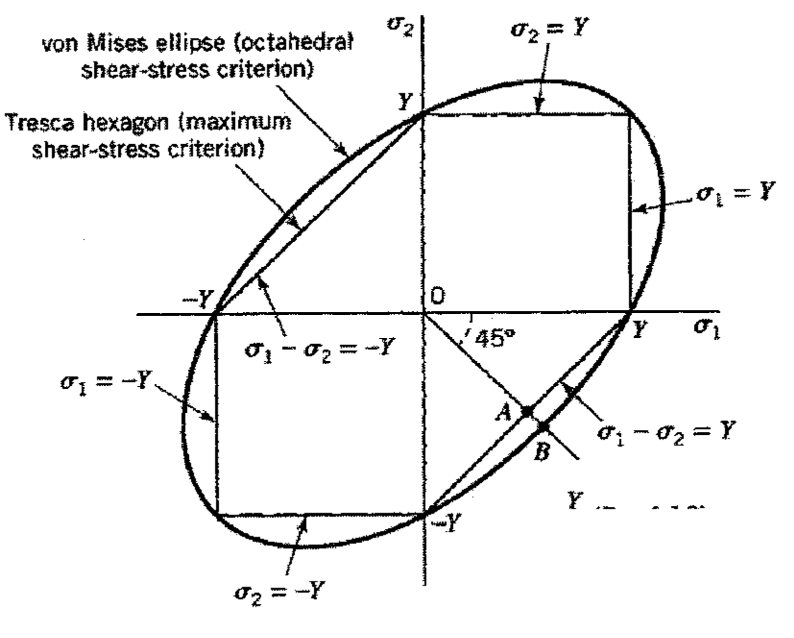

Figure 2.46 Yield surfaces for biaxial stress state ($\sigma_3 = 0$). For points A and B, $\sigma_1 = -\sigma_2 = \sigma$ (pure shear) (Boresi & Schmidt, 2003)

2.14 Concluding remarks

The following remarks are drawn leading to the gaps of the research study:

- In the past, many investigations were conducted to study the behaviour of RC beams with openings; such as in T-beams, continuous and simply-supported beams with the effects of openings size, shape and location subjected to bending, shear, torsion and combined loading.
- The numerical analyses found in literatures are mostly modelling of solid RC beams as well as strengthening of solid beams using FRP materials. However, numerical investigations or validation using a FE program to model the behaviour of RC beams with the presence of openings and strengthening by FRP materials are rather limited.
- Available literatures investigated the strengthening of RC beams with openings; such studies are mainly experimental based or partly experimental and partly theoretical. Very little research efforts are performed in both experimental and validation using FE based numerical analysis.

CHAPTER 3

RESEARCH METHODOLOGY

3.1 Introduction

This research study was divided into two major parts which comprised of:

i. Numerical modelling using a non-linear FE program, and
ii. Experimental investigation

In the first part, FE modelling and analysis were carried out to investigate the behaviour of control beams (without opening), beams with large openings (without CFRP) and beams with openings strengthened using CFRP laminates. Various strengthening configurations of CFRP laminates were designed around the openings, which should be beneficial to re-gain and restore the original structural capacities of the beams.

In the second part, an experimental program was conducted to study the behaviour of control beams and beams with openings (with and without strengthening). The most effective strengthening configuration of a particular beam with openings was chosen from a number of strengthening schemes that were analyzed in the FE analysis. In the final part, results of FE analysis were compared with the experimental results in order to determine the degree of agreement between the two results. Figure 3.1 shows the flowchart of the overall research methodology.

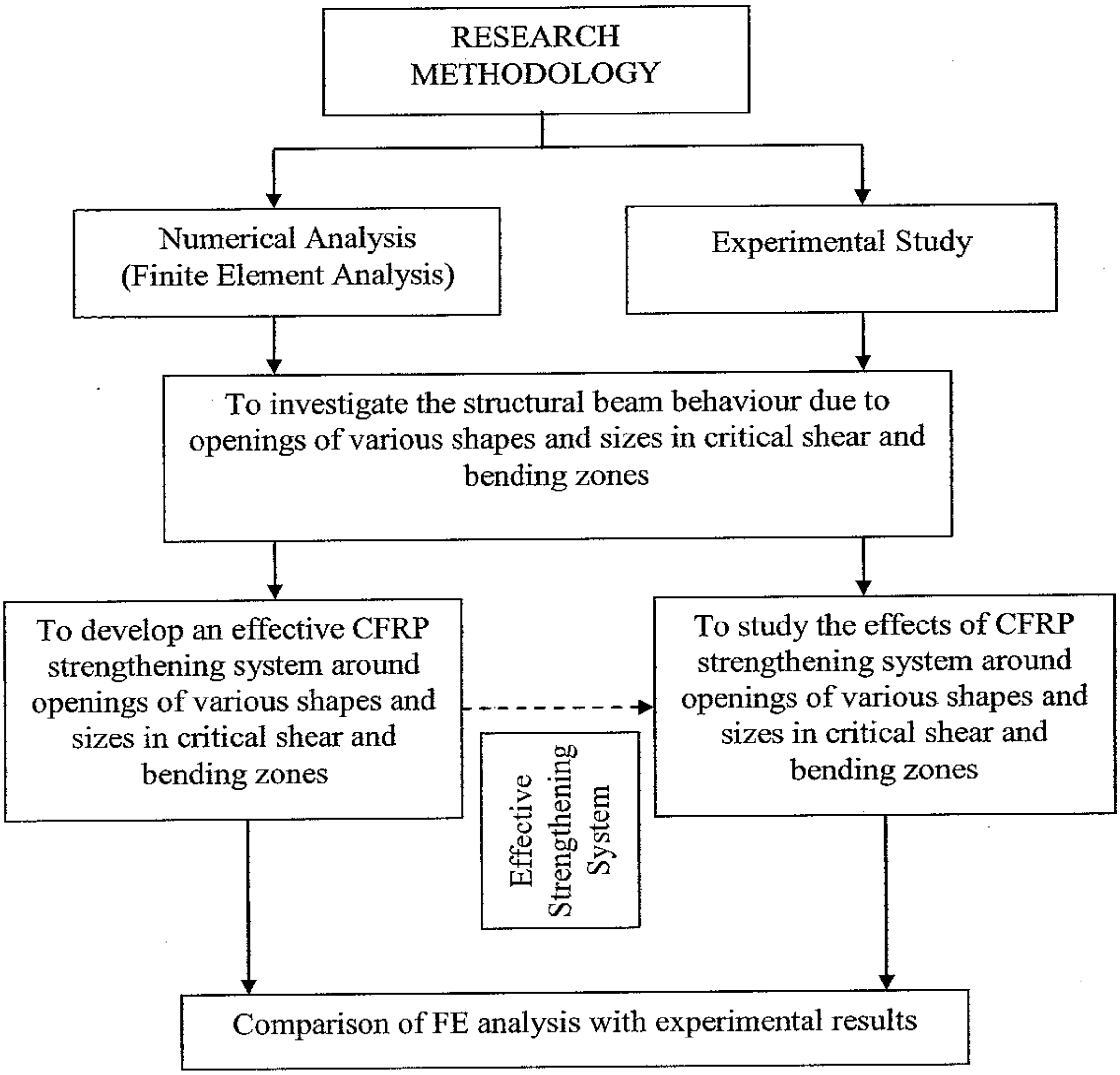

Figure 3.1 Flowchart of the research methodology

3.2 Numerical Modelling and Analysis

Details of the numerical modelling and analysis including the background and overview are presented.

3.2.1 Background

In the previous studies, various FE modelling tools, i.e. ANSYS, ABAQUS, ATENA were used to simulate the behaviour of RC beams (without opening) strengthened using FRP materials from linear and nonlinear response, which were extended up to failure. The studies focused on the numerical models for the analyses of beams strengthened with FRP using a nonlinear smeared fracture analysis of concrete. The analyses were conducted to gain a better understanding of the behaviour and characteristics of RC structures. However, the use of FE method to simulate the behaviour of beams with large openings strengthened with FRP materials was missing in the available literatures.

In the context of structural engineering, FE analysis determines the overall behaviour of a structure by dividing it into a number of simple elements; each has well-defined mechanical and physical properties. However, it is relatively not easy in FE analysis to model the complex behaviour of RC, which is non-homogeneous and anisotropic. Most of the early FE models of RC included the effects of discrete cracking concept. The change of the topology in the model is required to keep track of the crack propagation inside the element is a time consuming task and results in very limited acceptance of the discrete cracking concept for crack modeling in actual applications.

The subsequent model was developed with the concept of smearing the cracks by using isoparametric formulations to represent the cracked concrete as an orthotropic material. In the smeared cracking approach, when the principal stress exceeds the ultimate tensile strength, cracking of the concrete occurs. The elastic modulus of the material is then assumed to be zero in the direction parallel to the principal tensile stress direction. Thus, to simulate the behaviour and failure mechanisms of experimental beams, FE analysis with the smeared cracking concept was adopted throughout this study. Figure 3.2 shows the flowchart of the numerical modelling and analysis.

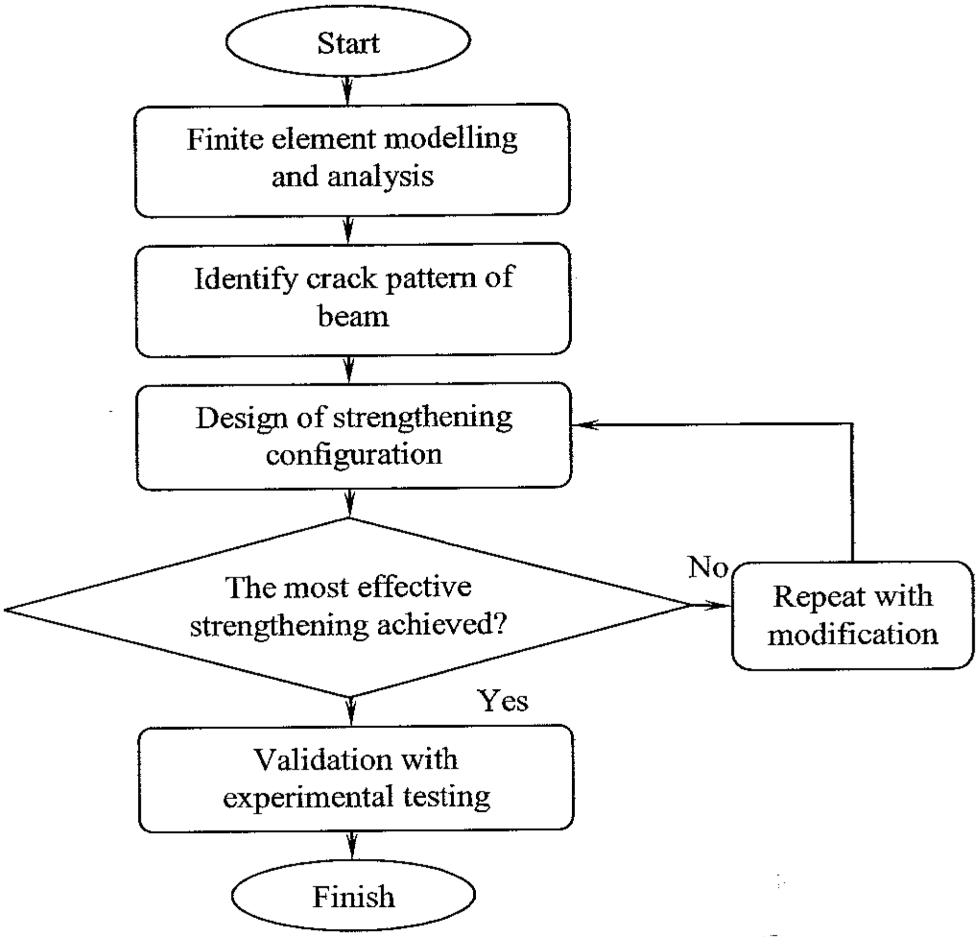

Figure 3.2 Flowchart of numerical analysis

3.2.2 Overview of FE Analysis using ATENA

2D modelling using a non-linear FE program, ATENA was adopted to simulate the behaviour of all beams. For modelling the material properties in the analysis; SBETA material model for 2D plane stress elements was used to represent concrete whereby the tensile behaviour of concrete is modelled by nonlinear fracture mechanics combined with the crack band method, in which the smeared crack concept was adopted. Longitudinal steel reinforcements, stirrups and CFRP laminates were modelled as discrete reinforcement represented by bar elements. Perfect bond was assumed between the steel reinforcements and the surrounding concrete whereas the bond slip relation of CFRP and concrete was defined and assigned in the properties of the discrete reinforcement bar of CFRP. Processes of FE modelling are explained in details in chapter 4, which includes a selection of material models, meshing, loading and boundary conditions. Meanwhile, the convergence of results it is assumed to be taken care by the software. To verify the efficiency and relevancy of the software, an example of RC beam in the ATENA example manual (Kabele et al., 2010) was performed and the results were found in good agreement, which is shown in APPENDIX A.

3.3 Experimental Investigation

Details of the experimental study are presented and discussed in the following sub-sections.

3.3.1 Background

In modern building constructions, openings in beams are often used to provide for the passage of utility ducts and pipes as this could impose a reduction in storey height and material cost. However, providing an opening in the beam causes crack around the opening which reduces the beams stiffness and resulted in a more complicated structural response. Various studies have been carried out to upgrade, strengthen and rehabilitate RC beams with openings using externally bonded FRP as a strengthening solution.

The effectiveness of strengthening using externally bonded reinforcement may be affected by several factors of the openings, which are due to the size, shape and location of the openings. From the previous studies, the openings investigated are mainly small openings; i.e. circular, square, while for large opening i.e. rectangular openings. Thus, further study is needed in order to investigate the behaviour of beams contained small and large openings in the bending and shear zones.

In terms of location of the openings, investigations on strengthening of beams with openings have mostly studied the openings located in the area near to the support and in the shear zone. This is because providing an opening at the shear zone can seriously impair the safety and serviceability of the structure. Thus a large number of researches are needed to further investigate on various sizes and shapes of the openings, especially large openings provided in the critical shear zone as well as flexure zone.

From the previous studies, investigations were conducted to strengthen openings in various types of RC beams, such as deep beams, T-beams, continuous beams and simply-supported beams. Further studies are needed for strengthening of openings in different type of beams as the current studies are rather limited. Also, various types of externally bonded strengthening material have been used in the previous studies for the strengthening of RC beams with opening such as using FRP plates, CFRP sheets, FRP rods and GFRP sheets. As the investigation is still rather limited, further study is needed for the different types of external strengthening material especially using the most commonly available externally bonded reinforcement CFRP sheets and laminates.

From the literatures, various strengthening configurations have been studied with respect to the openings in RC beams such as vertical and horizontal strengthening, FRP wrapping, and application of CFRP around the openings. The strengthening configurations reported in literatures mostly conducted only one or two strengthening configurations. This is mainly to check the potential and efficiency of using FRP materials as a strengthening solution. However, limited investigation focuses on the study and design of various strengthening configurations around the openings for the effective strengthening with CFRP laminates.

In addition, in most of the literatures, stirrups and U-shape stirrups were provided at the opening chords to replicate the actual case of providing an opening in existing beam. In contrast, there is a need to study the pure contribution and strengthening efficiency of CFRP around the openings by not providing any stirrups at the opening chords. The flowchart of the experimental program is shown in Figure 3.3.

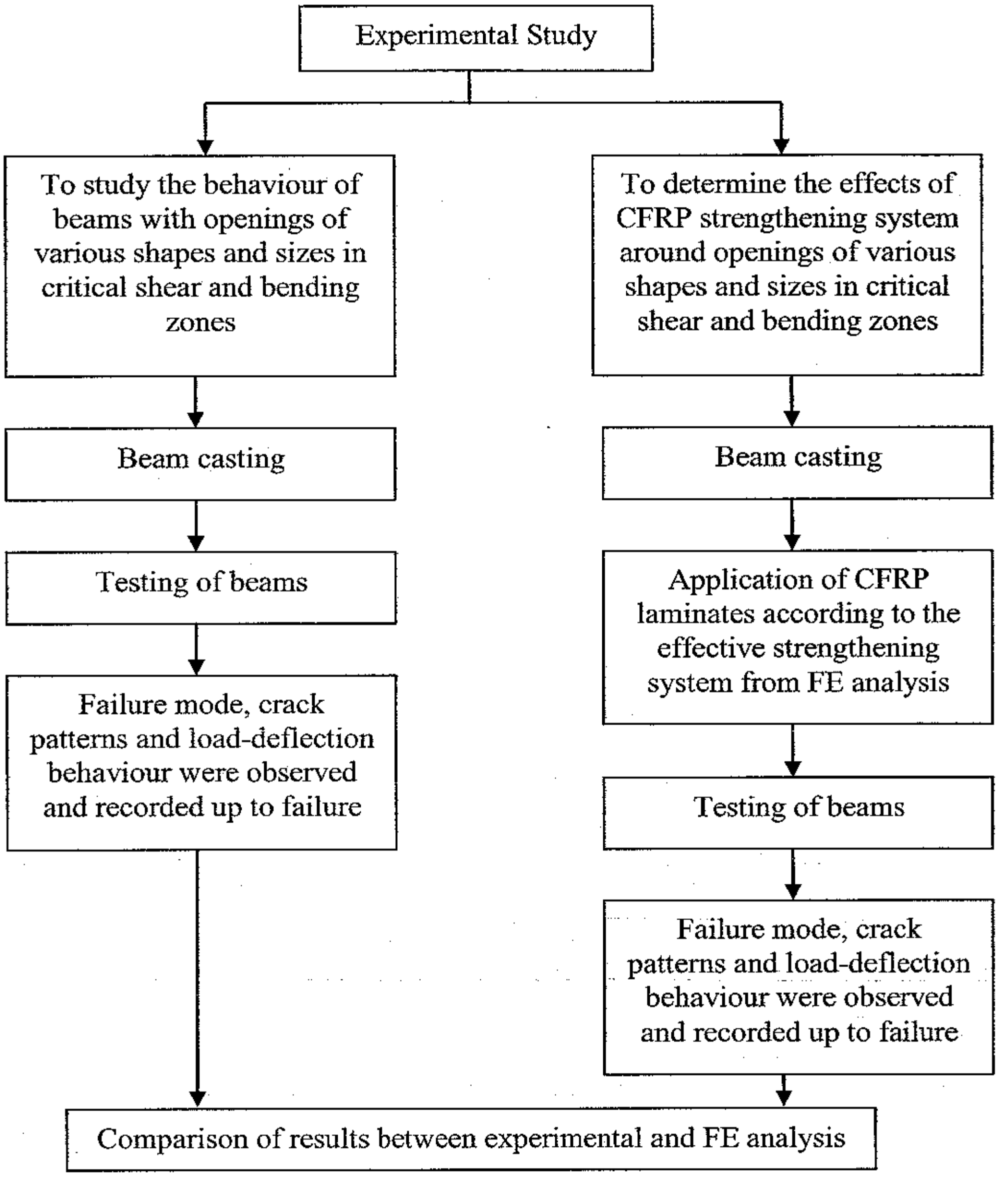

Figure 3.3 Flowchart of the experimental program

3.3.2 Test Matrix

An experimental study consisted of three (3) series of beams in which a control beam was cast at the time of each series, CB1, CB2 and CB3, respectively using ready-mixed concrete of grade 35 MPa. The three series of beams which comprised of twenty-seven (27) simply-supported RC beams of rectangular in shape were constructed and tested. Three (3) of them were control beams (without opening and strengthening), thirteen (13) beams were consisted of beams with openings without strengthening, and the remaining were beams with openings strengthened using CFRP laminates with the most effective strengthening configuration. The details of the test matrix are shown in Tables 3.1-3.2.

Table 3.1 Text matrix of un-strengthened openings

Beam No.	Beam Name	Opening				
		Size (mm)	Shape	Location		
				Flexure	Shear	
					Openings at both ends	Opening at one end only
					Distance from support	Distance from support
1	CB1	Control				
2	CB2	Control				
3	CB3	Control				
4	CF	230ø	Circular	Mid-span		
5	SF	210x210	Square	Mid-span		
6	LEF	140x800	Elliptical	Mid-span		
7	LRF	140x800	Rectangular	Mid-span		
8	C0S	230ø	Circular		zero	
9	S0S	210x210	Square		zero	
10	S0.5dS	210x210	Square		0.5d	
11	CdS	230ø	Circular		d	
12	SdS	210x210	Square		d	
13	S0.5dS1	210x210	Square			0.5d
14	CdS1	230ø	Circular			d
15	SdS1	210x210	Square			d
16	S1.5dS1	210x20	Square			1.5d

Specimen naming convention:

CB = **C**ontrol **B**eam
CF = **C**ircular **F**lexure
LEF = **L**arge **E**lliptical **F**lexure
C0S = **C**ircular (distance) **S**hear
S0.5dS = **S**quare (distance) **S**hear
SdS1= **S**quare (distance) **S**hear **1** (single opening)

Table 3.2 Test matrix of strengthened openings

Beam No.	Beam Name	Opening				
		Size (mm)	Shape	Location		
				Flexure	Shear	
					Openings at both ends	Opening at one end only
					Distance from support	Distance from support
17	CF-S	230ø	Circular	Mid-span		
18	SF-S	210x210	Square	Mid-span		
19	LEF-S	140x800	Elliptical	Mid-span		
20	LRF-S	140x800	Rectangular	Mid-span		
21	C0S-S	230ø	Circular		zero	
22	S0S-S	210x210	Square		zero	
23	S0.5dS-S	210x210	Square		0.5d	
24	CdS-S	230ø	Circular		d	
25	SdS-S	210x210	Square		d	
26	CdS1-S	230ø	Circular			d
27	SdS1-S	210x210	Square			d

Specimen naming convention:

CF-S = Circular Flexure –Strengthening
SF-S = Square Flexure - Strengthening

3.3.3 Beam Descriptions

The basic shape and dimension of the RC beams are illustrated in Figure 3.4. The basic beam geometry was 120 mm width, 300 mm height, and an effective span of 1800 mm. The bottom tension reinforcements consisted of two 12 mm ø deformed steel bars. The compression steel reinforcements consisted of two 10 mm ø deformed steel bars. Shear reinforcement consisted of steel stirrups with a diameter of 6 mm smooth bars. The stirrups were uniformly spaced at 300 mm, center to center. The tension test of reinforcing steel bars was performed and their engineering properties were reported in Section 3.3.6.2. The beams' effective depth to the main reinforcement, d = 280 mm. In the case of RC beams with openings, the area around the openings (at the top and bottom chords) is not reinforced by any shear reinforcement.

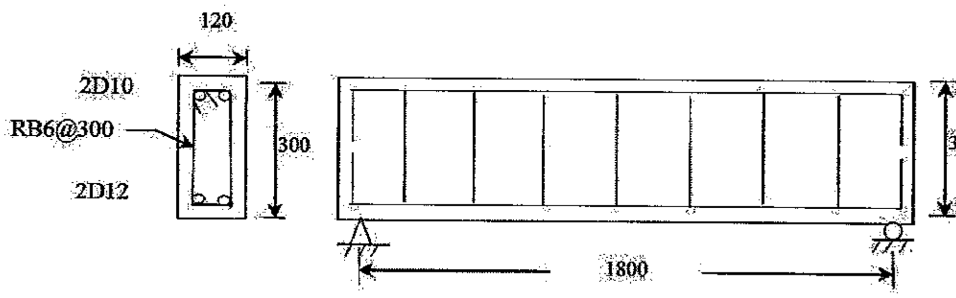

Figure 3.4 Beam geometry and reinforcement details of control beam

3.3.3.1 Size and Shape of Openings

The openings considered in this study included circular, square, large elliptical and large rectangular opening. The size of each respected shapes is presented and discussed, as described in Figure 3.5.

- **Circular**: The diameter of the circular opening investigated in this study was ø230 mm.
- **Square**: The dimension of the square shape was 210 x 210 mm.
- **Large Elliptical**: The cross section of the elliptical opening was 800 mm with a semi-circular curve in ø140 mm.
- **Large Rectangular**: The cross section of the rectangular opening was 140 mm x 800 mm.

The ratio of the opening size (square and circular) to the beam's effective depth was 0.75 and 0.82, respectively in which researchers classified them as large opening (Somes & Corley, 1974, Pimanmas, 2010).

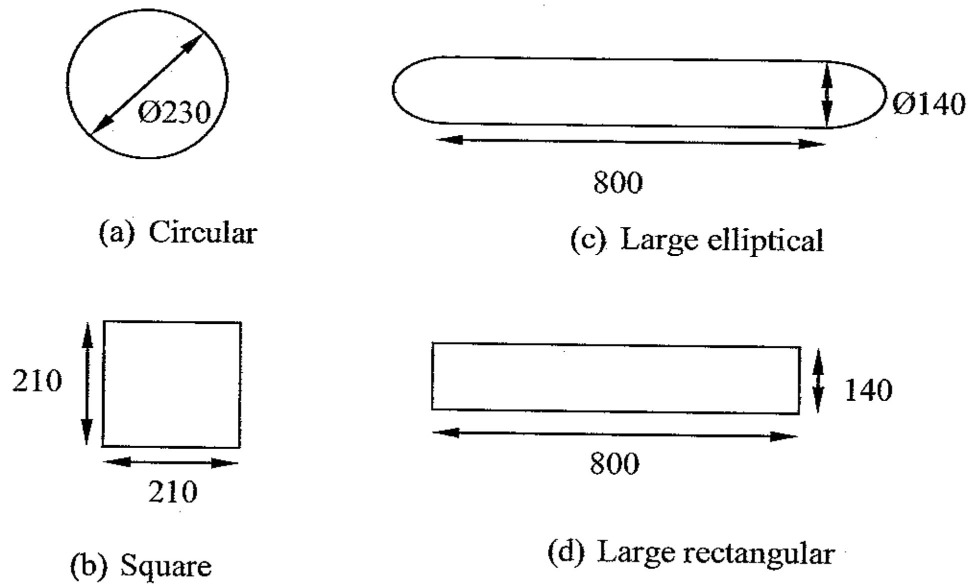

Figure 3.5 Shapes and sizes of openings

3.3.3.2 Location of Openings

The RC beams with openings in this study were located in bending and shear zones, as explained as follows:

- **Bending:** The opening was located at the beam mid-span.
- **Shear**: Opening at both ends: Location at (0, 0.5d, d) distances from the support.
  Opening at one end only: At distances 0.5d, d and 1.5d away from the support.

3.3.3.3 Construction of Openings

The openings were constructed with respect to the shape of the openings. Figure 3.6 shows the construction of various types of openings. The materials used are described as follows:

- **Square**: The square opening was formed by inserting a box fabricated from plywood (Figure 3.6(a)).
- **Circular**: The circular opening was formed by a circular polyvinyl chloride (PVC) pipe inserted in the beam before the casting of concrete (Figure 3.6(b)).
- **Large elliptical and rectangular**: The opening was created by using wooden planks for the rectangular formwork and wooden planks and aluminium foil were used for the shaping of the semi-circulars at both ends (Figure 3.6 (c) and (d)).

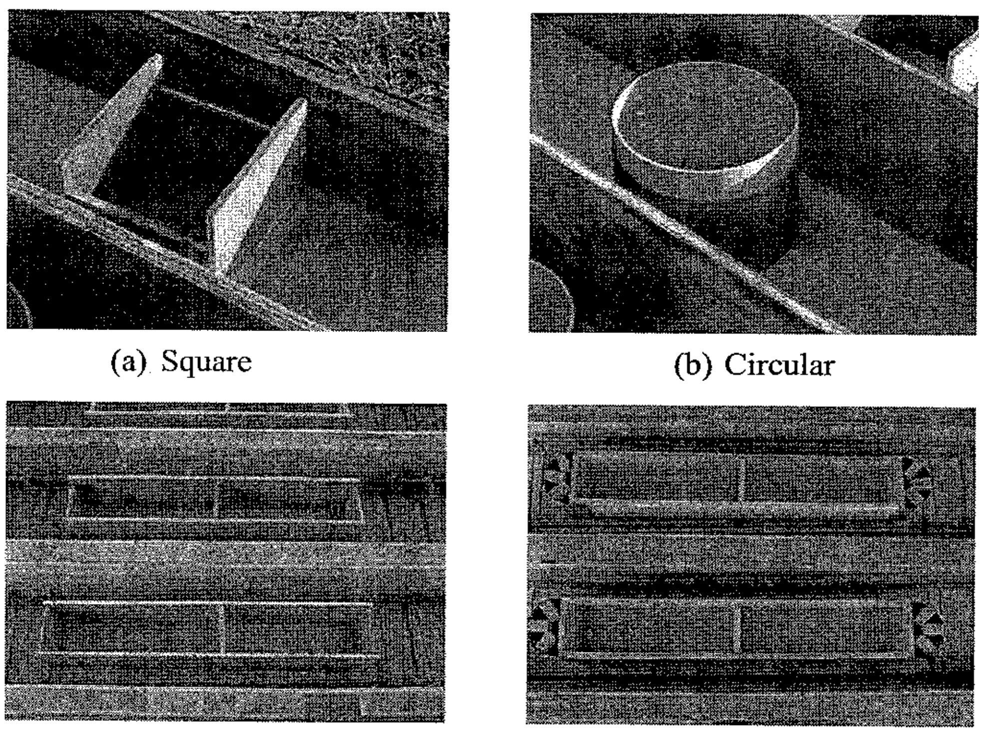

(a) Square (b) Circular

(c) Rectangular (d) Elliptical

Figure 3.6 Construction of openings

3.3.4 Casting and Curing of Concrete

The casting and curing of beams and cubes were conducted in the experimental program. Detailed descriptions are discussed in the following sections.

3.3.4.1 Beams

Figure 3.7 shows the construction procedure for the RC beams following typical construction practice. The reinforcing steel bars were prepared (Figure 3.7(a)) and the beams were cast in a horizontal position using plywood formwork (Figure 3.7(b)). All of the steel cages were placed inside wooden formwork (Figure 3.7(c)). Concrete spacer blocks were placed underneath the steel reinforcement at several points to provide the desired clear cover (20 mm) at the bottom of the beams. Ready-mixed concrete was used with a specified compressive strength of 35 MPa (Figure 3.7(d)). The concrete slump was obtained as 180 mm at the time of casting. After casting, plastic sheet was used to cover the beam specimens to prevent water evaporation. After 24 hours, the beam specimens were removed from the formwork and left for curing using wetted gunny bags for 28 days (Figure 3.7 (e) and (f)).

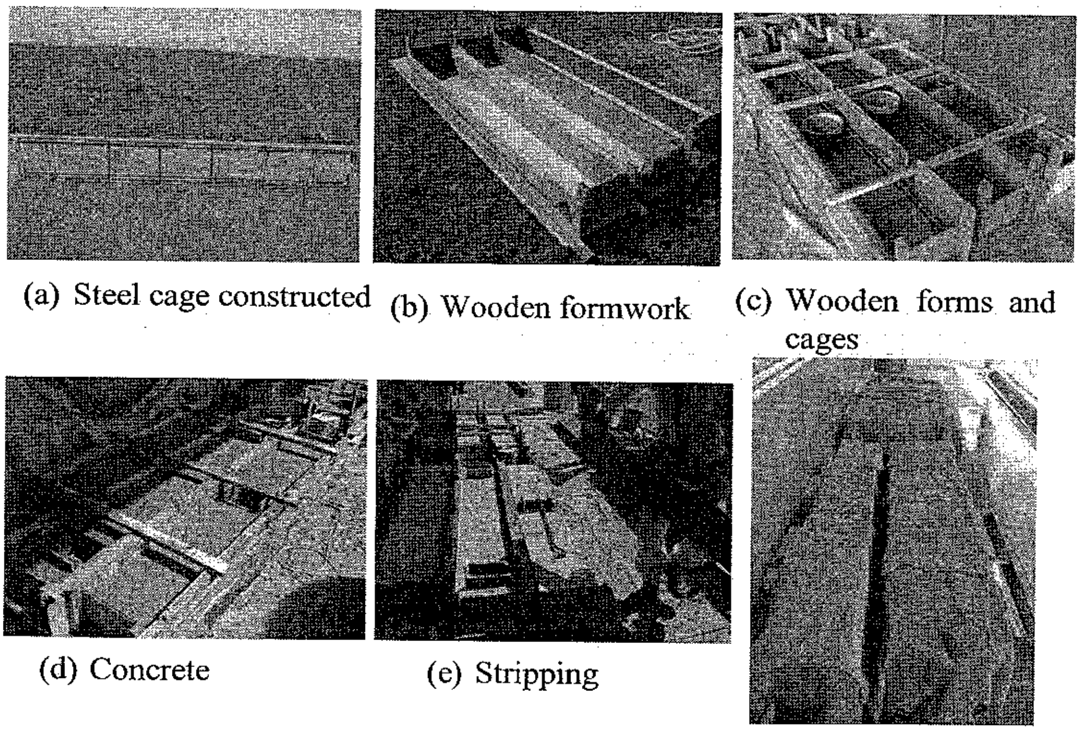

(a) Steel cage constructed (b) Wooden formwork (c) Wooden forms and cages

(d) Concrete (e) Stripping (f) 28 days moisture curing

Figure 3.7 Casting process of RC beams

3.3.4.2 Concrete cubes

Concrete cubes with the dimension of 100 x 100 x 100 mm were cast for testing at the age of 7, 14 and 28 days. The concrete cubes were cured in water bath. Figure 3.8 shows the curing method of concrete cubes.

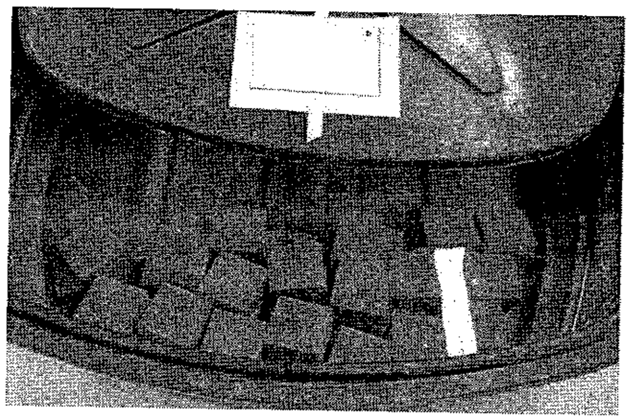

Figure 3.8 Concrete cubes in water bath

3.3.5 Specimens Preparation

The following steps were made to prepare the beam specimens and CFRP laminates for bonding purposes. The material handling and preparations are according to the standards provided by the manufacturer (Sika, 2010):

3.3.5.1 Concrete Surface Preparation

- The concrete surface of the beam specimens was roughened using sand paper and a mechanical grinder to remove the surface laitance.

3.3.5.2 CFRP Laminates Preparation

- The CFRP laminates were cut to the required width and length as designed in FE modelling using a mechanical shearing machine, as shown in Figure 3.9(a).

- The CFRP laminates were cleaned with methanol. The process was repeated until the washcloth was no longer blackened before pasting onto the concrete surface, as illustrated in Figure 3.9(b).

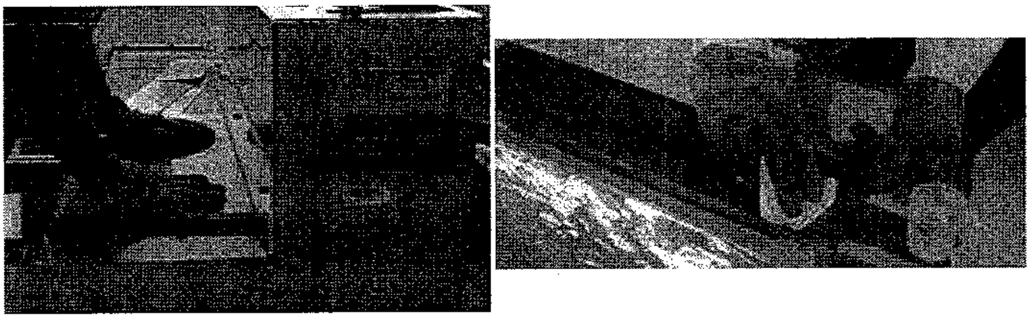

(a) Cutting of CFRP (b) CFRP surface

Figure 3.9 Cutting and surface preparation of CFRP laminate

3.3.5.3 Mixing of Epoxy resin – Sikadur®-30

- Figure 3.10(a) shows two types of component in Sikadur®-30. Three parts of 'Component A' and one part of 'Component B' by weight were added into a clean tray, as shown in Figure 3.10(b).
- Both components were mixed thoroughly for 3 minutes until the mixture turns greyish in colour, as shown in Figure 3.10(c).

(a) Epoxy resin Part A and Part B (b) Measurement of each part by weight (c) Mixture turns greyish in color

Figure 3.10 Mixing process of epoxy resin

3.3.5.4 Bonding of CFRP Laminates

- The mixed of Sikadur®-30 was applied onto the concrete and CFRP laminates to a nominal thickness of 1.5 mm each with a "roof-shaped" spatula as shown in Figure 3.11(a).

- The CFRP laminates were placed onto the concrete surface as soon as possible to avoid the hardening of epoxy.

- The laminates were pressed into the epoxy resin until the adhesive was forced out on both sides and excess adhesive was removed. The glue line was remained in 3 mm.

- The CFRP laminates were left undisturbed for a minimum of 24 hours and left for curing for 7 days, as shown in Figure 3.11(b).

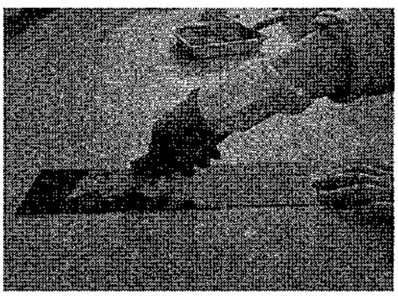

(a) Application of epoxy onto CFRP laminate

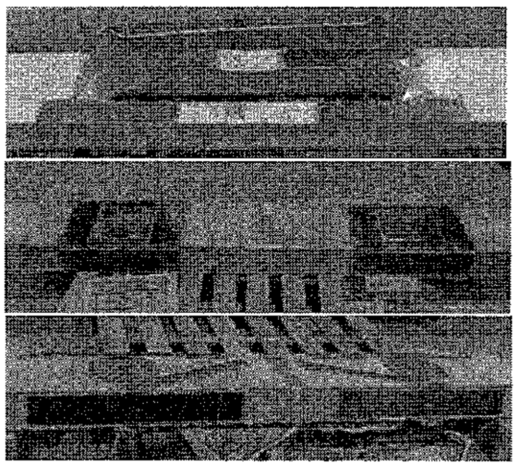

(b) The CFRP with epoxy were left 24 hours for curing

Figure 3.11 Preparation and bonding of CFRP

3.3.6 Material Properties

The materials used in the experimental work including concrete, steel reinforcements and CFRP laminates. In this section, their engineering properties are reported.

3.3.6.1 Concrete

Compression tests were performed using a compressive strength machine under a pace rate of 3.0 kN/s according to BS 1881: Part 116:1983 (British Standards Institution 1983) at 7 days, 14 days and 28 days of curing. Three concrete cubes were tested each time and the average strength was calculated. Figure 3.12 illustrates the average concrete cube strength with time. The average compressive strength obtained was 35.6 MPa at 28 days and in the range of 34.05~36.89 MPa at the time of testing. Hence, a concrete compressive strength of 35 MPa was used for the analysis of the beam. Figure 3.13 shows the failure mechanism of a concrete cube under compressive loading.

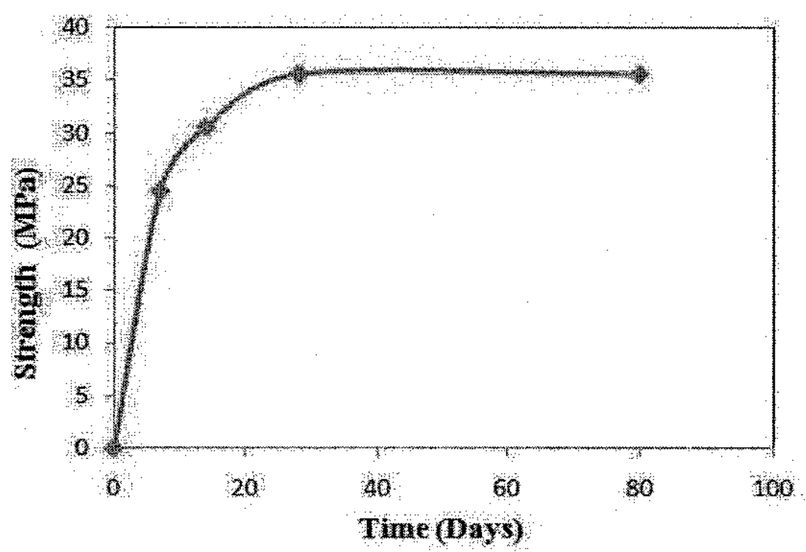

Figure 3.12 Concrete compressive strength versus time

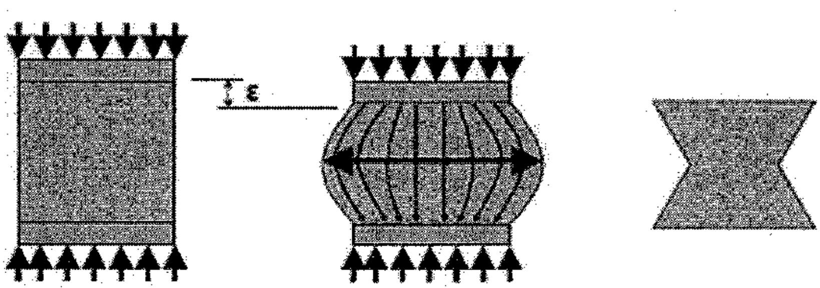

(a) Concrete cube under compression (b) Stress path in concrete under compression (c) Normal concrete cube failure

Figure 3.13 Tensile failure under compressive loading (Beushausen & Alexander, 2010)

3.3.6.2 Steel Reinforcement

Tensile testing of steel bars in this study was according to BS 4449:1997 (British Standards Institution, 1997). The test setup and ruptured steel bar are shown in Figure 3.14(a) and (b). The ultimate strain at rupture was calculated by measuring the final elongation between two points marked on the steel bar. The yield stress of steel was 410 MPa and the ultimate stress was 545 MPa. The ultimate strain at rupture was obtained as 0.018 (1.8%).

(a) Test setup of steel bar (b) Rupture of steel bar

Figure 3.14 Test setup and failure mode of 12 mm diameter steel bar

The stress-strain curve of the tested bar is shown in Figure 3.15. The steel behaviour includes elastic state, yielding of steel reinforcement; hardening and rupture were clearly observed. The slope of the stress-strain is the modulus of elasticity, which is shown in Eq. (3.1).

$$E = \frac{\sigma}{\varepsilon} = 210 \text{ GPa} \tag{3.1}$$

3.3.6.3 CFRP Laminates and Epoxy Adhesive

The CFRP composites are made up of two constituents, carbon fiber and epoxy adhesive. Commercially available carbon fiber (Sika® CarboDur® XS1014) and epoxy adhesive (Sikadur®-30 -Sika Malaysia) was used in this study. The properties of CFRP laminates and epoxy resin are described in Table 3.3 based on the data provided by the manufacturer (Sika, 2010).

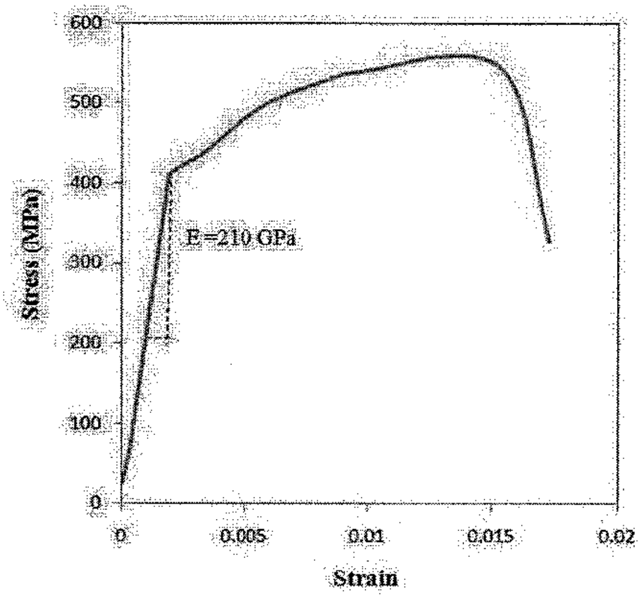

Figure 3.15 Stress-strain curve of steel reinforcement

A tension test of the CFRP laminates was carried out based on ASTM D3039 (ASTM International, 2008). The specimens were prepared with a length of 550 mm, width of 100 mm, and thickness of 1.4 mm. Steel tabs (thickness of 1.2 mm) were bonded to both ends of the specimens with epoxy adhesive. The test setup and failure mode of CFRP laminates are shown in Figures 3.16(a) and (b), respectively. The failure was with a sudden 'crack' sound resulted in cracks as described in Figure 3.16(b). The elastic modulus of CFRP laminates was 170 GPa about 3% higher than the value provided by the manufacturer.

Table 3.3 CFRP laminate and epoxy-resin material properties (Sika, 2010)

Material Type	Tensile Strength (MPa)	Elastic Modulus (GPa)	Elongation at break (%)	Adhesive strength on concrete (MPa)	Adhesive strength on steel (MPa)
Sika® CarboDur® XS1014	>2200	>165	>1.4	-	-
Epoxy resin Sikadur®-30	24.8	12.8	1	>4	>21

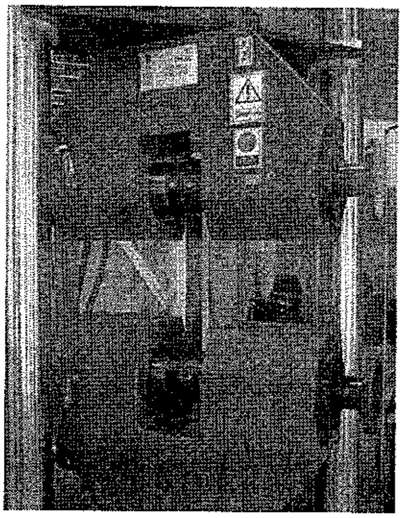

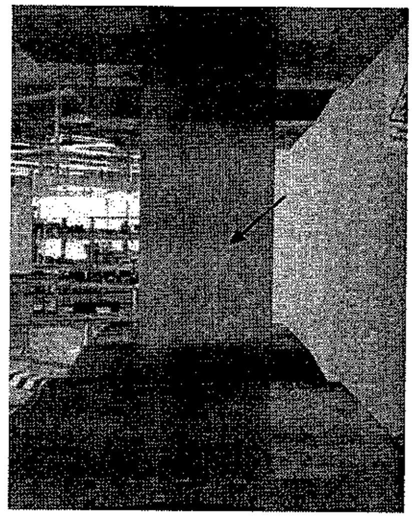

(a) CFRP laminate test setup (b) Failure mode of CFRP laminate

Figure 3.16 Test setup and failure mode of CFRP laminates

3.3.7 Test Setup and Instrumentation

The beam specimens were placed onto the support subjected to static load as shown in Figure 3.17. All the beams were tested to failure under four points loading using a Universal Testing Machine (UTM) of 500 kN. A spreader beam was used to transfer the load to the test specimens through two loading points at 500 mm apart.

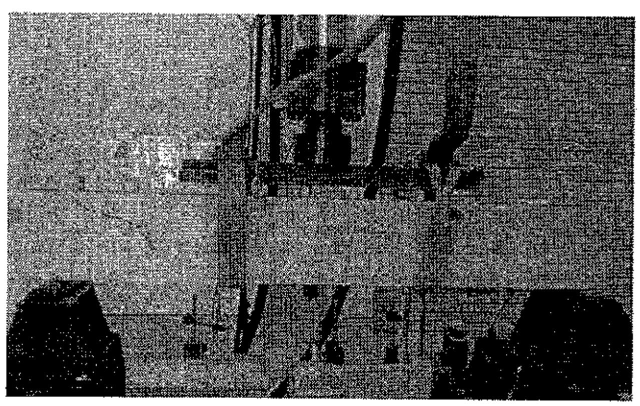

Figure 3.17 Test setup of control beam

3.3.7.1 Linear Variable Displacement Transducer (LVDT)

The beams deflection were monitored by three (3) numbers of LVDTs of 100 mm and 50 mm placed at the bottom soffit of the beams with a distance of 300 mm each. This is to measure the displacement of the beams. Figure 3.18 illustrates the location of the LVDTs at the bottom soffit of the beam.

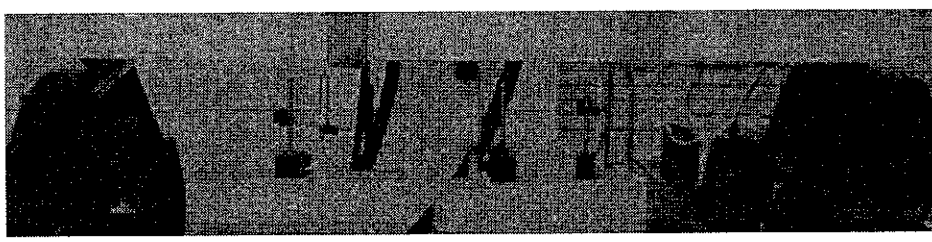

Figure 3.18 LVDTs at the bottom soffit of beam

3.4 Summary

In this chapter, the methodologies used in this research including numerical analysis and experimental investigation were discussed. Detail explanation of the experimental investigation was presented herein while the methodology of numerical analysis was presented in detail in Chapter 4.

CHAPTER 4

FINITE ELEMENT MODELLING

4.1 Introduction

This chapter presents the details of a numerical simulation analysis. The numerical analyses carried out in this study are based on a commercial package, ATENA (Cervenka & Cervenka, 2002). In this study, FE modelling was performed using 2D models on plane stress elements. The numerical models were developed to simulate the full scale RC beams contained small and large openings as well as strengthening using CFRP laminates. From the various FE software's such as ABAQUS, ANSYS, ADINA and DIANA; ATENA 2D is adopted as it is specialized in simulating experimental testing results for RC structures. This chapter focuses mainly on the construction of the numerical models with the applications of the correct material models and numerical procedures while details and results of the studies are presented in Chapter 5 and 7.

4.2 ATENA 2D

A 2D simplified version of ATENA 3D is known as ATENA 2D. It is a unique software for realistic 2D simulation of RC structures for engineers similar as ATENA 3D. Due to the user friendly environment, various analyses can be performed which include push over analysis, verify the load-carrying capacity of complicated reinforcement details, check crack widths or deflections by taking into account all important phenomena of RC materials, such as concrete cracking, crushing, reinforcement yielding or creep and shrinkage.

Furthermore, the results can be visualized even while during the analysis. This program also includes mesh generation capabilities for 2D meshes. In addition, ATENA has the ability to evaluate internal moments, shear and normal forces, also for solid elements. Arbitrary quantity can be displayed along a predefined section using the CUT feature of ATENA 2D (V. Cervenka & J. Cervenka, 2006).

4.2.1 Plane Stress

In 2D FE analysis, the models in this study were modelled as plane stress elements. Plane stress is defined to be a state of stress in which the normal stresses, σ_z and the shear stresses σ_{xz} and σ_{yz}, directed perpendicular to the x-y plane are assumed to be zero (UCSB College of Engineering, n.d.). All loading and deformation are restricted to this plane (Tarallo & Mastinu, n.d.). In terms of loading and boundary conditions, loadings may be point forces or distributed forces applied over the thickness, *h* e.g. of a plate as shown in Figure 4.1 whereas the supports may be fixed points or roller supports, as illustrated in Figure 4.2, respectively.

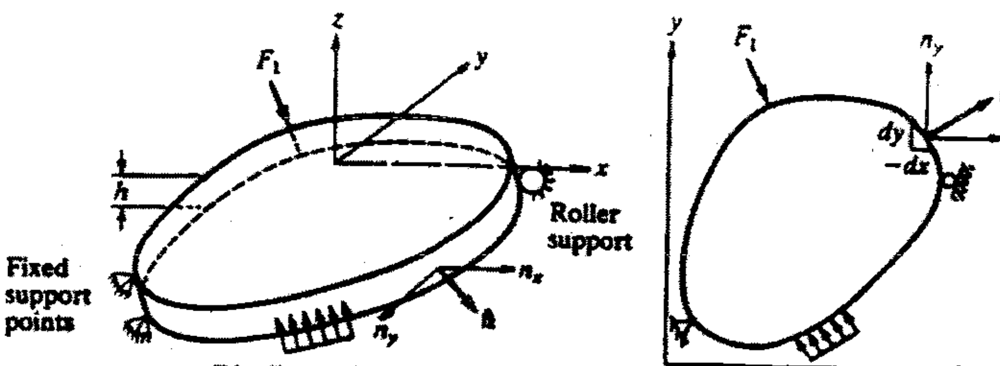

Figure 4.1 Loading conditions of plane stress system in 2D (UCSB College of Engineering, n.d.)

Figure 4.2 Support conditions of plane stress system (UCSB College of Engineering, n.d.)

4.2.2 Material Models

The program system ATENA offers a variety of material models for different materials and purposes. The most important material models in ATENA for RC structure are concrete and reinforcement. These advanced models take into account all the important aspects of real material behaviour in tension and compression (Cervenka et al., 2010).

4.2.2.1 Modelling of Concrete (CCSbetaMaterial)

The concrete model used for the numerical investigation is the SBETA constitutive model (Cervenka et. al., 2010) for 2D plane stress elements that is characterized by:

(i) Non-linear behaviour in compression, including hardening and softening;

(ii) Fracture of concrete in tension based on non-linear fracture mechanics

(iii) Biaxial strength failure criterion

(iv) Reduction of compression strength after cracking

(v) Tension stiffening effect

(vi) Reduction of shear stiffness after cracking;

(vii) Rotated crack direction

Where a perfect bond between concrete and reinforcement is assumed within the smeared crack concept.

The non-linear behaviour of concrete in the biaxial stress state was described in terms of effective stress and equivalent σ_c^{ef} uniaxial strain ε^{eq} (Cervenka et al., 2010). The equivalent uniaxial strain ε^{eq} can be considered as the strain that is formed from the stress σ_{ci} in a uniaxial test with the modulus of elasticity E_{ci} along the direction, *i*. For example,

$$\varepsilon^{eq} = \frac{\sigma_{ci}}{E_{ci}} \tag{4.1}$$

A biaxial stress failure criterion based on Kupfer et al (1969) was adopted in this model. The failure boundaries of the four stress states include (i) compression-

compression, (ii) tension-compression, (iii) compression-tension and (iv) tension-tension and are expressed in the following equations. In the compression-compression stress state, the compressive strength $f'_c{}^{ef}$ is:

$$f_c'^{ef} = \frac{1+3.65a}{(1+a^2)} f'_c \tag{4.2a}$$

$$a = \frac{\sigma_{c1}}{\sigma_{c2}} \tag{4.2b}$$

Where σ_{c1} and σ_{c2} are the principal stresses in concrete, and f'_c is the uniaxial concrete cylinder strength. Meanwhile, for the tension-compression stress state, the compressive strength $f'_c{}^{ef}$ can be expressed as:

$$f_c'^{ef} = r_{ec} f'_c \tag{4.3a}$$

$$r_{ec} = 1+5.3278 \frac{\sigma_{c1}}{f'_c} \tag{4.3b}$$

Where r_{ec} is the reduction factor of the compressive strength in a principal direction due to tensile stress in the other principal direction and it falls between the range of 0.9 and 1.0, i.e. $0.9 \leq r_{ec} \leq 1.0$. Likewise, for compression –tension stress state,

$$f_t'^{ef} = \left(1-0.8\frac{\sigma_{c2}}{f'_c}\right) f'_t \tag{4.4}$$

Where f'_t is the uniaxial tensile strength. Furthermore, tensile strength was assumed to be constant in tension-tension stress state and is equal to the uniaxial tensile strength f'_t, i.e.

$$f_t'^{ef} = f't \tag{4.5}$$

The concrete failure criterion suggested by Kupfer et al. (1969) is illustrated in Figure 4.3.

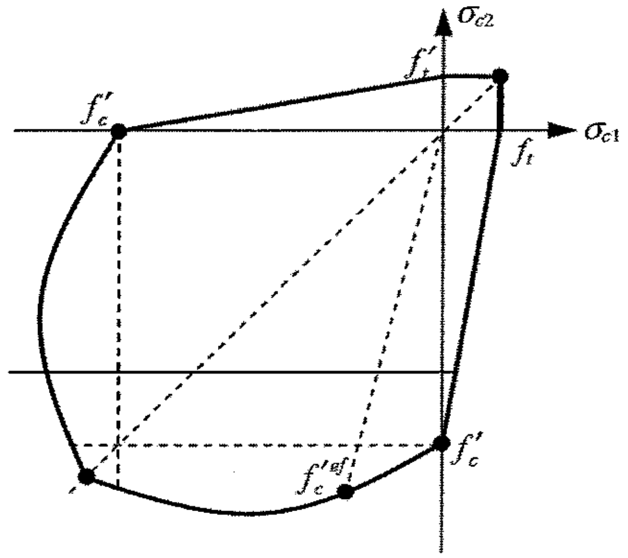

Figure 4.3 Biaxial failure function for concrete in ATENA (Cervenka & Cervenka, 2002)

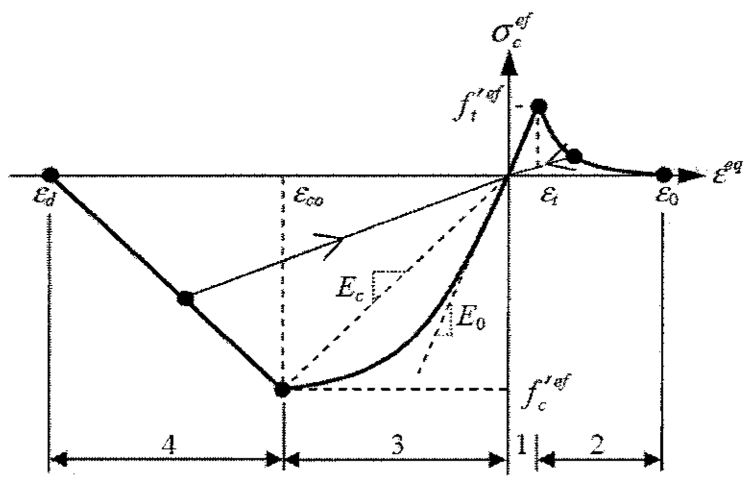

Figure 4.4 Uniaxial stress-strain relationship for concrete in ATENA (Cervenka & Cervenka, 2002)

The biaxial stress state as exhibited in Figure 4.3 was used to determine the peak values of the uniaxial stress-strain relationship of concrete which is depicted in Figure 4.4. For discussing the behaviour of concrete, it can also be divided into four different states which include (i) tension before cracking, (ii) tension after cracking, (iii) compression before peak stress and (iv) compression after peak stress. In state (i) the behaviour of concrete in tension without cracks is assumed to be linearly elastic as described in (4.6a), which is applicable to the limits defined in (4.6b)

$$\sigma_c^{ef} = E_0 \varepsilon^{eq} \tag{4.6a}$$

$$0 \leq \sigma_c^{ef} \leq f_t'^{ef} \tag{4.6b}$$

Where σ_c^{ef} is the concrete stress whereas E_0 is the initial elastic modulus.

The second state occurs after the concrete cracks in tension. A fictitious crack model which was derived experimentally by Hordijk (1991) was used to describe the relationship between the normal stress in the crack σ and the crack opening displacement w as follows:

$$\frac{\sigma}{f_t'^{ef}} = \left[1+\left(\frac{3w}{w_c}\right)^3\right] \exp\left(-\frac{6.93w}{w_c}\right) - \frac{28w}{w_c} \exp(-6.93) \tag{4.7a}$$

$$w_c = 5.14 \frac{G_F}{f_t'^{ef}} \tag{4.7b}$$

Where w_c is the crack opening (crack width) at the complete release of stress while G_F is the fracture energy needed to produce a unit area of crack surface. The displacement of crack opening, w can be computed as a total crack opening displacement within the crack band (Bazant and Oh, 1983), i.e.,

$$w = \varepsilon_{cr} L'_t \tag{4.8}$$

Where ε_{cr} is the crack opening strain, which is equal to the strain normal to the crack direction in the cracked state after the complete stress release. L'_t is the band size of the element in tension. Figure 4.5 describes the exponential crack opening law, which was adopted in this analysis.

In the third state, the concrete is subjected to compression but before reaching to the peak stress. The stress-strain formula recommended by CEB-FIP Model Code 1990 (Cervenka et al., 2010) was adopted, namely:

$$\sigma_c^{ef} = f_c'^{ef} \left[\frac{\left(\frac{E_0}{E_c}\right)\left(\frac{\varepsilon}{\varepsilon_{co}}\right) - \left(\frac{\varepsilon}{\varepsilon_{co}}\right)^2}{1+\left(\frac{E_0}{E_c}-2\right)\left(\frac{\varepsilon}{\varepsilon_{co}}\right)} \right] \tag{4.9}$$

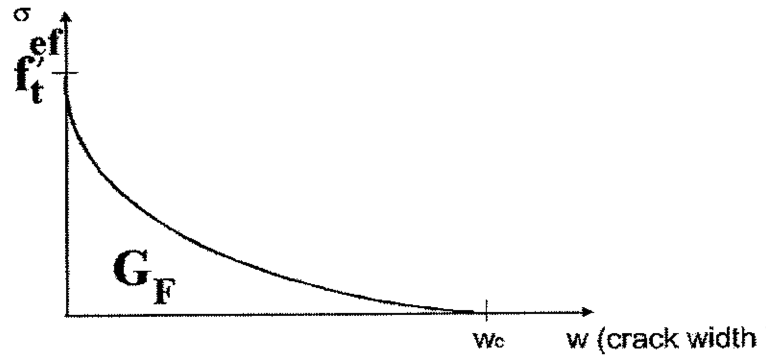

Figure 4.5 Exponential crack opening law (Cervenka et al., 2010)

Where ε represents the concrete strain; ε_{co} represents the strain at the peak stress $f'_c{}^{ef}$; E_0 represents the initial elastic modulus; and E_c represents the secant elastic modulus at the peak stress. Figure 4.6 illustrates the adopted stress-strain law in compression.

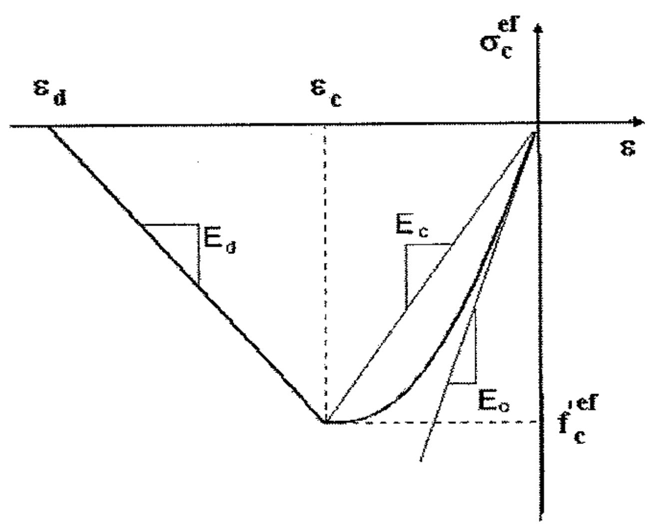

Figure 4.6 Compressive stress-strain diagram (Cervenka et al., 2010)

The fourth state is the post-peak range under compression. Concrete softening in compression was assumed linearly descending and a fictitious compression plane model was adopted in the NLFEA. This model is based on the assumption that compression failure is localized in a plane normal to the direction of compressive principal stress in which all post-peak compressive displacements and energy dissipation are localized in the plane. Van Mier (1986) confirmed experimentally that the displacement is independent of the size of the structure. Hence, the relationships of the limit compressive strain ε_d in terms of the concrete strain at the peak stress ε_{co}, the plastic displacement w_d and the band size of an element in compression L'_d can be expressed in the following equation:

$$\varepsilon_d = \varepsilon_{co} + \frac{w_d}{L'_d} \tag{4.10}$$

A value of w_d = 0.5 mm for normal concrete was adopted based on the experiments conducted by Van Mier (1986). Figure 4.7 explains the adopted softening displacement law in compression.

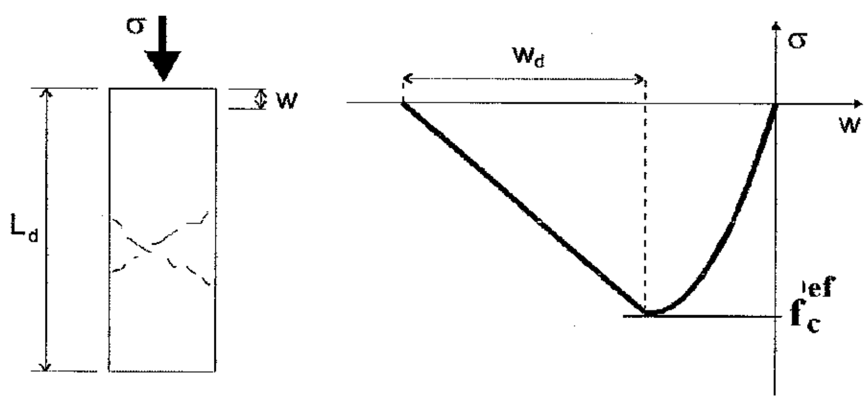

Figure 4.7 Softening displacement law in compression (Cervenka et al., 2010)

The analyses have also justified the unloading and later the reloading of concrete. During unloading, the stress and strain follow a straight line from the last loading point on the concrete stress-strain curve to the origin. The unloading is illustrated in Figure 4.4. Subsequently after unloading, reloading takes place. The reloading follows the linear unloading path until the last loading point is reached and eventually the original stress-strain curve is then resumed.

The analysis of concrete model requires the following as inputs to the concrete models, namely cylinder strength f'_c, initial elastic modulus E_0, uniaxial tensile strength f'_t, fracture energy, G_F, and Poisson's ratio v. The default formulas of material parameters were taken as:

$$f'_c = -0.85 f'_{cu} \qquad \text{(MPa)} \tag{4.11}$$

$$E_0 = (6000 - 15.5 f'_{cu})\sqrt{f'_{cu}} \qquad \text{(MPa)} \tag{4.12}$$

$$f'_t = 0.24 f_{cu}^{2/3} \qquad \text{(MPa)} \qquad (4.13)$$

$$G_F = 0.000025 f'^{ef}_t \qquad \text{(MN/m)} \qquad (4.14)$$

$$v = 0.2 \qquad (4.15)$$

Despite the above, the concrete properties are dependent on local concrete properties and methods of concreting. 2D models for each beam were used. The concrete beams were modelled by 2D macro elements.

4.2.2.2 Modelling of Reinforcement, Stirrups and CFRP Laminates

Reinforcement modelling could be discrete or smeared. In this research, a discrete modelling of reinforcement, stirrups and CFRP were conducted. Discrete reinforcement is in the form of reinforcing bars and is modelled by truss elements (Cervernka et. al., 2010). Figure 4.8 shows the geometry of the truss elements. The shape functions in natural coordinate system are shown in the following equations.

$$N_1 = \frac{1}{2}(1\text{-}r) \qquad (4.16a)$$

$$N_2 = \frac{1}{2}(1+r) \qquad (4.16b)$$

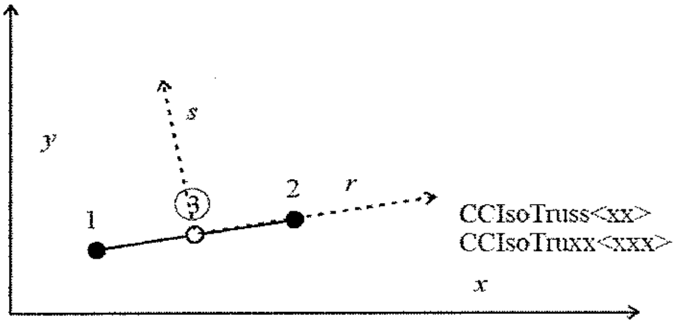

Figure 4.8 Geometry of CCIsoTruss<...> elements (Cervenka et al., 2010)

4.2.2.3 Modelling of Steel Plates

Steel plates were modelled by plane stress elastic isotropic. For linear isotropic material, plane stress state assumed that;

$$\sigma_z = \tau_{xz} = \tau_{yz} = 0 \tag{4.17a}$$

$$\gamma_{xz} = \gamma_{yz} = 0 \tag{4.17b}$$

as shown in Figure 4.9. The state of plane stress occurs in a thin plate subjected to forces acting in the mid-plane of the plate (Cervenka et. al., 2010). In addition, the state of plane stress also occurs on the free surface of a structural element or at any point of the surface not subjected to an external force.

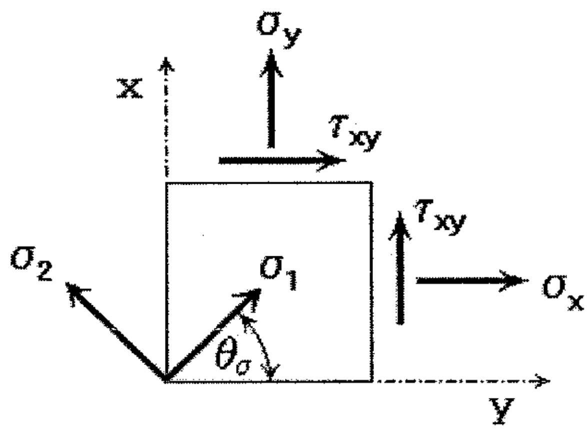

Figure 4.9 Components of plane stress state (Cervenka et al., 2010)

4.2.3 Material Properties

The material properties of concrete, steel reinforcement, CFRP and steel plates are presented as follows:

4.2.3.1 Concrete

In ATENA, concrete is represented by the SBETA material model. The physical properties of concrete are given in Table 4.1. The values are generated in ATENA for concrete compressive strength, $f_{cu} = 35$ MPa which used in this study.

4.2.3.2 Steel Reinforcement, Stirrups and CFRP Laminates

The input properties of steel reinforcement, stirrups and CFRP laminates in ATENA were obtained from the tensile tests conducted in the experimental program. The steel

Table 4.1 Material properties of concrete

Material Type		SBeta Material	
Elastic modulus	E_c	32.29	GPa
Poisson's ratio	ν	0.2	-
Compressive strength	f_c	29.75	MPa
Tensile strength	f_t	2.568	MPa
Type of tension softening		Exponential	
Fracture Energy	G_f	64.2	N/m
Crack Model		Rotated	

reinforcement, stirrups and CFRP laminates were modelled by a single straight line in a discrete manner (bar elements). Multi-linear law was adopted for the steel reinforcement, stirrups and CFRP in this study, which is shown in Figure 4.10. This law allows to model all four stages of steel behaviour which were obtained from the experimental results; namely elastic state, yield plateau, hardening and fracture. The bond between steel reinforcement and concrete was assumed as perfect bond. The material properties of steel reinforcement, stirrups and CFRP in this study are tabulated in Tables 4.2 – 4.4, respectively.

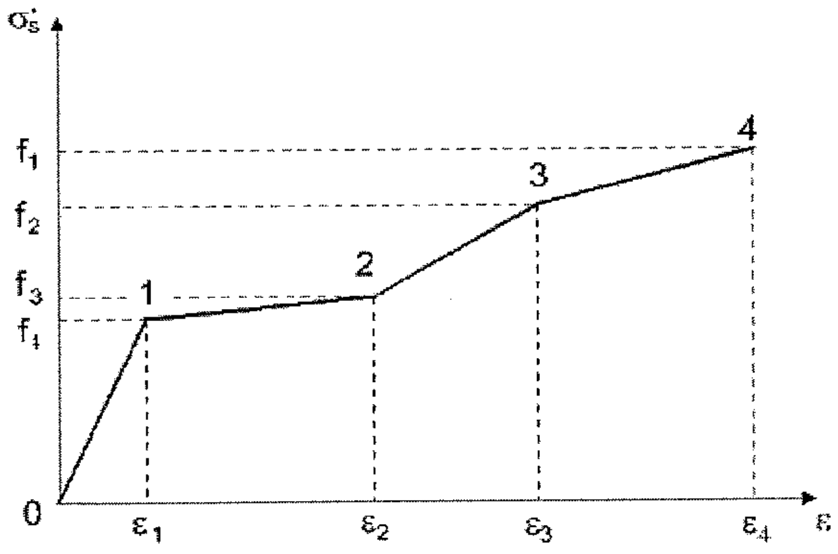

Figure 4.10 Multi-linear stress-strain law for reinforcement (Cervenka et al., 2010)

Table 4.2 Material properties of steel reinforcement

Material Type		Reinforcement	
		multilinear	
Elastic modulus,	E	210	GPa
Yield strength,	σ_y	410	MPa
Hardening		linear	

Table 4.3 Material properties of stirrups

Material Type		Reinforcement	
		multilinear	
Elastic modulus	E	240	GPa
Yield strength	σ_y	280	MPa
Hardening		linear	

Table 4.4 Material properties of CFRP

Material Type		Reinforcement	
		multilinear	
Elastic modulus	E	170	GPa
Yield strength	σ_y	930	MPa
Hardening		linear	

4.2.3.3 Steel Plates

The steel plates were assumed as elastic-perfectly plastic. The elastic modulus, E was 210000 MPa and Poisson's ratio, ν of 0.3, as summarized in Table 4.5. Figure 4.11 illustrates the bilinear stress-strain law adopted for the steel plates.

Table 4.5 Material properties of steel plates

Material Type		Reinforcement	Steel plates
		bilinear	
Elastic Modulus	E	210	GPa
Poisson's ratio	ν	0.3	
Hardening		perfectly plastic	

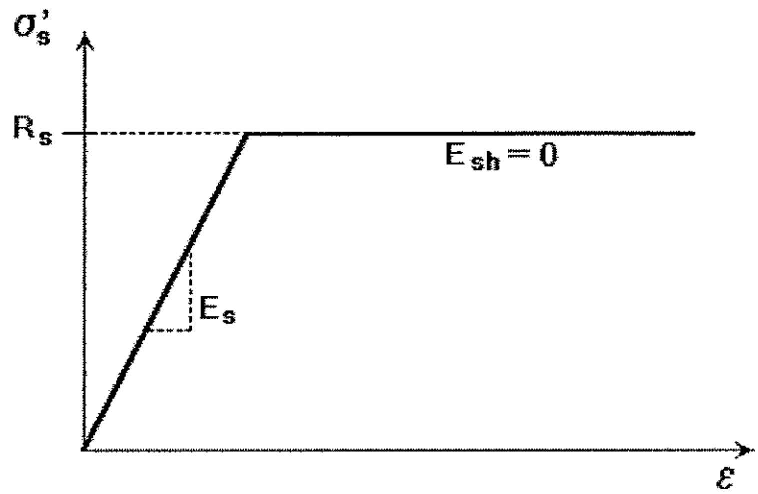

Figure 4.11 Bilinear stress-strain law (Cervenka et al., 2010)

4.2.4 CFRP/Concrete Interface

A bond slip between CFRP composites and concrete interface was considered in the analyses. The bond slip model developed by Lu et al., 2005 which is shown in Figure 4.12 was adopted. This bond slip model was considered as an accurate bond slip model that can be incorporated into the FE analysis. The mechanical behaviour of the CFRP/concrete interface was modelled as a relationship between the local shear stress, τ and relative displacement, s between the CFRP laminate and the concrete. The (τ –s) relationship was discussed in detail in section 2.12.7.

The difference in relative displacement between the concrete and CFRP laminate represents the slip at the interface. The interface elements are considered to act only in the directions parallel to the main fiber reinforcements. In ATENA, the bond slip relation of CFRP and concrete was defined in the 'bond for reinforcement' material type. In the bond for reinforcement, the material properties are defined and calculated based on the bond slip model equations by Lu et al., 2005. The widths of CFRP, b_w used in this study including 35, 45, 80 and 100 mm. Details of the bond stress and slip for the various CFRP widths, b_w are summarized in Table 4.6.

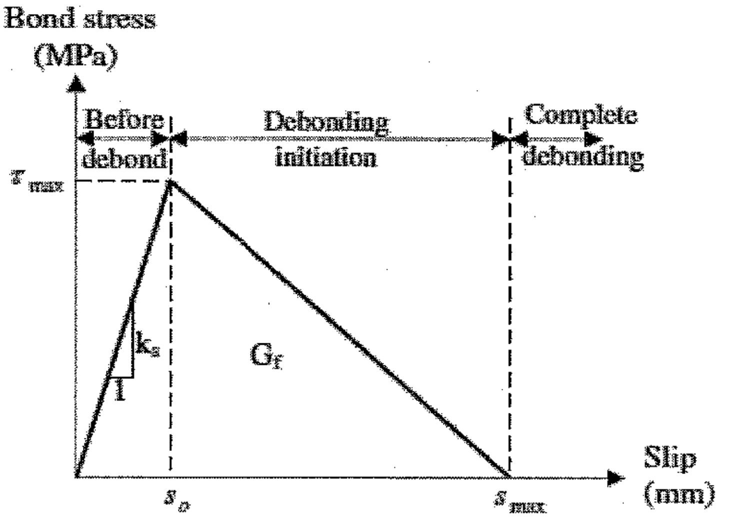

Figure 4.12 Bond slip model (Godat et al., 2012; Lu et al., 2005)

Table 4.6 Slip and bond stress values of CFRP width, b_w of 35, 45, 80 and 100 mm

CFRP width, b_w (mm)	Point (P)	Slip (m)	Bond Stress (MPa)
35	P1	0	0
	P2	5.64E-05	4.34
	P3	2.90E-04	0
45	P1	0	0
	P2	5.4E-05	4.14
	P3	2.75E-04	0
80	P1	0	0
	P2	4.56E-05	3.50
	P3	2.34E-04	0
100	P1	0	0
	P2	4E-05	3.20
	P3	2.1E-04	0

4.2.5 System of Meshing

After the material properties were specified in the numerical simulation, the structure was discretized into a mesh type of four-node isoparametric plane stress quadrilateral element as shown in Figure 4.13. Plane quadrilateral elements in ATENA are coded in a group of elements CCIsoQuad<xxxx>...CCIsoQuad<xxxxxxxxx>. The string in < > describes present element nodes. These are isoparametric elements integrated by Gauss integration at 4 or 9 integration points for the case of bilinear or bi-quadratic interpolation , i.e. for elements with 4 or 5 or more element nodes, respectively. This type of elements is suitable for plane 2D as studied in this research. The FE meshes for several beam specimens in ATENA are shown in Figure 4.14.

The FE mesh was automatically generated by the program and the size of each concrete element was 0.025 x 0.025 m (Cervenka et al., 2003; Kabele et al., 2010). For convergence, it is recommended to use a fine uniform mesh (element size of 0.025 m for quadrilateral) (Kabele et al., 2010) throughout the beam in order to minimize the effect of FE discretization on the formation and propagation of cracks, namely the inclined shear ones. The mesh size should be similar or comparable to the aggregate size to fulfill the basic assumption of modelling the concrete as a continuum (Kabele et al., 2010). For other 2D macro-elements, the size of each element was 0.06 m. The meshing of the reinforcement is a special case compared to the macro-elements. No mesh of the reinforcement is needed because the reinforcements were modeled in a single straight line in a discrete way. Table 4.7 summarizes the FE mesh properties including the FE type, element size, element shape smoothing and optimization used in the analysis. The analyzed beam models with the total number of nodes and elements are summarized in Tables 4.8 and 4.9, respectively.

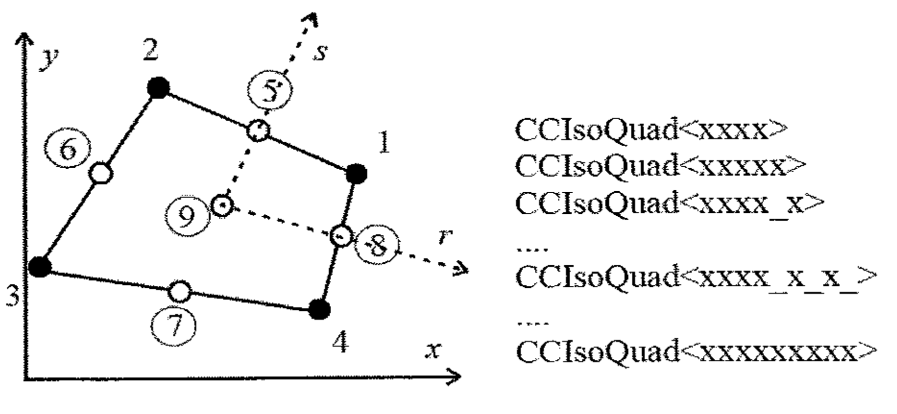

Figure 4.13 Geometry of CCIsoQuad<...>elements (Cervenka et al., 2010)

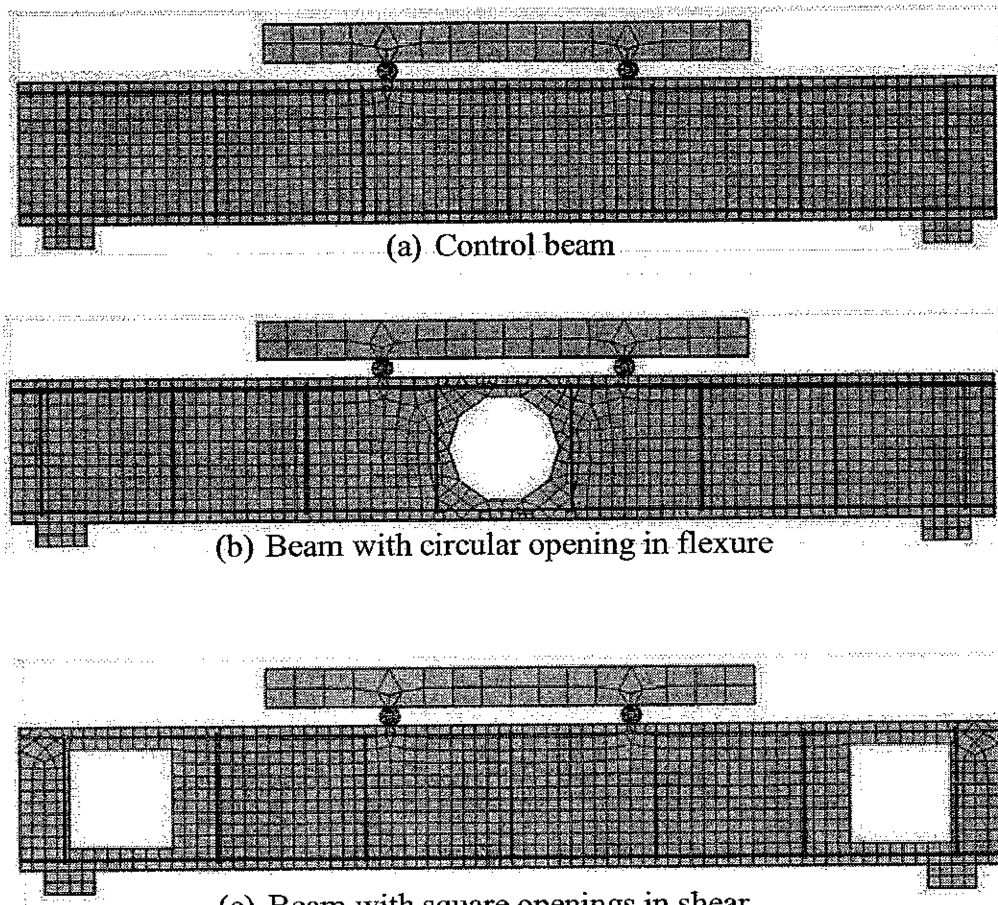

(a) Control beam

(b) Beam with circular opening in flexure

(c) Beam with square openings in shear

Figure 4.14 Finite element meshes for RC beam specimens in ATENA

Table 4.7 Finite element mesh properties

Finite Element Type	Quadrilateral (CCIsoQuad)	Unit
Element Size (Concrete)	0.025	m
Element Size (Others)	0.06	m
Element Shape Smoothing	on	
Optimization	Sloan	

Table 4.8 Total number of nodes and elements of analyzed beam models (control and un-strengthened beams)

Beam No.	Beam models	Openings	Total no. of nodes	Total no. of elements
1	CB	-	1479	1068
2	CF	1	1459	1010
3	SF	1	1443	1004
4	LEF	1	1265	796
5	LRF	1	1293	810
6	C0S	2	1370	934
7	S0S	2	1394	944
8	S0.5dS	2	1382	940
9	CdS	2	1436	964
10	SdS	2	1394	940
11	CdS1	1	1510	1010
12	SdS1	1	1496	1004
13	S1.5dS1	1	1481	986

Table 4.9 Total number of nodes and elements of analyzed beam models (strengthened beams)

Beam No.	Beam Models	Openings	Total no. of nodes	Total no. of elements
1	CF-S	1	1623	1010
2	SF-S	1	1506	1004
3	LEF-S	1	1339	796
4	LRF-S	1	1379	810
5	C0S-S	2	1561	934
6	S0S-S	2	1586	944
7	S0.5dS-S	2	1554	940
8	CdS-S	2	1609	964
9	SdS-S	2	1558	940
10	CdS1-S	1	1613	1010
11	SdS1-S	1	1578	1004

4.2.6 Loading and Boundary Conditions

In terms of boundary conditions, simple support and complex support boundary conditions represent boundary conditions of Dirichlet types i.e. boundary conditions that prescribed displacements. Dirichlet boundary conditions, which are usually referred to as left-hand side (LHS) BCs. A simple form of such BCs are:

$$u_l = 0, \quad l \in <1, m>,$$

$$u_l = u_{l0}, \quad l \in <1, m>. \tag{4.18}$$

These kinds of BCs typically represent structural supports with no displacements (the first equation) or with prescribed displacements u_{l0} (the second equation) (Jendele & Cervenka, 2009). Displacement boundary conditions are needed to restrain the models in order to obtain a unique solution.

To make sure that the FE models act similar as the experimental beams, boundary conditions need to be applied at the location where the supports and loading exists. In terms of symmetry, the beams were modelled having the full scale (exact beam size) as adopted in the experimental program in which the behaviour of beams with openings located in mid-span and in shear can be analyzed and compared. As in the experiment, loads and vertical support constraints were applied through steel plates to avoid local concrete crushing. The steel plates were assumed perfectly bonded to concrete.

Figure 4.15 shows the geometry and boundary conditions for the supports. At support 1, the support was considered as fixed support with constraints in both X and Y direction while for support 2, the support was restricted in Y direction only. The boundary lines between the steel plates and concrete were formed by connecting two joints, as shown in Figures 4.16 and 4.17, respectively. Loading was applied by prescribed vertical displacement at the middle point on top of the loading plates in constant increments of 0.1 mm as shown in Figure 4.18.

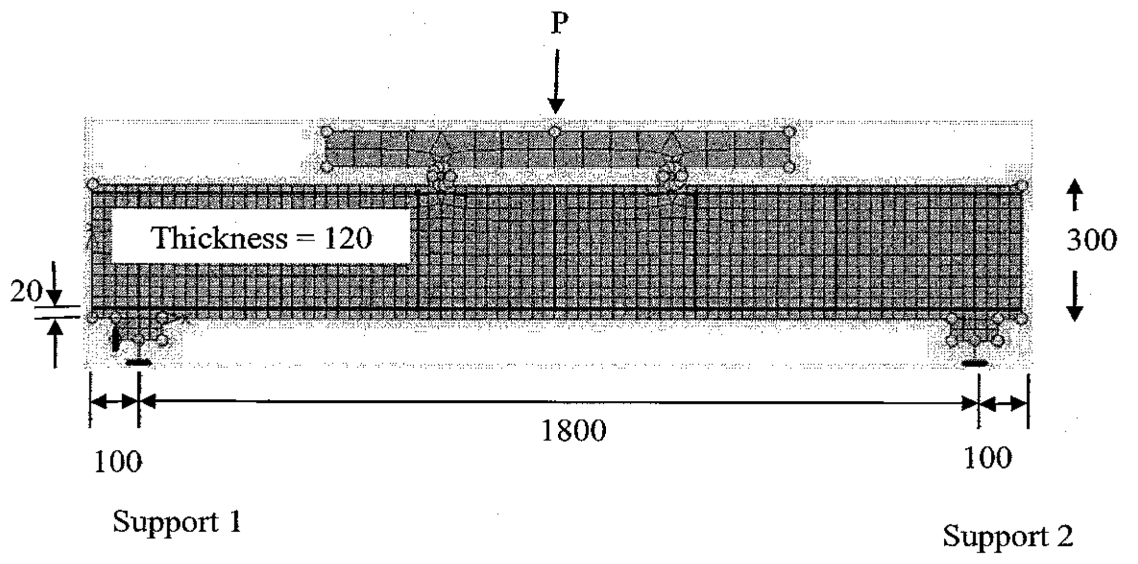

Figure 4.15 Geometry and boundary conditions of beam (dimensions shown in mm)

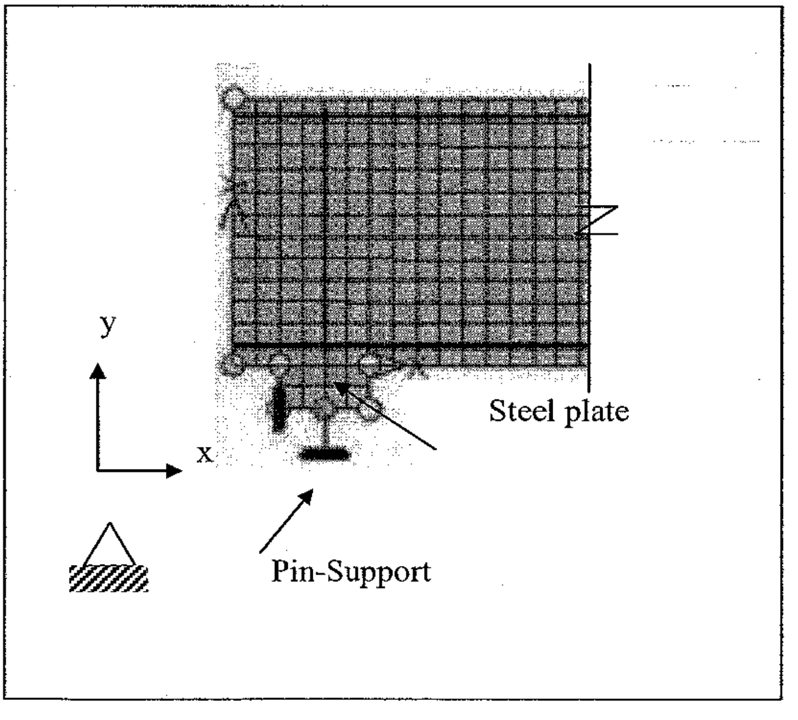

Figure 4.16 Details at support 1

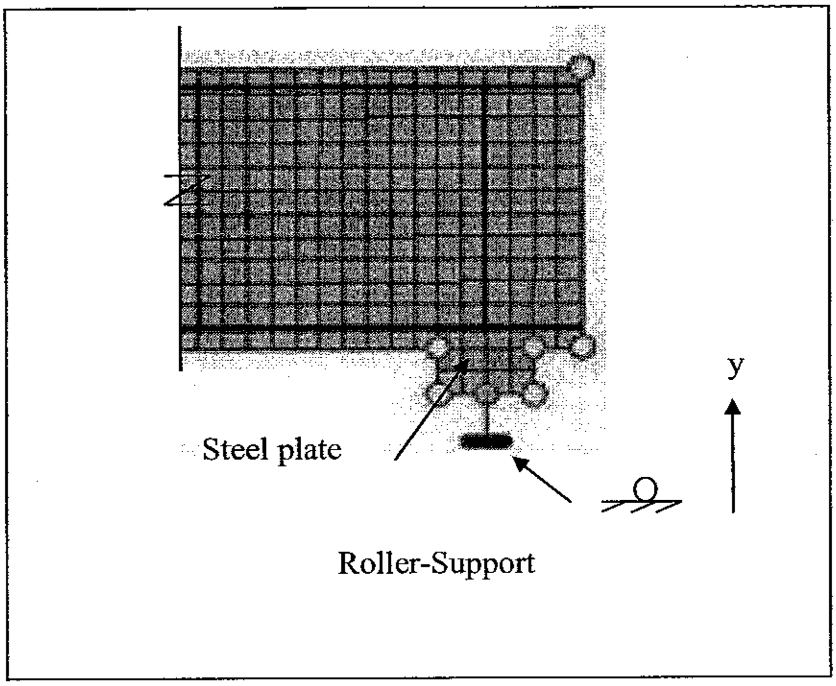

Figure 4.17 Details at support 2

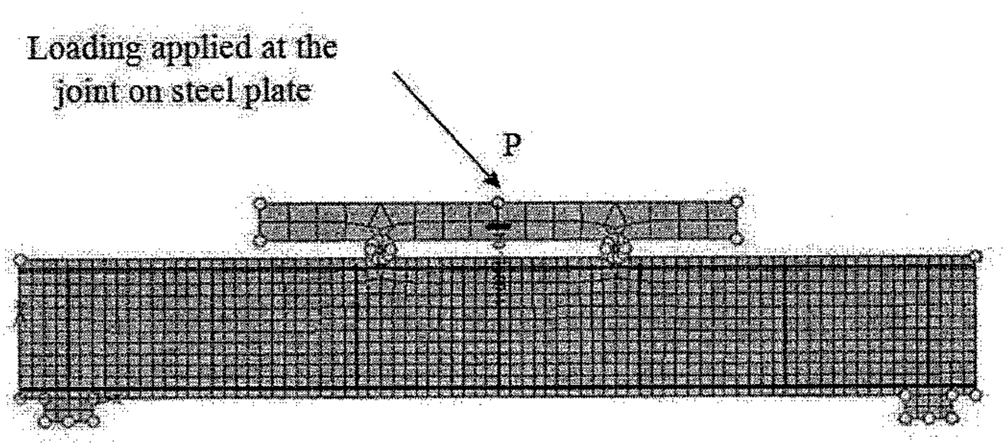

Figure 4.18 Boundary condition at the loading plate

4.2.7 Monitoring Points

During non-linear analysis in ATENA, it is useful to monitor forces, displacements or stresses in the model. The monitored data can provide important information about the state of the structure (Cervenka, 2001). Monitoring points serve to monitor the results during analyses which have similar meaning as measuring gauges in laboratory experiments. There are two kinds of monitoring points: (1) in nodes and (2) integration points. In nodes; external forces, reactions and displacements can be monitored. While in integration points; stress, strain, temperature, initial stress and strain, body forces and crack attributes can be monitored. The locations of the monitors are depicted on screen graphically as shown in Figure 4.19 in order to record the overall beam response (Cervenka, 2001).

As shown in Figure 4.19, the first monitoring point in a node (i) was added near the joint where the prescribed displacements were applied. The second component (y-direction) of nodal applied forces was monitored at this point. Meanwhile, the second monitoring point in a node (ii) was located at the middle of the beam near the bottom surface, where the largest vertical displacements were expected. The second component (y-displacement) of nodal displacements was monitored at this location. These two monitoring points provide the results of load-displacement curve during the non-linear FE analysis.

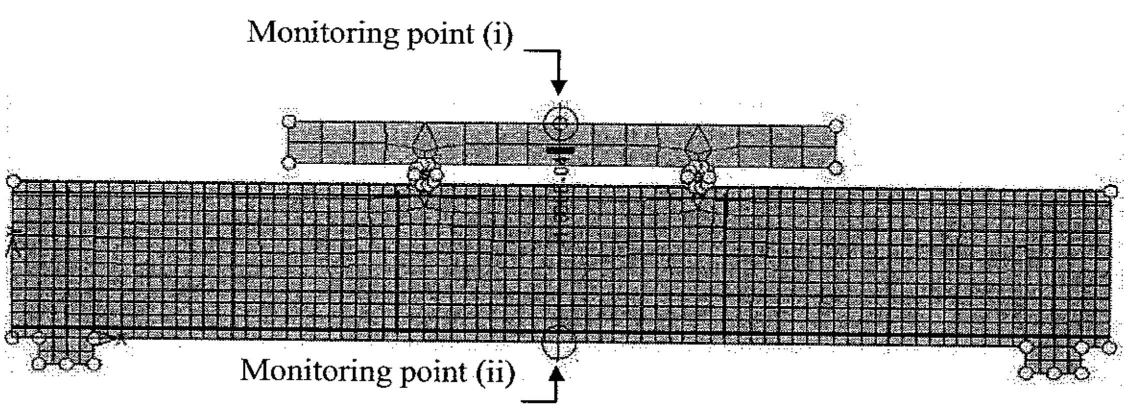

Figure 4.19 Monitoring points at top loading point and bottom of beam

4.2.8 Non-linear Solution

The greatest part of ATENA is the simplest way of solving the non-linear structural behaviour through FE method and its incremental loading criteria (Cervenka et. al., 2010). Various methods are available in ATENA for solving non-linear equations such as Linear Method, Newton-Raphson Method, Modified Newton-Raphson Method, and Arc Length Method. In this study, the Full Newton-Raphson Method is adopted.

In numerical analysis, Newton's method (or known as Newton Raphson Method) named after Issac Newton and Joseph Raphson is a method for finding successively better approximations to the roots of a real-valued function. The Newton-Raphson method is the true bridge between algebra (solving equations of the form $f(x) = 0$ and factoring) and geometry (finding tangent lines to the graph of $y = f(x)$) (Shiskowski & Frinkle, 2011). In addition, this method is based upon a knowledge of the tangent to the curve near the root. It is an "iterative" method in that it can be used repeatedly to continually improve the accuracy of the root. With the Newton-Raphson iterative formula, the iteration is begun with an initial estimate of the root, x_o, and continued using positive integer values of *n*, until a suitably accurate estimate of the position of the root is obtained. For e.g., if $f(x)$ has a simple root near x_n then a closer estimate to the root is x_{n+1} where as shown in Equation (4.19) (Engineering Mathematics, n.d.):

$$x_{n+1} = x_n - \frac{f(x_n)}{f'(x_n)} \tag{4.19}$$

4.2.8.1 Full Newton-Raphson Method

One approach of solving the non-linear solutions is to break the load into a series of load increments. The load increments can be applied either over several load steps or over several sub-steps within a load step. At the completion of each incremental solution, the program adjusts the stiffness matrix to reflect the non-linear changes in structural stiffness before proceeding to the next load increment.

The ATENA program overcomes this difficulty by using Full Newton-Raphson Method or Modified Newton-Raphson Method which drives the solution to equilibrium convergence (within tolerance limits) at the end of each load increment. In Full Newton-Raphson Method, it obtains the following set of non-linear equations:

$$\mathbf{K}(\underline{p})\Delta\underline{p} = \underline{q} - f(\underline{p}) \tag{4.20}$$

where $\underline{q}$ is the vector of total applied joint loads, $f(\underline{p})$ is the vector of internal joint forces, $\Delta\underline{p}$ is the deformation increment due to loading increment, $\underline{p}$ are the deformations of structure prior to load increment and $\mathbf{K}(\underline{p})$ is the stiffness matrix, relating loading increments to deformation increments.

The concept of solution non-linear equation set by Full Newton Raphson Method is illustrated in Figure 4.20. In Eq. (4.20), $\underline{q} - f(\underline{p})$ represents the out-of-balance forces during a load increment. The out-of-balance forces are the difference between internal forces at the end of the previous load step and the applied loads are evaluated in the Newton-Raphson Method. Then, a linear solution is performed in the program using the out-of-balance loads and checks for the convergence. If convergence criteria are not satisfied, the out-of-balance load vector is re-evaluated, the stiffness matrix is updated, and a new solution is attained. This iterative procedure continues until the problem converges (Cervenka et. al., 2010).

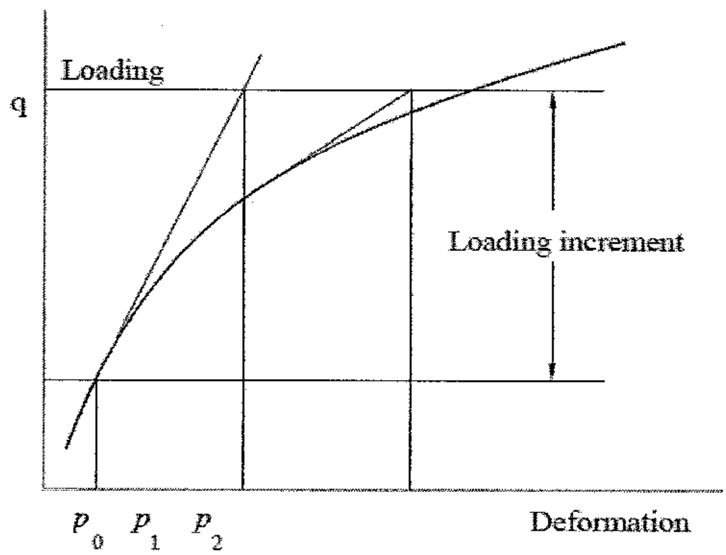

Figure 4.20 Full Newton Raphson Method (Cervenka et al., 2010)

In this study, the convergence of results is assumed to be taken care by ATENA using Full Newton-Raphson method to solve the non-linear behaviour of the full-scale beams and provide convergence at the end of each load increment within tolerance limits. Incremental displacement is gradually applied to the beam (displacement control). The values of the convergence tolerance limits (error tolerances) used in this study are set by default to 0.01 in ATENA as shown in Table 4.10. Four error tolerances are the limits for various criteria. The iteration stops when all criteria are satisfied. The error tolerances programmed in ATENA including displacement, residual, absolute residual and energy. The maximum number of iterations per loading increment used was 60. Line search was used in combination with the Newton-Raphson method in order to accelerate a convergence rate. Table 4.10 lists the solution parameters used in the FE modelling and analysis.

Table 4.10 Solution parameters

Solution Method	Newton-Raphson
Stiffness/update	Tangent/each iteration
Number of iterations	60
Error tolerance (displacement/residual/ absolute residual/energy)	0.01/0.01/0.01/0.0001
Line search	on, with iterations

4.3 Summary

The overall numerical analysis methodology is summarized in the following flow chart in Figure 4.21. The results of FE analysis are discussed in detail in Chapter 5.

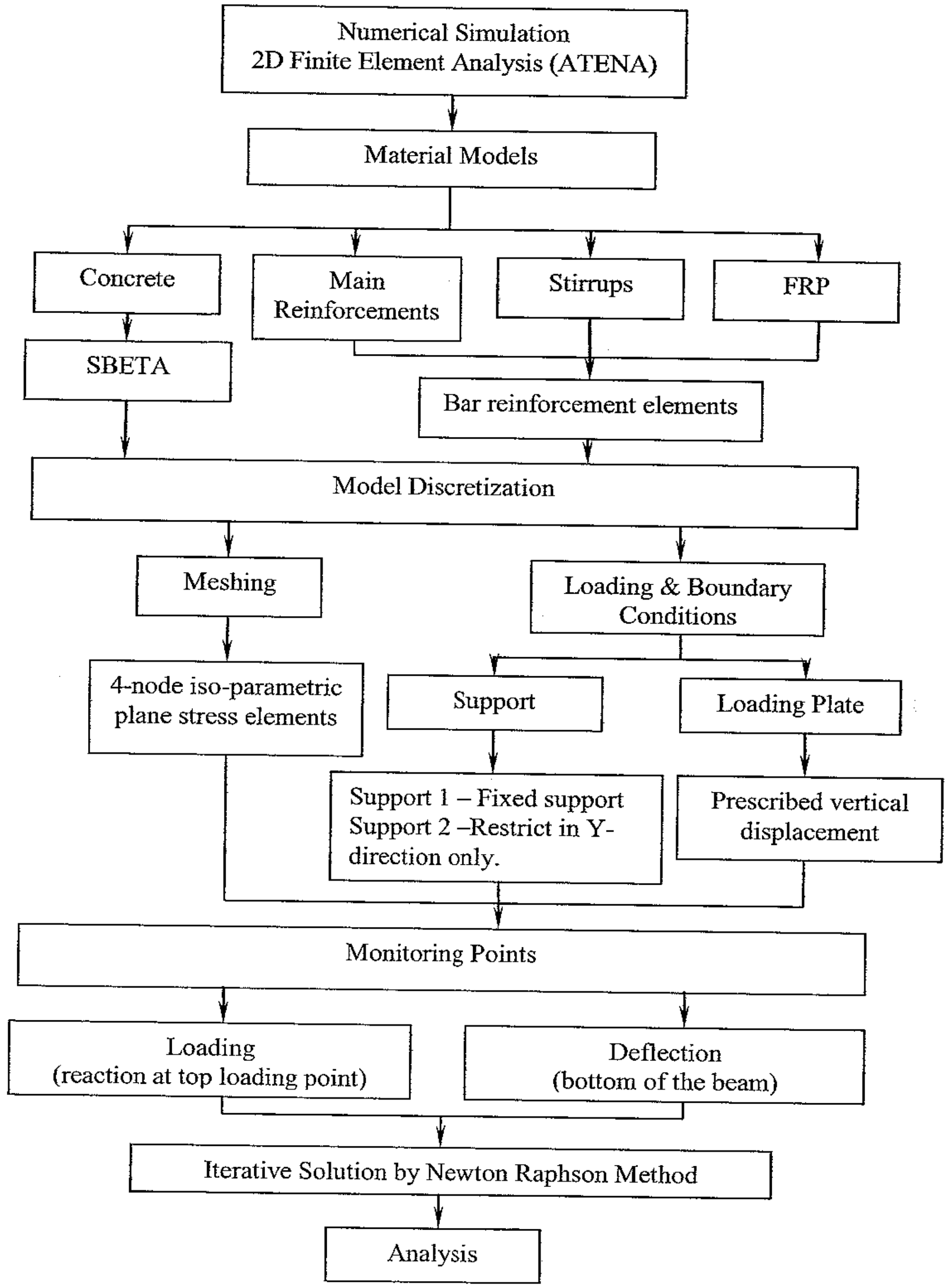

Figure 4.21 Flow chart of numerical analysis methodology

CHAPTER 5
RESULTS OF FINTE ELEMENT ANALYSIS

5.1 Introduction

This chapter presents and discusses the results of the numerical analysis using FE method of RC beams with different configurations of openings provided in bending and shear zones. The first part of the chapter discussed the effects of size and configuration of openings on load-deflection behaviour, crack patterns, stress and strain behaviour. In the second part, a number of possible strengthening options using CFRP were modelled and the results are discussed in terms of expected re-gain of the loss of capacity due to size, shape and configuration of openings. The purpose of several strengthening options was to choose the most effective strengthening options for simulation using experimental testing. All numerical calculations were performed using a non-linear FE program, ATENA in which more details are given in Chapter 4.

5.2 Investigating the Size, Shape and Configuration of Opening in Flexure Zone

The openings of various sizes, shapes and configurations considered in this study include circular, square, large rectangular and elliptical openings were modelled and the results are discussed in the following sub-sections. To achieve objectives no.1 (i) and 1(ii), the effects of openings on the structural behaviour of RC beams using FE analysis are discussed in terms of load-deflection behaviour and crack patterns in sections 5.2.1 – 5.2.3.

5.2.1 Generalized Load-Deflection Behaviour of RC Beam

Generalized load-deflection behaviour of all beams is illustrated in Figure 5.1 which is divided into four segments. From section (0)–(1), a linear line is observed indicating elastic behaviour. The linear elastic behaviour halted at a point (1) of which is the initiation of first crack, which may be called first yield. After point (1), there is a little drop in stiffness which lasted until second crack at point (2), which may be known as second yield. At that point, the beam was fully yielded. From section (2)-(3), the deflection was increased with almost constant load (plateau). In section (3)-(4), beam softening takes place until rupture at the point (4).

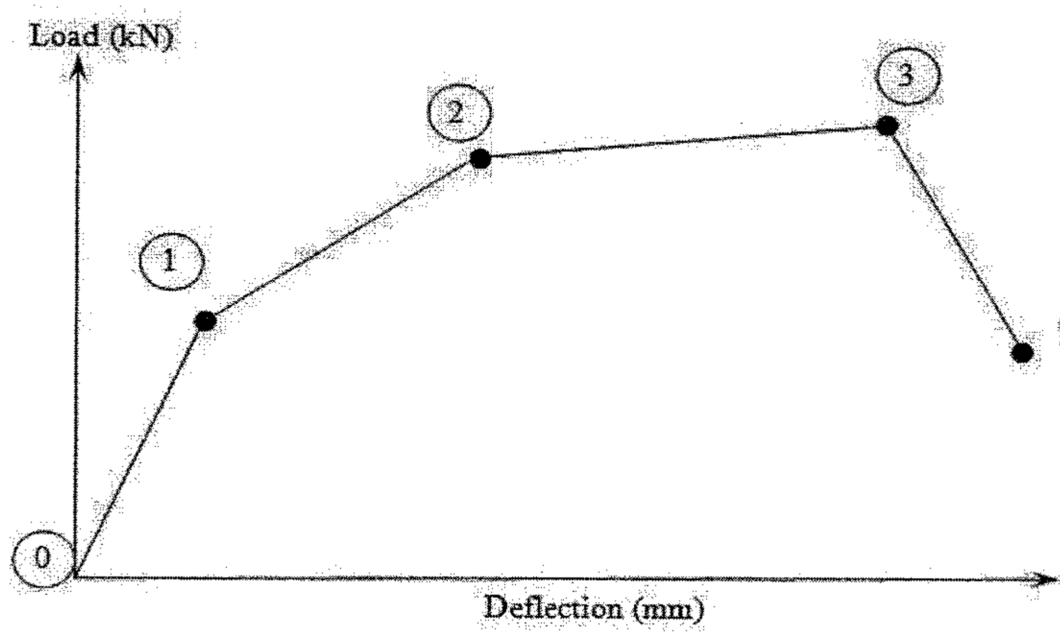

Figure 5.1 Generalized behaviour of load-deflection of a RC beam

5.2.2 Load-Deflection Behaviour of Un-Strengthened Beams

The numerical analysis using ATENA has the capability to produce results in the form of load-deflection, crack pattern, stress and strain contours. In this sub-section, load-deflection behaviour of un-strengthened beams as obtained from FE analysis has discussed, results are given in Table 5.1 and plotted in Figure 5.2. In the load-deflection curves, three points were identified, which are yielding point 1, yielding point 2 and ultimate point. The yielding load 1, P_{y1} is defined as the load recorded at the initiation of the first crack; yielding load 2, P_{y2} is defined as the load recorded at the initiation of the second crack, where the beam yielded and the maximum load recorded after passing the yield point is termed as ultimate load, P_u (Shafiq, 1987). The deflections measured at P_{y1}, P_{y2} and P_u are also denoted by Δ_{y1}, Δ_{y2} and Δ_u respectively. Effects of openings due to the size, shape and location are discussed in the following sub-sections and compared with the corresponding control beam.

5.2.2.1 Control beam (CB)

FE analysis of control beam is plotted in Figure 5.2 predicted the load-deflection behaviour as the elastic-plastic behaviour, which resembles to the load-deflection behaviour of a typical RC beam that could be obtained through experimental testing. It was obtained that until the initiation of the first crack that started at load, P_{y1} of 40.8 kN; the beam behaved as a stiffer beam because at this load the deflection Δ_{y1} was achieved as 0.7 mm. After the initiation of the first crack, a small dip in the load-deflection curve was observed as this may be due to the widening of cracks. Then, the beam has shown some hardening effects with a reduction of stiffness until the beam yielded at yield load 2, P_{y2} of 77.0 kN with a deflection Δ_{y2} of 3.9 mm. After the beam has yielded, it observed almost plateau load-deflection behaviour, at this stage the ultimate load, P_u was found as 86.7 kN at a deflection, Δ_u of 7.8 mm. Just after passing in this zone, the ultimate load of beam showed rapid softening and the failure was happened at the deflection of 7.6 mm.

5.2.2.2 Effects of Circular Opening, CF

A similar trend of load-deflection behaviour discussed for the control beam, CB was observed for the beam CF, which is plotted in Figure 5.2. The stiffness of the beam CF in the linear elastic region was found lower as compared to that obtained in beam CB. The reduction in stiffness may be due to the presence of circular opening. The linear elastic region halted at a point where the initiation of first crack of beam began to appear at load, P_{y1} of 43.0 kN at a deflection of 1.3 mm. After the first crack, the beam stiffness further reduced (as the load-deflection curve bent towards horizontal axis) with the effects of hardening until the beam yielded at second yield load, P_{y2} of 78.6 kN at a deflection of 3.9 mm. After that, the beam deflection rapidly increased by a constant increment of load until the ultimate load, P_u of 86.3 kN at a deflection of 8.4 mm. Eventually after the ultimate load was attained, softening of beam happened and caused a rupture of the beam.

The numerical analysis has shown that the circular opening provided in bending zone did not cause significant loss in the structural capacity, about less than 1%. It is due to the reason that the concrete is cut within the low stress zone within the section, which is the middle part of the section. It also increased the ductility of the beam, which means openings have provided some relief to the stress distribution. Hence, strengthening is not necessary for small opening provided in the mid-span. This shows that circular opening is a post-planned condition in which can be provided in the mid-span region of an existing beam without effecting the beam strength.

5.2.2.3 Effects of Square Opening, SF

The load-deflection curve of beam SF which is plotted in Figure 5.2 exhibited similar behaviour as that shown by CB and CF. In the initial stage, the linear elastic region of beam SF was observed similar to that of beam CF until the initiation of first crack occurred at load, P_{y1} of 32.0 kN at a deflection of 0.8 mm. After passing the first crack, the beam stiffness was slightly reduced as compared to the beam CF. The possible reason for this may be due to the provision of square opening. The load continuously increased as deflection increased by the effects of hardening until the initiation of next crack at load, P_{y2} of 79.1 kN at a deflection of 4.0 mm. Subsequently, a constant increment of load was observed with the rapid increase of beam deflection until the ultimate load, P_u of 85.5 kN at a deflection of 7.3 mm was observed. Beyond that point, the beam also followed the similar trend and that of the beam CB.

The load-deflection results show that the presence of a square opening did not cause much reduction in the beam capacity, less than 2% despite of the presence of sharp corners. The possible reason may be due to concrete loss because of the opening within the low stress zone in the mid-span. Thus, it is suggested that no strengthening is needed for small opening provided in the mid-span. It means that small openings in the mid-span can also be provided even the beam is already constructed, which means by hacking.

5.2.2.4 Effects of Large Rectangular (LRF)/Elliptical (LEF) Opening

In a situation when large openings (rectangular or elliptical) were placed in the middle-third span of the beam, loading points were applied within the upper chord as shown in Figure 5.3. In this case, hypothetically the applied load is mostly distributed in the upper chord while the lower chord is expected to be much relieved or lightly stressed. With increase load, cracks from the upper chord tend to propagate from the middle span towards the solid ends which eventually caused the formation of cracks at the corners. Hence, the failure of the upper chord happened that resulted in failure of the whole system whereas the lower chord was not fully utilized. It is the reason that in the softening stage after the ultimate load that caused the load-deflection curve of beams LRF and LEF was quite different from the control beam, CB, as shown in Figure 5.2.

In the early stage of loading i.e. until 10 kN, beam LRF behaved elastically that follow the similar trend as showed by the beams CB, CF and SF as shown in Figure 5.2. The initiation of the first crack was observed when the elastic region stopped at the load, P_{y1} of 23.9 kN at a deflection of 0.4 mm. After the first crack, the load-deflection curve of beam LRF was observed different from the beams CF and SF. The reason may be the extent of large rectangular opening covered the entire middle-third span of the beam. After passing the first crack, a slight reduction in load with the increase of deflection was observed until the second yield load, P_{y2} of 22.8 kN was noticed at a deflection of 0.9 mm. After that, the load is observed to increase with the reduction in stiffness due to the effects of hardening until the ultimate load, P_u of 40.4 kN at a deflection of 2.3 mm. The presence of a large rectangular opening in the middle-third span reduced 53% capacity as compared to that of the control beam, CB.

The load-deflection curve of beam LEF as plotted in Figure 5.2 shows a similar trend as that was discussed in beam LRF. The load-deflection curve remained linearly elastic until the initiation of first crack at the load, P_{y1} of 27.7 kN at a deflection of 0.4

mm. After the first crack, a decreased in load was observed with the increased of deflection until the second crack was initiated at the load, P_{y2} of 25.8 kN at a deflection of 0.8 mm. After passing the second crack, the load increased gradually with reduction in beam stiffness because of hardening effects until the ultimate load, P_u of 45.1 kN at a deflection of 2.2 mm. The softening trend of the beam was found similar as that of beam LRF. From the result, providing a large elliptical opening in the mid-span of the beam caused a reduction of 48% of the beam original structural capacity.

The provision of a large rectangular and elliptical opening in the beam mid-span had caused a reduction of beam capacity about 53% and 48%, respectively. Hence, appropriate strengthening option is required in order to restore the full capacity as of the control beam.

The changes made in the shape of the large rectangular opening with the additional of a semi-circular at both ends have transformed the shape from rectangular to elliptical. It was observed that beam LEF exhibited greater beam stiffness and ultimate load compared to beam LRF. This is because the stress distribution around the elliptical opening was reduced due to the absence of opening corners. Both large rectangular and elliptical openings created in the middle-third span of the beams have divided the beams into two sections with upper and lower chords that caused the beams to behave similarly to a Vierendeel panel at the opening section.

Table 5.1 FEA results of beam with un-strengthened opening in flexure

Beam	Yielding load 1 P_{y1} (kN)	Δ_{y1} (mm)	Yielding load 2 P_{y2} (kN)	Δ_{y2} (mm)	Ultimate load P_u (kN)	Δ_u (mm)
CB	40.8	0.7	77.0	3.9	86.7	7.8
CF	43.0	1.3	78.6	3.9	86.3	8.4
SF	32.0	0.8	79.1	4.0	85.5	7.3
LEF	27.7	0.4	25.8	0.8	45.1	2.2
LRF	23.9	0.4	22.8	0.9	40.4	2.3

*All abbreviations have explained in Chapter 3.

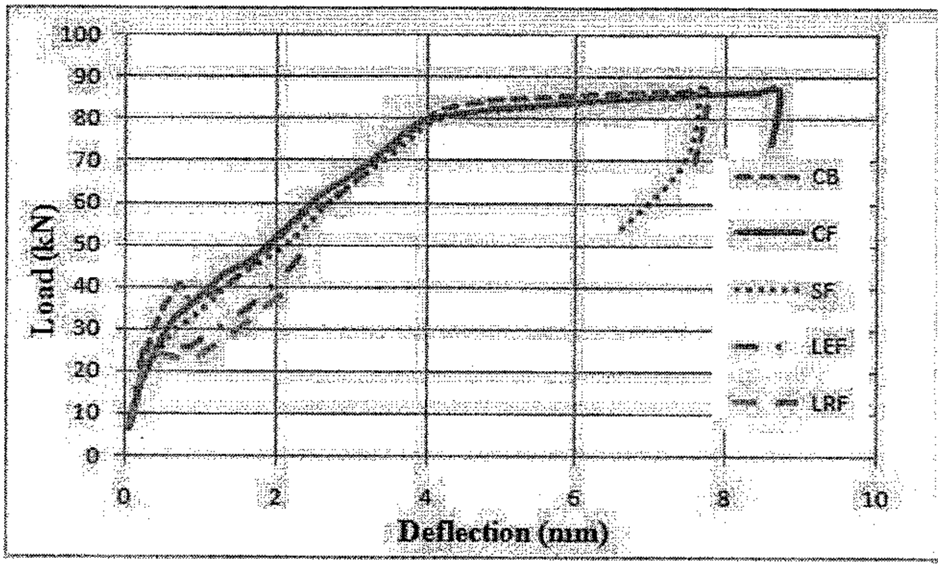

Figure 5.2 Load deflection analysis of beams with openings in the mid-span

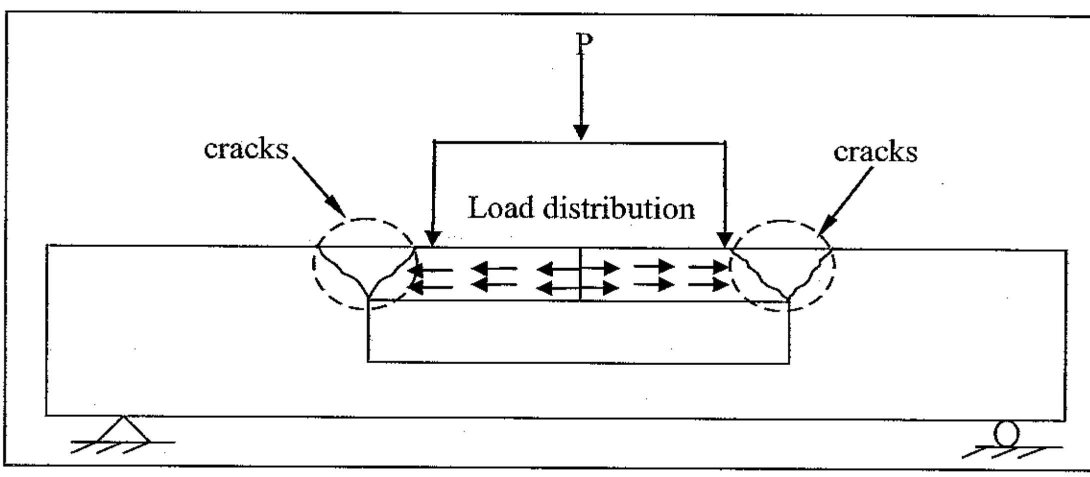

Figure 5.3 Load distribution and initiation of cracks in beam LRF

5.2.3 Crack patterns, Stress and Strain

In the subsequent sections, crack patterns, stress and strain contours of beams CB, CF, SF, LEF and LRF are discussed.

5.2.3.1 Control beam (CB)

Figure 5.4 presents the crack patterns, stress and strain contours of the control beam, CB. Vertical cracks were predicted as the first cracks to appear in the mid-span. Such cracks initiated from the bottom edge of the beam and radiated almost two-third depth of the beam; the height and thickness of cracks were reduced immediately after the mid-span. The vertical cracks were distributed within the middle-third span (more precisely within the extent of two loading points). After the loading point, the cracks tended to become diagonal. The length of diagonal cracks was higher near the loading point and beyond that until the beam support; the length of the diagonal cracks was reduced. In general, an idealized crack mapping is predicted at the two sides of the beam, which is illustrated in Figure 5.5.

Stress and strain contours as shown in Figure 5.4 showed that the neutral axis lied at the location prescribed by the codes such as Eurocode-2; in which the stress variation from higher stress to lower stress from the top, 0.4d to 0.45d (Mosley et al., 2007). Figure 5.6 presents the stress variation of triangular section in RC beams.

The stress contour showed that tensile stress was transferred to the bottom steel through concrete where the tensile stress was found about 4 – 7% of the compressive stress. The maximum compressive stress was recorded as 23 MPa, about 60 – 65% of the ultimate strength of 35 MPa. It is in line with the EC2 which allows the ultimate design stress as $0.567f_{ck}$, where it seems that the failure of the beam is governed by steel failure.

While in the strain contour, tensile strain in the vertical cracks which propagated a two-third of the beam depth in the tensile zone was found about 0.3 – 1.33%. The diagonal cracks beyond the loading point to the beam support exhibited minimum tensile strain which was about 0 – 0.3%.

5.2.3.2 Effects of Circular Opening, CF

The crack patterns, stress and strain contours of beam CF are illustrated in Figure 5.7 showed that the presence of circular opening has obstructed the predicted crack patterns as discussed in beam CB. Vertical cracks were predicted to appear at the bottom edge of the beam and propagated upward almost half of the beam depth below the opening. Similar crack patterns as observed in beam CB, the height and thickness of cracks were reduced after the mid-span. The vertical cracks were distributed below the opening within the middle-third span. After the loading point, the diagonal cracks were higher near the loading points and gradually reduced beyond that until the beam support. Horizontal cracks were predicted to form in the concrete above the opening.

The stress contour as illustrated in Figure 5.7 showed high tensile stress concentration around the circular opening, approximately about two-third of the beam depth in the mid-span. The tensile stress was observed along the tension zone of the beam as most of the tensile stress was transferred to the bottom steel in which the tensile stress was obtained about 5 – 8% of the compressive stress. The maximum compressive stress was recorded as 24 MPa, which was about 65 – 68% of the ultimate strength of 35 MPa.

The strain contour as shown in Figure 5.7 showed that the tensile strain of vertical cracks, which initiated from the bottom edge of the beam and moved upward to the bottom part of the opening and vertical cracks with higher height and thickness in the mid-span between the loading points were found in the range of 0.3 –1.38%. While the tensile strain in the cracks beyond the loading point to the beam support were reduced with the tensile strain obtained as 0 –0.3%.

5.2.3.3 Effects of Square Opening, SF

Figure 5.8 presents the crack patterns, stress and strain contours of beam SF has shown that the presence of square opening changes the idealized crack mapping as discussed in beam CB. The initiation of cracks was observed at the corners of the opening and at the bottom edge of the beam towards the bottom side of the opening in the middle-third span. The vertical cracks were predicted to propagate to two-third of the beam depth on both left and right sides of the opening. Horizontal cracks were also observed in the concrete above the opening. The stress and strain contours are illustrated in Figure 5.8.

From the stress contour, high tensile stress concentration was observed around the opening, especially two-third of the beam depth in the middle-third span. The tensile stress was also found along the tension zone indicating that the tensile stress was transferred to the longitudinal steel at the bottom where the tensile stress was found about 4 – 7% of the compressive stress. The predicted compressive stress above the opening was found about 7.5 – 9 MPa.

The strain contour showed that maximum tensile strain was observed below the square opening and in the middle-third span of the beam which was obtained as 0.3 – 0.7%. Beyond the loading point until the beam support, the tensile strain was reduced which was about 0 – 0.13%.

5.2.3.4 Effects of Large Elliptical Opening, LEF

The predicted crack patterns, stress and strain contours of beam LEF are shown in Figure 5.9; it was found different than as it was discussed in beams CB, CF and SF. This is because of the huge loss of concrete due to a large elliptical opening created in the middle-third span of the beam, which has hindered the propagation of cracks. The vertical cracks were predicted as the first crack to appear in the mid-span. These cracks initiated from the bottom edge of the beam and propagated in the lower chord of the opening. The vertical cracks were distributed within the middle-third span. With the increments of load, the vertical cracks tended to become diagonal at the bottom edge of the beam and radiated diagonally towards the opening approximately two-third of the beam depth. These diagonal cracks were observed from the upper turning point of elliptical opening to the beam support. Meanwhile, horizontal cracks were observed at the upper chord near the loading point while diagonal cracks were found at the turning point of the elliptical opening to the upper edge of the beam.

The stress and strain contours of beam LEF are described in Figure 5.9. The stress contour showed that the maximum tensile stress concentration was observed at the lower chord below the opening. This is because the tensile stress was transferred into the bottom steel which was found about 4 – 6% of the compressive stress. Compressive stress concentration was found at the upper chord, and at the left and right curves of the elliptical. The maximum compressive stress was recorded as 28

MPa, about 80% of the ultimate strength of 35 MPa. On the other hand, high strain concentration was observed at the upper chord near the right loading point with tensile strain about 0.4 – 1.13%.

5.2.3.5 Effects of Large Rectangular Opening, LRF

Figure 5.10 presents the predicted crack patterns, stress and strain contours of beam LRF. The crack patterns were found identical as of that discussed in beam LEF. Vertical cracks were first shown in the lower chord from the bottom edge of the beam. These cracks were distributed in the lower chord between two loading points within the middle-third span. The cracks became diagonal and the length of diagonal cracks was higher at approximately two-third of the beam depth at the corners of the opening after the loading point. The length of diagonal cracks was reduced beyond that until the beam support. In the upper chord above the opening, horizontal and diagonal cracks were observed near the applied load and corners of the opening.

The stress and strain contours in Figure 5.10 show that the maximum tensile stress concentration was observed at the lower chord below the opening. The reason is that the tensile stress was transferred into the bottom steel which was found about 8 – 10% of the compressive stress. Compressive stress concentration was found at the upper chord, at the left and right opening corners. The maximum compressive stress was recorded as 12 MPa, about 34% of the ultimate strength, 35 MPa. Meanwhile, the high tensile strain concentration was observed at the upper chord near the right loading point with strain about 0.6 – 1.12%, and maximum compressive strain at the top right corner, approximately 0.4 – 0.85%.

The crack patterns of openings provided in the flexure zone show that vertical cracks appeared in the middle-third span of the bottom chord and propagated towards the openings. For beam with circular and square openings, diagonal cracks were found diagonally at the loading point to the beam support, while such cracks appeared diagonally at the corners and semicircles of rectangular and elliptical opening, respectively.

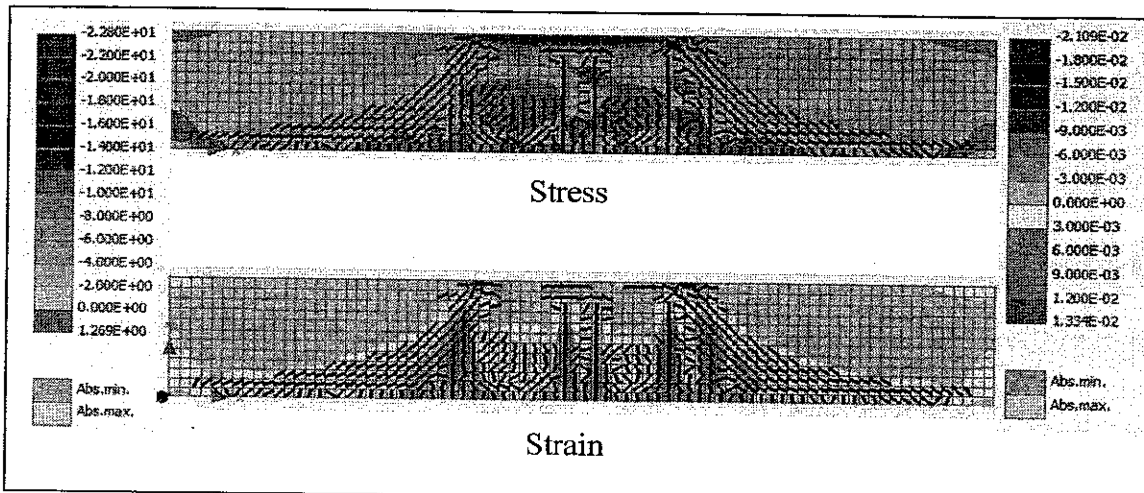

Figure 5.4 Crack patterns, stress and strain of control beam (CB)

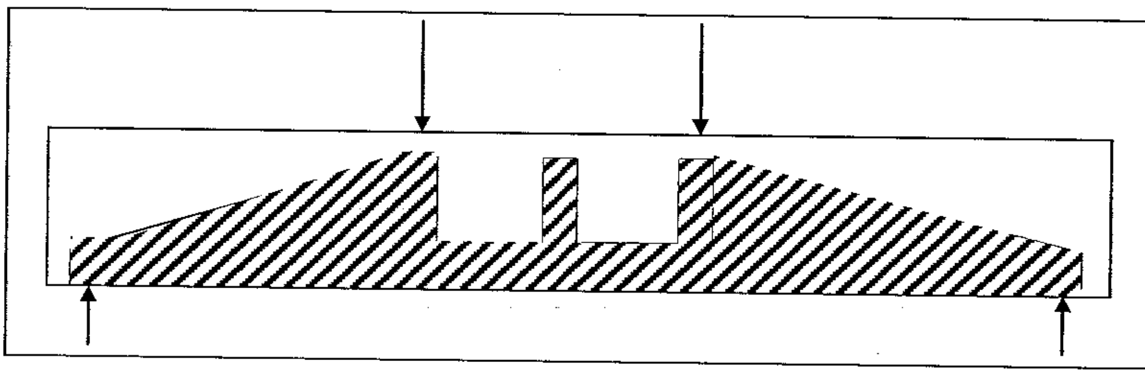

Figure 5.5 Idealized crack mapping in control beam (CB)

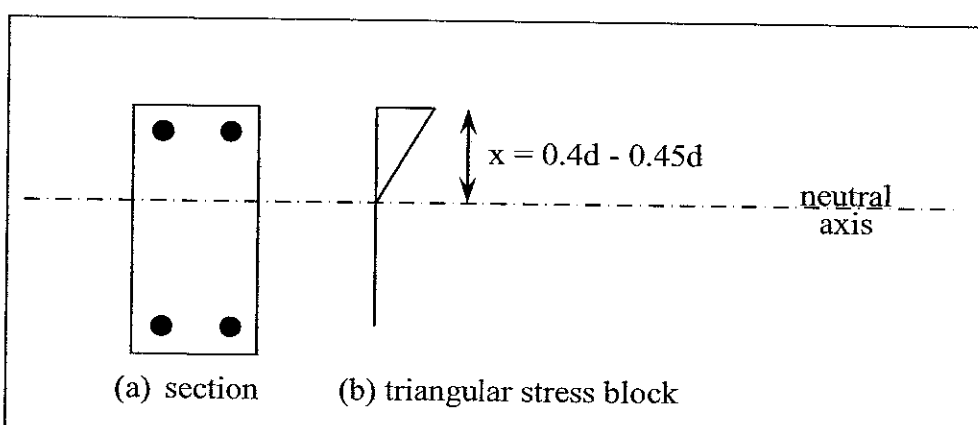

Figure 5.6 Triangular section in RC beam

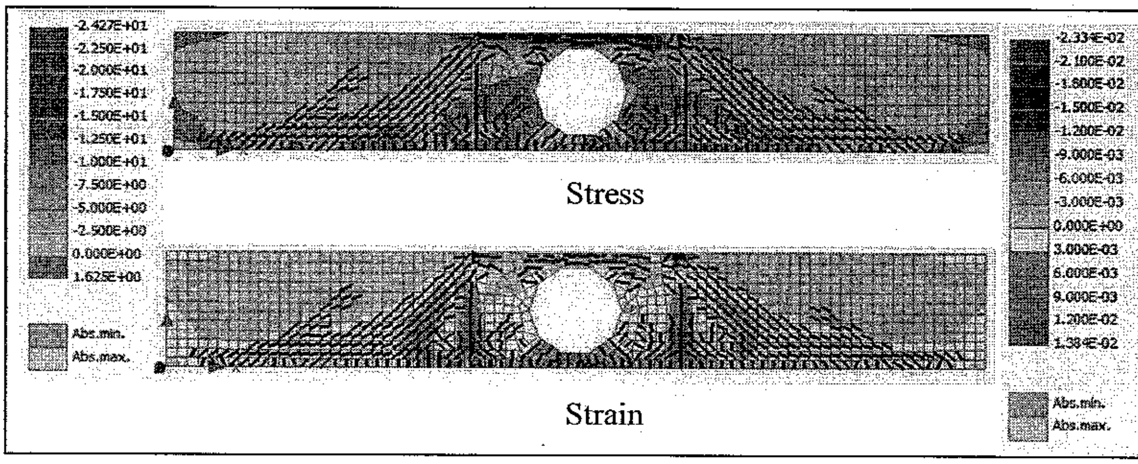

Figure 5.7 Crack patterns, stress and strain of beam CF

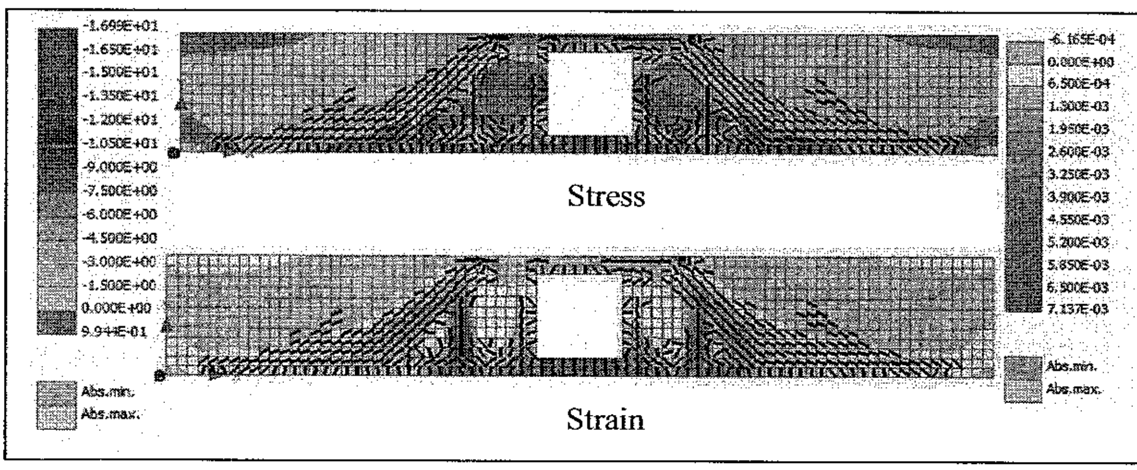

Figure 5.8 Crack patterns, stress and strain of beam SF

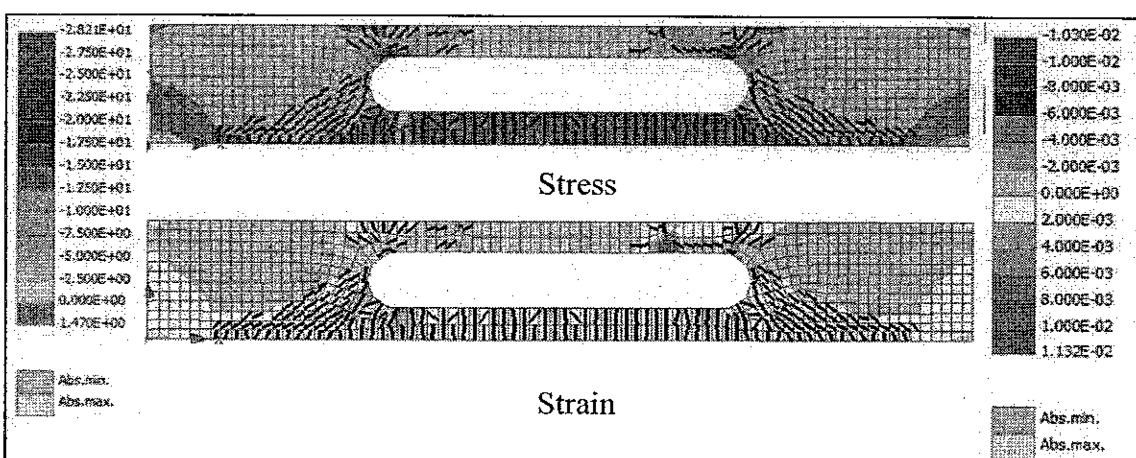

Figure 5.9 Crack patterns, stress and strain of beam LEF

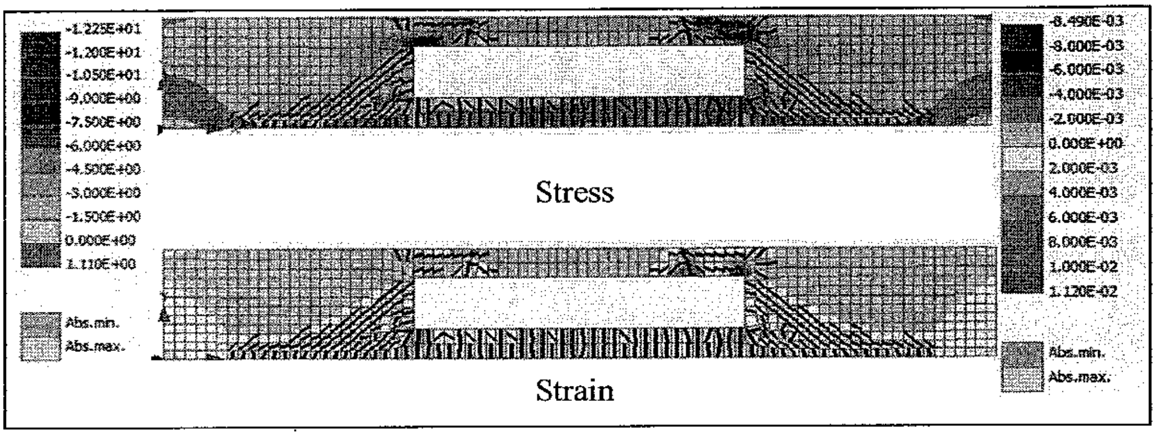

Figure 5.10 Crack patterns, stress and strain of beam LRF

5.2.4 Effects of CFRP Strengthening on Flexural Capacity

In the first part of the study, the effects of different shape, size and location of openings were investigated on the structural capacity, stress – strain behaviour and crack patterns. The second part of the study was dedicated to determine the most effective strengthening scheme to compensate the negative effects of openings in a particular beam. For this reason, many options were designed using numerical analysis and the most effective option was chosen to further validate through experimental testing in order to achieve objective no.2.

The term 'most effective scheme' means the strengthening scheme that utilizes the minimum amount of strengthening material and returns back the full losses in the structure those occurred due to openings.

5.2.4.1 Design Configuration of CFRP Laminates

In this sub-section, descriptions of the design configuration of CFRP laminates are given in Figure 5.11. In the figure, the chosen strengthening configurations for each beam are shown, whereas several strengthening options for a particular beam are given in the Appendix B – C.

CFRP lamination scheme in Figure 5.11(a) explain one of the strengthening configurations for beam with a large elliptical opening in the mid-span. CFRP laminates were positioned at the area where cracks appeared as discussed in Figure 5.9. Two longitudinal CFRP laminates were placed on the elevation face at the top chord; and two longitudinal CFRP laminates on the elevation face at the bottom chord, as shown in Figure 5.11(a). Anchorage margins for each length of CFRP laminates are considered.

Figure 5.11(b) illustrates one of the CFRP laminate configurations for beam with a large rectangular opening in the mid-span. Two CFRP laminates were placed on the elevation face at the top chord; and two CFRP laminates on the elevation face at the bottom chord. Two CFRP laminates were positioned on the left and right vertical surfaces of the opening as shown in Figure 5.11(b). The strengthening configuration was based on the crack patterns in the un-strengthened beam LRF as shown in Figure 5.10. The length of the CFRP laminates has considered for the anchorage margins.

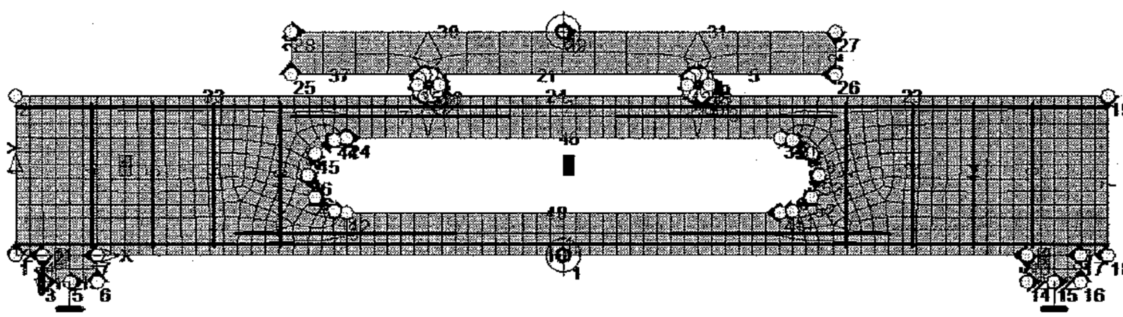

(a) LEF-S

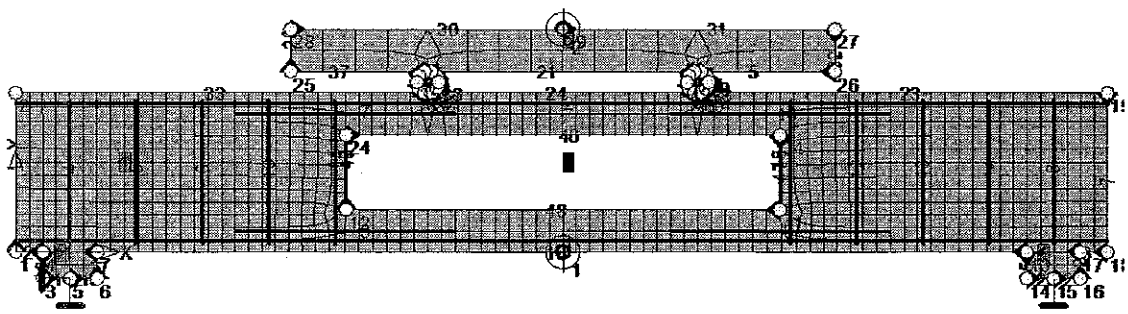

(b) LRF-S

Figure 5.11 CFRP strengthening schemes for beams with elliptical and rectangular openings in mid-span

5.2.4.2 Load-Deflection Behaviour

Table 5.2 summarizes the results of selected strengthening schemes analyzed for beams LEF-S and LRF-S. The load-deflection behaviour of the strengthened beams is illustrated in Figure 5.12. Effects of strengthening schemes are discussed in reference with the results of the control beam.

a) Strengthening for Large Elliptical Opening, LEF-S

The load-deflection curve of beam LEF-S as plotted in Figure 5.12 showed a different load-deflection trend compared to beam CB, CF-S and SF-S. In the initial stage; the extent of elastic region was rather short as the first crack was observed at the load, P_{y1} of 20.4 kN at a deflection of 0.1 mm. After the first crack, a significant drop in beam stiffness was noticed with the continuous increment in load due to the hardening effects. This may be due to the effects of reduction of concrete area in the middle-third span. The second yield load, P_{y2} of 35.8 kN was observed at a deflection of 0.7 mm. After that, the stiffness was found slightly increased with the increase of load and small deflection until the ultimate load, P_u of 63.9 kN at a deflection of 1.5 mm. The possible reason is that due to the effects of CFRP could have increased the beam stiffness and capacity to certain extent before failure. After the ultimate load, rapid softening occurs with a sharp decrease in load at a deflection of 1.2 mm. The provision of a large elliptical opening in the mid-span of a beam which caused a loss of 48% of original beam capacity as mentioned in section 5.2.2.4, the strengthening configuration with CFRP has re-gained the beam capacity of LEF-S to about 74% of the original beam structural capacity, CB. With this, theoretical analysis shows that the CFRP external strengthening scheme on beam with large size opening could not reinstate up to 100% design capacity.

b) Strengthening for Large Rectangular Opening, LRF-S

A similar trend of load-deflection behaviour that was discussed for beam LEF-S was observed in the beam LRF-S, which is plotted in Figure 5.12. In the elastic stage, the first crack was found at load, P_{y1} of 15.9 kN at a deflection of 0.1 mm. This beam has shown a lower yield load, P_{y1} due to the opening corners and concrete area loss in the middle-third span. After that, the load continuously increased with the reduction of beam stiffness until the initiation of the second crack at load, P_{y2} of 38.0 kN at a deflection of 0.8 mm. After the second crack, with a decrease in stiffness, the load increase with deflection until the ultimate load, P_u of 56.5 kN at a deflection of 1.8 mm. Compared to beam LEF-S, the beam stiffness in beam LRF-S was reduced, which may be due to the sharp corners effects. After the ultimate load was achieved, a sudden softening was observed at a deflection of 1.5 mm. As mentioned in section 5.2.2.4, providing a large rectangular opening in the mid-span of a beam greatly caused a loss of 53% of the original beam capacity. Strengthening of beam LRF-S with the chosen strengthening configuration has re-gained 65% of the original beam capacity, beam CB. From the results, FE analysis shows that the CFRP external strengthening configuration on beam with large size opening cannot reinstate up to 100% design capacity.

When additional stirrups were placed in the top and bottom chords of both beams with large elliptical (LEF-SS) and rectangular openings (LRF-SS) as shown in Figure 5.13; the beam stiffness, yield load and ultimate load as illustrated in Figure 5.12 and summarized in Table 5.2 were observed greater than those without additional stirrups, about 12% and 15%, respectively. This signifies that additional reinforcements are needed to strengthen around the opening which prone to localized shear failure (at the top chord) despite the presence of CFRP laminates in order to restore the full beam capacity. Such large openings cannot be provided in existing beams by hacking/drilling because the additional stirrups cannot be placed. Hence, large elliptical and rectangular openings are categorized as pre-planned openings in which adequate reinforcement around the openings should be considered during the preliminary design stage before construction.

Table 5.2 FEA results of beam with strengthened opening in flexure

Beam	Yielding load 1 P_{y1} (kN)	Δ_{y1} (mm)	Yielding load 2 P_{y2} (kN)	Δ_{y2} (mm)	Ultimate load P_u (kN)	Δ_u (mm)
CB	40.8	0.7	77.0	3.9	86.7	7.8
LEF-S	20.4	0.1	35.8	0.7	63.9	1.5
LRF-S	15.9	0.1	38.0	0.8	56.5	1.8
LEF-SS	25.0	0.1	37.4	0.4	72.5	1.5
LRF-SS	20.3	0.1	38.8	0.5	66.1	1.8

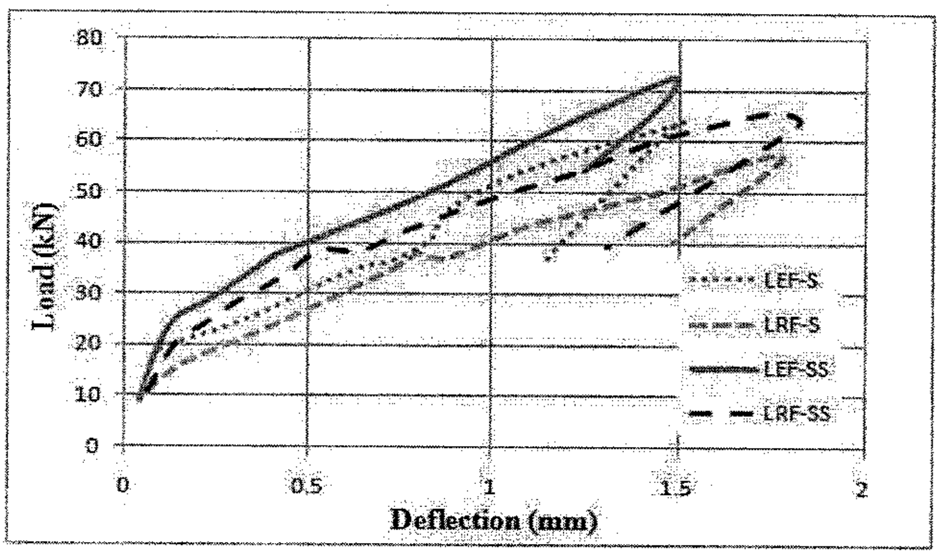

Figure 5.12 Load-deflection curves of beams with strengthened openings in the mid-span

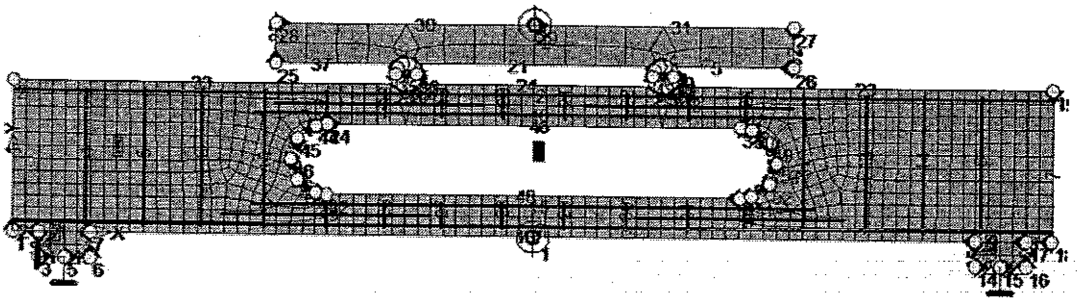

(a) LRF-SS

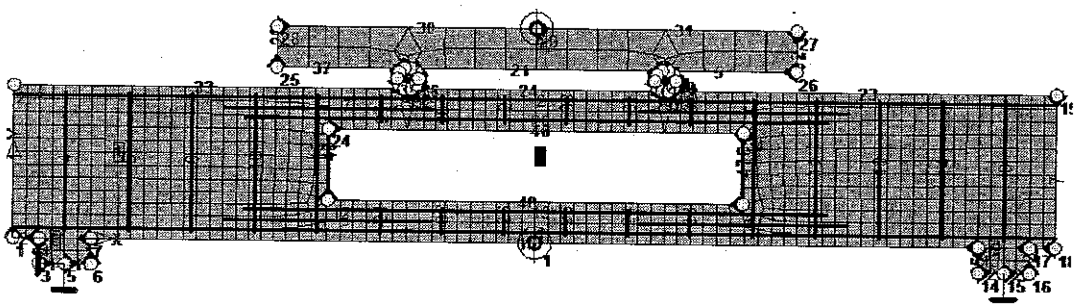

(b) LRF-SS

Figure 5.13 Additional stirrups around elliptical and rectangular openings

5.2.4.3 Crack patterns, Stress and Strain

This section presents the crack patterns, stress and strain behaviour of beams LEF-S and LRF-S as illustrated in Figures 5.14-5.15, respectively.

(a) Strengthening for Large Elliptical Opening, LEF-S

Figure 5.14 shows the crack patterns, stress and strain contours of beam LEF-S. The installation of CFRP in the chosen strengthening configuration has changed the crack patterns as that discussed for beam LEF, as illustrated in Figure 5.9. Vertical cracks were appeared in the lower chord of opening from the bottom edge of beam between two CFRP laminates. Such cracks propagated vertically through the lower chord until the bottom center of the opening. Eventually, diagonal cracks were formed at the left and right ends of CFRP laminates in the lower chord. The diagonal cracks were found about two-third depth of the beam near to the curve and their length increased as the cracks approached near to the beam support. In the lower chord, horizontal cracks were observed in the concrete. In the upper chord, similar to the lower chord, horizontal cracks were noticed in concrete. Only minor vertical cracks were observed in the top mid-span above the opening.

Stress contour showed that the maximum tensile stress was observed in the center of the lower and upper chords within the non-restricted area by CFRP laminates. This is because of the effects of CFRP that have shifted the tensile stress into the non-strengthened area in concrete. The maximum tensile stress was obtained as 1.74 MPa, about 6 – 8% of the compressive stress. The tensile stress was also observed at the end of each CFRP near to the beam support in the lower chord. The maximum compressive stress was recorded as 24 MPa which was approximately 69% of the ultimate design strength of 35 MPa. The maximum compressive stress was found diagonally from the loading point to the turning point of the opening.

The strain contour illustrated that the maximum tensile strain was observed in the center of the lower chord between two CFRPs where vertical cracks were significant. The tensile strain in concrete was found in the range of 0.29 – 0.53%. Mild tensile strain was noticed in the diagonal cracks near to the beam support at approximately 0.1 – 0.29%.

(b) Strengthening for Large Rectangular Opening, LRF-S

A similar trend of crack patterns, stress and strain distribution of beam LRF-S as discussed in Figure 5.15 was observed in the beam LEF-S. Vertical cracks appeared in the center of lower chord between two CFRP laminates. The vertical cracks penetrated from the bottom edge of the chord to the lower edge of the opening. The vertical cracks in the center of upper chord were not significant. Diagonal cracks were found at the end of each CFRP laminates in the lower chord. Beyond the loading points, these diagonal cracks were found along two-third of the beam depth from the top opening corners to the beam support, where the length of cracks was increased. Meanwhile, horizontal cracks were noticed in the concrete strengthened by CFRPs, both in the upper and lower chords.

In the stress contour, maximum tensile stress was found in the middle of upper and lower chords (above and below the opening) where the tensile stresses were obtained about 11 – 13% of the compressive stress. The maximum compressive stress was found in the upper chord, at the loading points to the opening corners, respectively was recorded as 12 MPa which is about 33 – 35% of the ultimate strength, 35 MPa.

The strain contour showed that the maximum tensile strain were observed in the center of lower chord and top left of the upper chord in which the presence of vertical cracks. The maximum tensile strain was in the range of 0.3 – 0.6% while the maximum compressive strain was found in the top left opening corner with the strain values of 0.4 – 0.7%.

From the crack patterns, it was found that external strengthening with CFRP laminates has caused the cracks to concentrate in the mid-span of the bottom chord; and diagonally from the opening corners to the beam support.

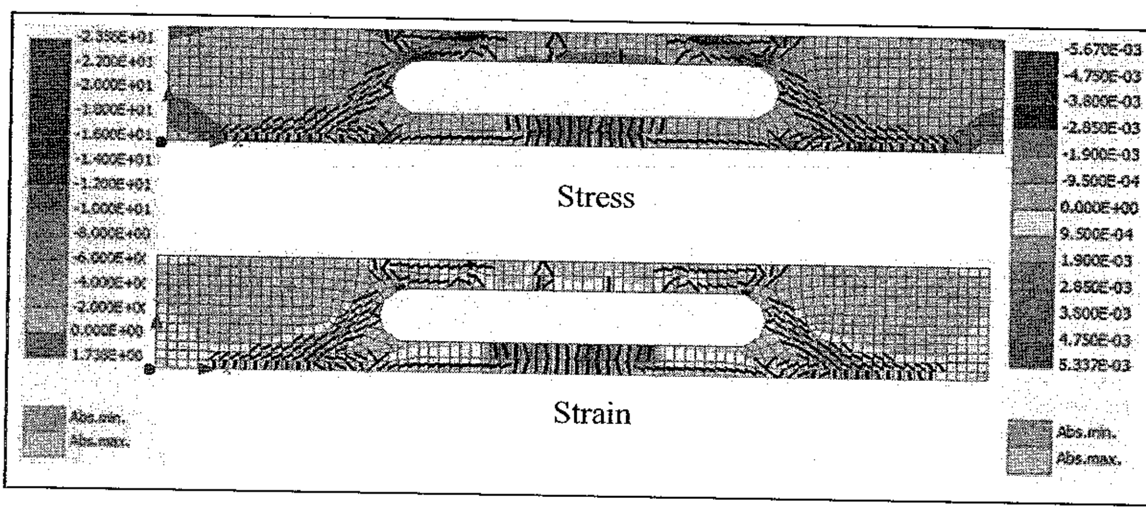

Figure 5.14 Crack patterns, stress and strain of beam LEF-S

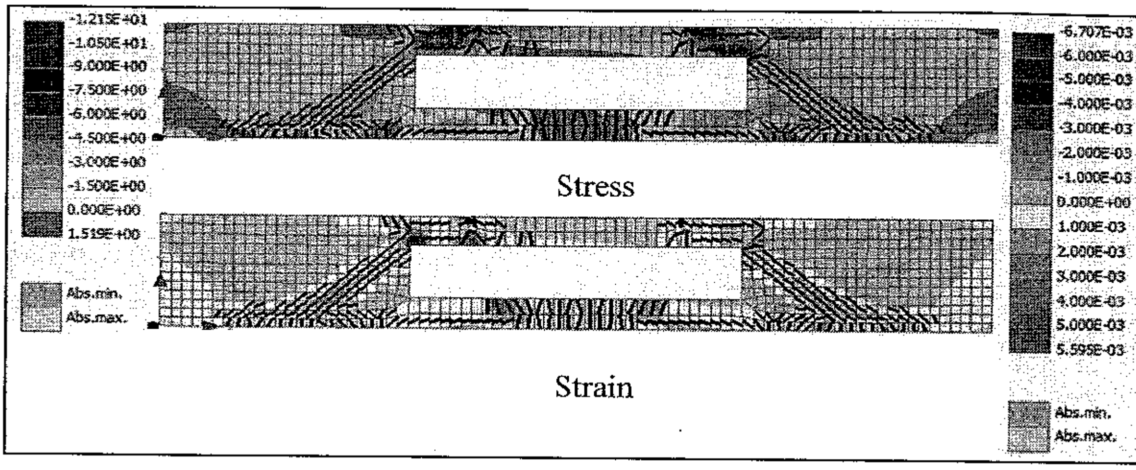

Figure 5.15 Crack patterns, stress and strain of beam LRF-S

5.3 Investigating the Size, Shape and Configuration of Openings in Shear Zone

Similar to the shape of openings adopted in the flexure zone, circular and square shapes were chosen to study the effects of the openings in the critical locations in the shear zone, which is considered at the distance of 0, 0.5d, d and 1.5d from the face of support. Most of the investigations reported in literatures were based on small circular and square openings and very little research was carried out using large circular and square opening in the shear zone (Abdalla et al. 2003; Allam 2005; Pimanmas 2010). The openings were placed into two sequences: (i) opening at both ends; (ii) opening at one end only. The purpose of such provision was that in some cases the openings are needed on one side only due to M & E requirements, whereas in another case, the openings may be needed on both sides. All the beams were modelled in ATENA and results are discussed in the following sub-sections in terms of load-deflection behaviour and crack patterns in section 5.3.1 and 5.3.2, respectively to achieve objectives no. 1(i) and 1(ii).

5.3.1 Load-Deflection Behaviour of Un-Strengthened Beams

Through FE analysis, load-deflection behaviour of different beams was investigated, which is plotted in Figure 5.16. As discussed earlier in the Section 5.2.1, three limiting loads, P_{y1}, P_{y2} and P_u together with the corresponding deflections were marked. Effects of openings on these limiting values are discussed with respect to the control beam in the following sub-sections.

5.3.1.1 Opening at Both Ends

The openings were placed on the face of support and at a distance 0.5d and d from the support, through FE analysis; any appreciable difference between the three load-deflection curves was not recognized. Therefore, Figure 5.16 plotted the generalized P-Δ curve for circular and square shape openings, which is valid for locations from the face of support until the distance d from the support.

(a) Effects of Circular Opening

At the initial stage, limiting load P_{y1} was obtained as 13.2 kN at the deflection of 0.3 mm. After that, the load continued to increase because of the effects of hardening until the next crack initiated at load, P_{y2} of 22.4 kN at a deflection Δ_{y2} of 1.6 mm. Following to this zone, a gradual increase in load as the deflection increase until the ultimate load, P_u of 26.2 kN at a deflection, Δ_u of 3.4 mm was observed. Just after ultimate load, the beam experienced softening that lasted until failure, at that point, the deflection was 4.9 mm. On comparing the load carrying capacity of such beams with the control beam, about 63 to 70% loss in load carrying capacity was observed. On the other hand, the effects of the circular opening on ultimate deflection were that it decreased by 53 – 56% as compared with that of the control beam.

(b) Effects of Square Opening

At the early stage, the limiting load, P_{y1} was obtained as 9.62 kN at a deflection of 0.5 mm. Then, the load was seen to increase with deflection due to the hardening effects until the second yield load, P_{y2} of 21.4 kN was noticed at a deflection of 2.5 mm. After the second crack, gradual increase in load was observed until the ultimate load was attained at load, P_u of 23.6 kN at a deflection, Δ_u of 4.6 mm. Just after the ultimate load, softening of beams was occurred gradually until failure in which the deflection was 5.2 mm. The load carrying capacity of such beams was being compared with the control beam and losses were found about 67% to 73%. Meanwhile, as compared with that of the control beam, the effects of square opening causes a decrease in ultimate deflection about 41% to 68%.

In general, either placing a circular or square opening at a distance 0 to d from each of the two supports have shown reduction in beam capacity at approximately 63 – 73% of the original beam capacity, CB. In terms of the effects of shape of the openings provided in this region, the load-deflection curve of the circular opening exhibited greater beam stiffness, yield load and ultimate load as compared to the square opening. This may be due to the effects of high stress concentration at sharp corners of the square opening that cause early diagonal cracking resulted in reduction of beam stiffness and strength.

The effects of changing the openings location from a distance 0 to d are not very significant, which was found within 5%. The obvious reason is that the shear stresses are distributed throughout the concrete section, in particular, in the middle-third cross-section, a larger portion of shear stresses are distributed which illustrated in Figure 5.17. It is also discussed in the various codes, i.e. Eurocode-2, Figure 5.18, showed the shear behaviour of RC beams according to Eurocode- 2 (Mosley et al. 2007). According to that, most critical location of shear stress is from the face until the distance d from the support. The code equations calculate approximately the same amount of shear stress within this zone. That is why no significant difference was found by changing the opening location from face of support to until the distance d.

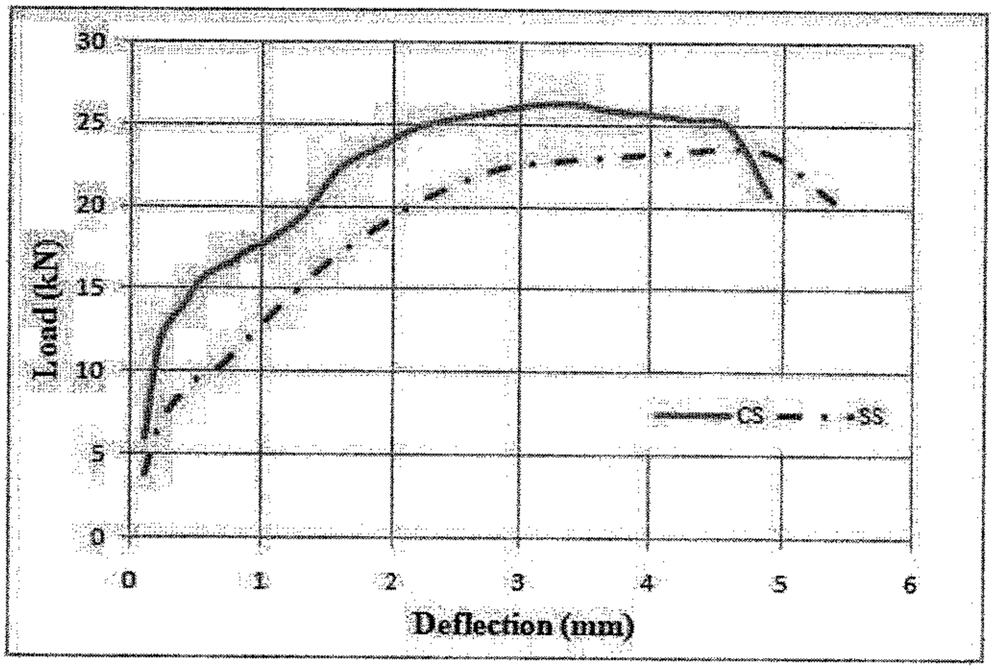

Figure 5.16 Load deflection analysis of beams with un-strengthened openings at both ends

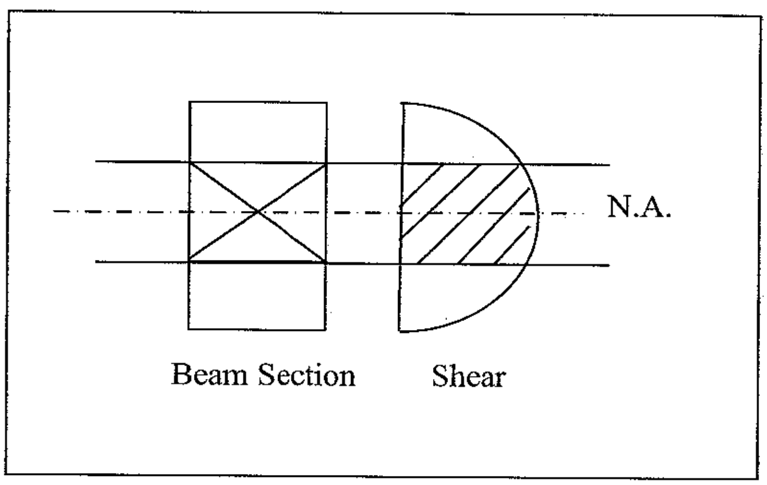

Figure 5.17 High shear stresses in middle-third cross section of beam

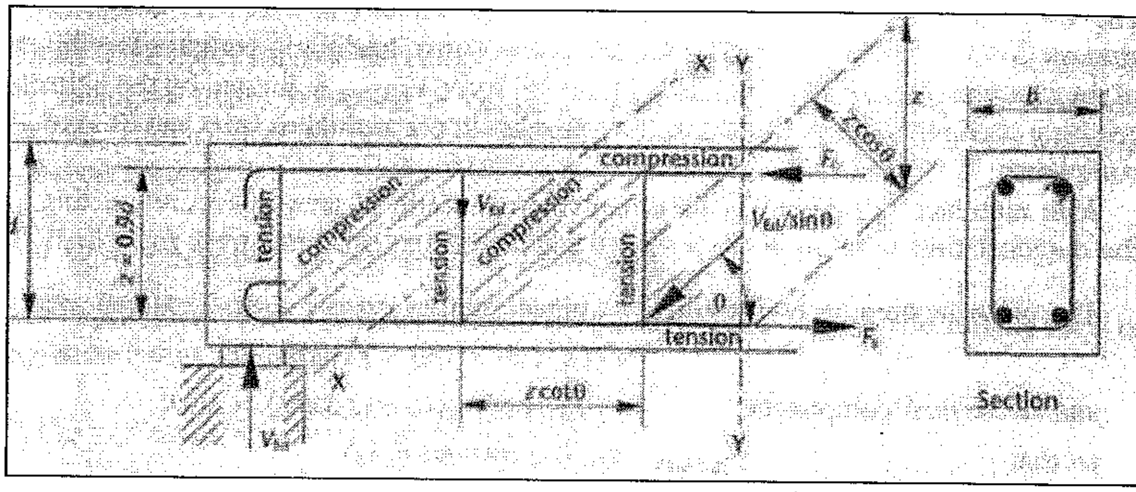

Figure 5.18 Shear stress model according to Eurocode-2 (Mosley et al. 2007)

5.3.1.2 Opening at One End Only

The openings were placed at 0.5d, d and 1.5d from the support with the method of FE analysis. Figure 5.19 plotted the load-deflection curves for circular and square openings which located from distance 0.5d, d and 1.5d from the support. The results obtained are summarized in Table 5.3.

(a) Effects of a Single Square Opening (at distance 0.5d from support), S0.5dS1

The linear state of the elastic region became non-linear as the first crack was initiated at load, P_{y1} of 9.07 kN at a deflection Δ_{y1} of 0.3 mm. After cracking, the load was increased due to hardening effects until the second crack at load, P_{y2} of 17.3 kN was noticed at a deflection Δ_{y2} of 0.9 mm. Following to this region, the load was gradually increased until the ultimate load was achieved at load, P_u of 20.4 kN at a deflection, Δ_u of 1.6 mm. Just after the ultimate load, the beam experienced softening that ended until failure in which the deflection was obtained at 2.8 mm. The load carrying capacity of beam S0.5dS1 was compared to the control beam, about 76% loss in load carrying capacity was observed. The effect of a square opening at 0.5d from the face of support on ultimate deflection was that it was decreased by 79% as compared to the control beam.

(b) Effects of a Single Circular Opening (at a distance d from support), CdS1

At the initial stage; the extent of elastic region was terminated within small deflection when the first crack was observed at load, P_{y1} of 9.07 kN at a deflection of 0.3 mm. After that, the load increase in a straight line with minimum deflection to the next yield load, P_{y2} of 20.0 kN at a deflection of 0.7 mm was observed. After cracking, the load was increased due to the effects of hardening in concrete. As the load kept increasing, the straight line became non-linear until the ultimate load was obtained at load, P_u of 23.6 kN at a deflection, Δ_u of 1.3 mm. After passing the point of ultimate load, rapid softening of the beam was noticed immediately. From the results, beam CdS1 has shown a significant loss of capacity which is about 73% compared to the load-carrying capacity of the control beam. The presence of a circular opening affected the ultimate deflection as it showed a decreased of about 83% as compared with that of the control beam.

(c) Effects of a Single Square Opening (at distance d from support), SdS1

In the early phase, the elastic state came to a halt when cracking was observed at load, P_{y1} of 7.28 kN at a deflection Δ_{y1} of 0.2 mm. After passing the first crack, the load was increased until the next crack at load, P_{y2} of 14.2 kN at a deflection Δ_{y2} of 0.6 mm was observed. Due to the hardening effects in concrete, the load increase non-linearly until the ultimate load, P_u of 20.1 kN at a deflection, Δ_u of 1.6 mm. Beyond that point, an immediate decrease in load was observed due to the softening effects in concrete. Compared to the load-carrying capacity of the control beam, a single square opening provided at a distance d from the face of support greatly reduced the beam capacity to approximately 77%. In terms of ultimate deflection, comparison with the control beam was made and found that it was decreased by 79%.

(d) Effects of a Single Square Opening (at distance 1.5d from support), S1.5dS1

The trend of load-deflection behaviour of beam S1.5dS1 was found similar to that of beam SdS1, as shown in Figure 5.19. At the initial period, the first crack was initiated at load, P_{y1} of 9.86 kN at a deflection of 0.3 mm. Following to that, the load was increased due to the effects of hardening in concrete, until the next yield load, P_{y2} of 16.8 kN was observed at a deflection of 0.7 mm. After that, the load was increased until the ultimate load, P_u of 20.9 kN was obtained at a deflection, Δ_u of 1.3 mm. Just after the point of ultimate load, the load decrease gradually due to the softening effects on the beam up to failure where the deflection was at 2.8 mm. A single square opening created at distance 1.5d from the face of support caused a decrease in beam capacity of about 76% as compared to the load-carrying capacity of the control beam. Comparing to the control beam, the effects of square opening on the ultimate deflection was that it was decreased by 83%.

Generally, the load-deflection curve of the beam with a circular opening at a distance d from the face of support, CdS1 as plotted in Figure 5.19 showed a different load-deflection trend as compared to the beams with square opening S0.5dS1, SdS1 and S1.5dS1. Comparing the shape of the opening, beam CdS1 exhibited greater beam stiffness and ultimate load compared to beams with square opening as this may be due to less stress concentration around the circular opening compared to the square opening with sharp corners. In terms of opening location, a similar trend of load-deflection curves of beams with square opening at distance 0.5d, d and 1.5d were observed. The effects of square opening placed at distance 0.5d, d and 1.5d were not significant, as the ultimate load was obtained within 5%, similar as observed and discussed in beams with openings at both ends at a distance 0 to d in section 5.3.1.1. Square opening provided in this region caused a reduction of beam capacity about 76-77% of the load-carrying capacity of the control beam.

Table 5.3 FEA results of beam with un-strengthened openings at one end only

Beam	Yielding load 1 P_{y1} (kN)	Δ_{y1} (mm)	Yielding load 2 P_{y2} (kN)	Δ_{y2} (mm)	Ultimate load P_u (kN)	Δ_u (mm)
CB	40.8	0.7	77.0	3.9	86.7	7.8
S0.5dS1	9.07	0.3	17.3	0.9	20.4	1.6
CdS1	12.4	0.3	20.0	0.7	23.6	1.3
SdS1	7.28	0.2	14.2	0.6	20.1	1.6
S1.5dS1	9.86	0.3	16.8	0.7	20.9	1.3

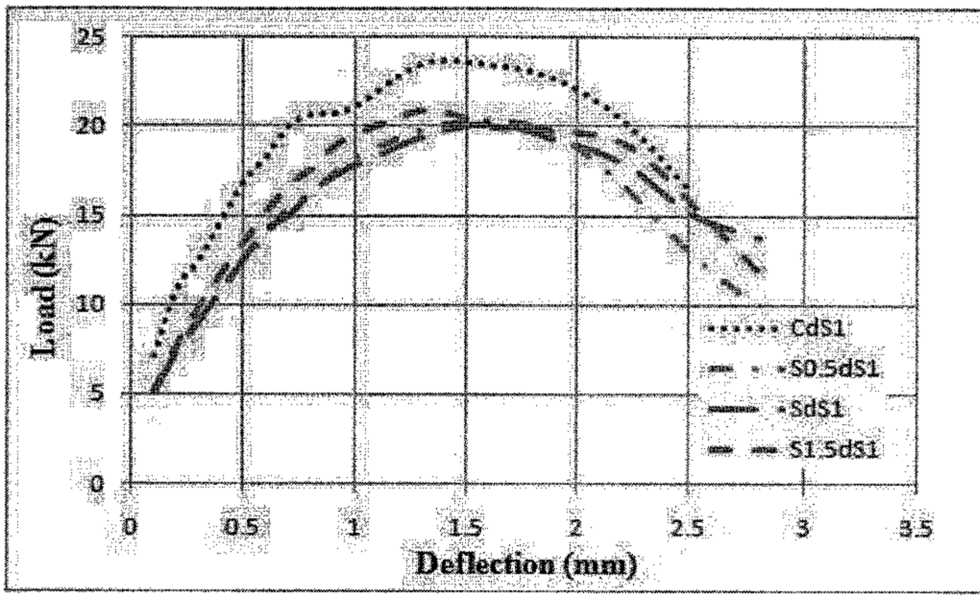

Figure 5.19 Load deflection analysis of beams with un-strengthened openings at one end only

5.3.2 Crack patterns and Stress Strain Distribution

During the FE analysis, crack patterns, stress-strain distribution on the beam faces were also observed. Effects of opening location, shape and sequence are also investigated, which is discussed in the following sub-sections.

5.3.2.1 Opening at Both Ends

This section presents and discusses the crack patterns, stress and strain contours of beams C0S, S0S, S0.5dS, CdS and SdS, respectively.

(a) Beam with Circular Openings (zero distance from support), C0S

Figure 5.20 presents the crack patterns, stress and strain contours of beam C0S. During analysis, first cracks observed were the vertical cracks in the mid-span, these cracks initiated from the bottom edge of the beam and propagated about one-third beam depth; moving away from the mid-span, the height and thickness of cracks were reduced whereas diagonal cracks were noticed at the opening, such cracks were initiated from the top side of the opening and then propagated until the load point. The cracks initiated from the bottom side of the opening were stretched all the way to the beam support. Such pattern of crack propagation is quite logical and comply the principles of fundamental mechanics.

The stress contour as shown in Figure 5.20 showed high tensile stress concentration, approximately within the two-third depth of the beam in the mid-span. The tensile stress was observed along the tension zone of the beam as most of the tensile stress was transferred to the bottom steel in which the tensile stress was found about 9 – 11% of the compressive stress. The maximum compressive stress was recorded as 18 MPa, which was about 50 – 52% of the ultimate design strength of 35 MPa. In the left circular opening, the compressive stress at the top was traced from the opening towards the loading point. Similar trend compressive stress distribution was noticed around the right circular opening.

The strain contour illustrated in Figure 5.20 showed that the tensile strain around the left and right circular openings were maximum; which stretched from the opening towards the loading point and beam support, respectively. The tensile strain was obtained in the range of 0.8 –1.8%. The color of the tensile strain was more intense at the bottom of opening until the beam support. The magnitude of tensile strain confirmed the occurrence of the wide diagonal cracks in that region, which is in concurrence with the observed crack patterns.

(b) Beam with Square Openings (zero distance from support), S0S

The crack patterns, stress and strain contours of beam S0S are illustrated in Figure 5.21 showed a different trend of the crack patterns around openings as compared to beam C0S. Prediction of FE analysis shows that initial diagonal cracks were formed at the corners of the square openings, which is due to the stress concentration at sharp corners. These cracks at the top corners stretched all the way to the top edge of the beam and the loading point, respectively whereas cracks at the bottom corners radiated diagonally towards the bottom edge of the beam and beam support, respectively. During the analysis, vertical cracks were seen distributed in the mid-span along the tension zone, where the cracks penetrated approximately one-third depth of the beam.

The stress distributions showed that high tensile stress concentration within the tension zone indicating that the tensile stress was transferred to the bottom longitudinal steel where the stress was found about 14 – 16% of the compressive stress. The compressive stress was at maximum with a recorded value of 16 MPa, which was about 44 – 46% of the ultimate strength of 35 MPa. These stresses were found maximum at the top edge of the beam above the opening corner near to the loading point and bottom corner of the opening near to the mid-span.

From the strain contour, maximum tensile strain was observed at the bottom corner near to the beam support, which was obtained about 0.3 – 0.8%. Meanwhile, the mild tensile strain concentration was found at the top corner near to the loading point approximately 0.2 – 0.4%. The maximum compressive strain was observed at the bottom corner near to the mid-span which was about 0.2 – 0.3%.

(c) Beam with Square Openings (at distance 0.5d from support), S0.5dS

In comparing to beam S0S, a different trend of crack pattern, stress and strain contours were observed in beam S0.5dS as the openings were shifted to a distance 0.5d from the face of support which is shown in Figure 5.22. The FE analysis predicted vertical cracks in the mid-span formed from the bottom edge of the beam and propagated about one-fourth of the beam depth whereas diagonal cracks were noticed at the sharp corners of the opening and radiated through the top and bottom edges of the beam, respectively. As the cracks approaching near to the loading point and beam support respectively, the height and length of cracks were increased.

The stress contour showed that high tensile stress concentration was found in the middle-third span as the stresses were transferred into the bottom steel reinforcements. The tensile stress was calculated approximately 10 – 12% of the compressive stress. Meanwhile, the maximum compressive stress was obtained as 22 MPa which was about 61 – 64% of the ultimate design strength of 35 MPa. Such stresses were found concentrated at the corners and top and bottom edges of the beam around the opening.

The strain contours illustrated that the tensile strain was noticed at the area of opening corners and at the top and bottom edges of the beam with the presence of cracks in concrete. The maximum tensile strain was obtained about 0.2 – 0.6%.

(d) Beam with Circular Openings (at distance d from support), CdS

Figure 5.23 illustrates the crack patterns, stress and strain distribution of beam CdS. Comparing to the crack patterns of beam C0S, the FE analyzed vertical cracks in the mid-span were reduced, which was about one-fourth of the beam depth from the bottom edge while diagonal cracks were found above the circular opening. Such cracks were initiated from the top side of the opening and then penetrated until the loading point. As the cracks stretching to the loading point from the top chord, the height and length of cracks were increased, where the horizontal cracks were formed. The cracks initiated from the bottom side of the opening were stretched all the way to the beam support.

From the stress contour, the tensile stress was noticed in high concentration in the mid-span between the circular openings; which signifies that the stresses were transferred to the longitudinal steel at the bottom where the stresses were about 10 – 12% of the compressive stress. The compressive stress was recorded maximum as 18 MPa, which was about 50 – 52% of 35 MPa, the ultimate design strength. These stresses were found concentrated at the top edge of the beam to the loading point and bottom edge of the beam to the beam support.

On the other hand, the tensile strain from the strain contour was found concentrated at the top side of opening to the loading point and bottom side of opening to the beam support. The maximum tensile strain was observed diagonally across the right circular opening which was obtained about 0.8 – 1.5%, while mild tensile strain was traced diagonally across the left circular opening which was about 0.4 – 0.8%.

(e) Beam with Square Openings (at distance d from support), SdS

As the openings were shifted into a distance d from the face of support, the trend of crack patterns, stress and strain distribution of beam SdS were observed rather different as compared to beams S0S and S0.5dS as illustrated in Figure 5.24. During the analysis, initial cracks were noticed diagonally at the corners of openings because of stress concentration. The cracks at opening corners in the top chord propagated diagonally to the top edge of the beam and the loading point respectively, whereas the cracks at opening corners in the bottom chord stretched diagonally to the bottom edge of beam and beam support, respectively. Meanwhile, vertical cracks were found distributed in the beam mid-span between two square openings along the tension zone where the cracks penetrated approximately one-fourth of the beam depth.

Tensile stress concentration from the stress contour was observed high along the tension zone; which means that the stresses were transferred to the bottom steel which was approximately 9 – 11% of the compressive stress. At maximum, the compressive stress was recorded as 20 MPa, which was about 56 – 58% of the ultimate strength of 35 MPa. The compressive stresses were found maximum at the top edge of the beam above the opening corner near to the loading point, bottom corner of the opening near to the mid-span and bottom edge of the opening near to the beam support.

Strain contour illustrated that the tensile strain was noticed at the opening corners and at the top and bottom edges of the beam, which was obtained about 0.3 – 0.6%. The tensile strain occurred due to cracking of concrete with the application of load, and because of the cracking effects, the opening was tilted upwards, hence the top edge of the beam was subjected to cracking.

The crack patterns of various beams with openings at both ends show that minor vertical cracks were formed along the mid-span of the beam. Most cracks appeared as diagonal cracks at the top and bottom sides of circular openings and at sharp corners of square openings.

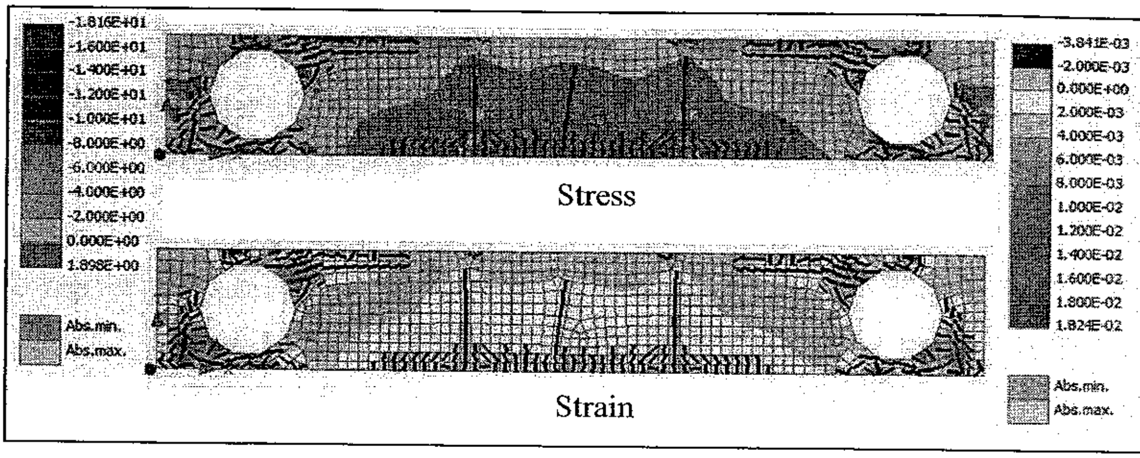

Figure 5.20 Crack patterns, stress and strain of beam C0S

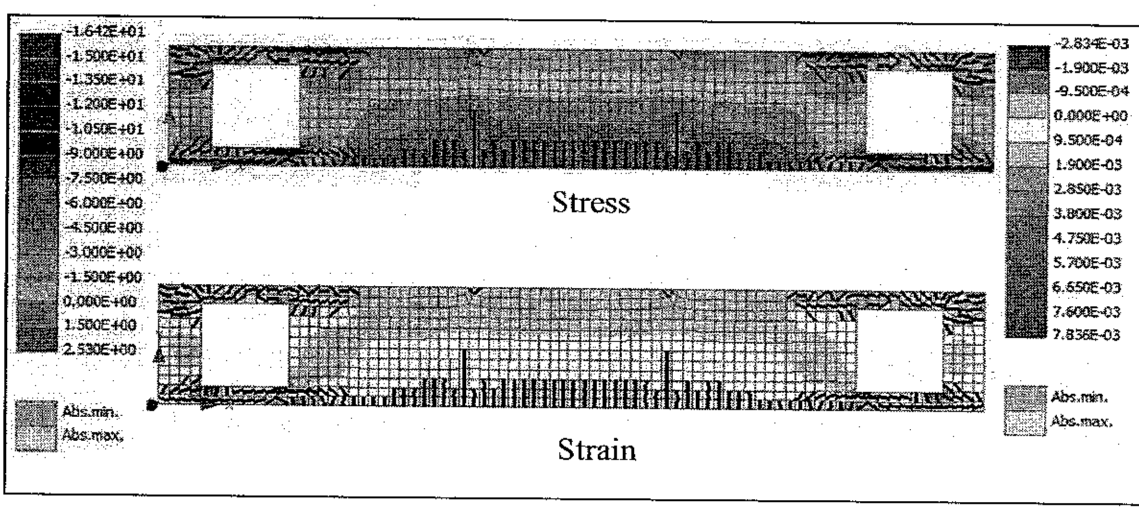

Figure 5.21 Crack patterns, stress and strain of beam S0S

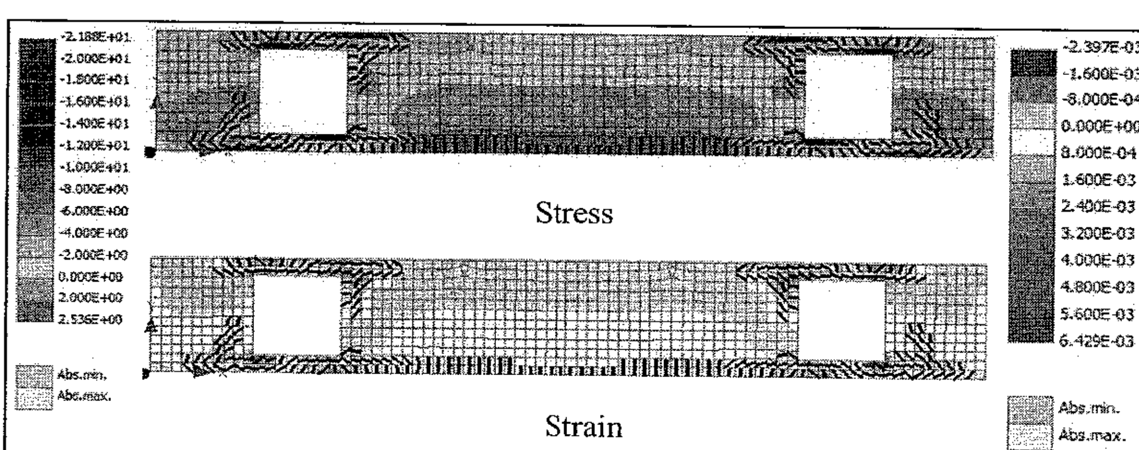

Figure 5.22 Crack patterns, stress and strain of beam S0.5dS

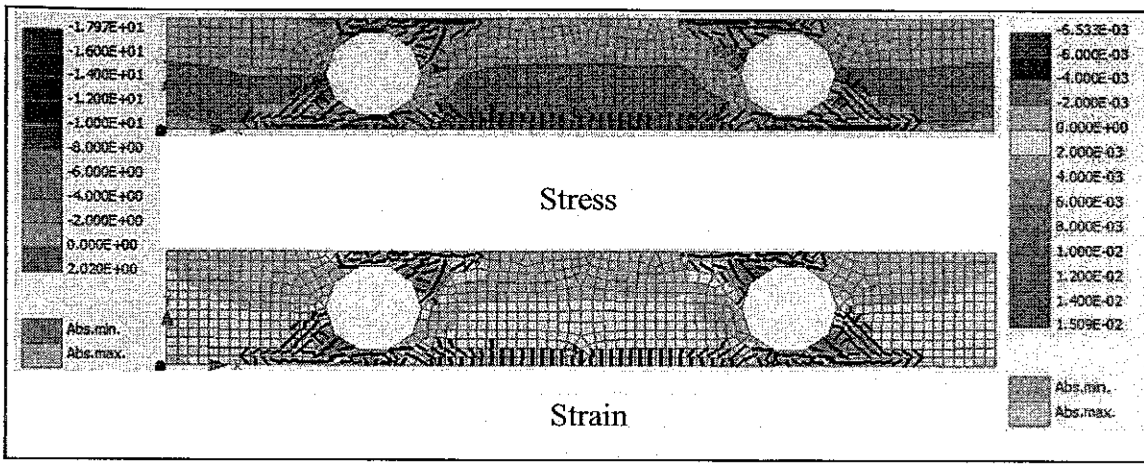

Figure 5.23 Crack patterns, stress and strain of beam CdS

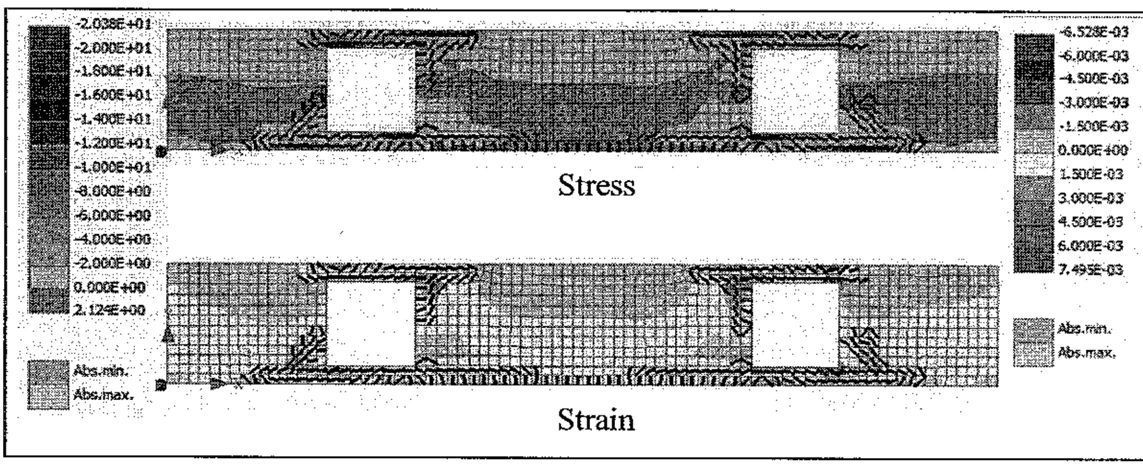

Figure 5.24 Crack patterns, stress and strain of beam SdS

5.3.2.2 Opening at One End Only

Crack patterns, stress and strain distributions of beams with a single opening at distance 0.5d, d and 1.5d from the face of support are presented in Figure 5.25 – 5.28, respectively.

(a) Beam with Single Square Opening (at a distance 0.5d from support), S0.5dS1

The crack patterns, stress and strain distributions of beam S0.5dS1 are presented in Figure 5.25. In the FE analysis, vertical cracks were observed in the middle-third span; about one-fourth of the beam depth from the bottom edge of the beam whereas diagonal cracks were noticed at the opening corners. The cracks at the top opening corners penetrated all the way to the top edge of the beam while the cracks at the bottom opening corners propagated to the beam support.

Based on the stress contour, tensile stress was observed maximum along the mid-span as such stresses were transferred into the steel at the bottom. These stresses were about 11 – 13% of the compressive stress. The maximum value of compressive stress was obtained as 15 MPa, which was about 42 – 44% of the ultimate strength of 35 MPa. The stresses were noticed at maximum at the top left and bottom right corners of opening and the top and bottom edges of beam towards the loading point and beam support, respectively.

The tensile strain from the strain contour showed that the strain was at maximum around the corners of opening located at the top right near the loading point and bottom left near the beam support. Similarly, it was also found in the top and bottom edges of the beam near the opening. The tensile strain was obtained in the range of 0.2 – 0.4%. Meanwhile, the compressive strain was observed at ultimate at the top left and bottom right corners of the opening, approximately 0.2 – 0.3%.

(b) Beam with Single Circular Opening (at a distance d from support), CdS1

Figure 5.26 illustrates the crack pattern, stress and strain contours of beam CdS1. During the analysis, vertical cracks were predicted to appear in the mid-span; such cracks initiated from the bottom edge of the beam and penetrated about one-third depth of the beam. The height and thickness of cracks were reduced as the cracks moved away from the mid-span region. Besides vertical cracks, diagonal cracks were noticed at the top and bottom sides of circular opening where the concentration and length of cracks increased as the cracks approaching the loading point and beam support, respectively.

According to the stress contours, tensile stress was in high concentration, approximately one-third depth of the beam in the mid-span. These stresses were noticed along the tension zone because the tensile stresses were transferred to the bottom longitudinal steel which was about 12 – 14% of the compressive stress. The maximum compressive stress was recorded as 15 MPa, which was about 42 – 44% of

35MPa, the ultimate design strength. These stresses were observed at ultimate at the top edge of the beam approaching the loading point and at the bottom edge of the beam to the support.

The strain contours illustrated that the tensile strain was found maximum at the diagonal cracks which formed at the circular opening towards the loading point and beam support, respectively. The tensile strain values were in the range of 0.4 –1.5%. The tensile strain signifies that wide diagonal cracks occurred in the concrete around the opening.

(c) Beam with Single Square Opening (at distance d from support), SdS1

The crack pattern, stress and strain distributions of beam SdS1 from the FE analysis are shown in Figure 5.27. The analysis predicted vertical cracks in the mid-span which initiated from the bottom edge of the beam and penetrated about one-third of the beam depth. As the cracks moved beyond the mid-span region, the height and thickness of cracks were reduced. Diagonal cracks were seen at the corners of the square opening and such cracks stretched all the way to the top and bottom edges of the beam, respectively.

Maximum tensile stress concentration in the mid-span was observed approximately one-third depth of the beam. It was found in the middle-third span since most of the tensile stresses were transferred to the bottom steel, approximately 10 – 12% of the compressive stress. The compressive stress was recorded at maximum as 16 MPa, which was about 44 – 46% of the ultimate design strength, 35 MPa. The high stresses were observed at the top edge of the beam near to the loading point and at the bottom edge of the beam near to the support; and at the top left and bottom right corners.

The tensile strain was observed maximum at the top right corner near to the loading point and bottom left corner towards the beam support; similarly at the top and bottom edges of the beam near to the opening corners. The tensile strain was recorded in the range of 0.1 –0.4% which signifies the formation of wide diagonal cracks at the opening corners. Meanwhile, maximum compressive strain was observed at the top left corner of the opening which was obtained as 0.2 – 0.3%.

(d) Beam with Single Square Opening (at a distance 1.5d from support), S1.5dS1

Figure 5.28 presents the crack patterns, stress and strain contours of beam S1.5dS1, with square opening located at distance 1.5d from the support. The crack patterns were found different than as it was discussed in beams S0.5dS1 and SdS1. From the prediction of FE analysis, vertical cracks were observed in the middle-third span, approximately one-fourth the depth from the bottom edge of the beam. These cracks were hindered by the presence of opening causing the reduction of height and length as the cracks moved towards the opening, leaving the mid-span region. Diagonal cracks were found at the opening corners and propagated to the top and bottom edges of the beam, respectively. The height and length of the diagonal cracks were reduced as compared to the cracks observed in beams S0.5dS1 and SdS1.

The tensile stress was found maximum in the middle-third span as shown in the stress contours, approximately 12 – 14% of the compressive stress. Meanwhile, compressive stress was observed ultimate at opening corners which located at the top left and bottom right of the opening; and also at the top edge of the beam. It was obtained as 15 MPa, which was about 41 – 43% of the ultimate design strength, 35 MPa.

At the opening corners, tensile strain was found maximum at the top right near to the loading point and bottom left near to the support; which obtained in the range of 0.2 – 0.5%. Compressive strain was noticed maximum at the top left corner of the opening, in which the strain value was about 0.2 – 0.3%.

In general, a similar crack pattern in beams with openings at one end only was traced as that of discussed for beam with openings at both ends. It was observed that vertical cracks that appeared in the tension zone were about one-fourth to one-third of the beam depth and as they moved away from the mid-span, the height and length decreased. Diagonal cracks were noticed at the corners of the square openings; and at the top and bottom sides of the circular openings.

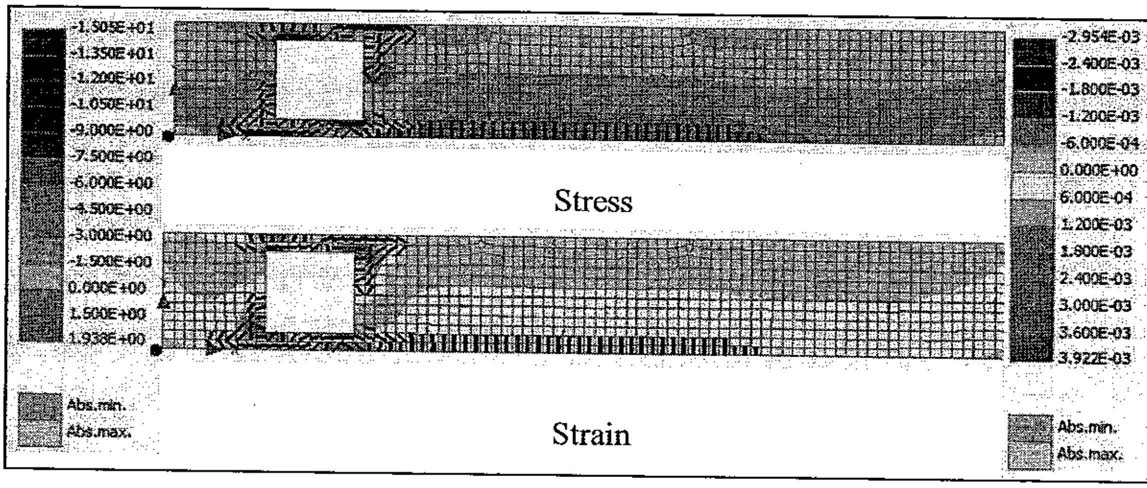

Figure 5.25 Crack patterns, stress and strain of beam S0.5dS1

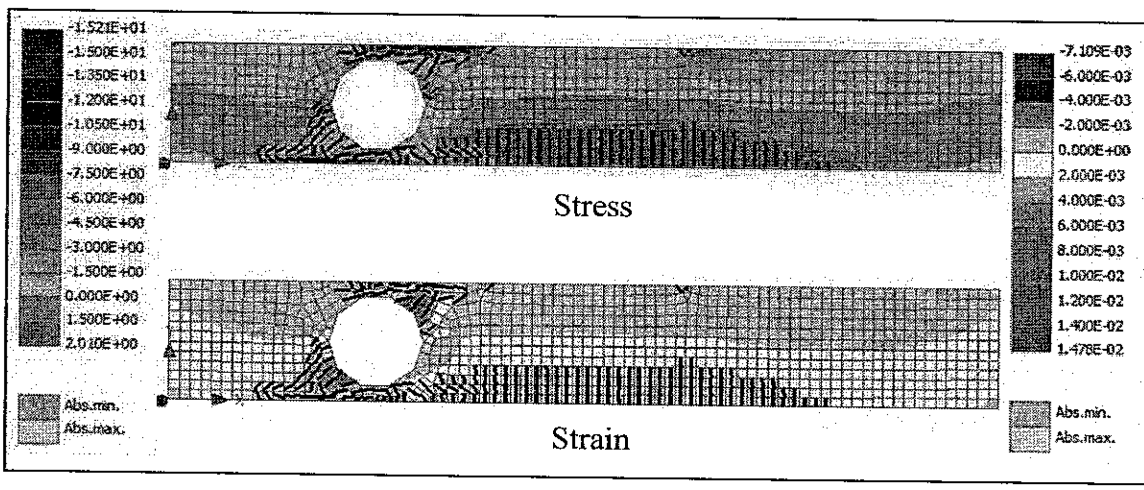

Figure 5.26 Crack patterns, stress and strain of beam CdS1

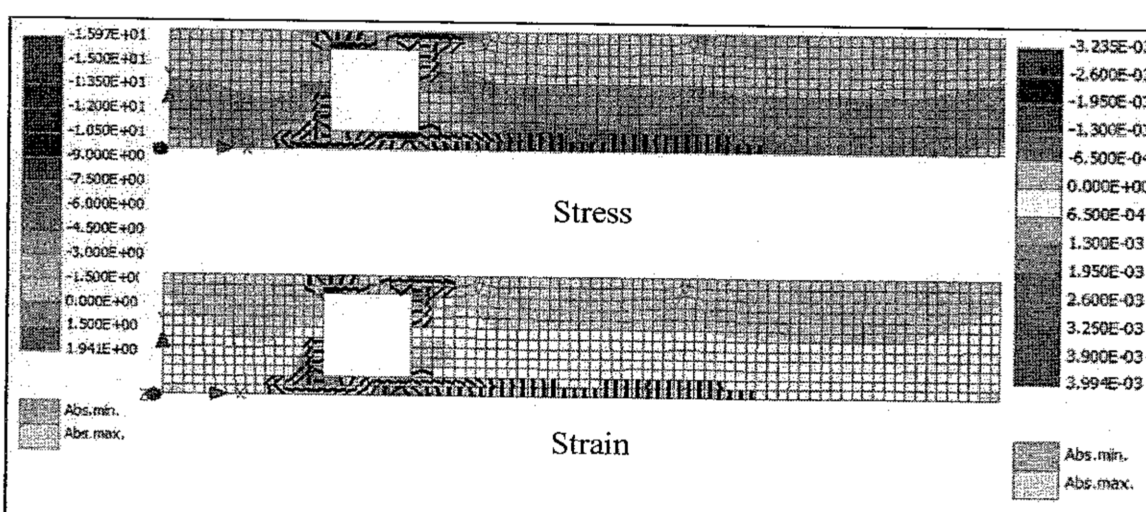

Figure 5.27 Crack patterns, stress and strain of beam SdS1

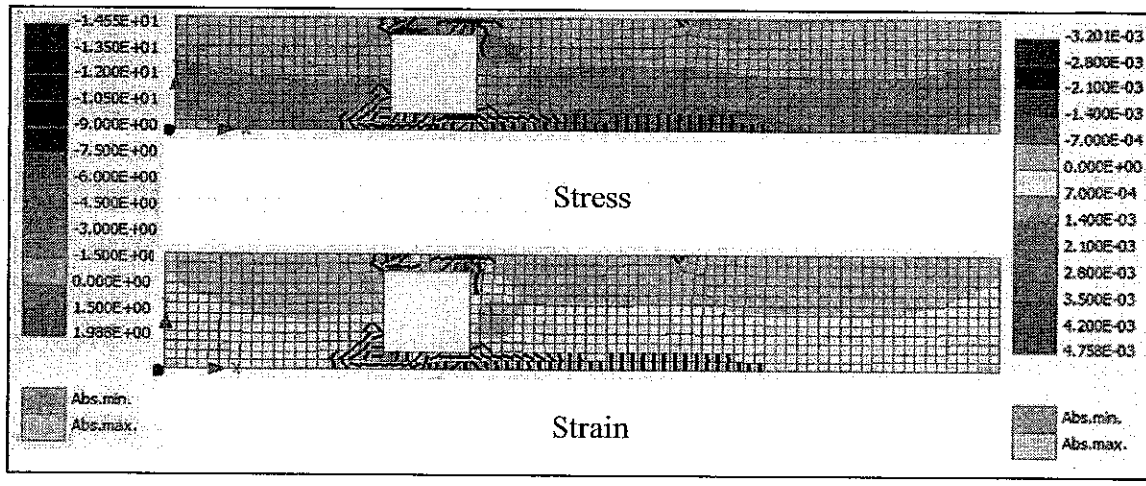

Figure 5.28 Crack patterns, stress and strain of beam S1.5dS1

5.3.3 Effects of CFRP Strengthening on Shear Capacity

As discussed in the earlier section; effects of opening in terms of shape, size and sequence on the reduction of capacity of beams were investigated. This section deals with the discussion on various strengthening options that if possible could return back the lost capacity. The results show that as a result of providing of opening in the shear zone, beams lost about 63 – 77% of design capacity. For this reason, many options were designed using numerical analysis and the most effective option was chosen to further validate using the experimental testing. All these are performed to achieve objective no. 2.

5.3.3.1 Design Configuration of CFRP Laminates

Descriptions of the strengthening configuration of CFRP laminates are given in Figure 5.29 for beams with openings at both ends and Figure 5.30 for beams with an opening at one end only. The strengthening configuration was selected from a number of strengthening options which is shown in Appendix D – I.

(a) Opening at Both Ends

Figure 5.29(a) illustrates one of the CFRP laminate configurations for beam C0S-S. A longitudinal CFRP laminate was placed on the elevation face of the top and bottom chords of the circular opening and on the bottom face of the beam below the opening. Additionally, a CFRP laminate was positioned diagonally next to each opening as shown in Figure 5.29(a). The strengthening configuration was designed according to the crack pattern which formed in un-strengthened beam, C0S as discussed in Figure 5.20. In designing the length of CFRP strip, the proper anchorage margin was also considered.

CFRP lamination scheme in Figure 5.29(b) explains one of the strengthening configurations for beam S0S-S. The CFRP laminates were placed around the square openings with a total of two longitudinal laminates at the top and bottom chords of the opening; two vertical laminates on the left and right sides of the opening; and two laminates longitudinally at the top and bottom beam surfaces above and below the opening. Crack patterns of the un-strengthened beam S0S were referred to the design of the strengthening configuration, as shown in Figure 5.21. To determine the length of CFRP laminates, adequate anchorage margin was also considered.

One of the strengthening configurations of beam S0.5dS-S with CFRP laminates is illustrated in Figure 5.29(c). The CFRP laminates were positioned around the openings similar as the strengthening configuration in beam S0S except that the length of vertical CFRP laminate on the left and right sides of the opening started and ended at the edge of the beam; while the length of longitudinal CFRP laminate at the top and bottom chords started at the edge of opening. Anchorage margin was considered in order to design the length of CFRP laminates. Likewise, the strengthening configuration of beam S0.5dS-S was adopted in beam SdS-S as shown in Figure 5.29(e). The CFRP lamination scheme is designed by referring to the crack pattern of the un-strengthened beams S0.5dS and SdS, respectively.

Figure 5.29(d) illustrates one of the CFRP laminate schemes for beam CdS-S. A longitudinal CFRP laminate was placed on the elevation face of the bottom chord of the circular opening and at the top beam surface above the opening; and a CFRP laminate was located diagonally next to each opening from the upper edge of the beam to the mid-span. The CFRP lamination scheme was designed according to the crack pattern that appeared in the un-strengthened beam, CdS as illustrated in Figure 5.23. The length of CFRP strips was designed based on the anchorage margin considered.

(b) Opening at One End Only

A chosen CFRP laminate configuration for beam CdS1-S is shown in Figure 5.30(a). A CFRP laminate was placed horizontally on the elevation face of the top and bottom chords of the opening. Similarly, same length of CFRP laminate was positioned longitudinally at the bottom surface of the beam. Between two horizontal aligned CFRP laminates at the top and bottom chords, a CFRP laminate was placed diagonally next to the opening. The strengthening configuration was designed by referring to the crack patterns in the un-strengthened beam CdS1 as discussed in Figure 5.26. The proper anchorage margin was considered to design the length of CFRP laminates.

Figure 5.30(b) presents one of the CFRP laminate schemes for beam with a single square opening at distance d from the face of support, SdS1-S. The strengthening scheme was designed based on the crack pattern in the un-strengthened beam SdS1 as illustrated in Figure 5.27. Similar to the strengthening configurations of beams S0.5dS1-S and SdS1-S, a CFRP laminate was placed vertically on the left and right sides of opening from the top to the bottom edges of the beam, a CFRP laminate was positioned longitudinally at the top and bottom surfaces of the beam and a longitudinal CFRP laminate was placed between the edges of opening corners at the top and bottom chords. To identify the length of CFRP needed, anchorage margin was taken into consideration.

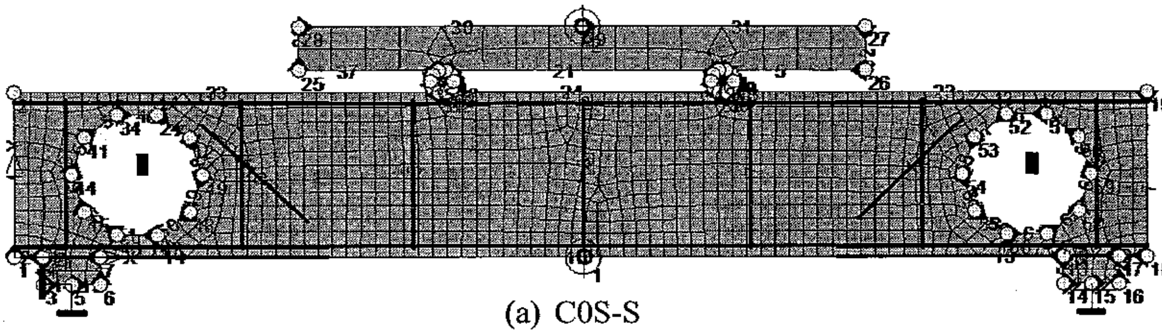

(a) C0S-S

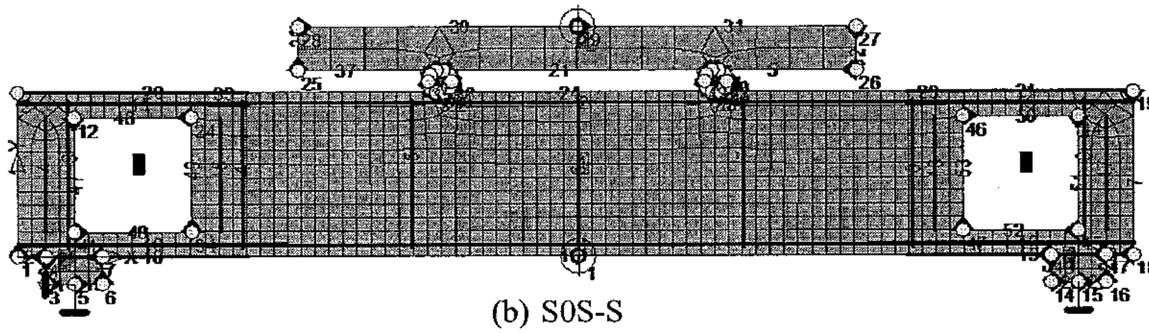

(b) S0S-S

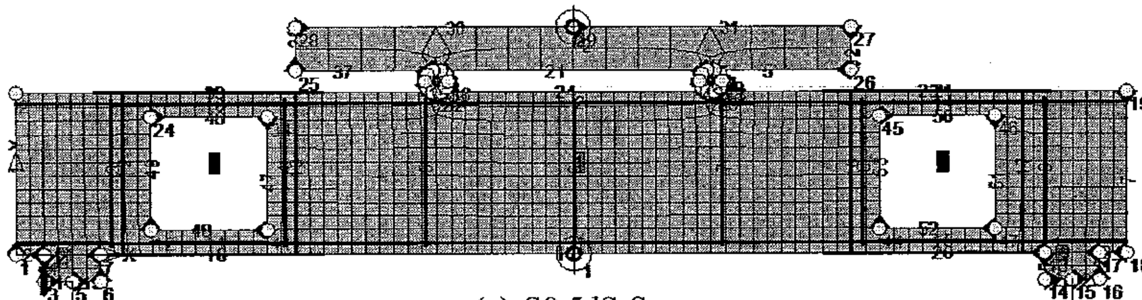

(c) S0.5dS-S

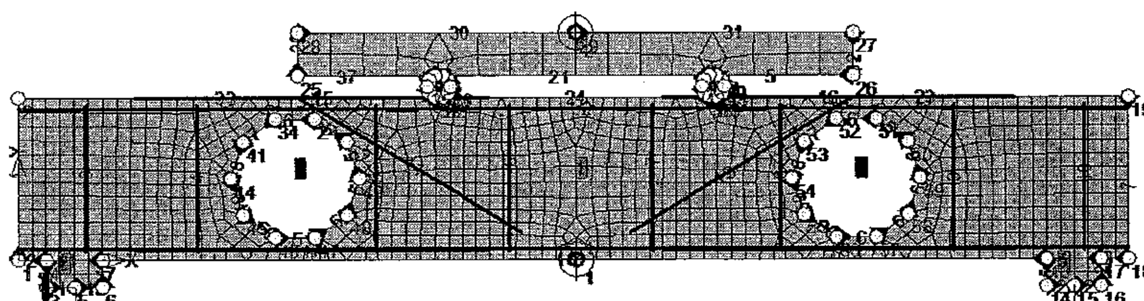

(d) CdS-S

Figure 5.29 CFRP strengthening scheme for beams with openings at both ends

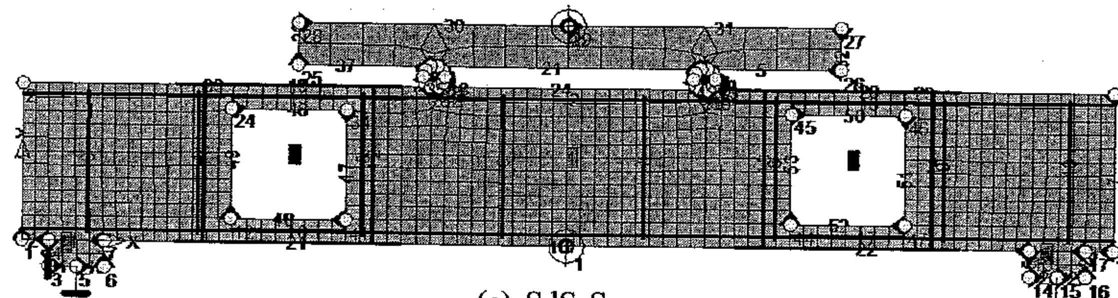

(e) SdS-S

Figure 5.29 CFRP strengthening scheme for beams with openings at both ends (Cont')

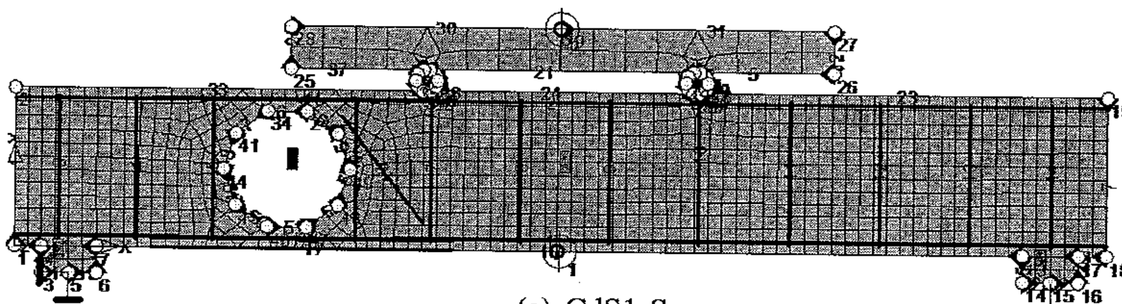

(a) CdS1-S

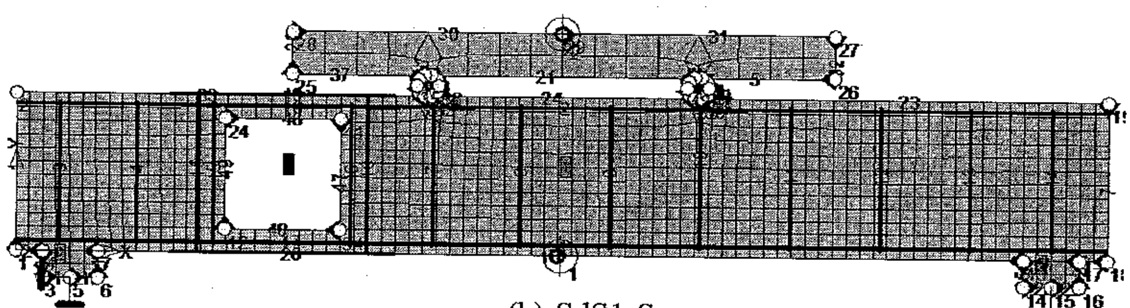

(b) SdS1-S

Figure 5.30 CFRP strengthening scheme for beams with an opening at one end only

5.3.3.2 Load-Deflection Behaviour

Load deflection behaviour as estimated using FE analysis of strengthened beams with openings at both ends is shown in Figure 5.31 and beams with an opening at one end only is given in Figure 5.32. The effects of the strengthening schemes with openings at various locations from the beam support are discussed as compared to the results of the control beam.

(a) Strengthening for Circular Openings (zero distance from support), C0S-S

In the initial phase of the elastic region, a linear elastic behaviour was observed until the first crack at the limiting load of P_{y1} was obtained as 29 kN at the deflection of 0.5 mm. After that, a small dip in the load-deflection curve was observed which may be due to widening of the crack. The beam loading then increases gradually with reduction in beam stiffness after some hardening effects until the second cracking at load, P_{y2} of 49.5 kN was observed at a deflection of 2.6 mm. The ultimate load was attained at load P_u of 50.4 kN at a deflection, Δ_u of 2.9 mm. Beyond that point, softening of beam took place and failure was at a deflection of 3.7 mm. As mentioned in section 5.3.1.1(a), providing a circular opening at each beam support significantly reduced 63 – 70% of the original beam capacity. The chosen strengthening scheme applied onto beam C0S-S has re-gained 58% of the original load-carrying capacity, CB. From the results, FE analysis shows that the external strengthening configuration could not fully reinstate the beam capacity.

(b) Strengthening for Square Openings (zero distance from support), S0S-S

The beam followed the similar trend as discussed for the beam C0S-S as plotted in Figure 5.31. However, the curve line deviated at the load of 20 kN, whereby the stiffness began to reduce until the first cracking at load, P_{y1} of 24.6 kN at a deflection of 0.4 mm. The early cracking may be due to the presence of sharp corners at square opening compared to circular. After that, gradual increase of load was observed with the reduction of beam stiffness due to cracking and hardening effects in concrete. A plateau-like load-deflection curve was noticed due to the minimal increment of load with deflection until the next cracking at load, P_{y2} of 35.1 kN with a deflection of 1.7 mm. The ultimate load, P_u of 36.9 kN was noticed at a deflection, Δ_u of 3.2 mm. The presence of square openings at the beam support greatly caused a loss of 67 – 73% of the original beam capacity, as discussed in section 5.3.1.1(b). External strengthening of the chosen configuration could re-gain the beam capacity to approximately 43% of the capacity of control beam, CB. Similar as discussed for beam C0S-S, external strengthening around openings provided at the beam support could not fully restore the beam original capacity.

(c) Strengthening for Square Openings (at distance 0.5d from support), S0.5dS-S

At the early stage, the elastic region ended as the first crack was initiated at load, P_{y1} of 21.8 kN at a deflection Δ_{y1} of 0.6 mm. The load increase gradually after that because of cracking and hardening effects in concrete until the second cracking at load, P_{y2} of 39.4 kN was observed at a deflection Δ_{y2} of 2.9 mm. After passing the second crack, the load increase with deflection until the ultimate load was obtained at load, P_u of 42.5 kN at a deflection, Δ_u of 3.8 mm. Softening of beam occurred just after the point of ultimate load and ended at a deflection of 5 mm. By providing a square opening at a distance 0.5d from the support at both ends, the loss of beam capacity was approximately 67-73%. With the strengthening configuration around the square openings, the beam capacity has re-gained 49% of load-carrying capacity of the control beam, CB.

(d) Strengthening for Circular Openings (at distance d from support), CdS-S

The initial stage of the elastic phase exhibited a linear straight line until the first crack which was observed at load, P_{y1} of 26.5 kN with a deflection of 0.2 mm. After that, a small dip in the load-deflection curve was noticed which may be due to the widening of cracks. With the increase of load, hardening effects in concrete lead to beam stiffness reduction until the next yielding load at P_{y2} of 49.0 kN at a deflection of 1.1 mm was observed. Soon after the second crack, the load increase until the ultimate load was obtained at load, P_u of 66.0 kN at a deflection, Δ_u of 2.0 mm. The possible reason may be due to the effects of CFRP laminates which could have increased the stiffness and capacity of the beam. After that, softening of beam happened rather rapidly and the deflection at failure was obtained at 2.3 mm. The un-strengthened beam with circular openings at distance d from the support has caused a loss of 63 – 70% of the beam original capacity, CB. Comparing to the control beam, strengthening of beam with the chosen strengthening configuration has re-gained the beam capacity to approximately 76%.

(e) Strengthening for Square Openings (at distance d from support), SdS-S

At the elastic period, the first crack was found at load, P_{y1} of 22.8 kN at a deflection of 0.7 mm. After passing the first crack, due to the hardening effects in concrete the load increase with deflection until the next cracking at load P_{y2} of 38.0 kN was observed at a deflection of 2.6 mm. The increment of load was observed up to the ultimate load, P_u of 41.8 kN at a deflection, Δ_u of 3.5 mm. Beyond that point similar to beam S0.5dS-S, effects of softening in beam were observed up to failure at a deflection of 5 mm. The presence of square openings at distance d from the face of support had caused a reduction of 67 – 73% of the load-carrying capacity of the control beam. Therefore, the strengthening configuration around the opening in this location has re-gained the beam capacity to approximately 48% as compared to the control beam.

From the results, strengthened beam with circular openings provided at distance d from the support, CdS-S exhibited higher beam stiffness and capacity as compared to opening that provided at the face of support, C0S-S. This shows that as the location of the opening was shifted to a region further away from the support, less critical condition of the beam was noticed.

In terms of square opening, the ultimate capacity of beams S0.5dS-S and SdS-S was found rather similar and greater than beam S0S-S. From the FE analysis of load-deflection, square openings provided at the face of support is the most critical location, while no significant difference was observed either the opening was located at distance 0.5d or at d from the support, as both locations gave almost the same beam stiffness and capacity, with a difference of 2%. Strengthening of beams with circular openings at the face of support and a distance d from the support with respect to their strengthening configuration has re-gained the beam capacity to approximately 58% and 76%, respectively. Meanwhile, strengthening configurations with CFRP in beams with square openings at the face of support and distance 0.5d and d from the support has re-gained 43%, 49% and 48%, respectively. In general, strengthening of beams with openings placed at critical region in the shear zone from the face of support up to distance d was found unable to return 100% beam capacity by any of the external strengthening performed. The maximum capacity can be re-gained by both internal and external strengthening.

Table 5.4 FEA results of beams with strengthened openings at both ends

Beam	Yielding load 1 P_{y1} (kN)	Δ_{y1} (mm)	Yielding load 2 P_{y2} (kN)	Δ_{y2} (mm)	Ultimate load P_u (kN)	Δ_u (mm)
CB	40.8	0.7	77.0	3.9	86.7	7.8
COS-S	29.0	0.5	49.5	2.6	50.4	2.9
SOS-S	24.6	0.4	35.1	1.7	36.9	3.2
S0.5dS-S	21.8	0.6	39.4	2.9	42.5	3.8
CdS-S	26.5	0.2	49.0	1.1	66.0	2.0
SdS-S	22.8	0.7	38.0	2.6	41.8	3.5

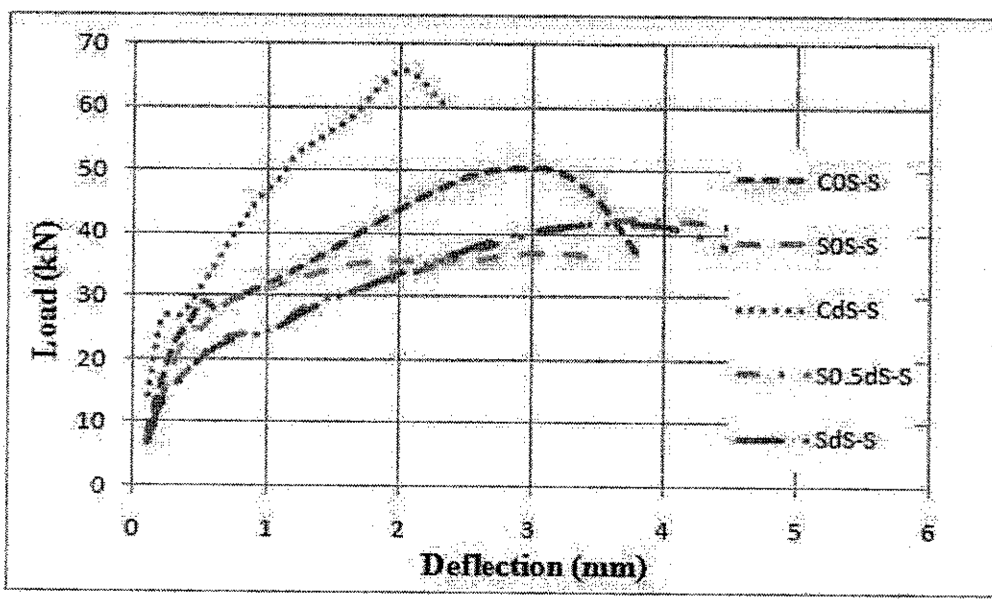

Figure 5.31 Load-deflection curves of beams with strengthened openings at both ends

(f) Strengthening for Single Circular Opening (at a distance d from support), CdS1-S

The load-deflection curve of beam CdS1-S is plotted in Figure 5.32. At the initial phase, a linear line was observed representing the elastic region until the initiation of first crack was observed at load P_{y1} of 18.2 kN at a deflection of 0.2 mm. After that, the load increase with reduction of stiffness due to cracking and hardening effects in concrete. The second yielding load, P_{y2} of 29.7 kN was observed due to cracking at a deflection of 1.0 mm. After passing that point, the stiffness was found slightly increased until the ultimate load, P_u of 34.9 kN at a deflection, Δ_u of 1.7 mm. The possible reason may be due to the strengthening effects which could have increased the beam stiffness and capacity to a certain level before failure. Softening of beam occurred immediately after the point of ultimate load and the load was noticed decreasing gradually until failure at a deflection recorded at 2.9 mm. A circular opening created at a distance d from the face of support caused a reduction of 73% of the original load-carrying capacity as discussed in section 5.3.1.2. As compared to the load-carrying capacity of the control beam, the strengthening scheme with CFRP laminates has re-gained the beam capacity of beam CdS1-S to about 40%. This signifies that the full capacity of the beam could not be reinstated by external strengthening around the opening provided at the critical shear zone.

(g) Strengthening for Single Square Opening (at distance d from support), SdS1-S

The trend of load-deflection behaviour discussed for beam CdS1-S was observed similar in beam SdS1-S as shown in Figure 5.32 except that beam SdS1-S exhibited lower in beam stiffness and capacity. In the early phase, the beam stiffness was found lower in the elastic region as compared to beam CdS1-S until the first crack which was initiated at load, P_{y1} of 19.6 kN at a deflection of 0.4 mm. After passing the first crack, the load increase gradually with the effects of hardening until the second cracking at load, P_{y2} of 25.7 kN was observed at a deflection of 0.9 mm. Similar as observed in beam CdS1-S, a slight increase in stiffness was observed after the second yielding and this may be due to the effects of CFRP laminates to increase the stiffness and capacity of the beam. The ultimate load, P_u of 34.8 kN was noticed at a deflection, Δ_u of 2.3 mm followed by softening effects of beam in which the failure was at a deflection of 3.2 mm. A square opening provided at a distance d from the face of support greatly reduced the beam capacity approximately 77% of the capacity of control beam, CB as reported in section 5.3.1.2. On comparison to the load-carrying capacity of the control beam, external strengthening with CFRP laminates around the square opening at this location has re-gained the beam capacity about 40%.

In general, strengthening of either a circular or square opening provided at a single end of the beam at a distance d from the face of support could only re-gained approximately up to 40% of the load-carrying capacity of the control beam. In other words, external strengthening of beams with opening provided at the critical shear zone could not fully reinstate the original beam structural capacity.

Table 5.5 FEA results of beams with strengthened openings at one end only

Beam	Yielding load 1 P_{y1} (kN)	Δ_{y1} (mm)	Yielding load 2 P_{y2} (kN)	Δ_{y2} (mm)	Ultimate load P_u (kN)	Δ_u (mm)
CB	40.8	0.7	77.0	3.9	86.7	7.8
CdS1-S	18.2	0.2	29.7	1.0	34.9	1.7
SdS1-S	19.6	0.4	25.7	0.9	34.8	2.3

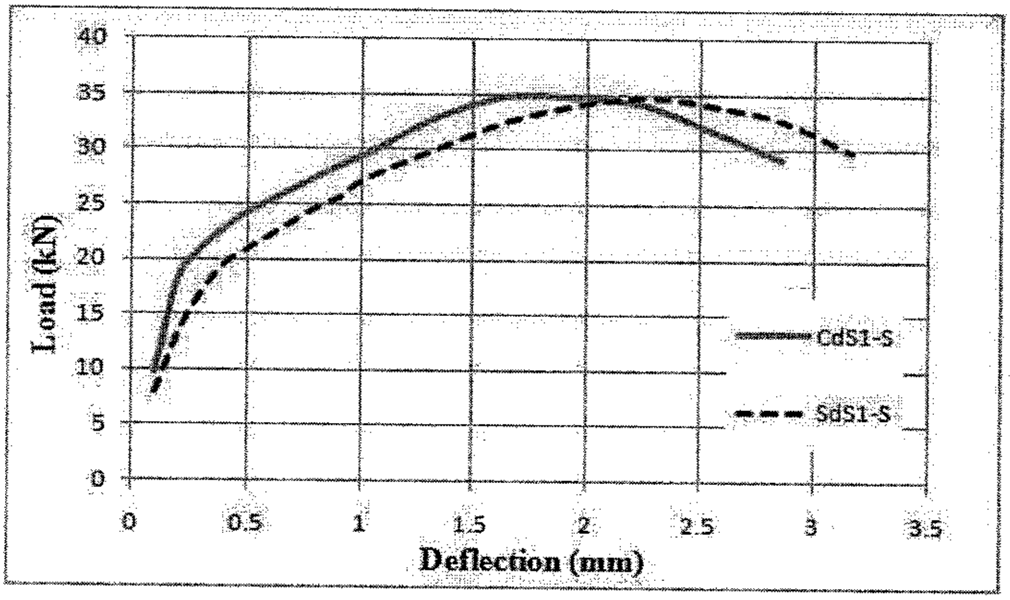

Figure 5.32 Load-deflection curves of beams with strengthened openings at one end only

5.3.3.3 Crack patterns and Stress Strain Distributions

In the following sub-sections, the effects of openings of various locations, shape and sequence strengthened with CFRP laminates in the FE analysis are investigated. During the analysis, crack patterns, stress and strain distributions of beams were observed.

(a) Strengthening for Circular Openings (zero distance from support), C0S-S

Figure 5.33 presents the crack patterns, stress and strain contours of beam C0S-S. From the FE analysis, vertical cracks appeared similar to that as discussed for un-strengthened beam, C0S in Figure 5.20 except the presence of concentrated diagonal cracks that appeared beyond the middle-third span. The possible reason may be due to the effects of CFRP laminates which hindered the propagation of cracks around the opening; hence the cracks appeared in the region away from the area strengthened by CFRP laminates which was in the mid-span. Cracks were predicted at the top side of the opening and penetrated diagonally through the top edge of the beam while the cracks at the bottom side of the opening propagated all the way to the bottom edge of beam near the support. As the cracks at the top side approaching the loading point whereas the cracks at the bottom side stretched towards the beam support, the height and length of cracks were reduced. It was observed that the cracks were more diagonally aligned in the strengthened beam compared to the cracks in un-strengthened beam which was more loosely dispersed. Some diagonal cracks were observed at the bottom edge of the beam near to the middle-third span as this may due to cracking at the end of CFRP laminates bonded with concrete.

Tensile stresses from the stress contours were found maximum in the middle-third span as the stresses were transferred into the bottom steel reinforcement. The ultimate tensile stress was obtained as 1.56 MPa, approximately 6 – 8% of the compressive stress. Compressive stress was recorded at maximum value of 20 MPa which was about 57% of the ultimate design strength, 35 MPa. It was noticed diagonally at the bottom of opening towards the beam support and the concrete cover at the loading points.

The strain contours illustrated that the tensile strain were noticed at maximum at the major vertical and diagonal cracks in the middle-third span. The presence of CFRP laminates has forced the cracks to be concentrated in the mid-span. The ultimate tensile strain was obtained in the range of 0.2 – 0.5% whereas compressive strain was found maximum diagonally at the bottom of the opening, 0.06 – 0.1%.

(b) Strengthening for Square Openings (zero distance from support), S0S-S

Crack patterns, stress and strain distributions of beam S0S-S as illustrated in Figure 5.34 showed that vertical cracks in beam S0S-S have increased to two-third of the beam depth as compared to one-third of the beam depth in beam S0S. In the FE analysis, major vertical cracks were also noticed as CFRP laminates strengthened zone has directed the crack propagation to appear in the middle-third span. In the top chord, the diagonal cracks at the corner of the opening were reduced due to the effects of CFRP laminates. These cracks were transformed into horizontal cracks at the top and bottom chords of the opening.

Stress contours showed that maximum tensile stress was found in the middle-third span with stress about 7 – 9% of the compressive stress as most of the stresses were transferred into the steel at bottom. The maximum compressive stress was obtained as 20 MPa which was about 56 – 58% of 35 MPa, the ultimate design strength. These stresses were found at the corners of the opening at the top and bottom chords.

Tensile strain was found maximum in the major vertical cracks in the mid-span about 0.09 – 0.6%. Similarly, such strain was noticed at the corners of the opening near to the beam support. Meanwhile, ultimate compressive strain was found at the opening corners near to the mid-span, approximately 0.3 – 0.4%.

(c) Strengthening for Square Openings (at distance 0.5d from support), S0.5dS-S

Figure 5.35 shows the crack patterns, stress and strain contours of beam S0.5dS-S. The prediction of FE analysis showed that major vertical cracks were formed with the height about one-third of the beam depth. The number of cracks increased in the middle-third span of beam S0.5dS-S as compared to un-strengthened beam S0.5dS as these cracks were directed from the restricted region with CFRP laminates. Similar crack pattern around the openings as discussed for beam S0S-S was observed in beam S0.5dS-S in which the diagonal cracks at the corners of the opening were replaced by horizontal cracks at the top and bottom chords of the openings.

As shown in the stress contours, the tensile stress in the middle-third span of the beam where the stress was at maximum, about 6 – 8% of the compressive stress. Meanwhile, the compressive stress was found maximum at the opening corners of the upper and lower chords was obtained as 21 MPa about 59 – 61% of the compressive stress.

A similar trend of tensile strain as discussed in beam S0S-S was observed in the beam S0.5dS-S. The maximum tensile strain was noticed at the major vertical cracks in the mid-span and at opening corners, about 0.1 – 0.5%. The compressive strain was found maximum in the opening corners as shown in Figure 5.35 about 0.2 – 0.3%.

(d) Strengthening for Circular Openings (at distance d from support), CdS-S

The FE analysis of crack patterns, stress and strain distributions of beam CdS-S is shown in Figure 5.36. CFRP strengthening around both openings had diverted the cracks away from the strengthened area into the middle-third span. Hence, the vertical cracks in beam CdS-S were found concentrated in the center of mid-span with cracks propagated to more than two-third of the beam depth from the bottom edge of the beam. The cracks at the top and bottom sides of openings were reduced due to the presence of CFRP laminates. Cracks were moved to the area without CFRP laminates in which the diagonal cracks at the openings appeared all the way to the beam support. The effects of CFRP laminates at the top chord had caused horizontal cracks to form at the concrete cover near to the loading points.

In the middle-third span, tensile stress was found maximum, about 7 – 9% of the compressive stress as the stresses were transferred into bottom reinforcement. At ultimate, the compressive stress was obtained as 18 MPa which was about 50 – 52% of the ultimate design strength, 35 MPa. It was found at the bottom chord below the left circular opening towards the beam support.

From the strain contours, maximum strain was observed at the major vertical cracks in the mid-span, approximately 0.6 – 2% while mild tensile strain was noticed at the diagonal cracks away from the strengthened zone, about 0.3 – 1.2%.

Compressive strain was found maximum at the top chord above the left opening which was recorded about 0.6 – 1.2%.

(e) Strengthening for Square Openings (at distance d from support), SdS-S

Crack patterns, stress and strain contours of beam SdS-S are presented in Figure 5.37. The strengthened beam showed that major vertical cracks appeared in the middle-third span with minor vertical cracks which propagated from the bottom edge about one-third of the beam depth. The concentration of cracks in the mid-span was increased as compared to the un-strengthened beam, SdS due to the effects of CFRP laminates around the openings which prevented the propagation of cracks and diverted the cracks into the middle-third span. Comparing to the un-strengthened beam SdS, less cracks were found around the openings of beam SdS-S.

Tensile stress from the stress contours showed that the maximum stress approximately 8 – 10% of the maximum compressive stress were found in the mid-span whereas compressive stress was found ultimate at the top and bottom chords near the opening corners, as shown in Figure 5.37, similar as observed in beam S0.5dS-S.

The tensile strain was found in the major vertical cracks in the mid-span, about 0.2 – 0.4%. It was also found at the corners of opening similar as discussed for beam S0.5dS-S. On the other hand, the maximum compressive strain was found in the opening corners, about 0.2 – 0.4%.

(f) Strengthening for Single Circular Opening (at a distance d from support), CdS1-S

Figure 5.38 presents the crack patterns, stress and strain distributions of beam CdS1-S. During the FE analysis, major vertical cracks penetrated from the bottom edge of the beam up to two-third of the beam depth. Diagonal cracks appeared at the top side and propagated to the loading point whereas cracks at the bottom side of opening stretched all the way to the beam support. Horizontal cracks were noticed along the bottom chord of opening from the face of support until the outer middle-third span.

These effects are due to the bonded CFRP laminates at the bottom chord of the opening.

Mild tensile stress was observed in the middle-third span about 1.5 MPa, approximately 9 – 11% of the compressive stress, as shown in the stress contours. Compressive stress was found maximum at the top side of opening diagonally to the loading point and at the bottom side of opening to the beam support. It was recorded as 15 MPa which was approximately 43% of the ultimate design strength, 35 MPa.

Strain contours illustrated that ultimate tensile strain was observed diagonally at the top side and bottom sides of the opening which was obtained in the range of 0.3 – 0.8%. The mild tensile strain was also observed around the major vertical cracks in the middle-third span which was about 0 – 0.2%.

(g) Strengthening for Single Square Opening (at distance d from support), SdS1-S

Crack patterns, stress and strain contours of beam SdS1-S are shown in Figure 5.39. The FE analysis predicted vertical cracks in the middle-third span penetrated about one-third of the beam depth from the bottom edge of the beam. Horizontal cracks at the top and bottom chords of the square opening were observed after strengthening by CFRP laminates.

The tensile stress of concrete was noticed in the middle-third span of the beam where the stresses are transferred into the bottom longitudinal steel, which was obtained as 1.5 MPa, approximately 8 – 10% of the compressive stress. Compressive stress was recorded maximum as 16 MPa which was found near the top left and bottom right corner of the opening along the horizontal cracks.

In the middle-third span, tensile strain was observed at the major vertical cracks, which was obtained as 0.09 – 0.3%. The maximum tensile strain was also found at the top right and bottom left of the opening corners and also at the bottom edge of the beam near the outer middle-third span. This may be due to the cracking and peeling effects at the end of CFRP and concrete. The compressive strain was noticed at ultimate at the top left corner of the opening, about 0.3 – 0.4%.

In general, it was found that the presence of CFRP laminates had transferred the cracks away from the strengthened area into the mid-span. Hence, the number of cracks has increased compared to the un-strengthened beams. Most of the diagonal cracks were replaced by horizontal cracks at the top and bottom chords of the opening.

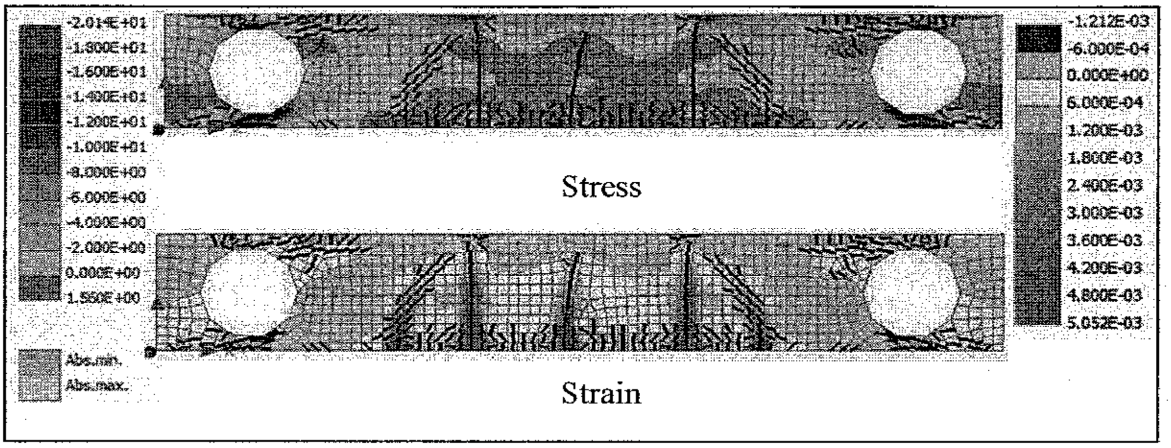

Figure 5.33 Crack patterns, stress and strain of beam C0S-S

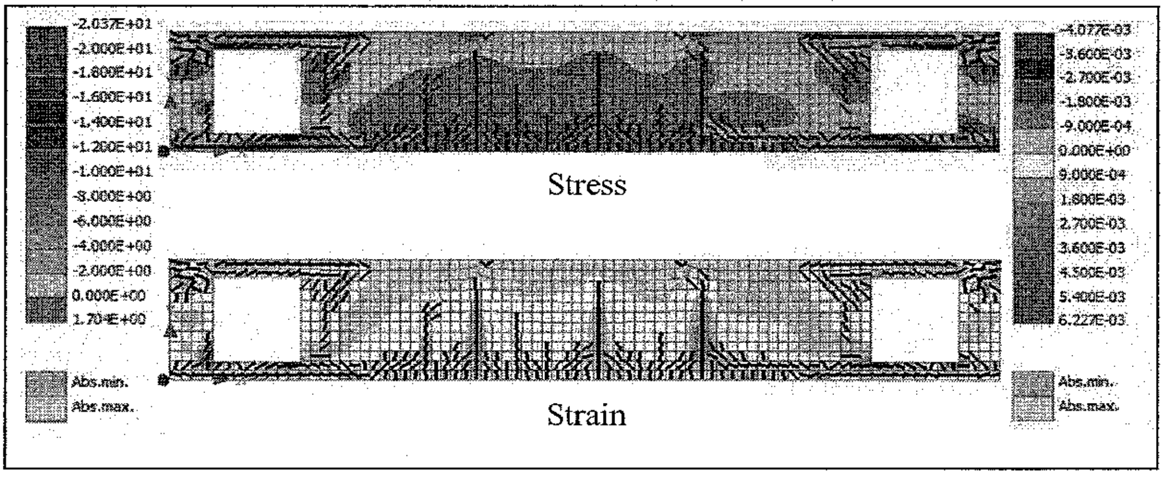

Figure 5.34 Crack patterns, stress and strain of beam S0S-S

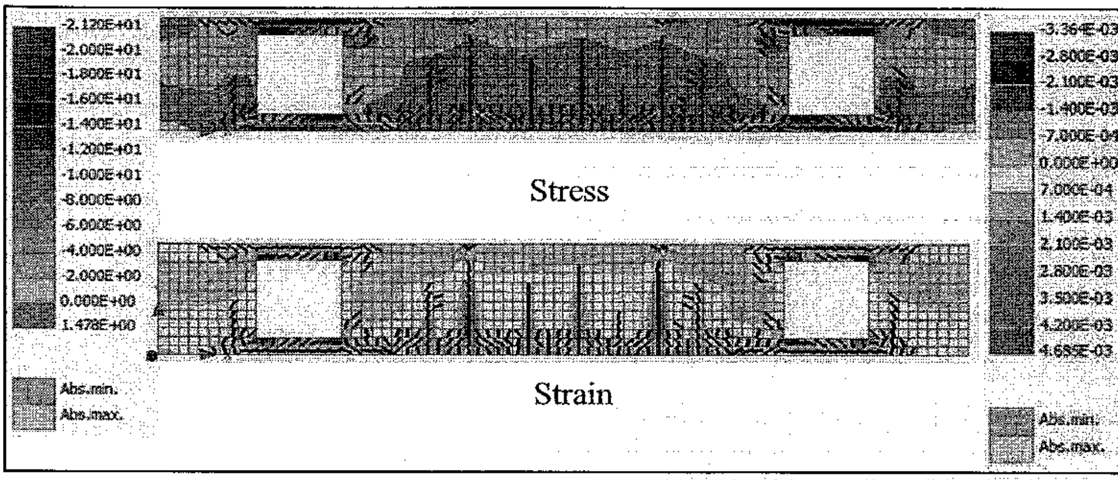

Figure 5.35 Crack patterns, stress and strain of beam S0.5dS-S

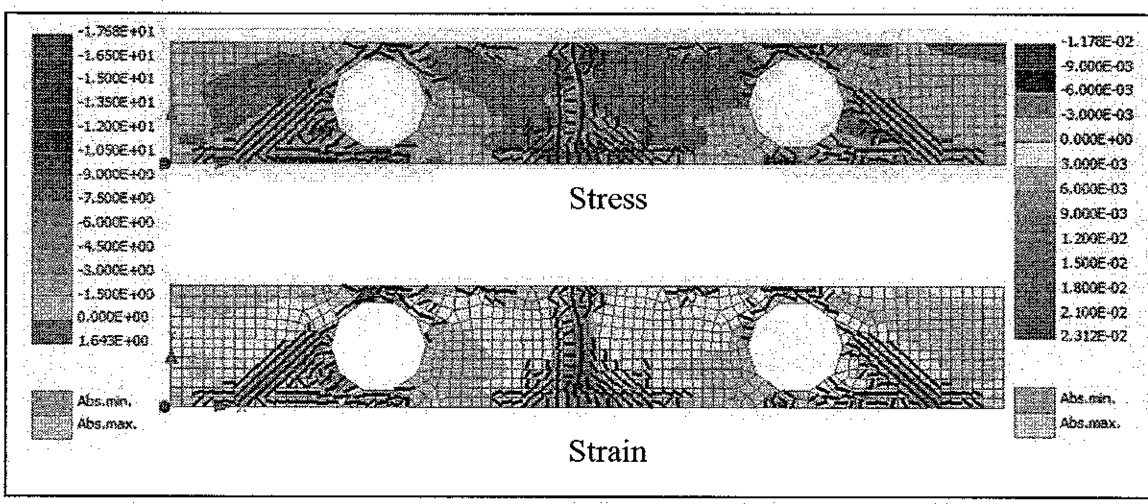

Figure 5.36 Crack patterns, stress and strain of beam CdS-S

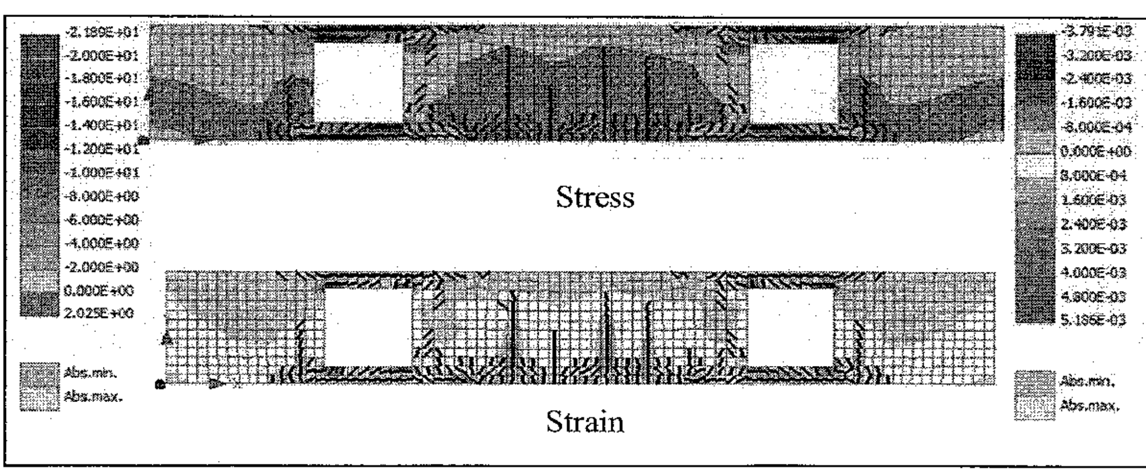

Figure 5.37 Crack patterns, stress and strain of beam SdS-S

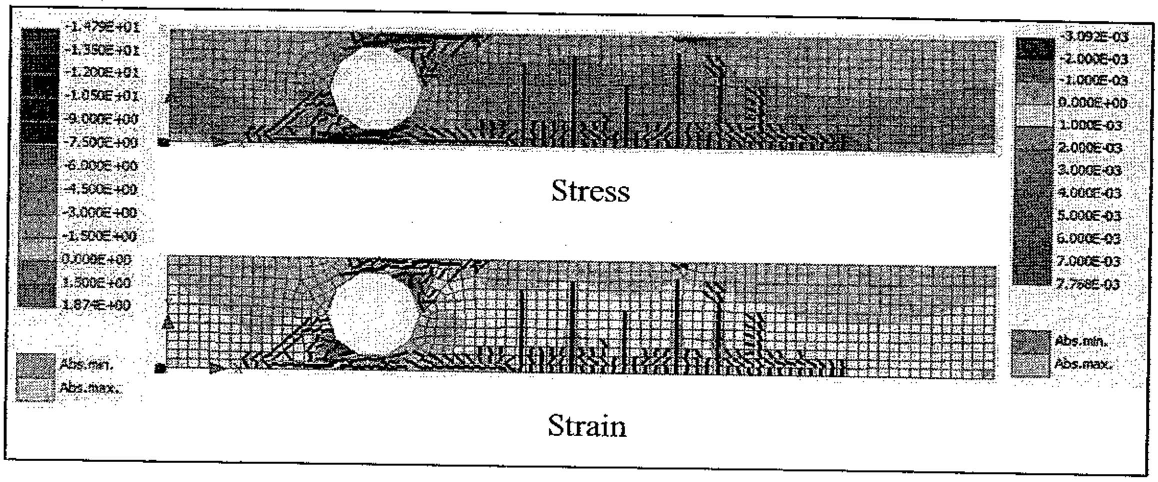

Figure 5.38 Crack patterns, stress and strain of beam CdS1-S

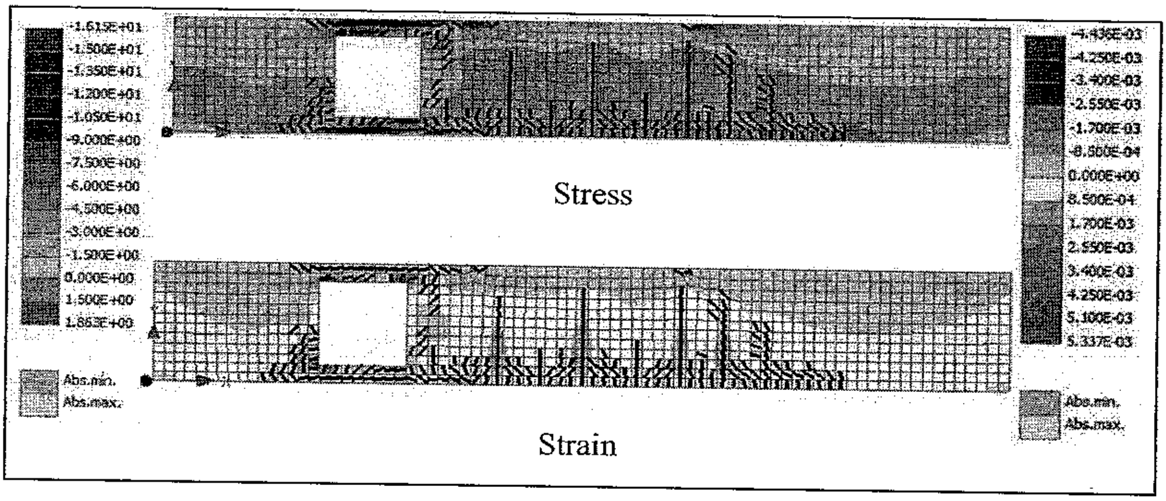

Figure 5.39 Crack patterns, stress and strain of beam SdS1-S

5.4 Summary

Based on the FE analysis, the following conclusions are made:

In terms of investigating the effects of openings provided in the flexure zone on the structural behaviour of the RC beams, circular and square openings provided in the flexure zone did not cause more than 2% reduction in the structural capacity. This may be due to the concrete loss within the low stress zone in the mid-span. This type of opening can be classified as 'small' opening as strengthening is not necessary in the mid-span. Small openings can be provided in RC beam by hacking/drilling which is not considered during the design stage. The presence of large rectangular and elliptical openings had caused a reduction of 53% and 48%, respectively of the capacity of control beam, CB. In general, elliptical openings showed greater beam stiffness and capacity compared to rectangular as the stress distribution around the openings was reduced due to the absence of opening corners.

The effects of openings provided in the shear zone on the structural behaviour of the RC beams show that circular and/or square openings at both ends had caused a reduction of 63 – 70% and 67 – 73%, respectively of beam capacity, CB. In terms of shapes, square openings caused a greater reduction due to high stress concentration at sharp corners of the openings which leads to early diagonal cracking. The effects of re-locating the openings from a distance 0, 0.5d and d from the support did not show significant difference, which was obtained as 5%. For beams with a circular and/or square opening at one end had caused a reduction of 73% and 76 – 77% of the capacity of beam CB, respectively. This is because of high stress concentration at the corners of square openings. Similar as obtained in openings at both ends, the effects of providing an opening at distances 0.5d, d and 1.5d from the support did not show significant difference, which was obtained as 5%.

In terms of crack patterns, openings either circular or square provided in the mid-span show that vertical cracks appeared in the middle-third span of the bottom chord and propagated towards the openings. Later, diagonal cracks were traced at the loading point to the beam support. Cracks also appeared diagonally at the corners and semicircles of rectangular and elliptical openings, respectively. On the other hand, the crack patterns of un-strengthened beams with openings at both ends show that minor vertical cracks were formed along the mid-span of the beams. Most cracks appeared as diagonal cracks at the top and bottom sides of circular openings and at sharp corners of square openings due to high stress concentrations. Crack pattern in beams with an opening at one end only was found to be similar to the beams with openings at both ends, as discussed earlier.

The most effective strengthening of opening using CFRP laminates using FE analysis was determined and summarized as follows:

In the flexure zone, the chosen strengthening configuration of beams LEF-S and LRF-S has increased the beam capacity to about 74% and 65% of beam capacity, CB. FE analysis shows that external strengthening with CFRP laminates could not 100%

reinstate the beam original capacity; hence, additional stirrups at the top and bottom chords of opening are needed. The large openings cannot be created in existing beams by hacking/drilling and sufficient reinforcement should be provided during the design stage. While in the shear zone, external strengthening using CFRP in the FE analysis shows that circular openings at both ends at distance zero (0) and d from the support has re-gained 58% and 76%, respectively of the beam capacity, CB while square openings provided at distance 0, 0.5d and d from the support has re-gained 43%, 49% and 48%, with respect to the control beam, CB. Similarly, strengthening with CFRP around an opening at one end only could only re-gained up to 40%. In general, openings placed at the critical region in the shear zone from the face of support up to distance d could not fully restore the original beam capacity, CB.

The crack patterns of the strengthened beams with an opening in the mid-span were seen concentrated in the beam mid-span at the bottom chord; and diagonally from the opening to the beam support. Meanwhile, strengthened beams around openings in the shear zone have transferred the cracks beyond the strengthened area into the mid-span. Hence, the number of cracks has increased compared to the cracks in un-strengthened beams. Most of the diagonal cracks were replaced by horizontal cracks at the top and bottom chords of the opening.

With the results obtained above, it is clearly shown that FE analysis using ATENA is helpful to the design engineers or planners for selecting the most appropriate opening(s) to facilitate the services requirements in buildings. Such analysis can save the cost of performing numerous experimental testing and enhanced the confidence of the designers to accurately determine the effects of opening sizes, shapes and locations in RC beams. It is also very useful to design the most effective strengthening schemes for the respective openings in order to fully reinstate the beam capacity.

CHAPTER 6

RESULTS OF EXPERIMENTAL STUDY

6.1 Introduction

This chapter presents the results of experimental study of RC beams with different configurations of openings. The main emphasis in the discussion was given to study the effects of size and configuration of openings on load-deflection behaviour, failure modes and crack patterns. In the second phase, beams were strengthened using CFRP laminates. Therefore, its effects are discussed in the later part of this chapter.

6.2 Effects of Openings on Flexural Capacity of Un-Strengthened Beam

In a simple beam, flexural stresses dominate in the middle third span where maximum bending moment usually occurs. Failure in bending usually occurs when the bending moment is sufficient to induce tensile stresses greater than the yield stress of the material throughout the whole cross-section. Therefore to study the effects of opening on flexural capacity, openings were provided in the mid-span of RC beams. The shapes of openings were circular, square, elliptical and rectangular, which covered about 8-24% of the beam elevation area and cut about 50-80% of the beam depth. The following sub-sections discuss the experimental results of the tested beams in terms of load-deflection behaviour, failure modes and crack patterns to attain objectives no. 1(i) and 1(ii).

6.2.1 Load-Deflection Behaviour

Figures 6.1 and 6.2 illustrate the load-deflection behaviour of RC beams with an opening in the flexure zone without any strengthening. The openings were classified as 'large', in which the criteria have been discussed in Section 2.6.1. Results of all such beams are compared with the results of the corresponding control beams, which are identified as CB1, CB2 and CB3. Table 6.1 summarizes the test results of such beams.

6.2.1.1 Control beam (CB1, CB2 and CB3)

There were three control beams CB1, CB2 and CB3 at the time of each series of casting. Therefore Figures 6.1, 6.2 and 6.3 showing the load-deflection curves of the three beams respectively. In the load-deflection curves, two (2) main points were identified, which are yielding point and ultimate point. The yielding load, P_y is defined as the load recorded at the initiation of the first crack and the maximum load recorded after passing the yield point is termed as ultimate load, P_u (Shafiq, 1987). The deflections measured at P_y and P_u are also denoted by Δ_y and Δ_u respectively. For further description, at yield point the load-deflection curve followed the sharp turn, which was observed in all of the graphs.

As shown in Figure 6.1, the load-deflection behaviour of CB1 is more ductile after the yielding load. For CB1, the load P_y was obtained as 79 kN at 5.4 mm deflection whereas the ultimate load, P_u was obtained as 116 kN at 29.5 mm deflection, which followed by a sudden collapse with little increment in load. Beam CB2 followed a similar trend until the first yield at point 'P'. It shows the yield load as 77 kN at 8.2 mm deflection. However, after the yield at point 'P', it exhibits more brittle behaviour and the ultimate load was found as 80 kN at 9.1 mm deflection. Although the 28 days compressive strength of CB1 and CB2 was the same, however due to different batches of casting, beam CB2 after casting may faced hot and dry weather condition during mixing and concrete hardening process that may cause some shrinkage cracks (Mosley et al., 2007), hence the post yielding behaviour had shifted to brittle. Similar to beam CB1, beam CB3 exhibited a similar trend of load-deflection behaviour. At point 'P' just before yielding of steel reinforcement, the yield load was obtained as 86 kN at 8.0 mm while the ultimate load was obtained as 96 kN at 36.4 mm. The increased in beam deflection with a constant load indicates that the beam demonstrates high ductile behaviour (Balaguru et al., 2008).

6.2.1.2 Effects of Circular Opening, CF

Circular opening in flexural beam covers 8% of the area and cut 77% of beam in the middle of the span. The load-deflection behaviour of beam CF plotted in Figure 6.1, which found of similar trend as that of the corresponding control beam, CB1. The beam has lost about 77% of its depth in the mid-span where most of the lost area is within the tension zone and 100% tensile stresses are transferred to the bottom steel. It is the main reason that the two load-deflection graphs (solid beam and with openings) are similar.

The lost area and depth of the beam causes a decrease in stiffness compared to control beam CB1, due to which higher ductility is shown by the CF beam. The yield strength of CF beam was obtained as 78 kN at a deflection of 7.7 mm, whereas the ultimate load as of 92 kN was observed at 16.7 mm deflection. The provision of the circular opening in flexure reduced 21% of the beam original structural capacity, which is not very significant. The reason is that the concrete area loss within the tension zone did not affect on the flexural capacity as all tensile stresses are transferred to tensile steel reinforcement (Mosley et al., 2007). The opening in the mid-span can serve as a spring. Hence, the ductility could be maintained to some extent. This signifies that providing a circular opening in the mid-span of a structure still be able to sustain large deformation without failure (Aly et al., 2003).

6.2.1.3 Effects of Square Opening, SF

Square opening size was adopted as 210 x 210 mm, which caused a reduction in the area as 8% and a concrete depth loss as 70%. Referring to Figure 6.1, the yield load of beam SF was obtained as 57 kN at 3.8 mm deflection whereas the ultimate load as of 75 kN was observed at 11.0 mm deflection. The inclusion of an opening in the mid-span caused a loss of 70% of the beam depth significantly reduced the beam capacity to 35%. Similar as beam CF, the deflection increased with an almost constant load, indicating ductile behaviour in which the ability to undergo deformations without a substantial reduction in the beam capacity (Olivia & Mandal, 2005; Balaguru et al., 2008).

As compared to circular openings, square openings caused an appreciable reduction in the beam capacity. It is because of the reasons that at the four corners caused stress concentration and change of stress flow path. A stress concentration is a location where stress is concentrated. This arises due to the various local changes in shape such as sharp corners and even curved members of sharp curvature (Huston & Josephs 2008). It was also evident that diagonal cracks were originated from the four corners, which is explained in detail in the section 2.6.2.2.

The increased stresses lower the resistance of the beam to impact and loading condition is one of the factors contributing to beam failure (Hsu et al. 2008). Stress concentration will decrease with increasing radii in the corners of the opening (Moreno, 2011) where circular shape is the symmetrical in nature that prevent stress concentration.

6.2.1.4 Effects of Large Elliptical Opening, LEF

Large elliptical opening, LEF provided of the dimension of 140 mm height and 800 mm length in the middle of the beam elevation. The semi-circles at both ends were about the diameter of 140 mm. The elliptical opening resulted in 24% of area loss and 47% of the beam depth loss.

This beam was cast in a second batch of casting, therefore to have realistic situation a control beam CB2 was cast for comparison. The large elliptical opening reduced the beam capacity by about 39% as compared to that of the beam CB2. As shown in Figure 6.2, the yield load, P_y of beam LEF was obtained as 32 kN at 2.0 mm deflection, whereas the ultimate load, P_u was found as 49 kN at 3.3 mm deflection. The load P_y for LEF was less than 50% of P_y of the beam CB2. One of the reasons is that 800 mm long opening turned the top and bottom part of the beam as the chord, therefore, when load was applied through the top chord it has affected (caused deflection) the top chord before transferring to the bottom chord. In a way, it was similar to a Vierendeel girder. From the load-deflection behaviour in Figure 6.2, it was observed that beam LEF exhibited a sharp reduction after failure. This is due to the stress concentration at the bend of the elliptical opening (Hsu et al. 2008).

6.2.1.5 Effects of Large Rectangular Opening, LRF

The large rectangular opening with a size of 140 mm width and 800 mm length were provided in the beam mid-span. The rectangular opening caused 21% of area loss and cut 47% of the beam depth.

Beam LRF was produced in a third batch of casting, hence for comparison reasons a control beam, CB3 was cast. The opening resulted in a decrease in beam capacity by about 59%, as compared to that of beam CB3. In Figure 6.3, the yield load was obtained as 34 kN at 2.5 mm deflection, whereas the ultimate load of 39 kN was observed at 3 mm deflection. Compared to the yield load, P_y of beam CB3, the yield load, P_y of beam LRF was found less than 59%. This is due to the similar phenomenon as observed in beam LEF, the 800 mm long and 140 mm depth opening separates the beam into two segments which consists of upper and lower chords. Hence, when load was applied through the top chord, the top chord deflected before the bottom chord. The beam behaves similarly to a Vierendeel panel at the opening segment which is explained in detail in the section 2.4.1.2. Referring to Figure 6.3, beam LRF exhibited a sharp decrease after the ultimate load was reached. One of the reasons is due to the discontinuity in the beam cross section provided by the opening whereby the stress concentration occurred at its corners. The stress concentration resulted in excessive cracking and caused premature failure of the beam (Mansur, 1983).

Table 6.1 Test results of RC beam with opening in flexure

Beam	Yielding load P_y (kN)	Δ_y (mm)	Ultimate load P_u (kN)	Δ_u (mm)	$\left(\frac{\text{Opening Area}}{\text{BEA}}\right)$ x 100%	$\left(\frac{\text{BCD}}{\text{TBD}}\right)$ x 100%
CB1	79	5.4	116	29.5	-	-
CB2	77	8.2	80	9.1	-	-
CB3	86	8.0	96	36.4	-	-
CF	78	7.7	92	16.7	8	77
SF	57	3.8	75	11.0	8	70
LEF	32	2.0	49	3.3	24	47
LRF	34	2.5	39	3.0	21	47

BEA = Beam Elevated Area
BCD = Beam Cut Depth
TBD = Total Beam Depth

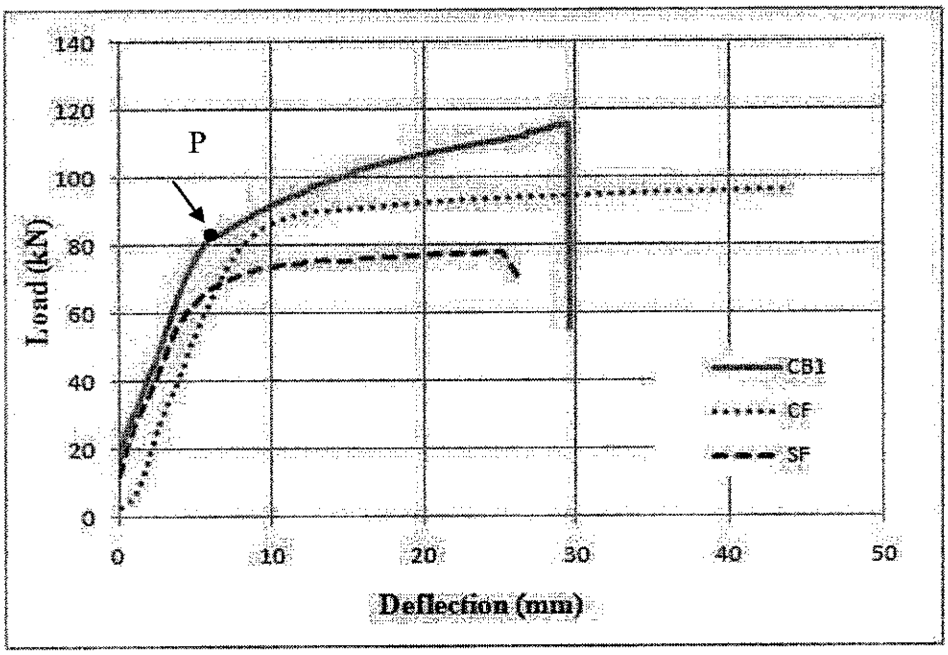

Figure 6.1 Comparison of the load-deflection behaviour of beams with un-strengthened opening in flexure

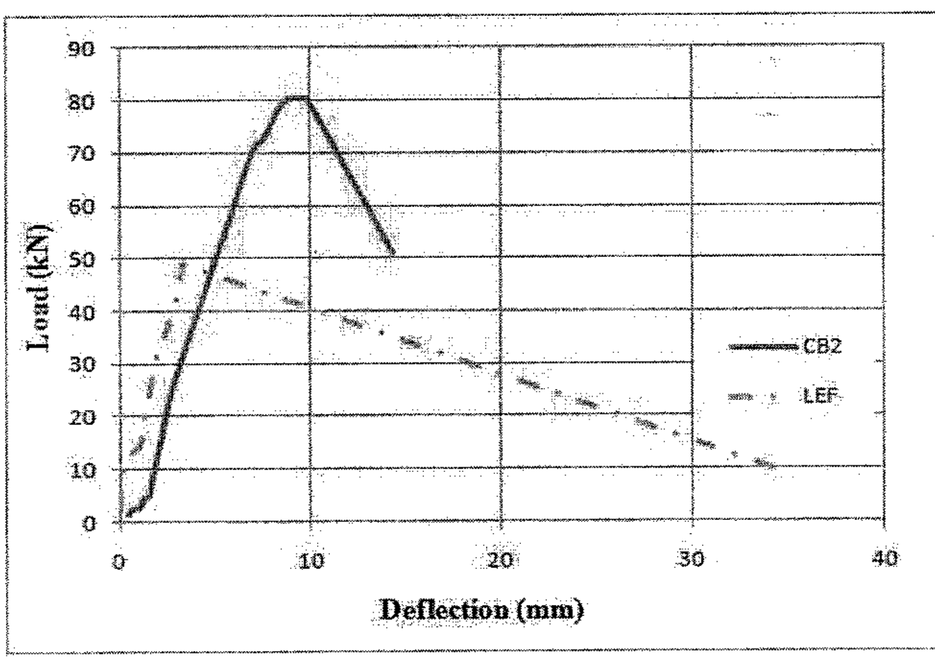

Figure 6.2 Comparison of the load-deflection behaviour of beams CB2 and LEF

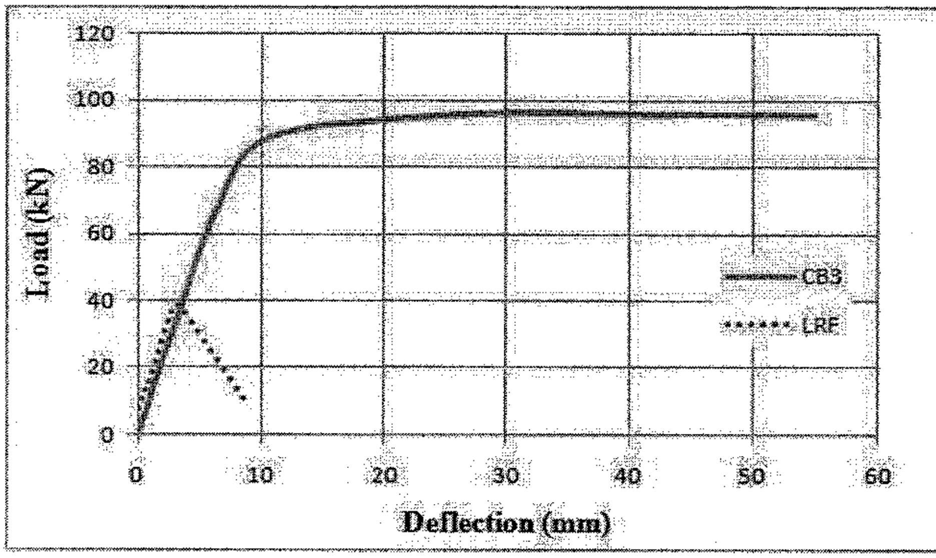

Figure 6.3 Comparison of load-deflection behaviour of beams CB3 and LRF

6.2.2 Failure Modes and Crack Patterns

In the following section, failure modes and crack patterns of control beams and un-strengthened beams with opening are presented and discussed. The results were observed and recorded up to failure.

6.2.2.1 Control Beams (CB1, CB2 and CB3)

Crack patterns of control beams, CB1, CB2 and CB3 are shown in Figures 6.4 to 6.6, respectively. Crack patterns of control beam, CB1 in which the first crack was observed in the mid-span of the beam is illustrated in Figure 6.4. As the load increased, cracks were formed along the tension zone of the beam length and eventually diagonal cracks appeared near to the support. The cracks appeared in the middle-third span of the beam were vertically aligned, which originated from the bottom edge of the beam and propagated upward. The mean length of such cracks was equal to about two third of the total depth of the beam; it means the cracks appeared mostly in the tension zone. Since no cracks were noticed in the upper part of this part of the beam, which means concrete crushing was not occurred. Cracks in this zone can be termed as the flexural cracks. The cracks appeared beyond this zone was typically diagonally aligned and penetrated towards the applied load as the load increased; such cracks are termed as shear cracks.

In general, failure of beam CB1 is governed by shear failure. The failure was initiated from the widening of diagonal cracks those initiated near to the support at the bottom edge of the beam. With the increment in load, concrete was completely spalled at the bottom of the beam and bottom bars were completely exposed. Therefore, on further increment in load the beam faced failure. The reason would be that the shear link or shear reinforcement was purposely provided as the minimum reinforcement.

Figure 6.5 illustrates the crack patterns of control beam CB2. The failure modes and crack patterns of beam CB2 were found similar to beam CB1. At an early stage, flexural cracks were found along the mid-span of the beam. With the increase of load, the flexural cracks slowly penetrated vertically towards the neutral axis of the beam as well as the formation of diagonal cracks near to the support. An abrupt shear failure occurred at the left support exhibiting a see-through gap where the top and bottom bars were noticed. Crushing of concrete cover was observed at the left loading point and support. Due to the shear failure, the diagonal crack width was significant between the loading point and support.

As mentioned earlier, the early cracks were appeared in flexure zone. It was observed that both beams CB1 and CB2 failed because of the diagonal cracks in the shear zone, which is called shear dominant failure. The failure happened in the left span, it may be due to the fact that the left end reached to failure before the other end. Diagonal cracks started to appear when the propagation of the tensile cracks was not resisted by the longitudinal tensile reinforcement. With the increase of load, the diagonal cracks extended into the compression zone, reducing the compression area to an ineffective amount; resulting in beam collapse (Larson, 1998).

Figure 6.6 shows the crack patterns of control beam CB3. Flexural cracks were observed in the middle-third span of the beam. The beam showed good ductility and failure was governed by flexure. Significant flexural cracks were observed, those penetrated up to the neutral axis before failure. The concrete cracks in the tensile strain region in which all the tension is carried by the reinforcement (Mosley et al., 2007). The beam fails when the bending moment is large enough for tensile stress to reach the failure stress of the material. The crack and failure patterns of CB3 were dissimilar to control beams CB1 and CB2. In the control beam CB3, the reinforcement was purposely increased by reducing the spacing of the link.

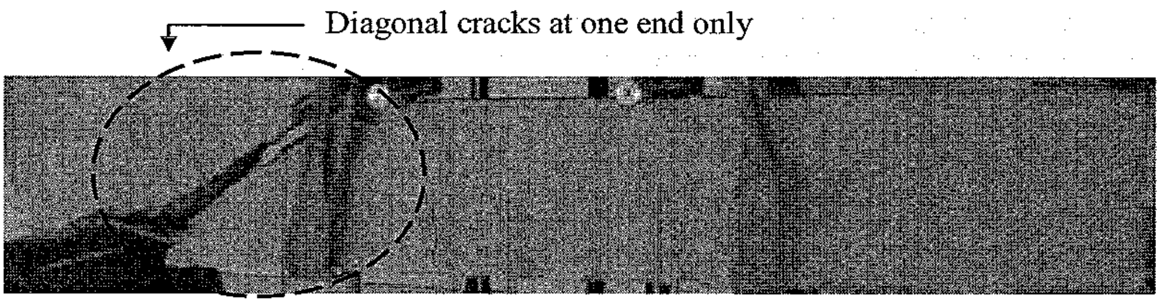

Figure 6.4 Crack patterns of control beam CB1

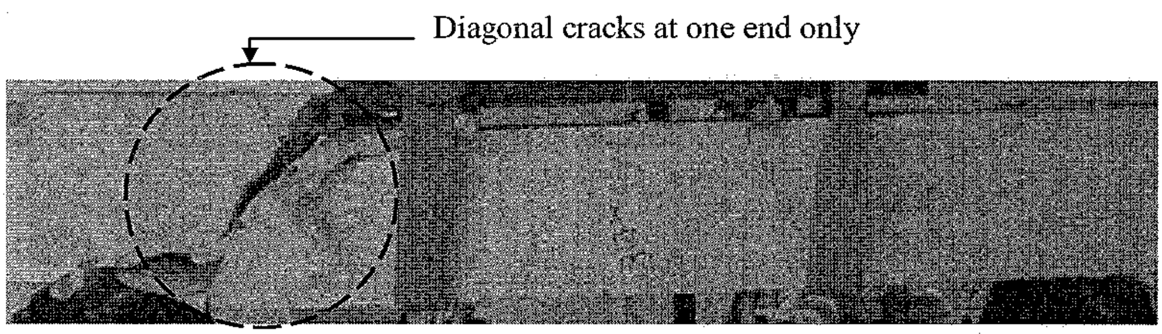

Figure 6.5 Crack patterns of control beam CB2

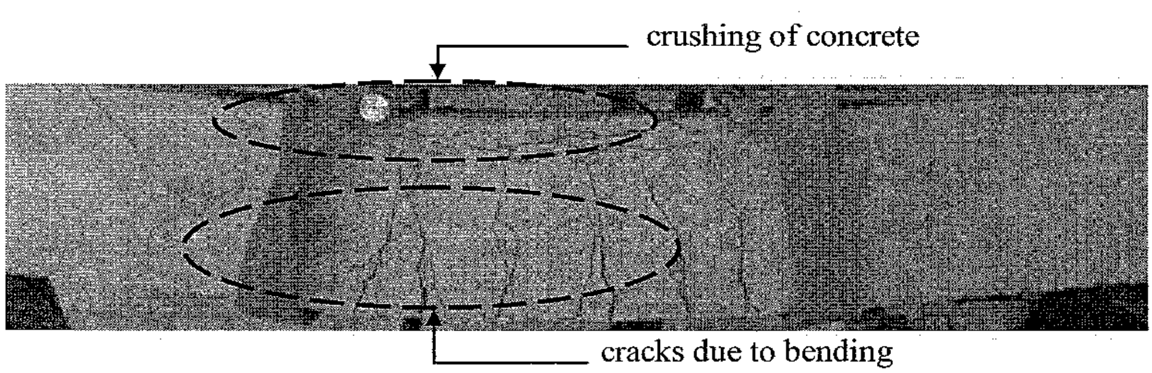

Figure 6.6 Crack patterns of control beam CB3

6.2.2.2 Effects of Circular Opening, CF

Effects of single circular opening in the mid-span on failure mode and crack patterns are illustrated in Figure 6.7. The early cracks were observed in the mid-span at the soffit of the beam, which then propagated at the left and right sides of the opening. Such cracks were diagonally aligned from bottom to top. When the beam showed noticeable deflection, cracks became prominent at the top chord of the opening; such cracks were horizontally aligned as shown in Figure 6.7 and later failure was happened by crushing of concrete in that chord. When the beam reached to an adequate deflection, the solid parts at the left and right sides of the opening exerted axial compression and tension on the top and bottom chords respectively, which is illustrated in Figure 6.7a. Due to 77% of the beam depth cut, the top chord area has reduced and the crushing was occurred, whereas most of the tension was transferred to the longitudinal bars.

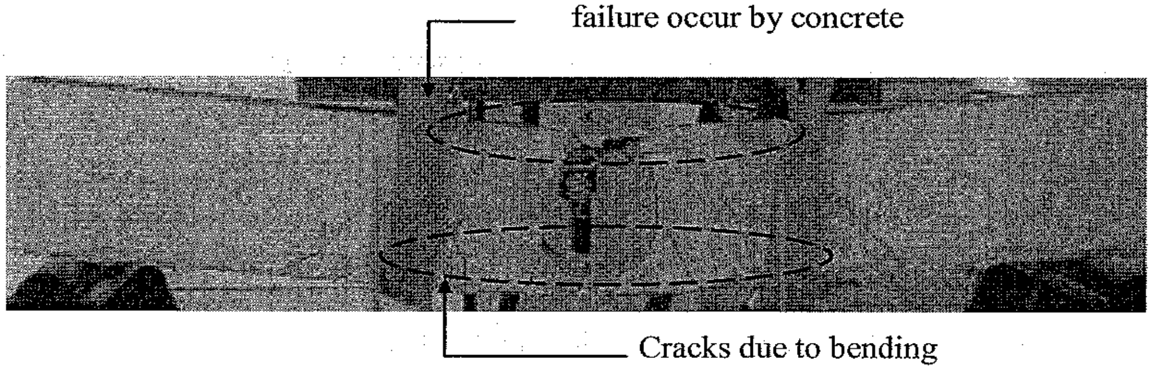

Figure 6.7 Crack patterns of un-strengthened beam CF

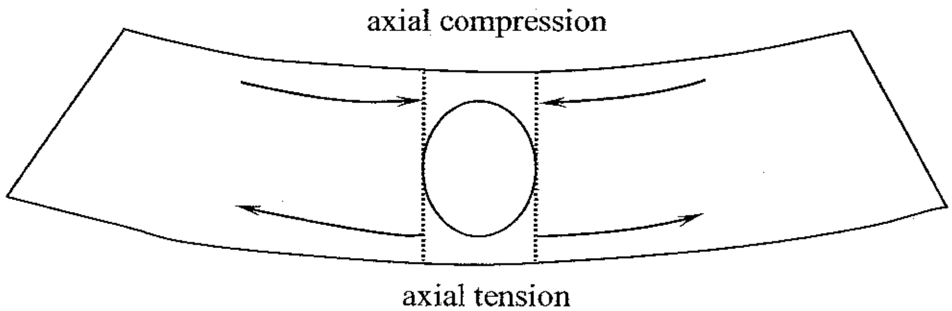

Figure 6.7a Axial compression and tension on top and bottom chord

6.2.2.3 Effects of Square Opening, SF

Figure 6.8 shows the effects of a single square opening in the mid-span on failure mode and crack patterns. The initial cracks were found in the mid-span at the soffit of the beam and then penetrated at the left and right sides of the opening. These cracks were diagonally aligned from the beam soffit towards the applied load. When visible deflection was observed, cracks became obvious at the top chord of the opening; such cracks were horizontally aligned with diagonal cracks at the applied load as illustrated in Figure 6.8. The failure occurred eventually with a slip in the top chord due to localized shear failure. As the beam undergone sufficient deflection, the solid sections on the left and right sides of opening applied axial compression and tension forces on the top and bottom chords respectively, which is shown in Figure 6.8a. Compared to circular section, the square shape has greater concrete area at the four corners which are subjected to high stress concentration that leads to early diagonal cracking (Mansur et al., 1992). One of the reasons is that because of stress concentration, failure is dominated in the bottom chord in which crushing of concrete was observed. Due to 70% of the beam depth loss, the top chord area has reduced with an increase in bottom chord when most of the tension was transferred to the bottom steel reinforcements.

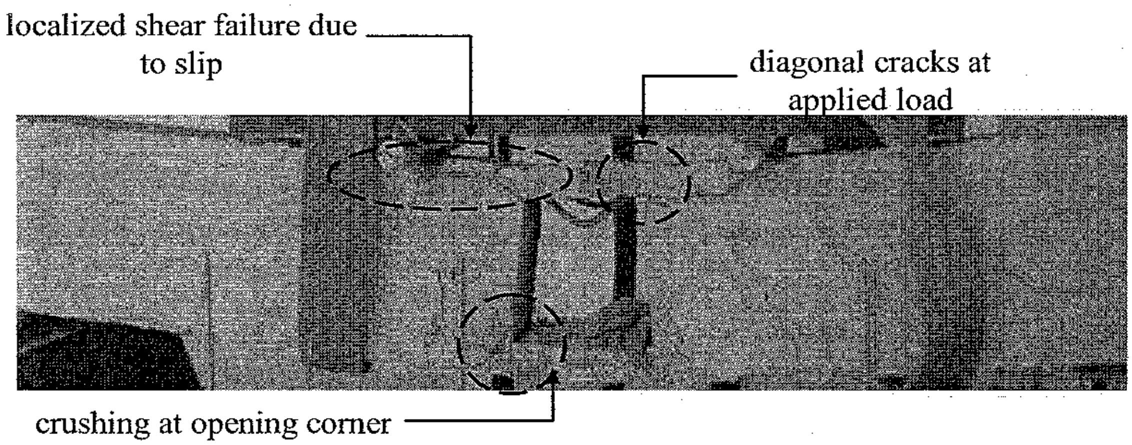

Figure 6.8 Crack patterns of un-strengthened beam SF

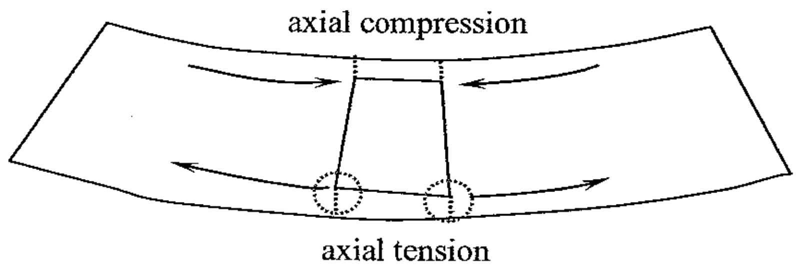

Figure 6.8a Axial and compression effect on top and bottom chord

6.2.2.4 Effects of Large Elliptical Opening, LEF

Failure mode and crack patterns of the effects of a large elliptical opening in the mid-span are illustrated in Figure 6.9. The large opening has divided the top and bottom parts of the beam into upper and lower horizontal chords, respectively. Due to that, early cracks were observed in the mid-span at the soffit of the beam that later propagated at the left side of the opening in the lower chord where such cracks were diagonally aligned from the bottom to one-third of the beam depth. When adequate deflection was reached, the solid segments of the beam at the left and right sides of opening exerted axial compression and tension forces on the upper and lower chords, respectively which caused deflection in the chord members similar to a Vierendeel action. Hence, the beam failed in shear at the upper chord due to localized shear failure with a diagonal crack near the point load and crushing of concrete in the lower chord were observed; while most of the tension was then carried by the bottom reinforcements.

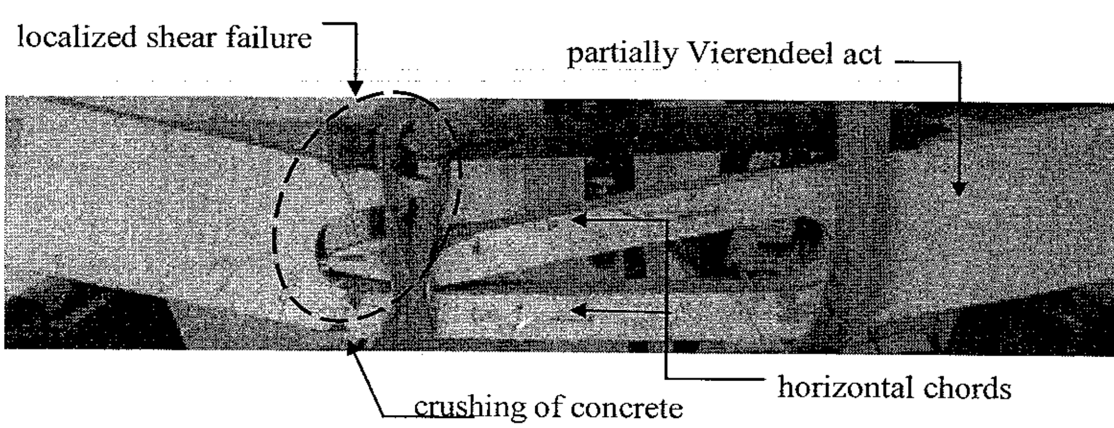

Figure 6.9 Crack patterns of un-strengthened beam LEF

6.2.2.5 Effects of Large Rectangular Opening, LRF

The effects of a large rectangular opening in the mid-span on failure mode and crack patterns are shown in Figure 6.10. The early cracks were found in the mid-span at the soffit of the beam which then appeared at the left side of opening in the bottom chord; such cracks were diagonally aligned. The solid parts of the beam at the left and right sides of the opening applied axial compression and tension forces on the upper and lower chords, respectively which caused deflection in the chord members similar to a Vierendeel action as the beam reached to sufficient deflection. Failure of the beam was in shear due to crushing of concrete in the top chord with a diagonal crack at the opening corner because of high stress concentration whereas most of the tension was transferred to the bottom longitudinal bars.

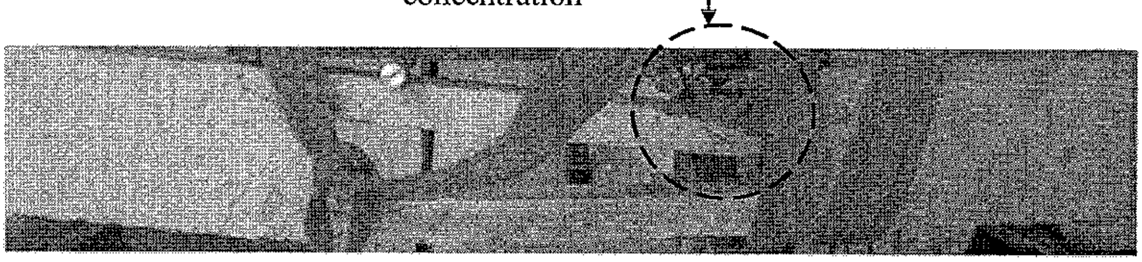

Figure 6.10 Crack patterns of un-strengthened beam LRF

6.2.2.6 Prevailing Shape of Opening

Based on Table 6.1, the highest ultimate load achieved were RC beams with the circular and elliptical shape of openings compared to square and rectangular openings. This can be explained as stress concentration will decrease with increasing radii in the corners of the opening. The maximum effect would be accomplished by having a circular opening without any sharp corners or 2 semi-circles on each end. The closest opening that approximates this shape is elliptical (Moreno, 2011).

6.2.3 Effects of CFRP Strengthening on Flexural Capacity

Based on the crack patterns and failure modes of un-strengthened beams, CF, SF, LEF and LRF; strengthening configurations using CFRP laminates were designed and applied around the openings. To design the strengthening configurations, solution from numerical studies were also referred, which are discussed in details in the earlier Chapter 5. The strengthening configurations for different size and configuration of openings are presented and discussed in this section in order to achieve objective no.2 in the research study.

6.2.3.1 Strengthening Configurations

The CFRP strengthening configurations are illustrated schematically in Figure 6.11. It is important for the CFRP laminates to intercept the potential cracks in order to contribute effectively in enhancing the beam flexural capacity. The qualitative arrangements of CFRP laminates were based on the failure mode and crack pattern results of the numerical analysis.

Referring to numerical analysis as mentioned in section 5.2.2.2, although it is found in FE analysis that strengthening is not necessary for beam with circular opening in mid-span, however minimum strengthening is needed due to the cracks observed in experimental beam CF for long term serviceability. Hence, the strengthening configurations for this beam were modelled in the FE analysis and the selected strengthening scheme was adopted in the experimental testing. The strengthening options of beam CF-S are presented in APPENDIX J.

Figure 6.11(a) describes the CFRP strengthening configuration applied onto beam CF-S as obtained from the numerical analysis. As discussed in section 6.2.2.2, the horizontal aligned cracks were observed between two applied loads in the top chord which was approximately 500 mm. Due to that, longitudinal CRFP laminates with a length of 630 mm (200 mm in both solid sections and 230 mm of the opening) were adopted to prevent further propagation of cracks beyond the applied load. The longitudinal CFRP laminates were bonded to the top and bottom chords of the opening with fibers oriented in a direction parallel to the longitudinal axis of the beam to resist the formation of horizontal aligned cracks and early cracks in the mid-span, respectively whereas at the top and bottom beam soffit to prevent local crushing of concrete. CFRP laminates in length of 290 mm oriented at 45° were designed and placed at the left and right sides of opening to restrict the diagonally aligned cracks that formed from bottom to top. The length was chosen because it adequately covered the area penetrated by such cracks.

Similarly, strengthening of beam with a square opening in flexure is not recommended in FE analysis as mentioned in section 5.2.2.3; however minimal strengthening with CFRP laminates is required due to cracks and small reduction of beam capacity in experimental beam SF and for long term serviceability of the structure. Thus, strengthening systems of such beams were modelled in FE analysis and the strengthening options are shown in APPENDIX K.

Four 210 mm-length of CFRP laminates with fibers oriented in the vertical and longitudinal direction were bonded in the square opening as illustrated in Figure 6.11(b). The CFRP laminates were arranged in such configuration to prevent crushing of concrete in the top and bottom chords. Meanwhile, a 610 mm longitudinal CFRP laminate with fibers oriented in a direction parallel to the longitudinal axis were applied at the bottom soffit of the beam. Referring to the selected strengthening option in the numerical solution, the designated length of CFRP laminates was sufficient to enhance concrete crushing in the bottom chord.

As shown in Figure 6.11(c), four longitudinal CFRP laminates of 400 mm length with fibers in a direction parallel to the longitudinal axis of the beam were bonded at the top and bottom chords of the large elliptical opening. The reason CFRP laminates were applied in such configurations was to resist the localized shear failure at the top chord and cracks in the bottom chord due to shear failure, as described in Figure 6.11(c). The crack pattern in section 6.2.2.4 with diagonal crack was approximately 250 mm in which 400 mm length of CFRP laminates were adequate to restrain the forming of these cracks.

Figure 6.11(d) illustrates the use of four 400 mm-length longitudinal CFRP laminates with fibers in a direction parallel to the longitudinal axis of the beam were bonded at the top and bottom chords of the large rectangular opening. This strengthening configuration was to prevent the crushing of concrete at opening corners due to high stress concentration. Based on the crack pattern results in section 6.2.2.5, the diagonal cracks at the top chord were approximately 250 mm in which the designated length, 400 mm were strong enough to control the forming of such cracks. While two 140 mm lengths of vertical CFRP laminates with the fibers perpendicular to the longitudinal axis of the beam in the rectangular opening were to further enhance the top and bottom chords from concrete crushing. This strengthening configuration from numerical analysis was referred.

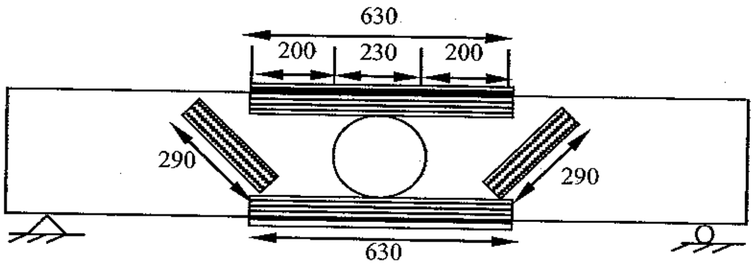

(a) CF-S

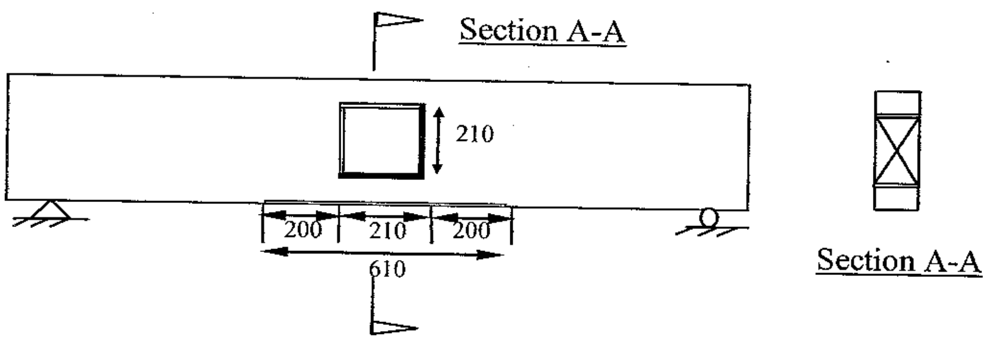

(b) SF-S

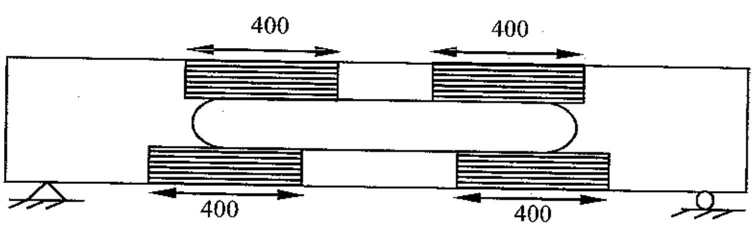

(c) LEF-S

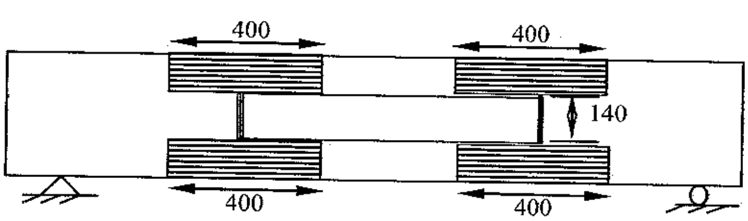

(d) LRF-S

Figure 6.11 CFRP strengthening scheme around various shape of openings in flexure

6.2.3.2 Load-Deflection Behaviour

Figures 6.12 to 6.14 illustrate the load-deflection behaviour of strengthening of beams with large openings using CFRP laminates. Results of all such beams are compared with the results of the corresponding control beams namely; CB1, CB2 and CB3. Table 6.2 summarizes the test results of the beams.

a) Strengthening for Circular Opening, CF-S

CFRP laminates around the circular opening covers 15% of the beam exposed area in the middle of the span. Strengthening using CFRP laminates managed to restore the beam capacity to approximately 92% of the control beam capacity, CB1. The load-deflection behaviour of beam CF-S plotted in Figure 6.12 which found of similar trend as that of the control beam, CB1. The yield strength of beam CF-S was obtained as 97 kN at 8.1 mm deflection, whereas the ultimate load as 107 kN was observed at 10.7 mm deflection. The strengthening of opening causes an increase in stiffness and reduces deflection compared to beam CB1 due to which a higher ductility is shown by the beam CF-S. One of the reasons is that higher yielding strength obtained in beam CF-S compared to CB1 is due to higher energy required to redirect the path of cracks through the un-reinforced area in which minimum energy is needed (Pimanmas, 2010).

b) Strengthening for Square Opening, SF-S

Strengthening configuration with CFRP laminates covers 11% of the beam exposed area. This arrangement could re-gain about 74% of the beam capacity of the control, CB1. As shown in Figure 6.12, the yield load, P_y of beam SF-S was as 73 kN at 4.7 mm deflection, whereas the ultimate load, P_u was obtained as 86 kN at 6.9 mm deflection. From the graph, strengthening using CFRP laminates increased the stiffness and enhanced deflection. Similar as of beam CF-S, the yield load of beam SF-S increased because of higher energy is needed to transfer the crack path through the un-strengthen area in which less energy is required (Pimanmas, 2010).

(c) Strengthening for Large Elliptical Opening, LEF-S

CFRP laminates configuration around the large elliptical opening which comprise 20% of the beam exposed area managed to restore 96% of the capacity of its corresponding control beam, CB2. In Figure 6.13, the yield load of beam LEF-S was obtained as 62 kN at 3.7 mm deflection, whereas the ultimate load of 77 kN was observed at 5.3 mm deflection. A sharp decrease in load was observed after the ultimate load was achieved, as illustrated in Figure 6.13. This indicates that the beam failed by crushing of concrete due to shear failure (Balaguru et al., 2008).

d) Strengthening for Large Rectangular Opening, LRF-S

CFRP laminates cover the area around the opening approximately 22% of the exposed area of beam LRF-S could re-gain 86% of the respective beam capacity, CB3. As shown in Figure 6.14, the yield strength was obtained as 72 kN at 6.6 mm deflection, whereas the ultimate load was found as 83 kN at 10.4 mm deflection. After the ultimate load was attained, the load decreased sharply indicating a brittle failure which is because of high stress concentration at the opening corners that later failed due to crushing of concrete.

In general, strengthening of beams with a large opening in flexure using CFRP laminates could re-gain and restore approximately 74% - 96% of their respective control beams depending on the strengthening configurations. Based on the load-deflection results of each type of beams, it is found that CFRP laminates bonded around the opening significantly increases the beam capacity to almost the same as the control beams. The increase in capacity in these beams was caused by the presence of CFRP laminates that interrupt the natural path of crack propagation, hence requiring a higher energy to redirect the path of cracks through the un-reinforced region. Furthermore, strengthening the opening region greatly increases the beam stiffness, enhances the deflection behaviour and controls cracks around the opening.

Table 6.2 Test results of CFRP strengthened openings in flexure

Beam	Yielding load P_y (kN)	Δ_y (mm)	Ultimate load P_u (kN)	Δ_u (mm)	Beam Exposed Area (BEA) (mm^2)	$\left(\frac{\text{Total CFRP Area}}{\text{BEA}}\right)$ x 100%
CB1	79	5.4	116	29.5	-	-
CB2	77	8.2	80	9.1	-	-
CB3	86	8.0	96	36.4	-	-
CF-S	97	8.1	107	10.7	1,296,000	15
SF-S	73	4.7	86	6.9	1,296,000	11
LEF-S	62	3.7	77	5.3	1,296,000	20
LRF-S	72	6.6	83	10.4	1,296,000	22

BEA= Beam Exposed Area

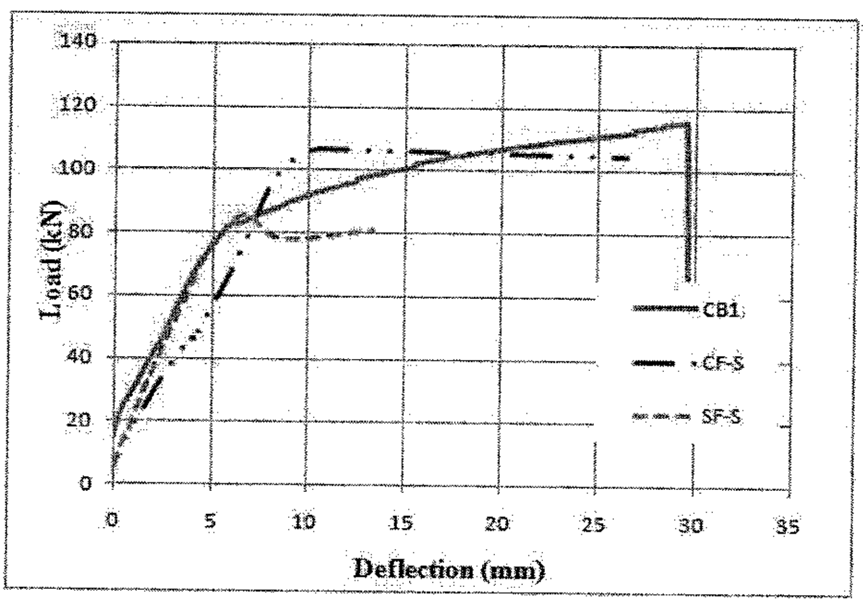

Figure 6.12 Comparison of load-deflection curves of beams CB1, CF-S and SF-S

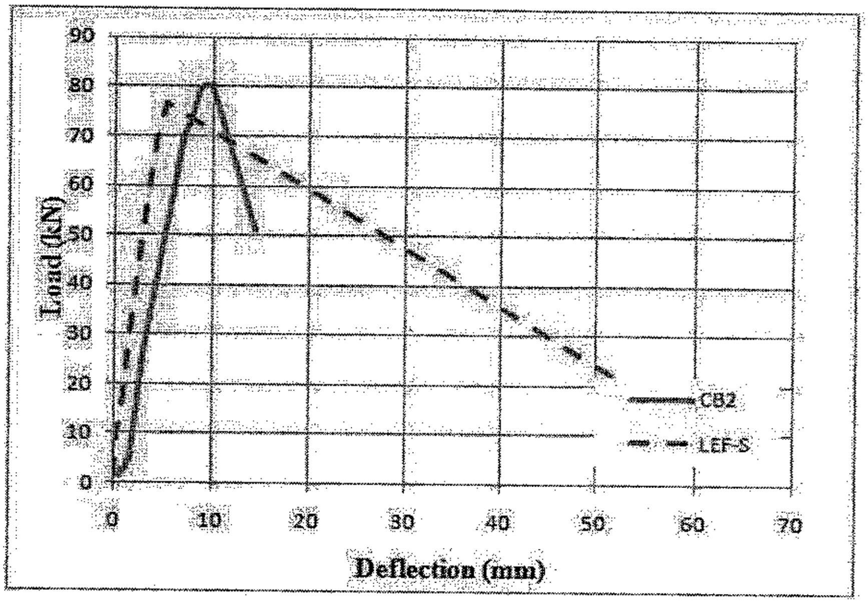

Figure 6.13 Comparison of load-deflection curves of beams CB2 and LEF-S

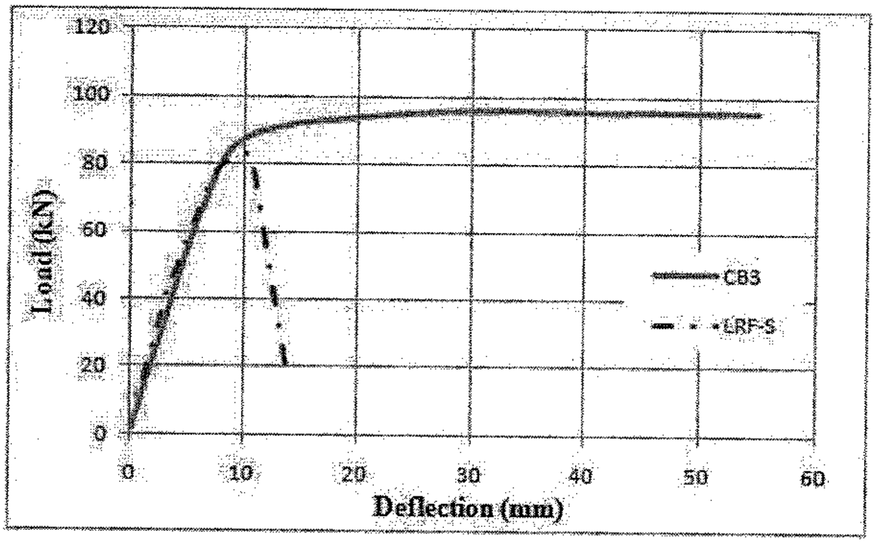

Figure 6.14 Comparison of load-deflection curves of beams CB3 and LRF-S

6.2.3.3 Failure Modes and Crack Patterns

This section includes the failure modes and crack patterns result of beams with strengthened circular, square, large elliptical and rectangular openings, CF-S, SF-S, LEF-S and LRF-S, respectively. The beams during experimental testing were observed up to failure.

(a) Strengthening for Circular Opening, CF-S

Effects of single strengthened circular opening in the mid-span on failure mode and crack pattern are illustrated in Figure 6.15. The early cracks were observed in the mid-span at the soffit of the beam away from the CFRP laminates, which then propagated at the left and right sides of the solid area near the 45° orientation of CFRP laminates. These cracks were diagonally aligned from bottom to top with the increasing of applied load and later failure was happened due to the widened diagonal crack which resulted in crushing of concrete. CFRP laminates in the top chord was partially ruptured with crushing of concrete near the applied load whereas crushing of concrete with exposed bottom longitudinal bars was observed in the bottom chord near the support.

Due to a higher reinforced area by CFRP laminates around the circular opening within the mid-span region, the failure of the beam is diverted to an area without the restriction of CFRP laminates. Hence, a sudden shear failure was observed at the diagonal crack which formed away from the strengthened area. This is due to CFRP laminates disturb the path of crack propagation which required a higher energy to extend the crack in a diverted direction (Pimanmas, 2010).

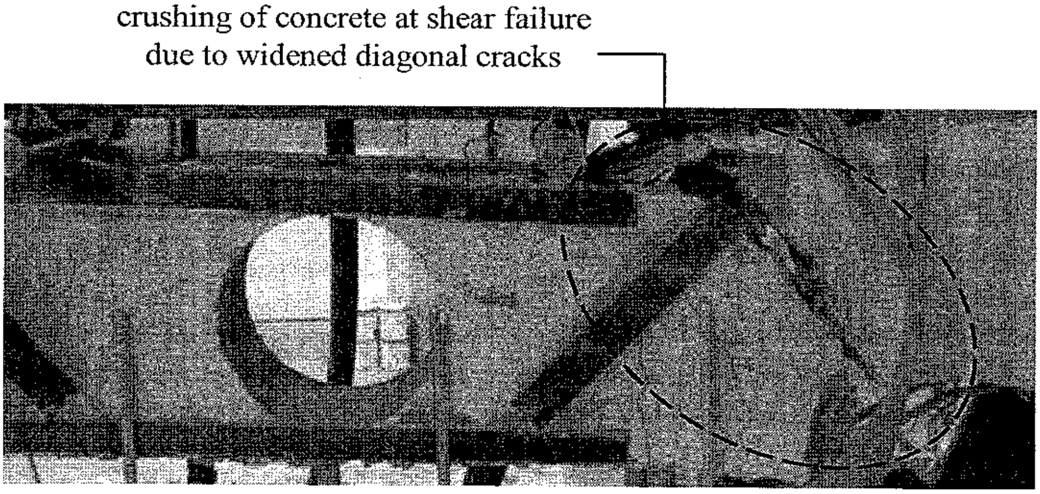

Figure 6.15 Crack patterns of strengthened beam CF-S

(b) Strengthening for Square Opening, SF-S

Figure 6.16 shows the effects of a square opening in mid-span on failure mode and crack pattern. The early cracks were found in the mid-span at a distance away from the soffit of the beam, in which the region was bonded by CFRP laminate; such cracks then propagated at the left and right sides of the opening was diagonally aligned from bottom to top. When the beam deflection was noticeable, cracks at the top chord of the opening were observed, such cracks were horizontally aligned and eventually failure was occurred due to crushing of concrete in the top chord. Diagonal shear failure was happened whereby the diagonally aligned cracks became prominent at failure. Upon reaching to adequate deflection, the solid parts at the left and right sides of opening exerted axial and compression forces on the top and bottom chords, respectively. Due to this effect, the top chord area has reduced and crushing of concrete was occurred which caused bending of CFRP laminate in the top inner surface of opening while the top longitudinal bars were exposed and bent in the opposite direction. Peeling of CFRP laminate and concrete at the soffit of the beam was observed due to the large deformation and partially detached from the beam.

It is found that CFRP laminates in the strengthening configuration controlled cracks around the four corners of the square opening and diverted the early cracks away from the region strengthened by CFRP laminate in the mid-span at the soffit of the beam, hence differs from the crack pattern of its counterpart beam with un-strengthened opening.

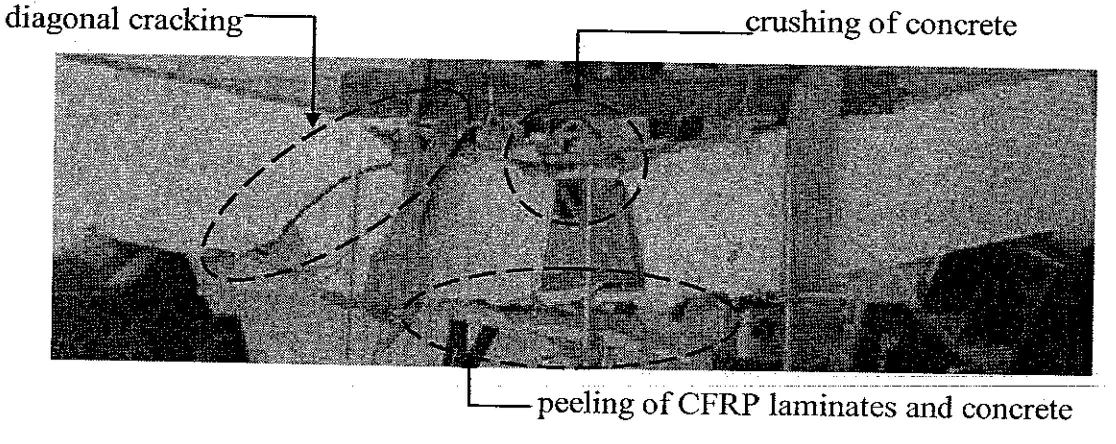

Figure 6.16 Crack patterns of strengthened beam SF-S

(c) Strengthening for Large Elliptical Opening, LEF-S

Failure mode and crack pattern of the effects of single large elliptical opening in the mid-span are shown in Figure 6.17. The initial cracks were observed in the mid-span at the soffit of the beam between two longitudinal CFRP laminates. Due to the presence of CFRP laminates, these cracks eventually was observed on the left and right sides of the CFRP laminates away from the mid-span; such cracks were diagonally aligned which penetrated from bottom to top. When the beam reached to adequate deflection, the numbers of early cracks in the mid-span and diagonal cracks away from CFRP laminates were increased and later failure was happened due to localized shear failure at the top chord in which a diagonal crack with the crushing of concrete was observed. This caused the longitudinal CFRP laminates to partially delaminated from the concrete surface whereas vertical crack in the mid-span near the right longitudinal CFRP laminates were noticeable.

CFRP laminates in this strengthening arrangement have directed the early cracks to form in the mid-span at the beam soffit between the two longitudinal CFRP laminates and controlled crushing of concrete from occurring at the bottom chord as the beam reached to adequate deflection.

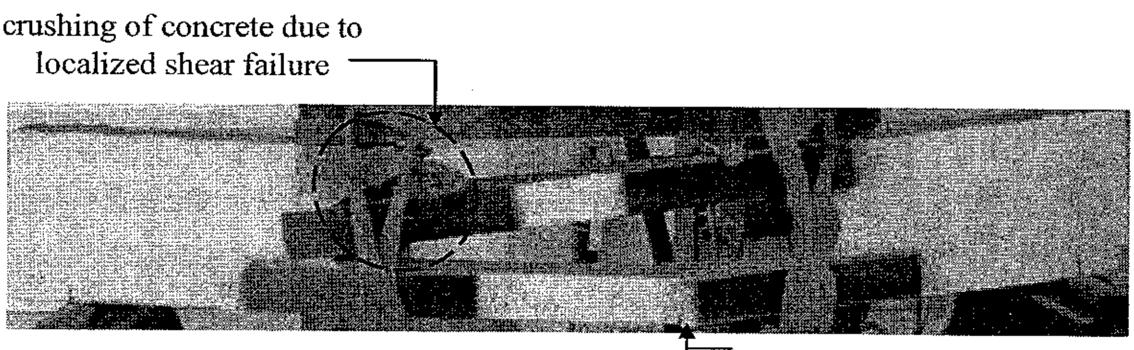

Figure 6.17 Crack patterns of strengthened beam LEF-S

(d) Strengthening for Large Rectangular Opening, LRF-S

Effects of a large rectangular opening in the mid-span on failure mode and crack patterns are illustrated in Figure 6.18. The early cracks were found in the mid-span at the soffit of the beam in between two longitudinal CFRP laminates. These cracks then propagated at the left and right sides away from the CFRP laminates and penetrated diagonally from the bottom. When the beam reached to its sufficient deflection, more cracks were observed in the mid-span between the two CFRP laminates and diagonally aligned cracks propagated from bottom towards the top near the CFRP laminate as shown in Figure 6.18. The failure was happened due to shear by crushing of concrete in the top chord with the shearing of CFRP laminate fibers in the middle.

The CFRP laminates in this configuration managed to control cracks in the mid-span and left and right sides away from the CFRP laminate in the bottom chord. Although crushing of concrete was occurred in the top chord which caused shearing of CFRP laminate fibers, however the CFRP laminate was still bonded intact to the concrete surface.

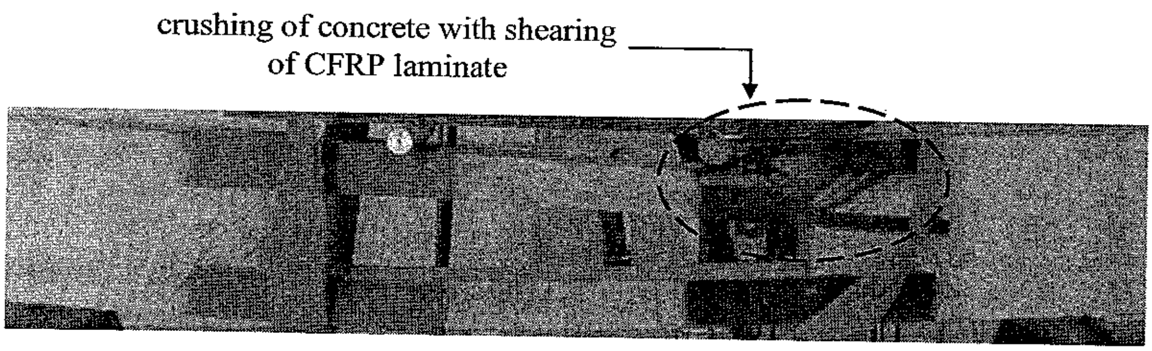

Figure 6.18 Crack patterns of strengthened beam LRF-S

6.2.3.4 Effective Strengthening Configuration

Comparing the results, it can be seen that CFRP strengthening around the openings in flexure significantly restore the beam capacity. Beam CF-S achieved a higher beam capacity compared to beam SF-S was presumably due to the CFRP strengthening configuration around the opening as well as the corners of the square opening which is subjected to stress concentration. Meanwhile, comparing beam LEF-S and LRF-S, both yield strength and ultimate load were found almost similar except that beam LRF-S exhibited a larger deflection at ultimate load. This may be due to the stress concentration at opening corners in the rectangular opening. Among beams CF-S, SF-S, LEF-S and LRF-S strengthened using CFRP laminates, RC beam with an elliptical opening in flexure, LEF-S could remarkably restore 96% of the load-carrying capacity of its corresponding control beam, CB2.

6.3 Effects of Openings on Shear Capacity of Un-Strengthened Beam

Apart from flexural failure, another type of beam failure is shear failure. It is well known that shear failure is sudden and brittle in nature. Hence, it is less predictable and gives no advance warning prior to failure which is more dangerous than flexural failure. In a simply supported beam, the critical shear region is at maximum near to the support. Hence, to study the effects of openings on shear capacity, openings were provided at the following location: (i) at the face of support; (ii) at distances 0.5d, d and 1.5d away from the support. Openings provided at both ends and at one end only were considered in this study. The shapes of openings are circular and square which covered about 8-16% of the beam elevation area and cut about 70-154% of the beam depth. To achieve objectives no.1 (i) and 1(ii), the experimental results of the tested beams are presented and discussed in the following sub-sections.

6.3.1 Load-Deflection Behaviour

Load-deflection behaviour of beams with openings in shear without the applications of CFRP laminates are presented in Figures 6.19-6.21. These beams were compared with their respective control beams, CB1, CB2 and CB3, respectively. The test results are summarized in Table 6.3.

6.3.1.1 Openings at Both Ends

In this section, the load-deflection curves of beams with circular and square openings at both ends are presented in Figures 6.19 – 6.20. The beams are compared with their corresponding control beams CB1 and CB2, respectively.

(a) Beam with Circular Openings (zero distance from support), C0S

Circular openings with a diameter of 230 mm were provided at both ends cover 15% of the area and cut 154% of beam at both ends. The load-deflection plots of beam C0S is shown in Figure 6.19. A decrease in beam stiffness was observed at the initial stage due to early cracking around the openings. This has changed the initial linear response to nonlinear. The yield strength of beam C0S was obtained as 21 kN at deflection of 2.1 mm, whereas the ultimate load as of 23 kN was observed at 2.8 mm deflection. At failure, a rapid decrease in load was observed indicating brittle shear failure. On comparing to the control beam without opening, CB1, about 80% loss of beam capacity was found in beam C0S. The results show that providing circular openings at both ends in the shear zone significantly decreases the ultimate capacity of the beam.

(b) Beam with Square Openings (zero distance from support), S0S

Square openings provided at both ends cover 16% of the area and cut 140% of the concrete depth, as listed in Table 6.3. At the early phase of loading, a linear elastic response was terminated after cracking in which a sudden decrease in the slope of the load-deflection curve was observed in Figure 6.19. The reduction of beam stiffness was due to the crack initiation and at opening corners showing a non-linear behaviour in the post-cracking region. The yield strength of beam S0S was obtained as 22 kN at a deflection of 5 mm while the ultimate load as of 25 kN at 7 mm deflection. In the post-yielding stage, after the ultimate load was achieved, an immediate decrease of load was observed upon failure. The beam capacity of beam S0S reduced approximately 78% as compared to the load-carrying capacity of the control beam, CB1.

(c) Beam with Square Openings (at distance 0.5d from support), S0.5dS

At the initial phase of loading, the elastic state of beam ended after a short period as the slope of the load-deflection curve decrease after the first cracking as shown in Figure 6.20. The stiffness of the beam reduced with the increase of load until the fully yield condition of beam. The yield load of beam S0.5dS was obtained as 18 kN at 3.9

mm deflection, whereas the ultimate load was found as 20 kN at 8.4 mm deflection. Beyond the point of ultimate load, a rapid decrease of load was observed which indicates softening of beams in a brittle behavior. The presence of square openings in beam S0.5dS caused a reduction of 75% in the beam capacity as compared to the corresponding control beam CB2.

(d) Beam with Circular Openings (at distance d from support), CdS

The load-deflection curve in Figure 6.20 shows that beam CdS possessed high stiffness at initial state in the early phase of loading. The high inclination of slope declined after that due to cracking of the beam. After cracking, the load was seen to increase until the beam fully yielded at a point where the yield strength of beam CdS was obtained as 18 kN at a deflection of 1.8 mm while the ultimate load was achieved as of 20 kN at 4.6 mm deflection. Just after the maximum point, a quick drop in load was observed exhibiting brittle shear failure. Comparing to the load-carrying capacity of the respective control beam CB2, a loss of beam capacity about 75% was observed in beam CdS.

(e) Beam with Square Openings (at distance d from support), SdS

The load-deflection curve of beam SdS as shown in Figure 6.20 exhibits a similar response to that of beam S0.5dS. A decrease in the slope of the load-deflection curve was observed at the initial stage of loading due to cracking around the openings. Such cracking reduced the beam stiffness; causing a nonlinear behaviour in the post-cracking stage. The yield load of beam was obtained as 24 kN at 14.4 mm deflection while the ultimate load was as of 25 kN at a deflection of 17.6 mm. In the post-yielding stage, decreasing of load was observed immediately upon failure of the beam. It was found that beam SdS exhibits less brittle behaviour compared to beam S0.5dS due to the higher plastic deformation as shown in the load-deflection curve which means the beam possessed greater ductility behaviour. The beam capacity of beam SdS exhibited a loss of about 69% as compared to the load-carrying capacity of the control beam, CB2.

For all the beam specimens in this section with openings at both ends, a non-linear load deflection response was observed indicating a higher rate of crack initiation, widening and growth where the load path was partially or fully interrupted by the openings (El Maaddawy & Sherif, 2009). Comparing the size and shape of openings, circular opening tends to exhibit a smaller deflection in the load-deflection curve within a range of 0-5 mm while square openings demonstrated load-deflection curve having a deflection in a range of 0-20 mm. This indicates that failure in circular opening was immediate and brittle because of the large size reduction in beam with 154% losses in the cut area compared to square opening.

6.3.1.2 Opening at One End Only

Beams with a circular or square opening created at one end are presented and discussed in this section. All the beams are compared with their respective reference beam, CB3 as shown in Figure 6.21.

(a) Beam with Single Square Opening (at distance 0.5d from support), S0.5dS1

The results of beam S0.5dS1 as plotted in the load-deflection curve showed that in the early phase of loading, the beam exhibited higher stiffness in the elastic region. The beam stiffness eventually reduced after cracking occurred in the beam in which a decrease of the slope was observed. The load was noticed increasing with the reduced stiffness until the yielding point of the beam where the yield load of the beam was obtained as 21 kN at a deflection of 2.3 mm. After the fully yielded condition, the increase of the load was noticed maximum in which the ultimate load was attained as of 23 kN at 3.3 mm deflection. After surpassing the maximum point, the line of the load deflection curve was noticed in a descending order indicating an abrupt failure. The provision of a single square opening at a distance 0.5d away from the face of support exhibited a loss of load-carrying capacity about 76% as compared with the beam capacity of the reference beam, CB3.

(b) Beam with Single Circular Opening (at a distance d from support), CdS1

The load-deflection curve of beam CdS1 shows a linear line at a high inclination at the early period of loading. The inclination of the slope declined eventually after the occurrence of cracks in the beam. After cracking, the increase of the load was noticed until the beam was fully yielded at a load of 20 kN and 0.8 mm deflection. The beam then reached the ultimate beam capacity which was obtained as 22 kN at 1.8 mm as the load was increased after passing the fully yielded condition. The line of load-deflection was observed to decrease immediately beyond the ultimate point exhibiting brittle shear failure. From the load-deflection curve, the beam CdS1 showed a reduction of beam capacity approximately 77% as compared to the maximum load-carrying capacity of the corresponding control beam, CB3 as of 96 kN.

(c) Beam with Single Square Opening (at distance d from support), SdS1

As shown in the load-deflection plots of beam SdS1 during the loading condition at an early stage, the initial stiffness of the beam was found similar as observed in beam S0.5dS1. The beam remained in the elastic condition until cracking was happened that eventually leads to reduction of beam stiffness. After that, the line of load-deflection was noticed in an ascending mode with declining of the slope up to the fully yielded condition of beam which yielded at a load of 25 kN at a deflection of 3.8 mm. When the line of the load-deflection curve was at its highest state, the ultimate load of beam was obtained as 27 kN at 5.1 mm. The beam eventually failed after exceeded the peak by exhibiting a sharp drop in load indicates brittle type of failure. This caused a significant loss of beam capacity of about 72% when being compared with the beam capacity of the reference beam.

(d) Beam with Single Square Opening (at distance 1.5d from support), S1.5dS1

The load-deflection curve trend of beam S1.5dS1 were noticed having similar development of the initial state of loading as observed in the load-deflection curves of beams S0.5dS1 and SdS1. The beam possessed high stiffness during loading at early phase demonstrating steeper inclination line of the load-deflection; however the outbreak of cracking in beam resulted in a reduction in beam stiffness showing declination of slope. Then, the load was observed to increase with lower stiffness until the yielding point where the yield strength of beam was obtained as 27 kN at a deflection of 3.3 mm. Beam S1.5dS1 then experienced a small plastic flow after yielding before the ultimate load was reached at a load of 31 kN at 6 mm deflection. A quick slump in loading was observed just after passing the maximum point demonstrating softening of the beam. On comparing to the load-carrying capacity of the control beam, the presence of a square opening at a distance 1.5d from the face of support causes a loss of beam capacity about 68%.

The load-deflection curves of the beams with an opening at a single end at a distance 0.5d, d and 1.5d away from the face of support achieved their maximum load within 23-31 kN whereas the beams mostly failed at a deflection from 0-10 mm. This may be because of the natural load path was not interrupted initially as the cracks tend to develop in the tensile region of the beam; therefore illustrating a linear elastic response. However, once the opening intervenes into the load path in one of the shear region where cracks initiated at the corners of the opening, this resulted in an abrupt and brittle shear failure.

Table 6.3 Test results of un-strengthened beams with openings in shear zones

Beam	Yielding load P_y (kN)	Δ_y (mm)	Ultimate load P_u (kN)	Δ_u (mm)	$\left(\frac{\text{Opening Area}}{\text{BEA}}\right)$ x 100%	$\left(\frac{\text{BCD}}{\text{TBD}}\right)$ x 100%
CB1	79	5.4	116	29.5	-	-
CB2	77	8.2	80	9.1	-	-
CB3	86	8.0	96	36.4	-	-
COS	21	2.1	23	2.8	15	154
SOS	22	5.0	25	7.0	16	140
S0.5dS	18	3.9	20	8.4	16	140
CdS	18	1.8	20	4.6	15	154
SdS	24	14.4	25	17.6	16	140
S0.5dS1	21	2.3	23	3.3	8	70
CdS1	20	0.8	22	1.8	8	77
SdS1	25	3.8	27	5.1	8	70
S1.5dS1	27	3.3	31	6.0	8	70

BEA = Beam Elevated Area
BCD = Beam Cut Depth
TBD = Total Beam Depth

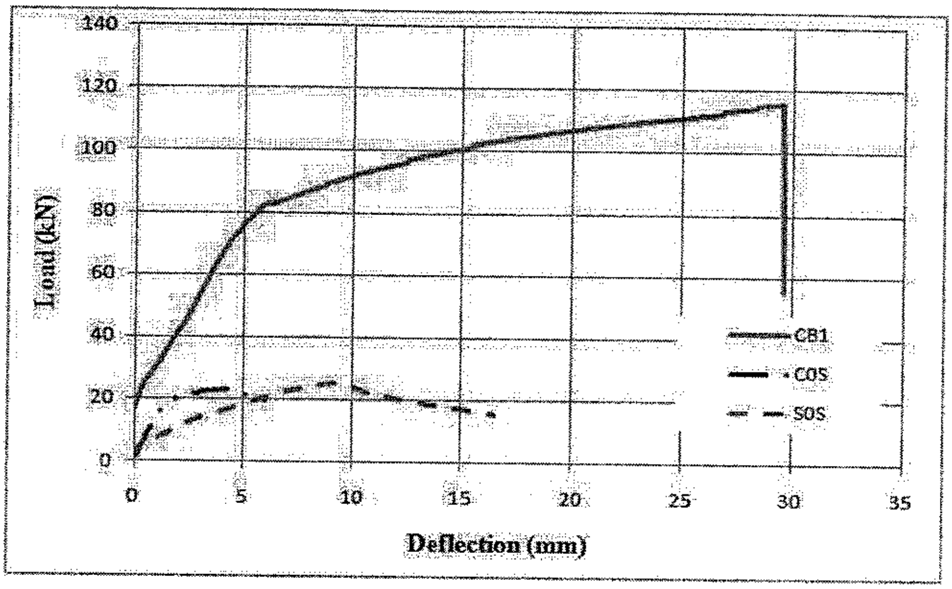

Figure 6.19 Comparison of the load-deflection curves of beams with un-strengthened openings at the face of support and beam CB1

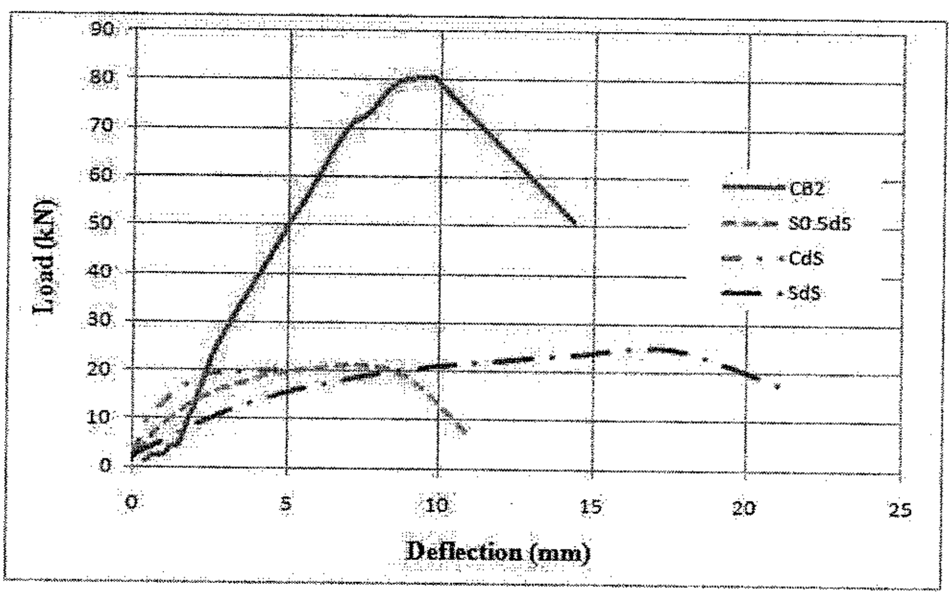

Figure 6.20 Comparison of the load-deflection curves of beams with un-strengthened openings at distance 0.5d and d from the support and beam CB2

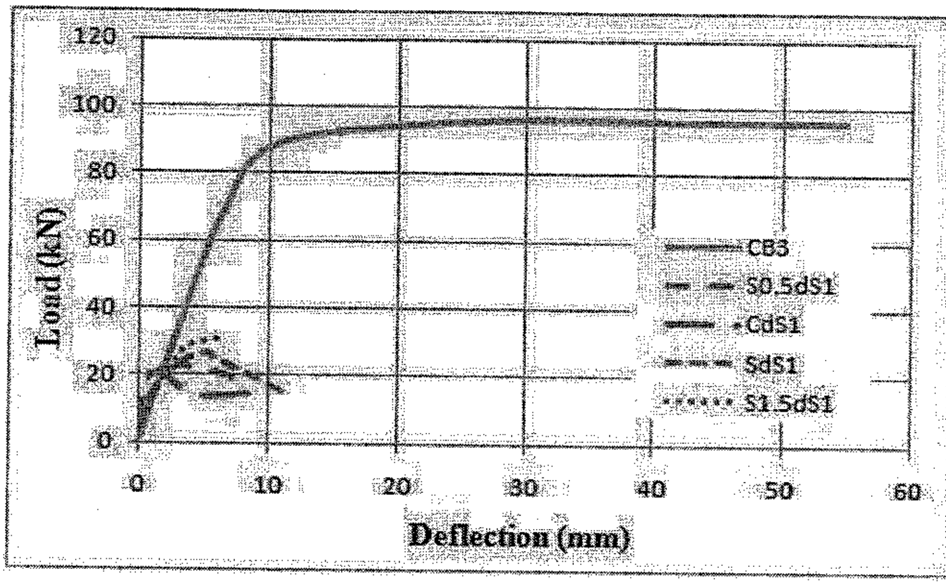

Figure 6.21 Comparison of the load-deflection curves of beams with un-strengthened opening at one end only and beam CB3

6.3.2 Failure Modes and Crack Patterns

In the following section, failure modes and crack patterns of un-strengthened beams with openings provided at both ends as well as at one end only are presented and discussed. Observations of such beams during experimental testing were recorded up to beam failure.

6.3.2.1 Openings at Both Ends

Crack patterns and failure modes of beams with un-strengthened openings at both ends are presented in Figures 6.22 – 6.26.

(a) Beam with Circular Openings (zero distance from support), C0S

Effects of circular openings at both ends placed at the face of support on failure mode and crack patterns are presented in Figure 6.22. It was observed that early cracks were initiated at the top chord of the opening, which then the cracks were diagonally oriented to the applied load. On the other hand, cracks appeared at the bottom chord of the opening which propagated diagonally to the beam support. Just before beam failure, these cracks at the top and bottom chords become prominent and exhibited a wide see-through gap exposing the top and bottom steel reinforcements at the opening. The wide cracking at the top chord of opening eventually leads to separation of concrete cover diagonally oriented from the opening towards the applied load. Due to about 154% of the beam depth cut at both ends at the support, a brittle shear failure was observed in the beam during failure.

It is found that the failure mode around the openings was frame-type failure when two independent diagonal cracks were formed, one on each of the chord member above and below the openings. Each of the members behaves independently similar to the members in a framed structure in which each chord member requires independent treatment (Mansur, 1998; Mansur, 2006). The circular opening in this study was classified as 'large' opening according to (Somes & Corley, 1974) and (Mansur, 2006).

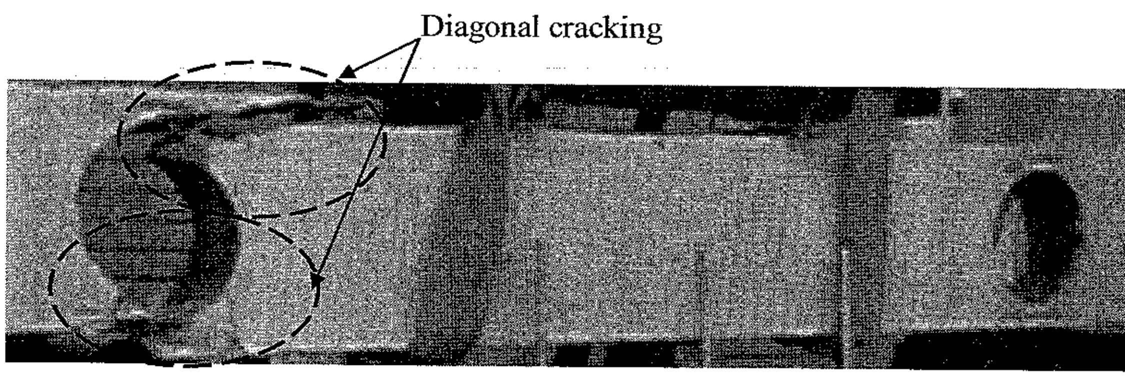

Figure 6.22 Crack patterns of un-strengthened beam C0S

(b) Beam with Square Openings (zero distance from support), S0S

Figure 6.23 shows the effects of square openings provided at both ends on the face of support on failure mode and crack patterns. Initial cracks were formed at the corners of the square openings at the top and bottom chords. The cracks at the corners of the opening at the top chord penetrated vertically to the top edge of the beam as well as diagonally oriented to the applied load. On the other hand, cracks at the opening corners at the bottom chord elongated vertically to the bottom edge of the beam and propagated vertically to the face of beam support, respectively. During beam failure, cracks at the opening corners became significant and eventually leads to crushing of concrete at the top edge of the beam and wide cracks at the corner of the opening in the top chord. Meanwhile, crushing of concrete was observed at the bottom side of the opening in which horizontal aligned see-through gap at the bottom chord was formed and penetrated to the face of support leading to the crushing of concrete from the support to the outmost edge of the beam. Furthermore, a see-through gap was observed vertically to the edge of the beam from the corner of opening at the bottom chord. This phenomenon happened because of about 140% beam depth were cut at the shear zone, the opening area which created mainly in the middle-third cross section of beam consist most of the shear stresses that caused brittle failure in shear.

It was observed that when square openings created at zero distance from the support, the failure mode at the four corners of the square opening were similar to the formation of a mechanism with four hinges in the chord members, one at each corner of the opening as illustrated in Figure 2.7 (Mansur et al., 1984).

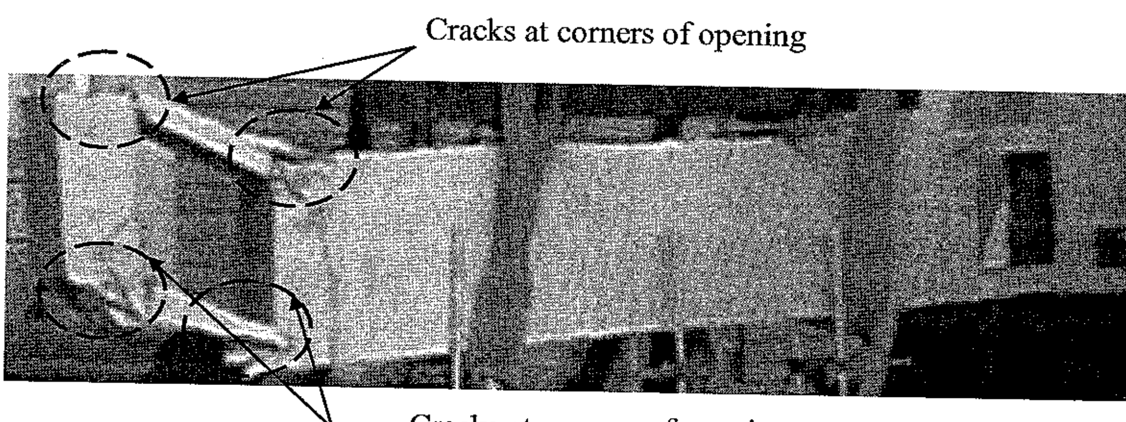

Figure 6.23 Crack patterns of un-strengthened beam S0S

(c) Beam with Square Openings (at distance 0.5d from support), S0.5dS

Effects of providing square openings at both ends at a distance 0.5d from the support on failure mode and crack patterns are shown in Figure 6.24. At the early phase of loading, early cracks were observed initiated at the corners of the square openings both top and bottom chords. At the top chord, the cracks at opening corners propagated vertically to the top edge of the beam and diagonally oriented from the corner of the opening to the applied load, respectively. While at the bottom chord, these cracks were seen penetrated vertically aligned from the opening corners to the bottom edge of the beam and stretched out diagonally to the direction of beam support penetrating through the solid concrete up to the edge of the beam, respectively. As the beam was almost failed, the cracks at opening corners became more visible. Failure of beam occurred when a see-through gap of diagonal cracks was formed from the opening corner to the applied load causing crushing of concrete cover at the top chord where the top steel reinforcements were noticeable. In addition, significant gap was observed at the opening corner at the bottom chord to the beam support. This type of beam failure was sudden and brittle.

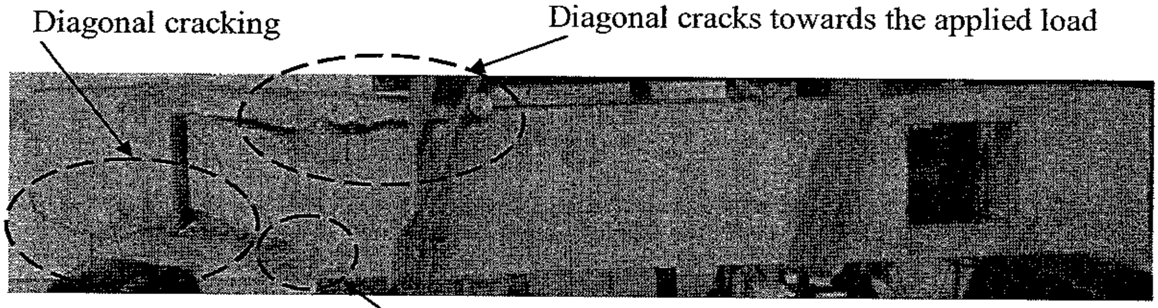

Figure 6.24 Crack patterns of un-strengthened beam S0.5dS

(d) Beam with Circular Openings (at distance d from support), CdS

Figure 6.25 illustrated the failure modes and crack patterns due to the effects of circular openings placed at both ends at a distance d from the support. The early cracks were observed both at the top and bottom sides of the opening. Cracks at the top side of opening were seen penetrated through the top edge of beam vertically whereas such cracks were noticed elongated in a diagonal approach to the applied load. On the other hand, cracks which formed at the bottom side of opening propagated all the way diagonally to the beam support. Just before the failure of the beam, cracks became obvious at the top side and bottom side of circular opening. The failure occurred eventually with the crushing of concrete cover at the top chord. A see-through gap was observed along the diagonal cracking at the top side of opening towards the applied load where the top steel reinforcements were noticeable. Meanwhile, the failure of the beam had caused a slip at the bottom chord causing a significant wide gap of diagonal cracks at the bottom side of opening to the beam support exposing the bottom steel reinforcements. The bottom chord was dislocated from the face of support due to shear failure.

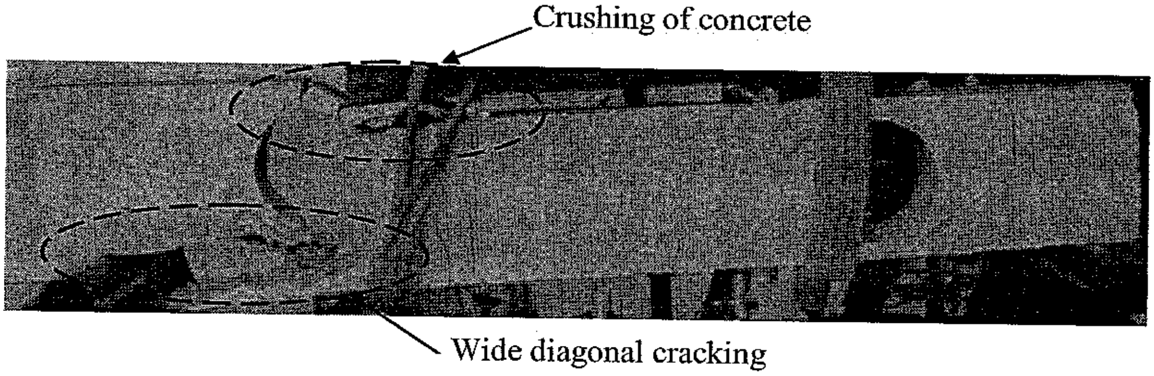

Figure 6.25 Crack patterns of un-strengthened beam CdS

(e) Beam with Square Openings (at distance d from support), SdS

Effects of square openings provided at both ends at a distance d from the face of support are shown in Figure 6.26. It was observed that initial cracks were formed at the corners of the square openings. At the top chord, cracks at the opening corners penetrated vertically to the top edge of the beam as well as diagonally towards the point of loading. While at the bottom chord, cracks were seen elongated to the bottom edge of the beam and propagated diagonally to the beam support. Just before failure of the beam, the cracks became prominent at top and bottom chords of the opening; such cracks were diagonally aligned to the applied load and diagonally oriented to the beam support, respectively. After that, failure was happened by crushing of concrete cover at the top and bottom chords in which the top and bottom steel reinforcements at the opening were exposed.

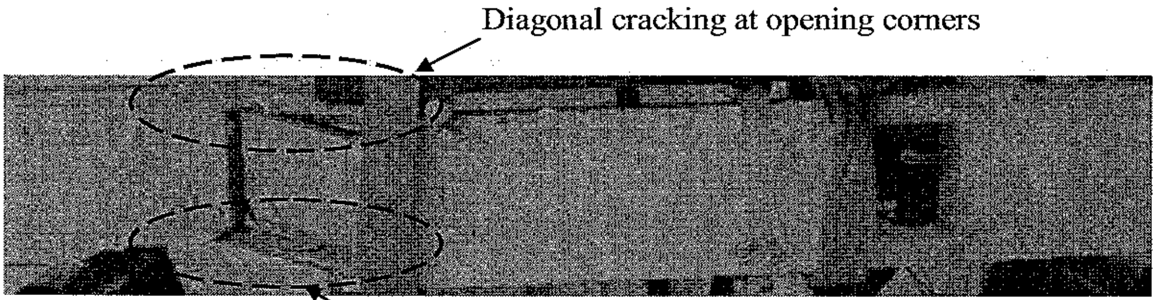

Figure 6.26 Crack patterns of un-strengthened beam SdS

6.3.2.2 Opening at One End Only

Crack patterns and failure modes of the beams with un-strengthened opening at one end only are shown in Figures 6.27 – 6.30.

(a) Beam with Single Square Opening (at distance 0.5d from support), S0.5dS1

Crack patterns and failure modes of beam S0.5dS1 are illustrated in Figure 6.27 in which the first crack was observed at the corners of the square opening. As the load increased, cracks were formed at the top chord where such cracks were vertically aligned to the top edge of the beam and diagonally oriented to the loading point. Cracks at the bottom chord were noticed vertically aligned to the bottom chord from the opening corners and diagonally elongated to the beam support and propagated to the solid part of the beam. The failure was initiated from the widening of diagonal cracks those initiated at the top chord near to the applied load and diagonal cracks that initiated near to the support which then penetrated through the solid part of concrete up the edge of the beam. In general, failure of beam S0.5dS1 is governed by shear failure due to about 70% of the beam depth cut at one end. With the increment in load, the enlargement of crack width at the opening corners, both at the top and bottom chords were clearly seen. Therefore, on further increment in load the beam faced failure in which spalling of concrete cover was happened causing top bars above the opening were completely exposed.

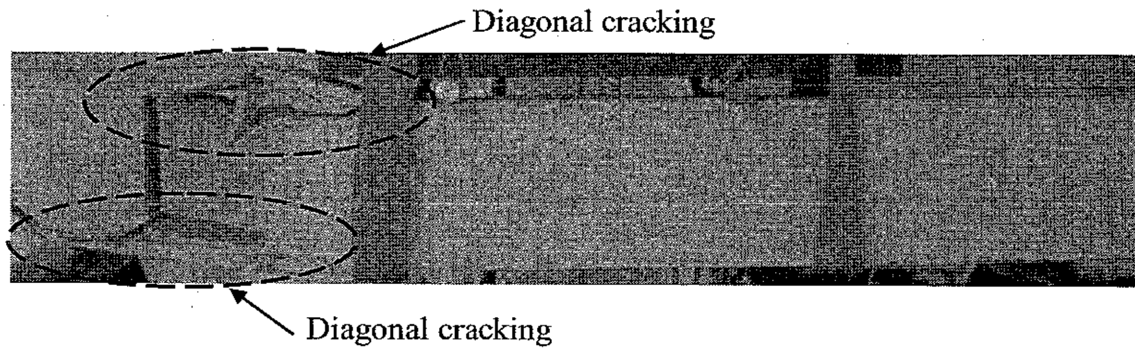

Figure 6.27 Crack patterns of un-strengthened beam S0.5dS1

(b) Beam with Single Circular Opening (at a distance d from support), CdS1

Figure 6.28 shows the crack patterns and failure modes of beam CdS1 on the effects of a single circular opening created at a distance d from the face of support. At early stage of loading, cracks appeared at the top side and bottom side of opening. With the increase of load, the cracks slowly penetrated vertically to the top edge of the beam as well as the formation of diagonally oriented cracks to the applied load. Meanwhile, cracks at the bottom side of opening propagated vertically to the bottom edge of the beam and the development of diagonal cracks to the beam support. With the increase of load, an abrupt and brittle shear failure was observed during the failure of the beam as the beam depth was cut about 77% at one end. Both widening of diagonal cracks at the top and bottom chords of opening became prominent just before failure. This phenomenon had caused the formation of a wide gap at the top chord exposing the top bars whereas spalling of concrete was occurred at the bottom chord near to the support revealing the bottom bars.

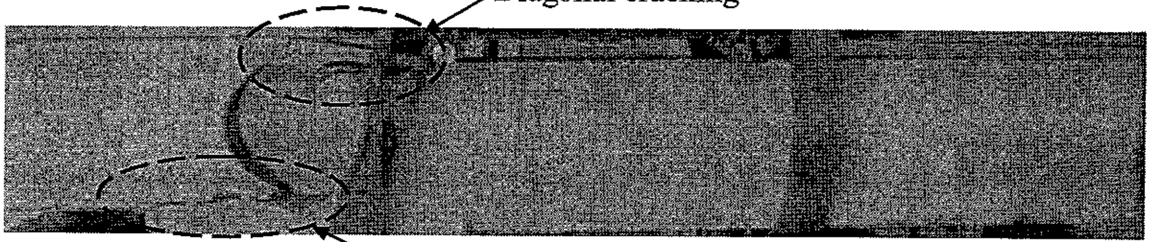

Figure 6.28 Crack patterns of un-strengthened beam CdS1

(c) Beam with Single Square Opening (at distance d from support), SdS1

Effects of a single square opening provided at one end at a distance d from the support on the failure modes and crack patterns are shown in Figure 6.29. The crack patterns were mainly consisted of shear and flexural cracks. It was observed that early cracks were formed at the corners of the square opening at the initial phase of loading. Such cracks at the top corners penetrated vertically to the top edge of the beam as well as forming diagonal cracks to the applied load. Meanwhile, cracks at the bottom corners propagated vertically to the bottom edge of the beam and elongated diagonally towards the beam support. Flexural cracks in the formed of vertically aligned from the bottom edge of the beam was clearly seen in the middle-third span of the beam. With the increment in load, such cracks at the top and bottom chords of opening became more significant. After further increment in load, the beam failed suddenly with the crushing of concrete at the top and bottom chords of opening leaving the bottom bars below the opening completely uncovered with concrete.

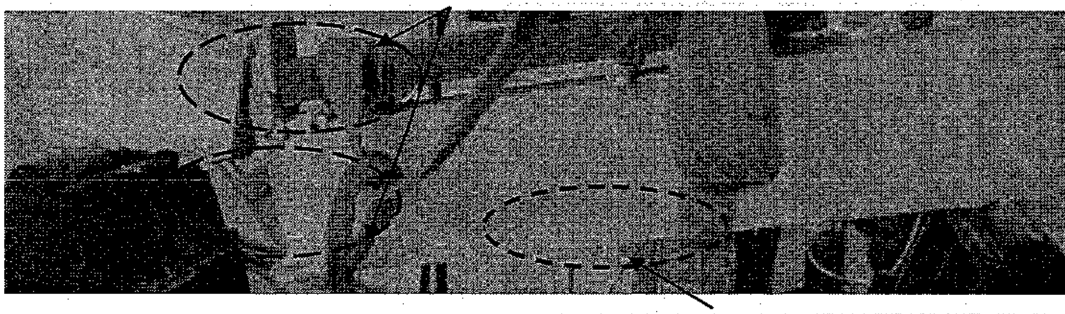

Figure 6.29 Crack patterns of un-strengthened beam SdS1

(d) Beam with Single Square Opening (at distance 1.5d from support), S1.5dS1

Figure 6.30 presents the crack patterns and failure modes of beam S1.5dS1. The trend of crack patterns were found similar as in beam SdS1 in which the cracks are composed of shear and flexural cracks. The early cracks were initiated at the corners of the opening at the initial stage of loading. These cracks were seen elongated vertically to the top edge of the beam as well as diagonally oriented to the applied load at the top chord. Meanwhile, cracks at the bottom corners were observed propagated downwards to the bottom edge of the beam and diagonally towards the beam support. On the other hand, vertically aligned cracks from the bottom edge of the beam were flexural cracks appeared in the middle-third span. The cracks at the opening corners were more noticeable with the increase of load. Just before beam failure, widening of cracks increased at the corners of opening especially at the top chord that resulted in crushing of concrete where the top bars above the opening were exposed.

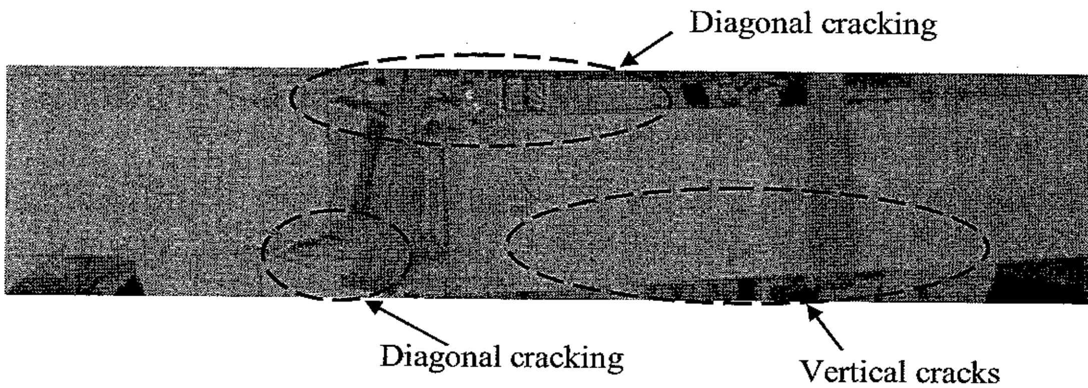

Figure 6.30 Crack patterns of un-strengthened beam S1.5dS1

6.3.2.3 Prevailing Shape of Opening

From Table 6.3, it shows that the ultimate loads of beams with circular and square shapes of openings in the shear zone were not significant. Similarly, the ultimate loads of beams with openings placed either at both ends or a single opening at one end only were found of no significant difference. The provision of circular and square openings in the critical shear region at the face of support and distance 0.5d, d and 1.5d from the support have shown a significant loss of beam capacity of about 68% - 80% as compared to the load-carrying capacity of their respective control beams. On the other hand, the failure modes of both types of shapes of opening were observed similar, which is typically an abrupt and brittle shear failure. Square shape of openings shows disadvantages because of the sharp corners that are subjected to stress concentration which originate initial cracks to form at the corners resulting in diagonal cracking before brittle failure of beams. As for beams with circular opening, two independent diagonal shear cracks were formed in the upper and lower chords of the opening near to the applied load and support. The openings in this study are classified as large openings; hence a smaller size of openings is well suited to provide at the shear zone provided at a less critical location further from the support, e.g. 2d from the support.

6.3.3 Effects of CFRP Strengthening on Shear Capacity

This section shows the strengthening configurations using CFRP laminates for circular and square openings located at both ends and at one end only. The strengthening configurations are the chosen strengthening schemes that were designed in the FE analysis, as discussed in Chapter 5. The most effective strengthening of openings using CFRP laminates in the tested beams is performed in order to achieve objective. no.2.

6.3.3.1 Strengthening Configurations

Figures 6.31 – 6.32 present the schematic diagram of CFRP strengthening configurations for beams with openings at both ends and at one end, respectively. The presence of CFRP laminates is essential to interrupt the probable cracks so as to effectively enhance the beam strength. The CFRP laminates arrangements were based on the FE analysis results on the crack patterns.

Figure 6.31(a) illustrates the CFRP strengthening configuration around the openings of beam COS-S. Referring to the crack pattern results of un-strengthened beam, COS at failure in section 6.3.2.1(a), wide diagonal cracks were formed at the top side of opening which measured approximately 350 mm. Therefore, a longitudinal CFRP laminates in a length of 550 mm with considered anchorage margins were adopted to prevent any penetration of cracks to the applied load. The longitudinal CFRP laminates were applied at the top and bottom sides of the opening with the orientation of fibers parallel to the longitudinal axis of the beam as well as at the bottom surface of the beam as shown in Section A-A. Such placement is to prevent the formation of diagonal cracks both at the top and bottom chords. Meanwhile, 260 mm length of CFRP laminate was placed next to the opening as shown in Figure 6.31(a) in which to restrict the penetration of diagonal oriented cracks towards the opening. This type of strengthening arrangement was also applied onto beam CdS1-S as illustrated in Figure 6.32(a); horizontal aligned CFRP laminates parallel to beam axis were 550 mm length based on the crack pattern results of experimental and numerical analysis were referred.

CFRP laminates configuration around the square openings of beam S0S-S as illustrated in Figure 6.31(b) are referred to the results of FE analysis. The strengthening configurations were mainly consist of horizontally and vertically aligned CFRP laminates around the opening due to the initiation of cracks at the corners of the opening, as observed in the un-strengthened beam, S0S. To prevent the propagation of cracks vertically and diagonally to the top and bottom chords of the opening, horizontal aligned CFRP laminate with fibers parallel to the longitudinal axis of the beam was bonded at both top and bottom chords with a length of 410 mm. The measurement of length has taken into consideration of the margins. In addition, 210 mm vertical aligned CFRP laminates with fibers oriented in a direction perpendicular to the longitudinal axis of the beam were bonded between two horizontally aligned CFRP laminates as shown in Figure 6.31(b). CFRP laminates with a length of 410 mm with fibers oriented parallel to the longitudinal axis were bonded at both top and bottom surfaces of the beam as shown in Section B-B to avoid crushing of concrete at the top and bottom chords of the opening, as observed in the un-strengthened beam.

Figures 6.31 (c) and (e) and Figure 6.32(b) present the strengthening configurations of CFRP laminates of beams S0.5dS-S, SdS-S and SdS1-S, respectively. These beams were bonded with the same CFRP arrangements around the openings which mainly composed of horizontal and vertical aligned CFRP laminates. Vertically oriented CFRP laminates with the fibers perpendicular to the longitudinal beam axis of 300 mm long were applied onto both sides of openings from the top edge to the bottom edge of the beam. Meanwhile, 210 mm long CFRP laminates with fibers in an orientation parallel to the longitudinal beam axis were placed in between two vertical CFRP laminates, at the top and bottom chords. This type of strengthening configurations around the openings were adopted to prevent the early forming of cracks at the corners of the opening as well as the penetration of vertical and diagonal cracks to the top and bottom chords. CFRP laminates in a length of 410 mm with fibers oriented parallel to the longitudinal beam axis were bonded at the top and bottom surface of the beam as depicted in Section C-C in which to prevent concrete crushing at the top and bottom chords. The lengths of CFRP laminates covered the potential length of cracks as well as additional margins were considered.

Strengthening configurations of CFRP laminates of beam CdS-S is shown in Figure 6.31(d). The CFRP laminates arrangements were mainly comprised of horizontally and diagonally aligned laminates around the openings. According to the crack patterns at failure as observed in the un-strengthened beam CdS and by referring to the results of numerical analysis, horizontal aligned CFRP laminates with fibers in an orientation parallel to the longitudinal beam axis were bonded at the top surface and bottom chord of opening as shown in Figure 6.31(d). The length of the longitudinal CFRP laminates was 630 mm. This CFRP arrangement was designed to prevent crushing of concrete at the top and bottom chords due to formation of vertical and diagonal cracks. To prevent the initiation of diagonal cracks from the opening to the applied load, CFRP laminates were placed diagonally oriented next to the circular opening from the top chord to the middle-third span approximately 480 mm as illustrated in Section D-D. The length of CFRP laminates has taken into consideration of additional margins for an effective bonding.

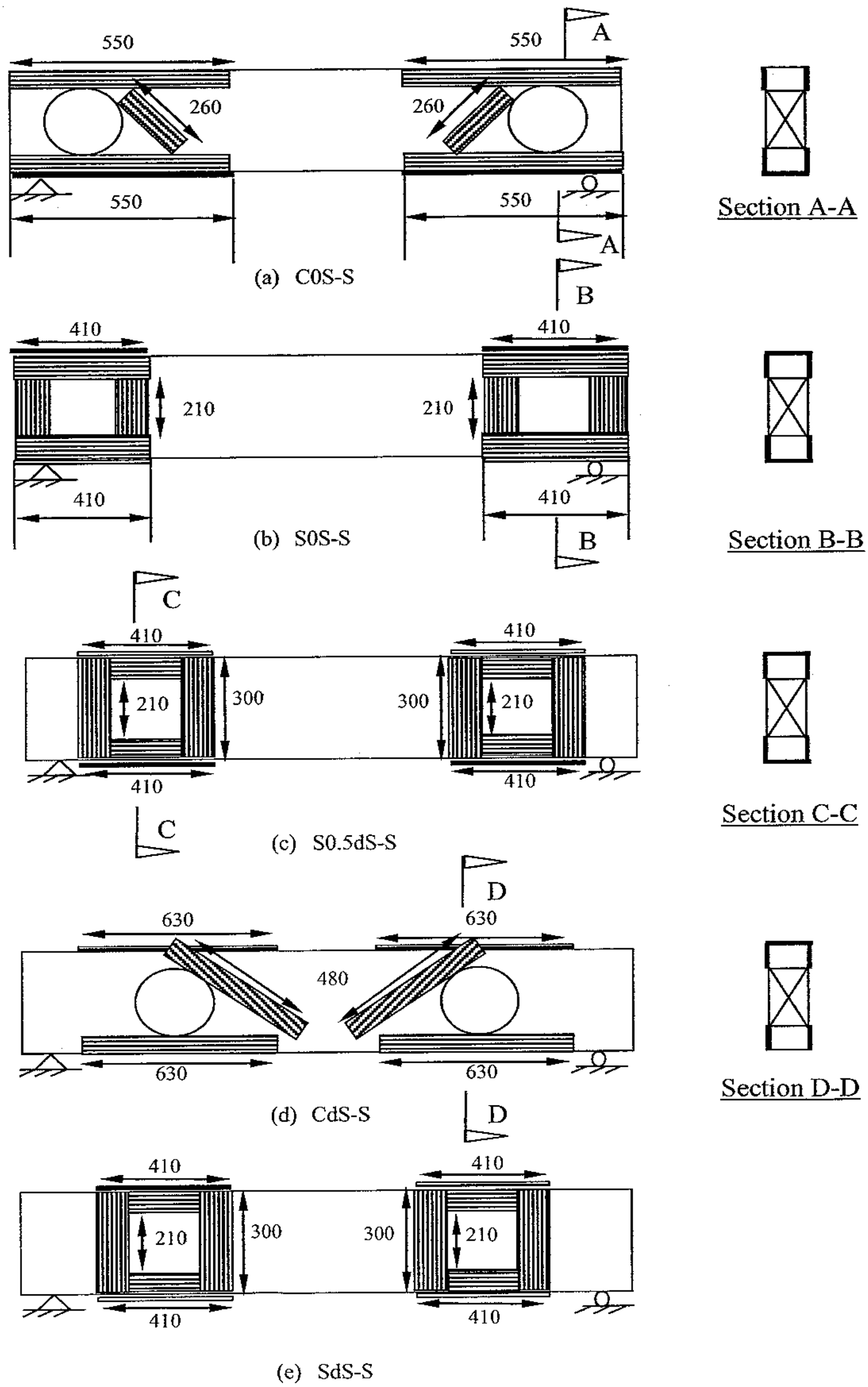

Figure 6.31 CFRP strengthening scheme around openings at both ends

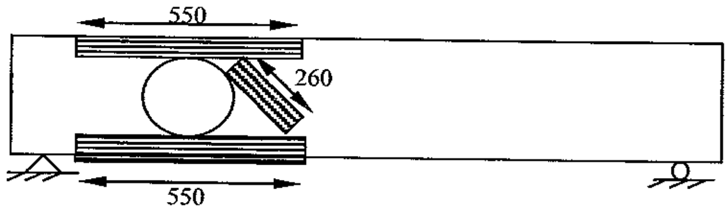

(a) CdS1-S

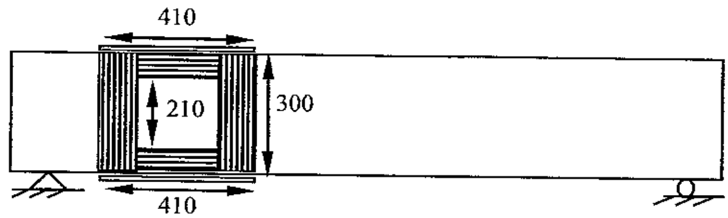

(b) SdS1-S

Figure 6.32 CFRP strengthening scheme around a single opening at one end only

6.3.3.2 Load-Deflection Behaviour

Load-deflection behaviour of beams with openings created at both ends and at one end only strengthened using CFRP laminates are shown in Figures 6.33 – 6.35. The beam results are compared with the results of the corresponding reference beams, which are identified as CB1, CB2 and CB3. A summary of the results is presented in Table 6.4.

(a) Strengthening for Circular Openings (zero distance from support), C0S-S

The area of CFRP laminates strengthened around the circular openings at both ends covers 16% of the beam exposed area. Figure 6.33 shows the plotted load-deflection curves of beam C0S-S. During the initial phase of loading, the beam exhibited elastic behaviour in which the CFRP laminates in the strengthening configuration able to divert the potential cracks to un-reinforced area. Due to this, the beam possessed high stiffness with curve line almost parallel to the load-deflection curve of beam CB1. After initiation of the first crack, the beam stiffness was found slightly reduced with the increment in load until the beam was fully yielded. The yield strength of beam

C0S-S was obtained as 38 kN at a deflection of 4 mm. Further increment in load, the peak point was reached with a maximum load of 40 kN at 4.4 mm deflection. Just after passing the ultimate load, a sharp decline of the slope was observed which indicates an abrupt failure. CFRP strengthening around the openings in this case could re-gain the load-carrying capacity of beam C0S-S to approximately 34% of the load-carrying capacity of the reference beam, CB1.

(b) Strengthening for Square Openings (zero distance from support), S0S-S

The total area of CFRP laminates used to strengthen the area around square openings at both ends covers 37% of the beam exposed area. Load-deflection curve trend of beam S0S-S is illustrated in Figure 6.33 shows a response similar to that as observed in beam C0S-S. It was observed that beam S0S-S experienced high stiffness at the early stage of loading. This may be due to the effects of CFRP laminates which was able to control the formation of cracks at openings' corners as well as top and bottom chords. After that, the beam stiffness was reduced as the load-deflection curve shows a decrease in steepness, which is slightly lower than the stiffness of beam C0S-S. The increase in load was observed until the fully yield condition of the beam. The yield load of beam was obtained as 37 kN at 4 mm deflection whereas the ultimate load was attained as 38 kN at a deflection of 4.3 mm. Beyond the ultimate point, the load-deflection curve exhibited a sudden drop in load indicating brittle failure with a maximum deflection at 7 mm. It is found that the CFRP strengthening configurations around the square openings could re-gain the capacity of beam S0S-S to about 33% of the load-carrying capacity of the reference beam, CB1.

(c) Strengthening for Square Openings (at distance 0.5d from support), S0.5dS-S

CFRP laminates configuration around the square openings composed of about 37% of the beam exposed area. Figure 6.34 presents the load-deflection curve of beam S0.5dS-S. At the initial stage of loading, the beam was high in stiffness due to the steep line of load-deflection. However, the steepness of the line was seen to decline after the formation of cracks. With the increment in load up to the yielding point, the yield strength of beam was obtained as 32 kN at 3.2 mm deflection. Further increment in load, the ultimate load of the beam was attained as 37 kN at 4.1 mm. Softening of the beam was noticed immediately after the point of ultimate load with an abrupt decrease in loading. The strengthening scheme with CFRP laminates of beam S0.5dS-S could re-gain the beam capacity to approximately 46% of the beam capacity of the respective control beam, CB2.

(d) Strengthening for Circular Openings (at distance d from support), CdS-S

The area of CFRP laminates with the strengthening configuration around circular openings at both ends covers 23% of the beam exposed area. The load-deflection curve of beam CdS-S as plotted in Figure 6.34 shows that the beam possessed high stiffness at the early phase of loading. The stiffness of beam CdS-S was observed greater than the stiffness as exhibited in beam S0.5dS-S and SdS-S. The load-deflection curve remained essentially in a sharp inclination until the cracking stage of the beam. Due to cracking, a slight decline of the slope was observed which indicates a reduction in stiffness. After that, the load was noticed increasing up to the fully yield condition and eventually passing the peak point before a sharp drop in load was observed due to failure of the beam. The failure mode was abrupt and brittle. The yield load of beam was obtained as 29 kN at a deflection of 1.2 mm whereas the ultimate load was 50 kN was noticed at 3.1 mm deflection. The presence of CFRP laminates in the strengthening arrangements could re-gain the beam capacity to approximately 63% of the ultimate load capacity, of the reference beam, CB2.

(e) Strengthening for Square Openings (at distance d from support), SdS-S

As shown in Table 6.4, the total area of CFRP laminates bonded around the square openings at both ends of beam SdS-S contained about 37% of the beam exposed area. It was observed that the load-deflection behaviour of beam SdS-S contained similar response as discussed in beam S0.5dS-S. In the early phase of loading, high stiffness in beam SdS-S was observed in the elastic region as shown in Figure 6.34. As the load increase, the line was found parallel to the load-deflection curve of beam S0.5dS-S;

however after the cracking of the beam, the stiffness of beam SdS-S remained in a stiff state despite a slight reduction in beam stiffness was noticed. The beam then exhibited plastic flow as the yield strength of beam was obtained as 36 kN at 3 mm deflection while the ultimate load was reached at a load of 37 kN at 3.3 mm. Just after the ultimate point, a sudden decrease of load was observed which shows a softening of the beam due to failure. The strengthening configurations with CFRP laminates could re-gain the beam capacity to about 46% of the beam capacity of control beam, CB2.

(f) Strengthening for Single Circular Opening (at a distance d from support), CdS1-S

The area of CFRP laminates with the strengthening configuration around a circular opening at one end covers 12% of the beam exposed area. Figure 6.35 shows the load-deflection curve of beam CdS1-S. In the preliminary stage of loading, the load-deflection curve exhibits a straight line indicating linear elastic response similar to the response of the corresponding control beam, CB3. The yield load of beam was obtained as 29 kN at 1.8 mm deflection whereas the ultimate load was 31 kN at 2.5 mm deflection. An abrupt reduction of applied load was observed in post-yielding stage due to beam failure. Strengthening with CFRP laminates could increase the beam capacity to approximately 32% of the ultimate load capacity of beam CB3.

(g) Strengthening for Single Square Opening (at distance d from support), SdS1-S

The area of CFRP laminates of the strengthening configuration which bonded around the square opening at one end covers 19% of the beam exposed area. The load deflection curve of beam SdS1-S as shown in Figure 6.35 exhibits behaviour similar to beam CdS1-S. In the early phase of loading, a high inclination of the slope was observed similar to the response of beams CB3. In the plastic zone of the beam, the load-deflection curve was observed nonlinear as a result of cracking before the yielding of the beam. The yield load of beam SdS1-S was obtained as 25 kN at 1.2 mm deflection while the ultimate load as 28 kN was noticed at a deflection of 3.5 mm. An immediate drop in load was observed after the ultimate load was attained.

Strengthening with CFRP laminates managed to re-gain the beam capacity to about 29% of the load-carrying capacity of control beam, CB3.

In general, strengthening using CFRP laminates could re-gain the beam capacity to a certain extent however could not fully reinstate the original beam capacity as of their respective control beams, CB1, CB2 and CB3. The openings may need both internal and external strengthening to fully restore the beam capacity. The beam behaviour depended primarily on the degree of interruption of the natural load path. In this case, the load path was interrupted as the opening was strengthened using CFRP laminates exhibited almost a linear relationship up to failure (El Maaddawy & Sherif, 2009). Results show that beams with circular openings tend to exhibit greater beam stiffness than square shape opening due to the high stress concentration at opening corners. The presence of CFRP laminates around the openings greatly enhances the beam stiffness and reduces beam deflection.

Table 6.4 Test results of CFRP strengthened openings in shear

Beam	Yielding load P_y (kN)	Δ_y (mm)	Ultimate load P_u (kN)	Δ_u (mm)	Beam Exposed Area (BEA) (mm^2)	$\left(\frac{\text{Total CFRP Area}}{\text{BEA}}\right)$ x 100%
CB1	79	5.4	116	29.5	-	-
CB2	77	8.2	80	9.1	-	-
CB3	86	8.0	96	36.4	-	-
COS-S	38	4.0	40	4.4	1,296,000	16
SOS-S	37	4.0	38	4.3	1,296,000	37
S0.5dS-S	32	3.2	37	4.1	1,296,000	37
CdS-S	29	1.2	50	3.1	1,296,000	23
SdS-S	36	3.0	37	3.3	1,296,000	37
CdS1-S	29	1.8	31	2.5	1,296,000	12
SdS1-S	25	1.2	28	3.5	1,296,000	19

BEA= Beam Exposed Area

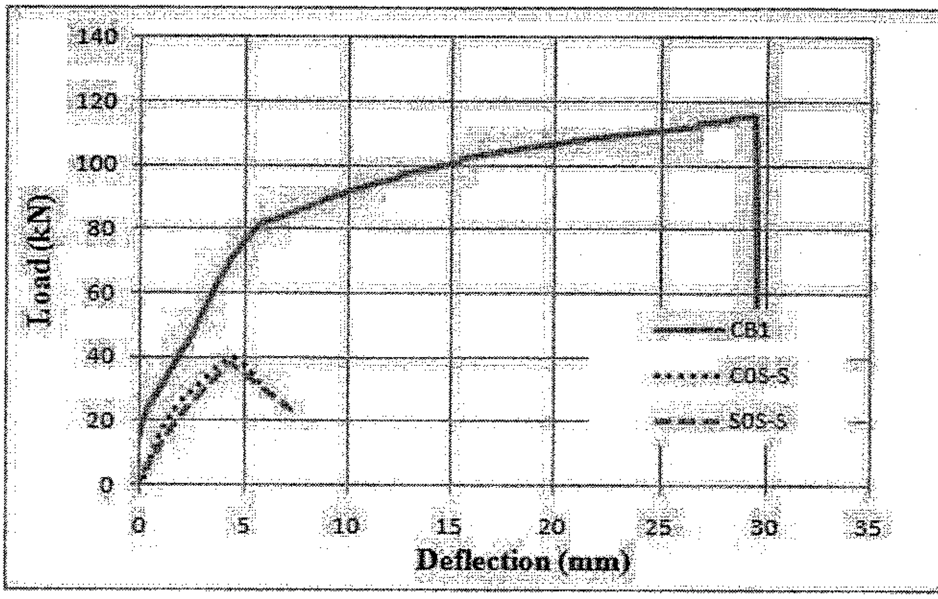

Figure 6.33 Comparison of load-deflection curves of strengthened beams with openings at the face of support and beam CB1

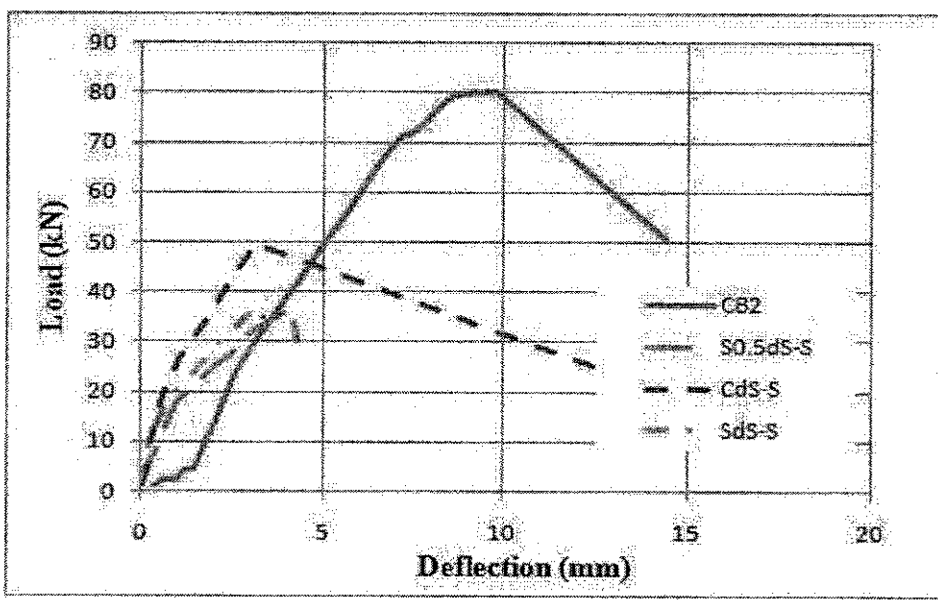

Figure 6.34 Comparison of load-deflection curves of strengthened beams with openings at distance 0.5d and d from the support and beam CB2

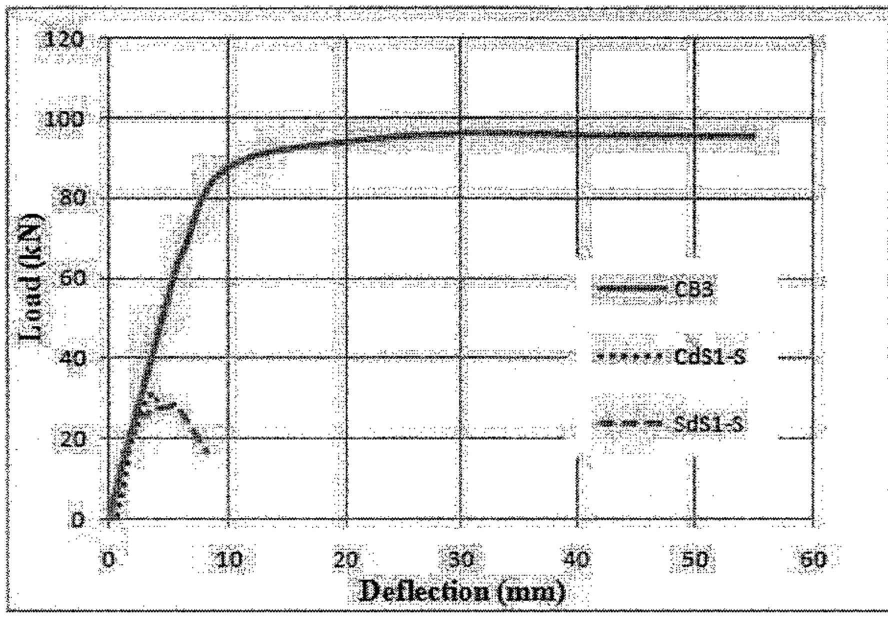

Figure 6.35 Comparison of the load-deflection curves of strengthened beams with opening at one end and beam CB3

6.3.3.3 Failure Modes and Crack Patterns

Figures 6.36 – 6.42 show the failure modes and crack patterns of beams with strengthened openings at both ends and at one end only. The failure modes and crack patterns of such beams during experimental testing were recorded up to failure.

(a) Strengthening for Circular Openings (zero distance from support), COS-S

Effects of strengthened circular openings at both ends at the face of support on failure modes and crack patterns are shown in Figure 6.36. The early cracks were observed in the middle-third span in which the formation of flexural cracks in the form of vertical aligned cracks from the bottom edge of the beam. Such cracks were noticed distance away from the strengthened area as the presence of CFRP laminates around the circular openings interrupted the natural load path of crack propagation (Pimanmas, 2010). Meanwhile, due to the effects of CFRP laminates at the top and bottom chords of openings, cracks at the top side of opening eventually became horizontally elongated to the loading point. These cracks were formed along the outer edges of CFRP next to the opening. On the other hand, diagonal cracks were formed at the bottom side of opening; such cracks then penetrated to the face of support. This phenomenon eventually caused peeling of CFRP laminates at the bottom chord of the opening. During the experimental testing, a sudden failure was observed in this beam indicating brittle shear failure.

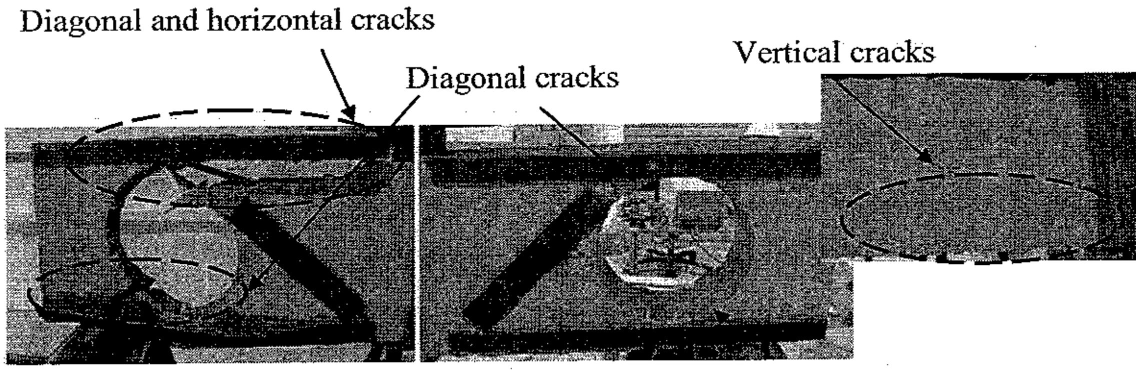

Figure 6.36 Crack patterns of strengthened beam COS-S

(b) Strengthening for Square Openings (zero distance from support), SOS-S

Figure 6.37 illustrates the failure modes and crack patterns of beam SOS-S due to the effects of CFRP laminates which bonded around square openings placed at both ends at the face of support. During the initial stage of loading, vertical cracks were found in the middle-third span of beam away from the strengthened area. With the increase of load, such cracks penetrated about one-third of the beam depth from the bottom edge of the beam. Soon after that, an abrupt and brittle shear failure was observed during the failure of the beam. Crushing of concrete cover at the top chord was observed due to the formation of diagonal and horizontal cracks at the top corner of opening to the loading point. On the other hand, diagonal and horizontal cracking at the bottom chord of the opening leads to crushing of concrete which then exposed the bottom bars and stirrups at the opening.

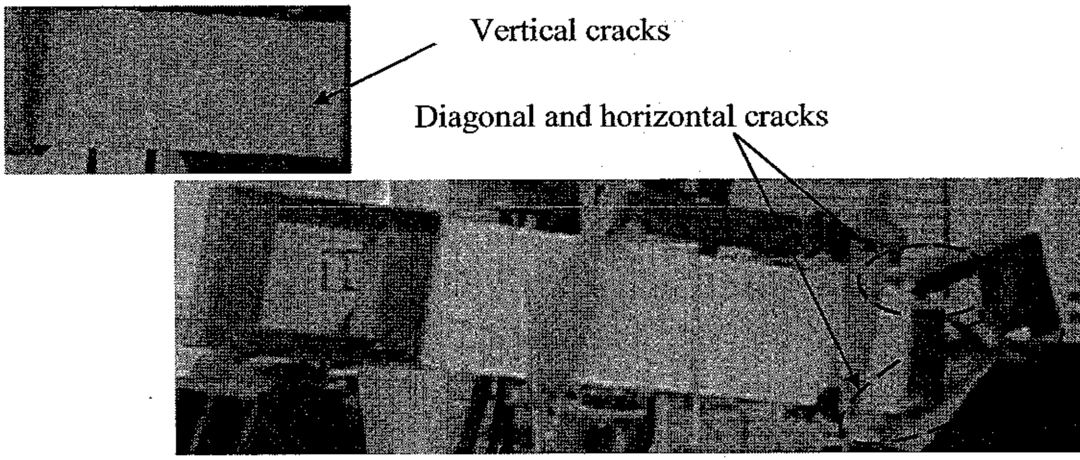

Figure 6.37 Crack patterns of strengthened beam S0S-S

(c) Strengthening for Square Openings (at distance 0.5d from support), S0.5dS-S

Effects of strengthened square openings at both ends at a distance 0.5d from the support on failure modes and crack patterns are shown in Figure 6.38. During the loading process, initial cracks in the form of flexural cracks appeared in the mid-span away from the opening region strengthened using CFRP laminates. This is due to the presence of CFRP laminates that diverted the crack propagation to non-restricted areas. Such cracks propagated vertically from the bottom edge of the beam to about half of the beam depth with the increment of load. Further increase of load, a sudden shear failure was observed at the top chord with diagonal cracking at the point of loading towards the top corner and horizontal cracking at the top side of the opening, respectively. At the top chord, this phenomenon resulted in crushing of concrete with peeling of concrete edges (bonded with CFRP laminates) at both ends with delamination of horizontally aligned CFRP laminates from the concrete surface which then exposing the top bars. Meanwhile at the bottom chord, horizontal cracks were noticed at the corner of the opening and elongated to the beam support. Such cracks lead to the crushing of concrete near the beam support and peeling of CFRP laminates at the edge. Bottom reinforcements were noticeable at the bottom side of opening.

Diagonal and horizontal cracks

Vertical cracks

Figure 6.38 Crack patterns of strengthened beam S0.5dS-S

(d) Strengthening for Circular Openings (at distance d from support), CdS-S

Figure 6.39 shows the failure modes and crack patterns of beam CdS-S due to the effects of CFRP laminates around the openings. At the early stage of loading, flexural cracks were formed in the middle-third span of beam at the area without strengthening of CFRP laminates. With the increase of load, flexural cracks in the form of vertically aligned cracks were initiated at the bottom edge of opening and penetrated upwards about one-third of the beam depth. Further increment in load, an abrupt shear failure was observed and recorded. At the top chord, crushing of concrete was observed at the top side of opening. This had caused partial delamination of CFRP laminates at the top surface of opening as well as at the top chord next to the opening. The top reinforcement bars at the opening were also visible. While at the bottom chord, initial diagonal cracks were noticed at the bottom side of opening; such cracks became horizontal aligned as the cracks elongated along the edges of CFRP laminates to the beam support. This eventually resulted in partial dislocation of bottom chord at the bottom side of the opening from the beam support in which the bottom bars were obviously seen.

Figure 6.39 Crack patterns of strengthened beam CdS-S

(e) Strengthening for Square Openings (at distance d from support), SdS-S

Crack patterns and failure modes of strengthened beam SdS-S due to the effects of CFRP laminates are illustrated in Figure 6.40. The trend of crack patterns was found similar as discussed in beam S0S-S and S0.5dS-S; flexural cracks were formed in the tension zone away from the strengthened region by CFRP laminates. Such cracks then penetrated vertically from the bottom edge of the beam to about one-third of the beam depth with the increase of load. The beam then failed suddenly by diagonal and horizontal cracking at the top chord whereas crushing at the bottom chord was observed as the load was further increased. At the top chord, diagonal and eventually horizontal cracks were observed at the loading point to the top corner of the opening. This had caused peeling of concrete cover at the top surface of the opening. Also, the top bars at the top side of the opening were exposed. On the other hand, diagonal and horizontal cracks were formed at the bottom chord which eventually resulted in partial displacement of bottom chord from the beam support. The bottom bars at the bottom side of the opening were noticeable due to the concrete crushing.

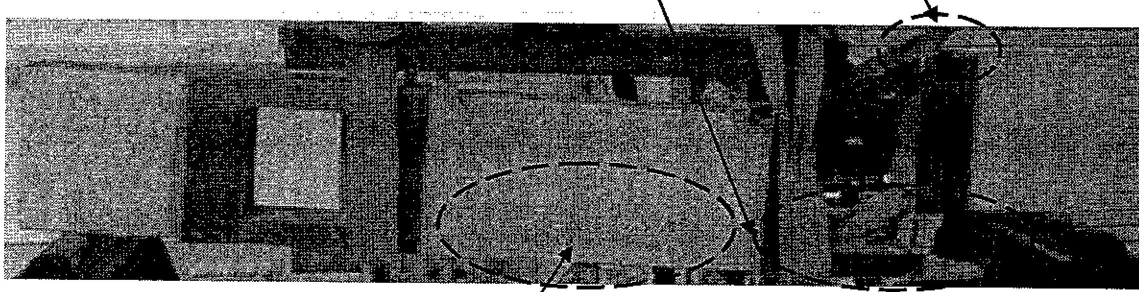

Figure 6.40 Crack patterns of strengthened beam SdS-S

(f) Strengthening for Single Circular Opening (at a distance d from support), CdS1-S

Figure 6.41 shows the failure modes and crack patterns of beam CdS1-S due to the effects of CFRP laminates around the circular opening at one end a distance d from the support. During the initial stage of loading, flexural cracks were observed along the mid-span. This is because the area subjected to the formation of diagonal cracks at the top and bottom sides of the opening was restricted by CFRP laminates in this strengthening configuration. As the load increased, these flexural cracks propagated vertically from the bottom edge of the beam to about 1/4 – 1/3 of the beam depth. The beam with strengthened circular opening at one end failed abruptly in a brittle shear manner. Cracks at the top side of opening penetrated vertically to the top edge of the beam and diagonally to the loading point which had caused delamination of horizontally aligned CFRP laminates at the top chord. While at the bottom side of the opening, diagonal cracks were first initiated followed by the formation of horizontal aligned cracks; such cracks penetrated along the edges of longitudinal CFRP laminates at the bottom chord to the beam support. This condition of cracks resulted in partial displacement of bottom chord from the beam support.

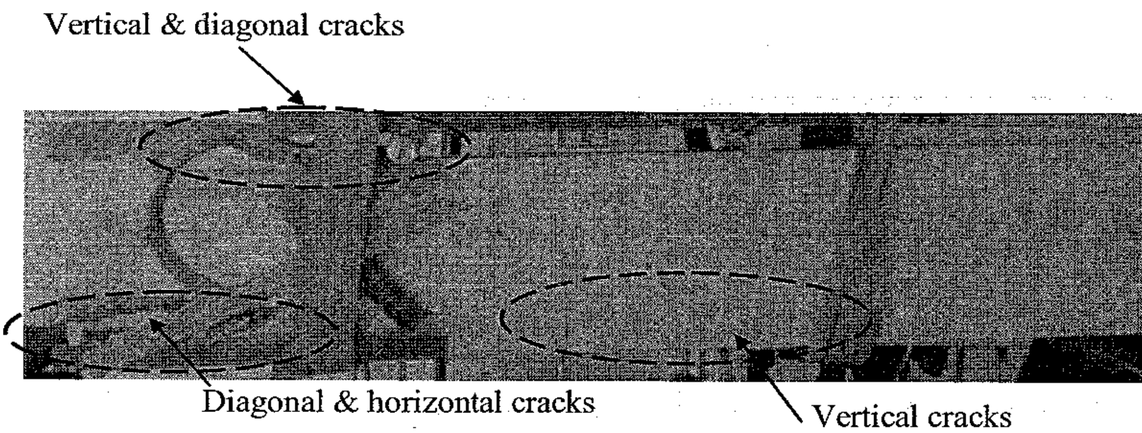

Figure 6.41 Crack patterns of strengthened beam CdS1-S

(g) Strengthening for Single Square Opening (at distance d from support), SdS1-S

Effects of CFRP laminates on the failure modes and crack patterns of beam SdS1-S are shown in Figure 6.42. Early cracks were observed in the tension zone during the early phase of loading away from the strengthened region. These cracks were flexural cracks which initiated at the bottom edge of the beam and penetrated vertically to about 1/3 of the beam depth. With the increase of load, concentration of cracks increases in the mid-span. Upon failure, a sudden and brittle shear failure at the opening was observed. Horizontal cracks were found at the top chord of the opening which resulted in peeling of concrete cover. These cracks at the top chord caused the delamination of horizontally aligned CFRP laminates. Meanwhile at the bottom chord, horizontal cracks were noticed along the bottom side of opening and elongated to the beam support. This resulted in partial dislocation of bottom chord from the beam support, as shown in Figure 6.42. The bottom reinforcements were clearly seen due to concrete spalling at the bottom side of opening.

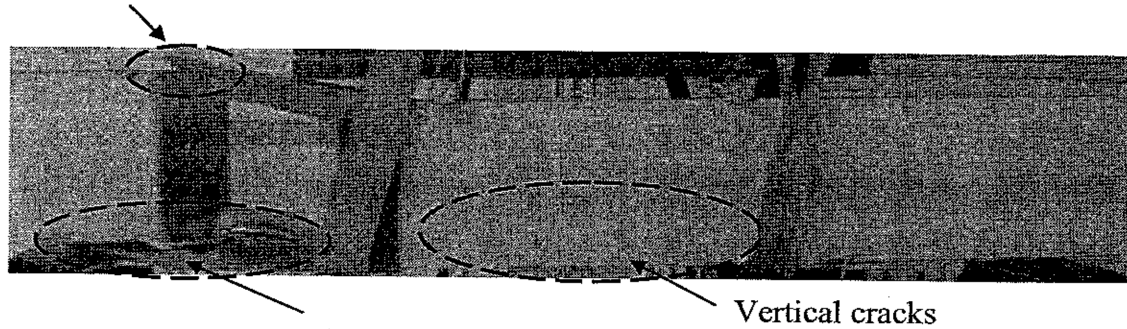

Figure 6.42 Crack patterns of strengthened beam SdS1-S

6.3.3.4 Effective Strengthening Configuration

With their respective strengthening configurations, results of strengthened circular and square openings at both ends and at one end only with CFRP laminates could re-gain the beam capacity to about 30% - 60% and 30% - 50%, respectively of their respective control beams. In terms of failure modes, both circular and square openings failed in an abrupt and brittle shear failure with their corresponding crack patterns as discussed in the earlier sections. In general, the results show that strengthened beams with openings either circular or square in shapes provided at both ends and at one end only did not show significant difference in terms of beam capacity. The presence of CFRP laminates that disturbs the natural path of crack propagations which requires a higher energy to redirect the path of the cracks to the un-strengthened area, this causes an increase in beam capacity to a certain state before failure occurred.

6.4 The Effects on Shear and Flexural Capacity

Figure 6.43 illustrates the comparison of openings provided in flexure and shear zones in the relationships of percentage ratio of opening area and beam elevated area as well as the percentage ratio of CFRP area and beam exposed area.

Referring to Figure 6.43, it can be seen that openings located in the shear zone show a greater percentage of CFRP area needed to strengthen the area around the openings compared to the openings in flexure. It is found that the highest utilization of CFRP area needed to strengthen the area around the openings were located at distances of 0, 0.5d and d away from the support.

Comparing the shape of openings in shear, square openings needed the most CFRP laminates to strengthen the area around the openings compared to the circular ones. This is because the sharp corners of the square openings are subjected to stress concentration which eventually leads to early diagonal cracking.

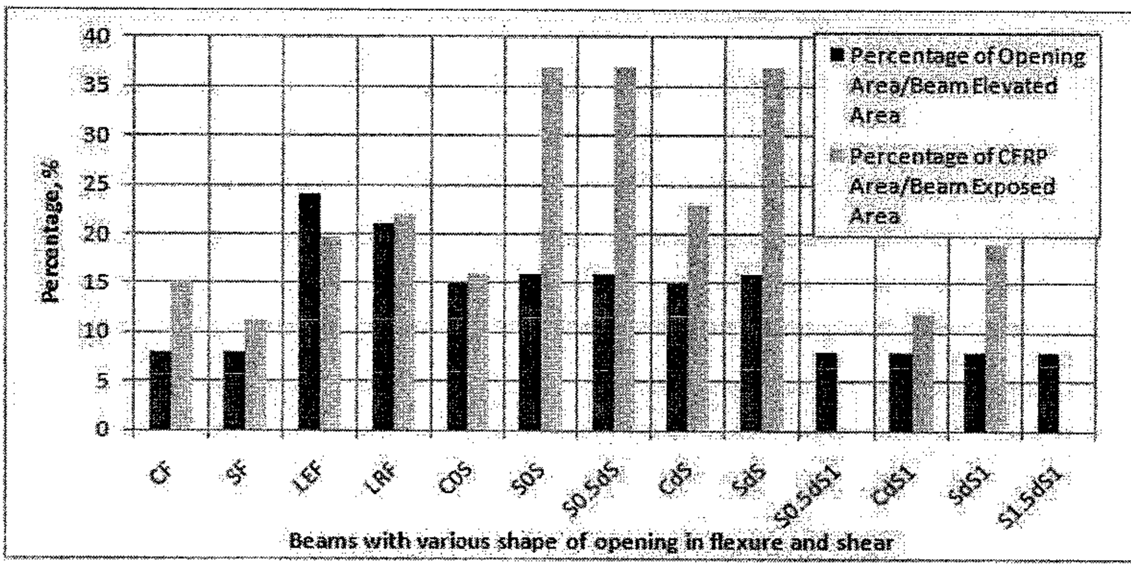

Figure 6.43 Comparisons of openings in flexure versus shear

6.5 Summary

The following experimental results in terms of beam capacity (load-deflection and crack pattern) as well as the effects of openings due to shapes and sizes are obtained and summarized as follows:

The presence of openings in the mid-span of RC beams had caused the reduction of beam capacity to a range of 21% - 59%; with the lowest reduction caused by the provision of the circular opening while the highest reduction was because of the rectangular opening. When providing openings in the shear zone of RC beams, the beam capacity was significantly reduced either with openings provided at both ends or a single opening provided at one end only. Openings provided at both ends caused a reduction of 69% - 80%. Meanwhile, a single opening at one end caused a decrease of

68% - 77%. Circular and square shape openings provided at distances 0, 0.5d, d and 1.5d away from the support did not show significant difference in the beam capacity.

The crack pattern results of beams with circular and square openings in the mid-span show that vertical cracks were formed along the tension zone at the bottom chord and then propagated towards the openings. Diagonal cracks were then observed at the loading point towards the beam support. Such beams failed mainly due to bending failure. On the other hand, stress concentration at the sharp corners of the rectangular opening in the mid-span resulted in the formation of diagonal cracks towards the loading point, which leads to localized shear failure. Meanwhile, the results of the crack pattern of beams with openings at both ends and at one end only show that diagonal cracks was formed at the top and bottom sides of the circular openings. On the other hand, diagonal cracks were initiated at the four corners of the square openings due to concentration of stress. Such cracks then penetrated diagonally to the top and bottom chords, respectively. The failure modes of such beams were in shear.

To determine the most effective strengthening of openings using CFRP laminates experimentally, the following summaries are drawn:

For CFRP strengthened openings in flexure, the presence of CFRP laminates managed to restore approximately 74% - 96% of the beam capacity for the control beam. Remarkable restoration of beam capacity is found in beams with circular and elliptical openings rather than beams with square and rectangular openings. Thus, it is recommended that circular and elliptical openings are best-suited shape of openings to be provided in the flexure location in RC beams in practice. On the other hand, the results of beams with CFRP strengthened openings in shear show that the strengthening configuration managed to re-gain the beam capacity of beams with openings located at both ends and one end only to approximately 30% - 60% of the original beam capacity. The enhancement of the load-carrying capacity of beams with openings in the shear region could be increased by the provision of smaller openings in the shear zone and the distance from the support should be greater than a distance d.

CFRP strengthening configuration around circular and square openings located in the beam mid-span had caused the vertical cracks to appear in the mid-span away from the strengthened region. The failures of such beams were a combination of bending and shear failure. The strengthening configurations of CFRP around large elliptical and rectangular openings force the vertical cracks to appear at the bottom chord between the CFRP laminates. The failure mode of such beams is due to diagonal cracking at the loading point to the opening corner at the top chord that caused localized shear failure. The crack patterns of the strengthened circular and square openings at both ends and at one end only appeared vertically along the beam mid-span away from the area strengthened by CFRP laminates. Shear failure was observed in these beams. Diagonal and horizontal cracks were observed at the top and bottom sides of circular opening. Similarly, such cracks were also found at the opening corner of square openings.

CHAPTER 7

EXPERIMENTAL STUDY VERSUS FE ANALYSIS

7.1 Introduction

This chapter presents the comparative study of experimental and FE analysis results. The comparison of results was made in two parts: in the first part, the results of the un-strengthened beams are discussed while in the second part, the results of the strengthened beams are presented and discussed. This comparative study has shown the confidence level of the numerical analysis. There were about 80% of the results found in very close agreement with each other. Therefore, numerical analysis can be used to find the optimal solution for dealing with the openings in beams.

7.2 Flexural Analysis of Un-Strengthened Beams

In the following sub-sections, comparative analysis of the load-deflection behaviour and crack patterns of the un-strengthened beams contained different opening configurations are performed and discussed in order to achieve objective no. 1(iii). For this discussion, beams contained openings in the flexural zone are considered whereas control beam, CB is considered as the reference beam.

7.2.1 Load-Deflection Behaviour

Tables 7.1 and 7.2 contain the summary of results derived from the load-deflection curves of FE analysis and experimental testing as shown in Figures 7.1 – 7.5.

7.2.1.1 Control beam, CB

Figure 7.1 shows the load-deflection curves of beam CB, which were obtained from FE analysis and the experimental testing. Both the curves show that at the early stage of loading, the beam possessed high stiffness because of the steepness. The steepness of the line declined after the formation of the first crack, the two lines (FE and EXP) seemed parallel to each other, which was observed until the fully yield condition. After the fully yield condition, FE results show a smaller plastic zone, which is about 20% of that exhibited by experimental testing, which means experimental beam has shown higher ductility because the failure was happened at the deflection of 29.5 mm as compared to that of the theoretical beam that showed a deflection of 7.8 mm. One of the reasons is that soon after the failure position, the beams came down quickly that is recorded by the LVDT, whereas the theoretical beam marked the deflection at the point where failure is expected to happen. The experimental beam was yielded at 79 kN at 5.4 mm whereas the theoretical analysis predicted the yielding load as 77 kN at 3.9 mm deflection, which in very good agreement.

7.2.1.2 Effects of Circular Opening, CF

Load deflection behaviour of the beam CF as obtained from FE analysis and experiment is compared in Figure 7.2. Both the curves show that at the initial phase of loading, the beam experienced high stiffness because of the steepness. The line of steepness declined after the first crack was formed, both the line of experimental and FE seemed parallel to each other which was observed until the fully yield condition. Beyond the point of yielding, FE results show a smaller plastic zone, which is about 50% of that exhibited by experimental testing, which means experimental beam has shown higher ductility because the failure was happened at the deflection of 16.7 mm as compared to that of the theoretical beam that showed a deflection of 8.4 mm. The experimental beam was yielded at 78 kN at 7.7 mm whereas the theoretical analysis predicted the yielding load as 79 kN at 3.9 mm deflection, which shows a good match between both results.

7.2.1.3 Effects of Square Opening, SF

Figure 7.3 shows the load-deflection curves of beam SF that obtained from experimental testing and the FE analysis respectively. The beam followed the similar trend as discussed for the beam with circular opening. Both of the curves show a linear elastic behaviour until the first yield observed. After yielding was observed, both the curves demonstrated an almost constant load with the increase of deflection, which means a plastic flow in the beam. The extent of flow of theoretical curve was about half of the experimental curve. Experimental beam was failed at the deflection of 11 mm and 75 kN. On the other hand, the theoretical beam was failed at 7.3 mm and 86 kN. At the yielding point, deflections were quite similar in both the curves, i.e. 3.8 mm and 4 mm. There was observed a difference of about 30% in the yielding load of experimental beam with the theoretical results. One of the reasons could be due to the opening corners which subjected to high stress concentration which may cause the beam to experience yielding at early stage.

7.2.1.4 Effects of Large Opening (Elliptical and Rectangular)

Effects of large elliptical opening on load-deflection behaviour as obtained using numerical analysis and experimental testing are shown in Figure 7.4. Similar behaviour was observed as discussed in the earlier i.e. during linear elastic response the beam showed high stiffness, after experiencing the first crack a drop in stiffness was observed. However, both experimental testing and FE analysis showed a continuous increase in load until it reached to the maximum value of 49 kN and 45 kN, respectively by experimental testing and FE analysis. The maximum experimental load of 49 kN was achieved at 3.3 mm deflection whereas theoretical load was obtained at 2.2 mm deflection. As the length of opening was extended beyond the load points on both sides, therefore after reaching to the peak theoretical load of 45 kN there was no further load-deflection was recorded; which means collapse is expected at this point. On the other hand, experimental graph has shown a sudden drop of load with large plastic deformation. It is because of the reason that when peak load was achieved, after that the beam deflected down quick that was recorded by LVDT, which was not predicted by FE analysis.

Figure 7.5 presents the effects of large rectangular opening on load-deflection behaviour as obtained using numerical analysis and experimental testing. The beam behaviour was observed similarly as discussed in the earlier i.e. the beam showed high stiffness at the state of elastic response, reduction in stiffness was observed after the first cracking. However, both the curves of experimental and FE results showed a continuous increase in load until it reached to the ultimate value of 39 kN and 40 kN, respectively by experimental testing and FE analysis. The ultimate experimental load of 39 kN was achieved at 3 mm deflection while the theoretical load was obtained at 2.3 mm deflection. As the length of opening was extended beyond the load points on both sides, therefore after reaching to the peak theoretical load of 40 kN there was no further load-deflection was recorded; which means collapse is expected at this point. In contrast, experimental graph has shown a sudden fall of load with large plastic deformation. Similarly as observed in the elliptical opening, it is because of the reason that when peak load was attained, then the beam deflected downwards in which was recorded by LVDT, which was not predicted by FE analysis.

A comparison of the experimental with predicted ultimate loads of the beam specimens is given in Table 7.2. As shown, a good agreement between the experimental and analytical results is achieved. The ratios of the predicted to experimental ultimate strength for the beams CB, CF, SF, LEF and LRF are 0.75, 0.93, 1.15, 0.92 and 1.03, respectively. The theoretical results were found slightly greater than the experimental ones in beams SF and LRF; and similar to the experimental results in beams CF and LEF. The average numerical-to-experimental ratio and its standard deviation were found as 0.96 and 0.15, respectively, which indicates a close agreement. The experimental study and the numerical analysis have proved that providing a small opening in the beam mid-span did not significantly affect the structural capacity; hence no CFRP strengthening is required. The comparison results also proved that the theoretical models are reliable because the theoretical results are found close and in good agreement with the corresponding experimental results.

Table 7.1 Comparison of experimental and FEM results of un-strengthened beams

Beam	EXP				FEM			
	Yielding load P_y (kN)	Δ_y (mm)	Ultimate load P_u (kN)	Δ_u (mm)	Yielding load P_y (kN)	Δ_y (mm)	Ultimate load P_u (kN)	Δ_u (mm)
CB	79	5.4	116	29.5	77	3.9	87	7.8
CF	78	7.7	92	16.7	79	3.9	86	8.4
SF	57	3.8	75	11.0	79	4.0	86	7.3
LEF	32	2.0	49	3.3	26	0.8	45	2.2
LRF	34	2.5	39	3.0	23	0.9	40	2.3

Table 7.2 Comparison of experimental and FEM ultimate loads of beams

Beam	Ultimate load, P_u (kN)		FEM/EXP
	EXP	FEM	
CB	116	87	0.75
CF	92	86	0.93
SF	75	86	1.15
LEF	49	45	0.92
LRF	39	40	1.03

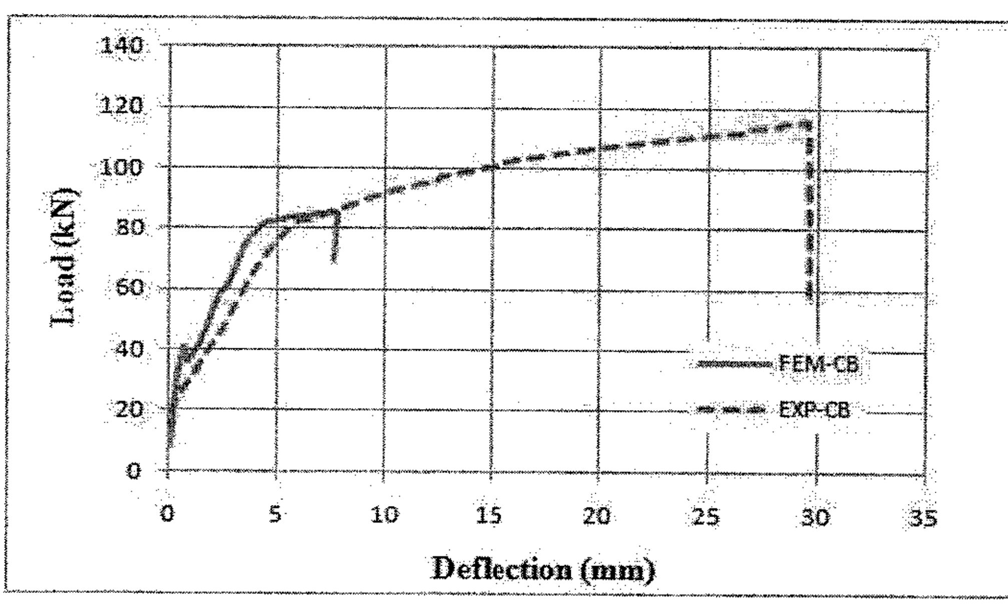

Figure 7.1 Experimental and FEM load-deflection behaviour of control beam, CB

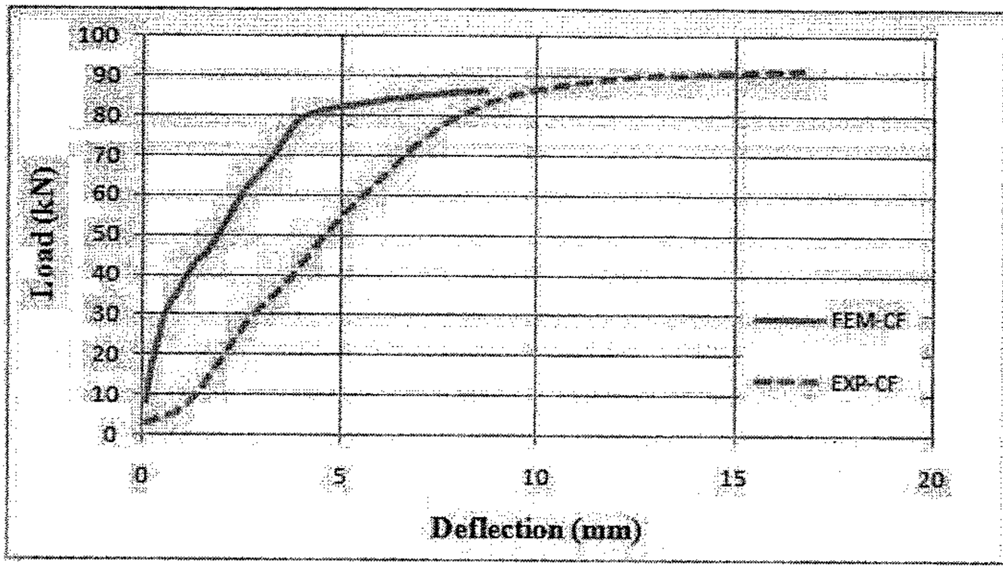

Figure 7.2 Experimental and FEM load-deflection behaviour of beam CF

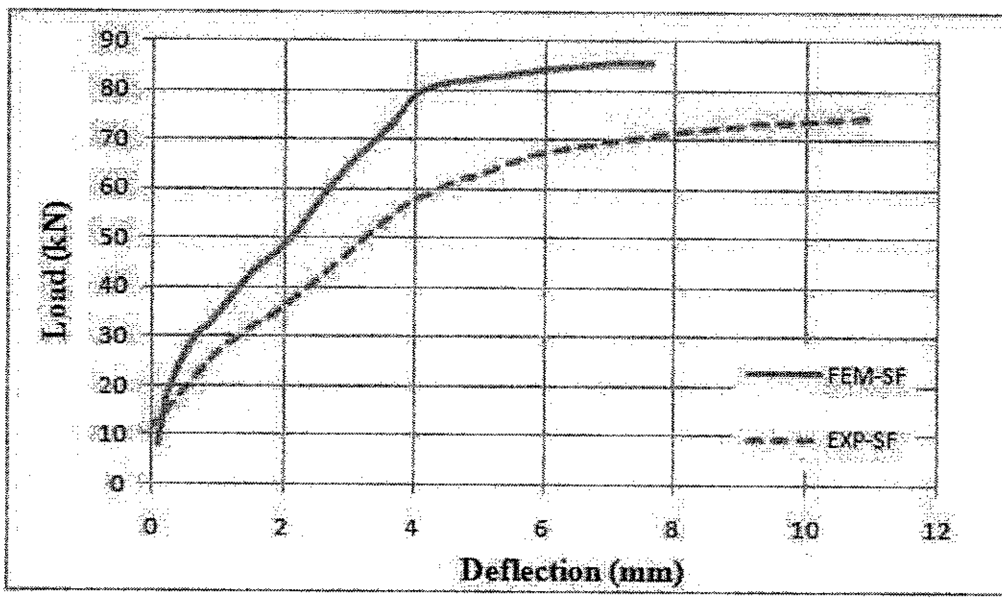

Figure 7.3 Experimental and FEM load-deflection behaviour of beam SF

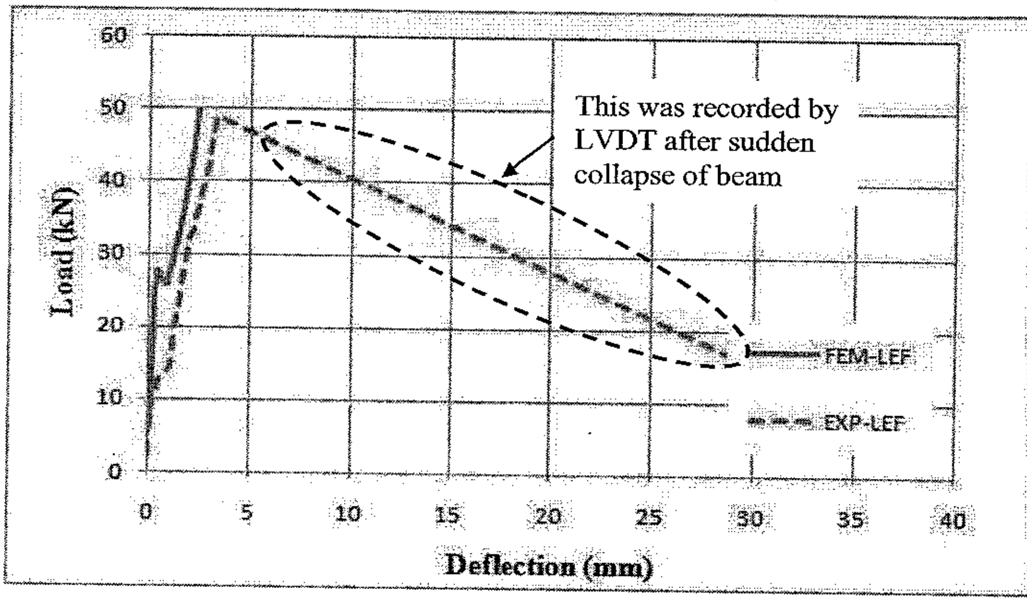

Figure 7.4 Experimental and FEM load-deflection behaviour of beam LEF

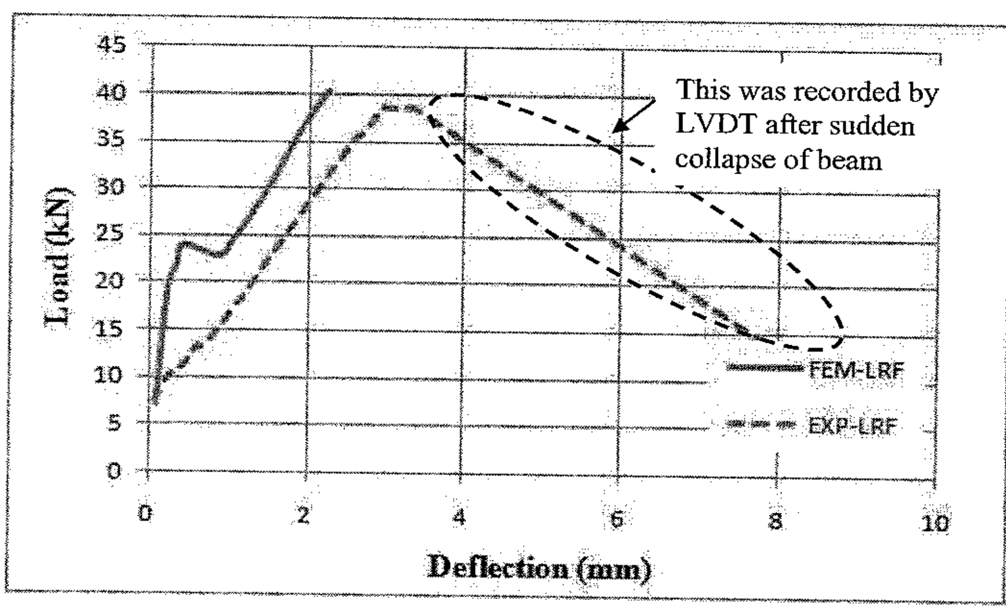

Figure 7.5 Experimental and FEM load-deflection behaviour of beam LRF

7.2.2 Crack Patterns

This section presents the comparative analysis of the crack patterns as observed during testing and drawn by FE analysis, which is shown in Figures 7.6 – 7.10.

7.2.2.1 Control beam, CB

Control beam is the solid beam, referring to Figure 7.6, theoretical results and tested beam showed the similar crack patterns, which are composed of flexural and shear cracks. The flexural cracks were vertically aligned from the bottom up to middle-third of the depth of the beams, such cracks were observed within the middle-third span. The shear cracks were diagonally oriented, which originated from loading points at the top side of the beam and elongated diagonally to the bottom near to the supports. At the point of failure, the main diagonal cracks were very wide, which formed see-through gap. Therefore, it can be concluded that the failure was governed by the shear failure.

7.2.2.2 Effects of Circular Opening, CF

The FE analysis crack pattern of beam CF is compared with the crack pattern of experimental testing as shown in Figure 7.7. The crack patterns were mainly composed of flexural cracks formed in the middle-third span vertically from the bottom edge of the beam up to the bottom side of opening whereas shear cracks in the form of diagonal cracks appeared in the region away from the mid-span. Within the loading points, the height and length of diagonal cracks were increased and eventually reduced as the cracks moved beyond the loading point to the beam support. At the top side of the opening, FE analysis captured horizontal cracks between the loading points indicating concrete crushing; this behaviour was also observed in the experimental beam. Therefore, in this case the failure was mainly due to bending which indicates a close match of crack patterns between the two results was observed.

7.2.2.3 Effects of Square Opening, SF

Figure 7.8 presents the crack pattern comparison of beam SF from FE analysis and tested beam. From the numerical analysis, flexural cracks were predicted vertically aligned from the bottom edge in the middle-third span of the beam. Then, these cracks became diagonally oriented as the cracks approaching the beam support. The height and length of diagonal cracks increase at the loading points at the top side of the beam and elongated diagonally to the bottom near to the supports. On the other hand, diagonal cracks at the opening corners at the top chord seemed horizontally aligned as the cracks penetrated to the loading points; similar as observed in the experimental beam. A good agreement is obtained between the crack pattern of FE results and experimental beam.

7.2.2.4 Effects of Large Opening

Comparison of the produced and experimentally observed crack patterns of the beams with large elliptical and rectangular opening are shown in Figures 7.9 and 7.10, respectively. Similar as observed in the experimental beam, the theoretical results exhibited vertical aligned flexural cracks in the bottom chord from the edge of the beam which distributed along the length of the opening. Diagonally oriented shear cracks were noticed at the point of curve formation to the beam support where the number of cracks was increased. On the other hand, diagonal cracks were seen propagated from the points of the curve towards the loading points at the top chord which eventually leads to localized shear failure, as observed in the experimental beam. The crack pattern of the FE analysis matches well with the observed beam.

Similarly, the crack patterns of beam with a large rectangular opening in flexure as shown in Figure 7.10 were found similar in beam with an elliptical opening. The vertical cracks from the numerical analysis were initiated from the bottom edge of the beam along the length of opening in the middle-third span. Diagonally oriented cracks were found at the opening corners and propagated its way to the beam support. FE analysis also captured diagonal and horizontal cracks at both opening corners at the top chord which resulted in localized shear failure at the right corner of the opening, as traced in the experimental beam.

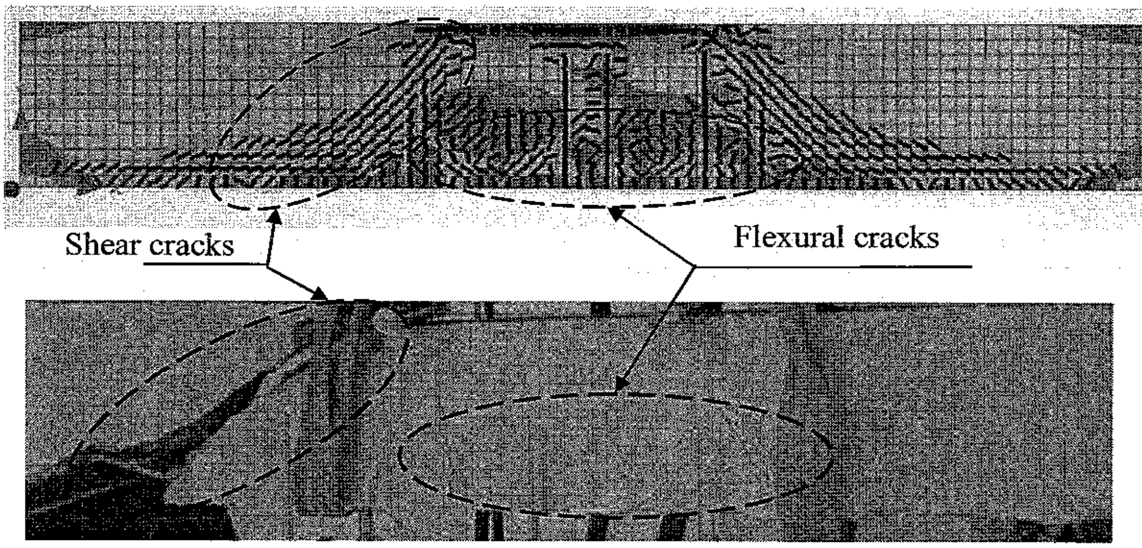

Figure 7.6 Comparison between experimental and FEM crack patterns of beam CB

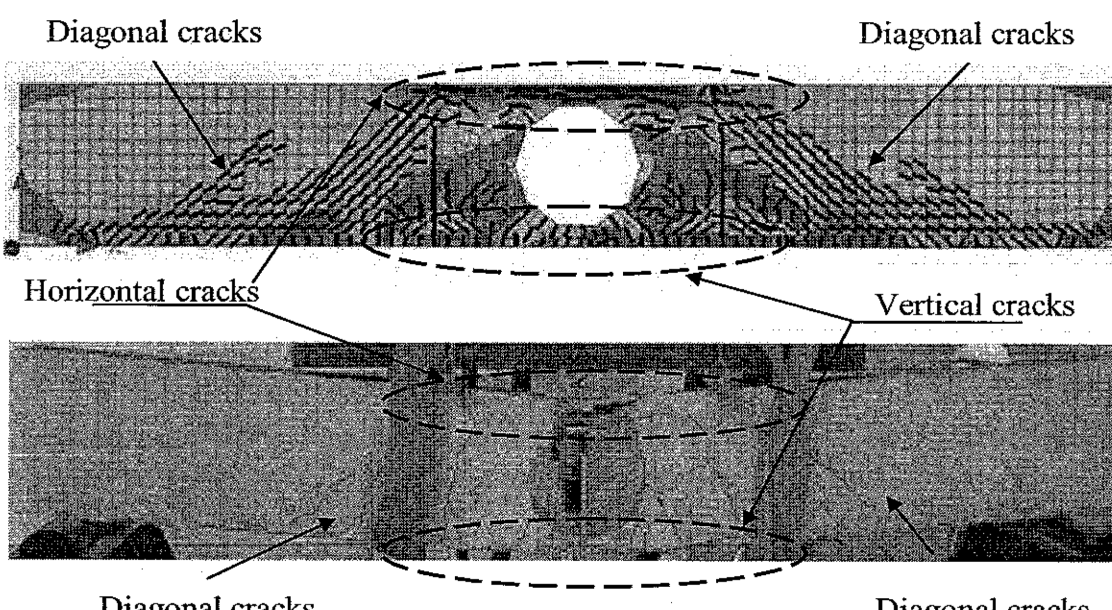

Figure 7.7 Comparison between experimental and FEM crack patterns of beam CF

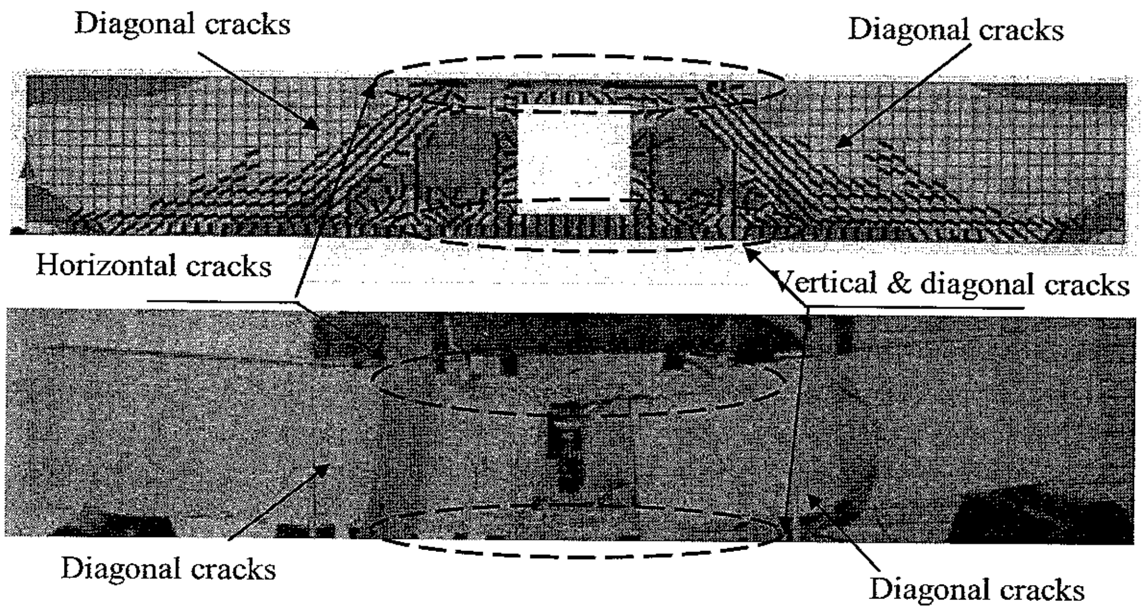

Figure 7.8 Comparison between experimental and FEM crack patterns of beam SF

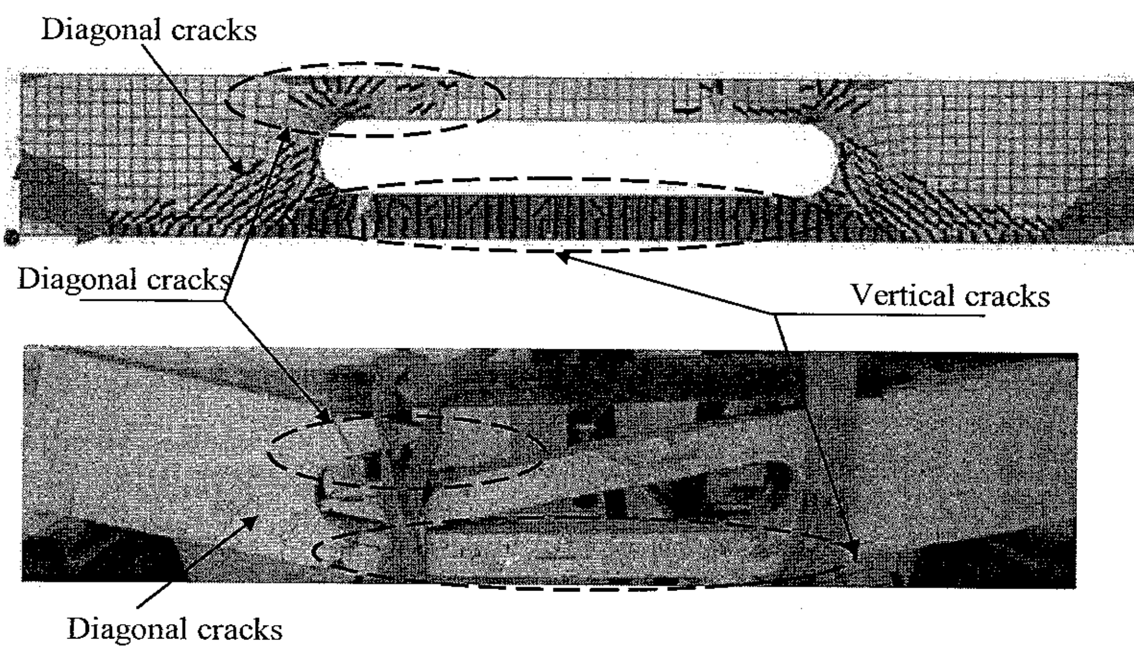

Figure 7.9 Comparison between experimental and FEM crack patterns of beam LEF

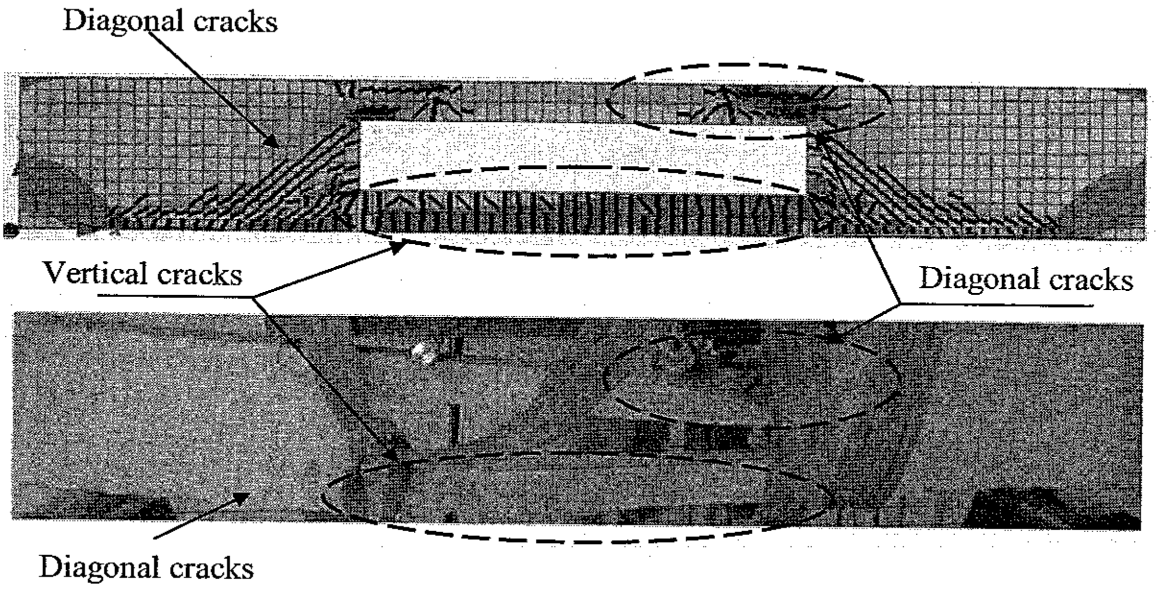

Figure 7.10 Comparison between experimental and FEM crack patterns of beam LRF

7.2.3 Flexural Analysis of Strengthened Beams

To attain objective no. 2, comparison and analysis of load-deflection behaviour and crack pattern results of experimental and FE analyzed beams are presented and discussed in the following sub-sections. This discussion covers the strengthening of beams with different opening configurations provided in the flexure zone.

7.2.3.1 Load-Deflection Behaviour

The load versus mid-span deflection plots obtained from numerical analysis along with the experimental results are presented and compared in Figures 7.11 – 7.14. Tables 7.3 and 7.4 summarize the results from the load-deflection curves of FE analysis and experimental testing.

a) Strengthening for Circular Opening, CF-S

As discussed in Chapter 6, the presence of the circular opening in the mid-span reduced about 21% of the beam original structural capacity. Although strengthening is not necessary in the numerical analysis of the beam CF as reported in section 5.2.2.2; however due to the cracks observed and losses of beam capacity in the experimental beam CF, external strengthening with CFRP laminates is needed for long term serviceability of the structure. The CFRP strengthening configuration of experimental beam CF-S was referred to the chosen strengthening scheme in FE analysis.

Load deflection behaviour of the beam CF-S as obtained from FE analysis and experiment is compared in Figure 7.11. At the start of loading, the load-deflection curve of FE analysis generated a stiff behaviour in the elastic region compared to the experimental curve. The stiffness of both curves declined after the first crack was formed, both the line of experimental and FE continuously increase until the fully yield condition. After the fully yield condition, FE results show a smaller plastic zone, which is about 30% of that exhibited by experimental testing, which means experimental beam has shown higher ductility because the failure was happened at the deflection of 26 mm as compared to that of the theoretical beam that showed a deflection of 10.1 mm. The experimental beam was yielded at 97 kN at 8.1 mm whereas the theoretical analysis predicted the yielding load as 94 kN at 2.7 mm deflection, which shows a good agreement between both results.

b) Strengthening for Square Opening, SF-S

The presence of square opening in the flexure zone had caused a reduction in beam capacity about 35%, as discussed in Chapter 6. As for the theoretical results in Chapter 5, it is suggested that strengthening is not necessary for small opening provided in the mid-span; however, because of loss of beam capacity and the formation of cracks in the experimental beam, strengthening is required for long-term serviceability of the structure. The strengthening scheme of this beam refers to the chosen strengthening configuration in the FE analysis.

Figure 7.12 shows the load-deflection curves of beam SF-S, which were obtained from FE analysis and the experimental testing. Both the curves show that at the early stage of loading, the beam exhibited high stiffness. The stiffness then declined after the formation of the first crack, the two lines of FE and experiment seemed parallel to each other, which was observed until the fully yield condition. After the yielding point, FE results show a greater plastic zone, which is about double of the experimental testing, which indicates that FE analyzed has shown slightly higher in ductility until the ultimate load was achieved at load of 87 kN at 7.9 mm whereas 86 kN at 6.9 mm of the experimental beam.

c) Strengthening for Large Opening (Elliptical and Rectangular)

Load-deflection behaviour of beam LEF-S obtained from FE analysis and experiment is compared in Figure 7.13. At the early phase of loading, both the curves exhibited high stiffness. The stiffness of the beam reduced after the formation of the first crack. Both the lines of experimental and FE continuously increase until the fully yielded condition. After passing the ultimate point, a quick drop in FE results was noticed. The theoretical beam was failed at 1.5 mm at 64 kN while the experimental beam was failed at the deflection of 5.3 mm at 77 kN. There was observed a difference of about 40% in the yielding load of experimental beam with the theoretical results.

Figure 7.14 shows the comparison of load-deflection plots of beam LRF-S from experimental testing and FE analysis. Similar to the trend of the load-deflection curve as discussed for beam LEF-S was observed in beam LRF-S. Both the curves possessed high stiffness in the initial stage of loading until the first crack was occurred. The curves of experiment and FE analysis remained linear in the plastic zone although reduction of beam stiffness was observed. After the complete yield condition, the line of experimental results shows a constant plane before the softening of beam; which indicates that the experimental beam has shown ductile behaviour as the actual failure was occurred at the deflection of 10.4 mm and 83 kN. On the other hand, the curve of the FE results was failed at 1.8 mm deflection at 57 kN load after the fully yielded state followed by rapid softening effects. A difference of about 47% was observed in the yielding load of experimental beam with the theoretical results.

Table 7.4 summarizes and compares the ultimate loads from experiment and predicted loads from FE analysis. It was found that the FE-to-experiment ultimate load ratio of beams CF-S and SF-S, 1.07 and 1.01 were slightly greater than beams LEF-S and LRF-S, 0.83 and 0.69, respectively. The calculated average ratio and standard deviation of FE-to-experiment are 0.90 and 0.17, respectively, which indicates that the results are comparable between the FE and experimental results.

Table 7.3 Comparison of experimental and FEM results of strengthened beams

Beam	EXP				FEM			
	Yielding load P_y (kN)	Δ_y (mm)	Ultimate load P_u (kN)	Δ_u (mm)	Yielding load P_y (kN)	Δ_y (mm)	Ultimate load P_u (kN)	Δ_u (mm)
CF-S	97	8.1	107	10.7	94	2.7	115	10.1
SF-S	73	4.7	86	6.9	78	4.0	87	7.9
LEF-S	62	3.7	77	5.3	36	0.7	64	1.5
LRF-S	72	6.6	83	10.4	38	0.8	57	1.8

Table 7.4 Comparison of ultimate loads from experimental and FEM results

Beam	Ultimate load, P_u (kN)		FEM/EXP
	EXP	FEM	
CF-S	107	115	1.07
SF-S	86	87	1.01
LEF-S	77	64	0.83
LRF-S	83	57	0.69

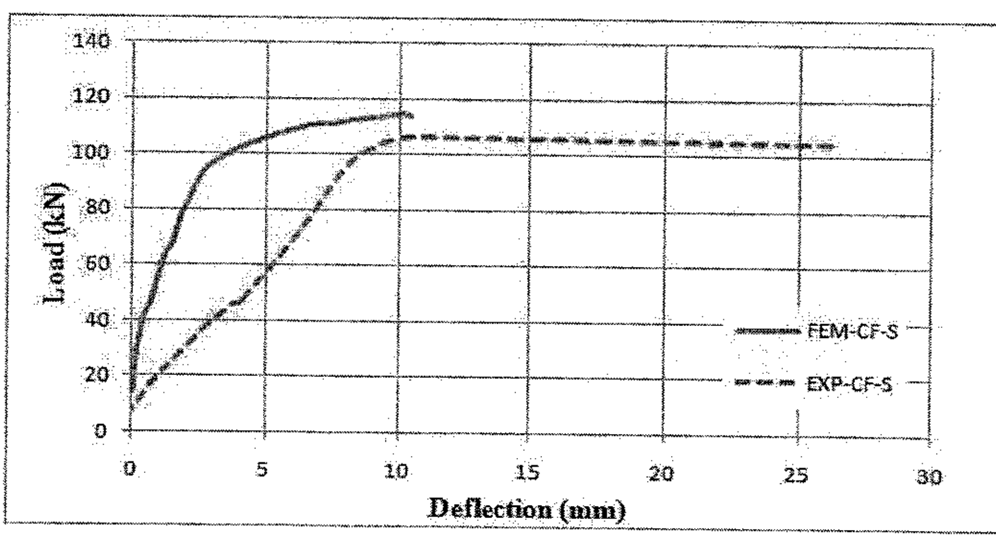

Figure 7.11 Experimental and FEM load-deflection behaviour of beam CF-S

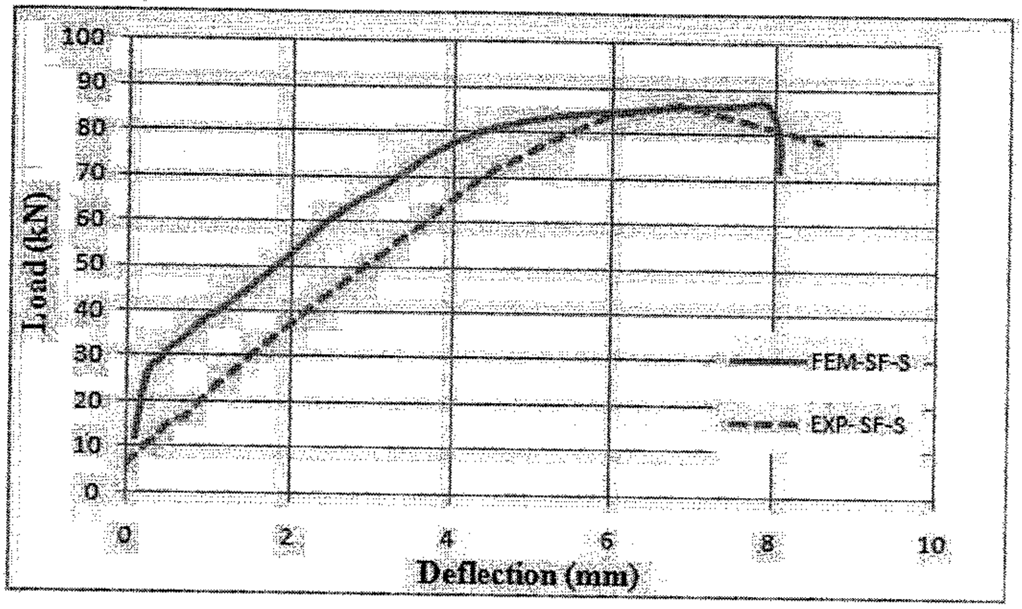

Figure 7.12 Experimental and FEM load-deflection behaviour of beam SF-S

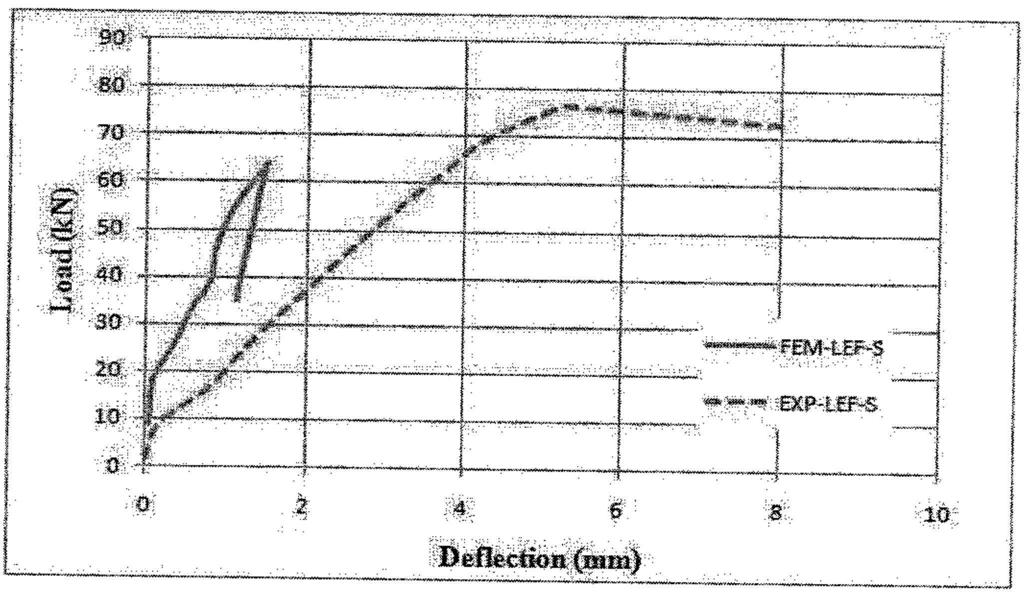

Figure 7.13 Experimental and FEM load-deflection behaviour of beam LEF-S

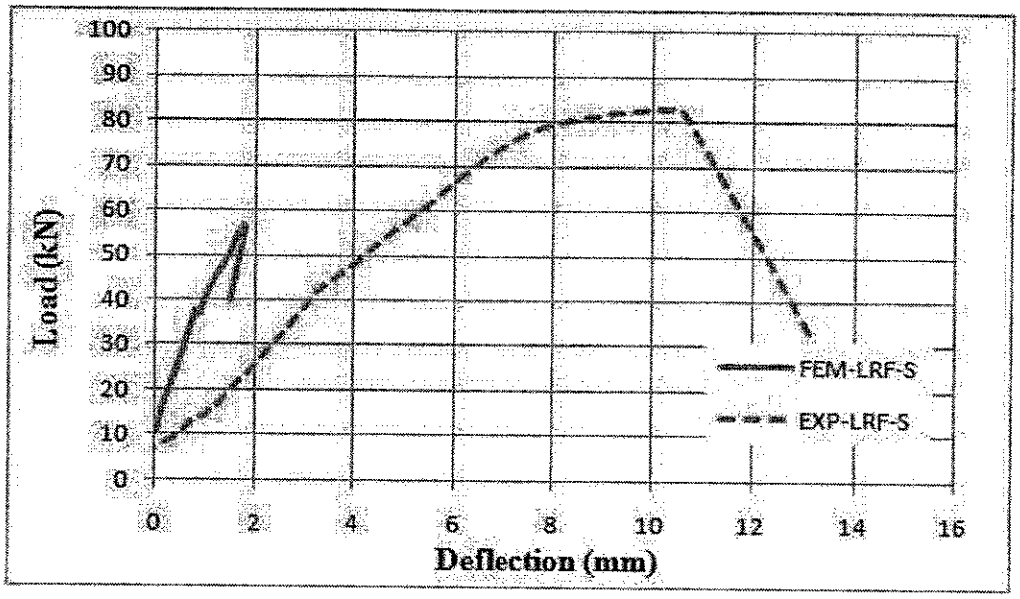

Figure 7.14 Experimental and FEM load-deflection behavior of beam LRF-S

7.2.3.2 Crack Patterns

Figures 7.15 – 7.18 present the crack patterns comparison of strengthened beams obtained from experimental testing and numerical analysis.

a) Strengthening for Circular Opening, CF-S

The FE analysis crack patterns of beam CF-S is compared with the crack patterns of experimental testing as shown in Figure 7.15. Similar to the experimental beam, the FE analysis predicted the flexural cracks that appeared vertically at the bottom edge of beam away from the strengthened area. These cracks were also noticed at the diagonally oriented CFRP laminates in the middle-third span. On the other hand, high stress concentration at the end of CFRP laminates with horizontal cracks at the top chord was observed in the analyzed beam. This resulted in horizontal cracking of concrete cover in the top chord similar as observed in the tested beam. Continuation from the horizontal cracks at the loading point, FE analysis predicted shear cracks that formed diagonally penetrating from the loading point to the beam support. A good match was obtained between the crack pattern results from FE analysis and experimental testing.

b) Strengthening for Square Opening, SF-S

Figure 7.16 presents the crack pattern comparison of beam SF-S from theoretical results and tested beam. In the bottom chord, theoretical analysis predicted diagonal cracks at the corners of the opening and horizontal cracks along the area strengthened by CFRP laminates in the mid-span. Hence, large horizontal cracks in the mid-span were observed in the experimental beam which leads to peeling of concrete cover. While in the top chord, FE analysis captured high stress concentration within two loading points where horizontal cracks were formed, similar as observed in the experimental beam. This phenomenon caused crushing of concrete cover along the horizontal cracks with exposed of top steel reinforcement was noticed between the applied loads in the actual beam. On the other hand, formation of diagonal shear cracks was observed from the bottom edge of the beam at the space beyond the CFRP laminates approaching the applied loads, similar to that as observed in the tested beam. Therefore, a close agreement was observed between the two results.

c) Strengthening for Large Opening

Comparative analysis of FE results and experimentally observed crack patterns of strengthened beams with large elliptical and rectangular opening is presented in Figures 7.17 and 7.18, respectively. The FE analysis captured flexural cracks that vertically aligned from the bottom edge of beam in the mid-span which restricted by two CFRP laminates at the bottom chord. Diagonally oriented shear cracks which initiated at the bottom edge of the beam at the end of both CFRP laminates at the bottom chord penetrated all the way to the point of curvature at the top chord, similar to that as observed in the experimental beam. At the top chord, similarities between the crack pattern of analyzed and experimental beams were found. The FE analysis predicted high stress concentration diagonally at the loading points to the opening which eventually leads to diagonal cracking due to localized shear failure in concrete of experimental beam. The crack pattern of FE analysis agrees well with the observed beam.

Figure 7.18 shows the crack patterns of strengthened beam with large rectangular opening obtained from FE analysis and experimental testing. A similar trend of the crack pattern as discussed for beam LEF-S was observed in beam LRF-S. The flexural cracks were vertically aligned from the bottom up to the bottom chord within the middle-third span due to the effects of CFRP laminates. On the other hand, shear cracks diagonally oriented from the bottom edge of the beam at the end of CFRP laminates and propagated through the space without CFRP up to the opening corners at the top chord, as observed in the tested beam. The FE analysis exhibited high stress concentration diagonally at the loading points to the opening corners at the top chord. This resulted in the formation of diagonal cracks due to localized shear failure in the predicted beam; similarly in the experimental beam in which wide diagonal cracking was observed at the loading point to the corner of opening at the top chord.

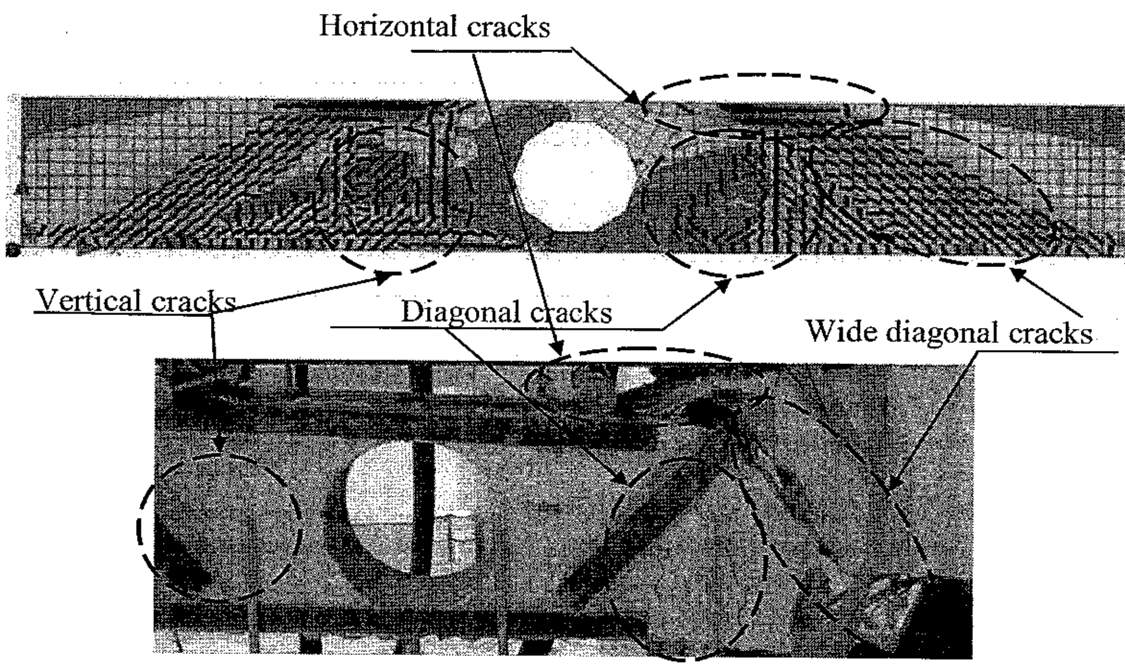

Figure 7.15 Comparison of experimental and FEM crack patterns of beam CF-S

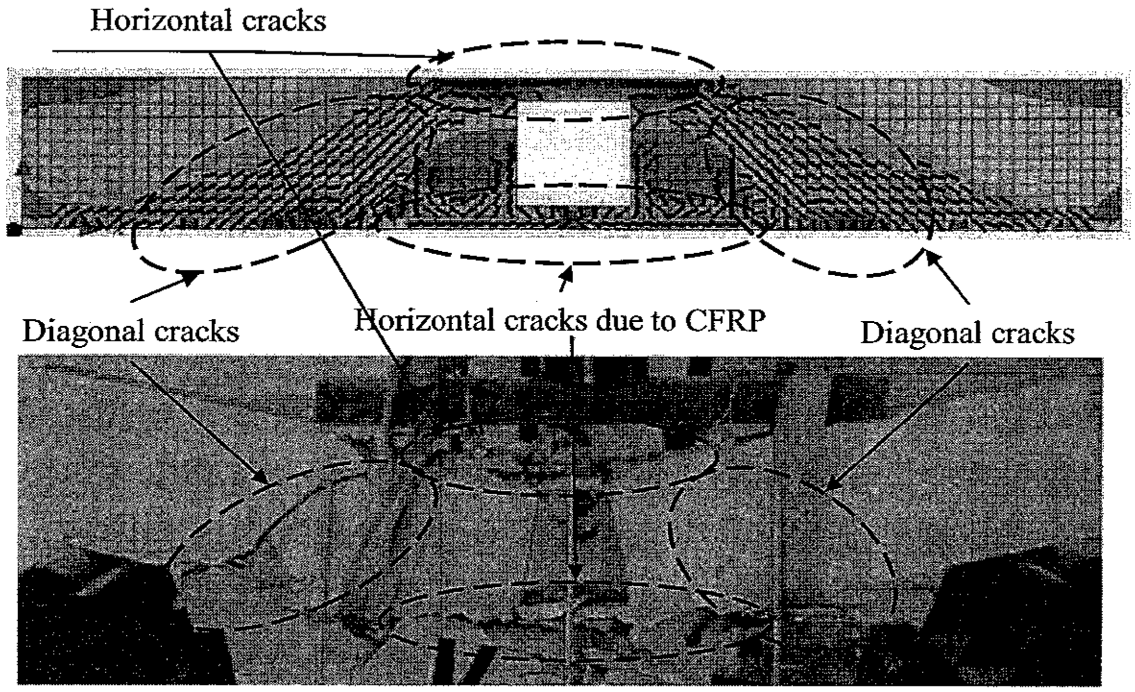

Figure 7.16 Comparison of experimental and FEM crack patterns of beam SF-S

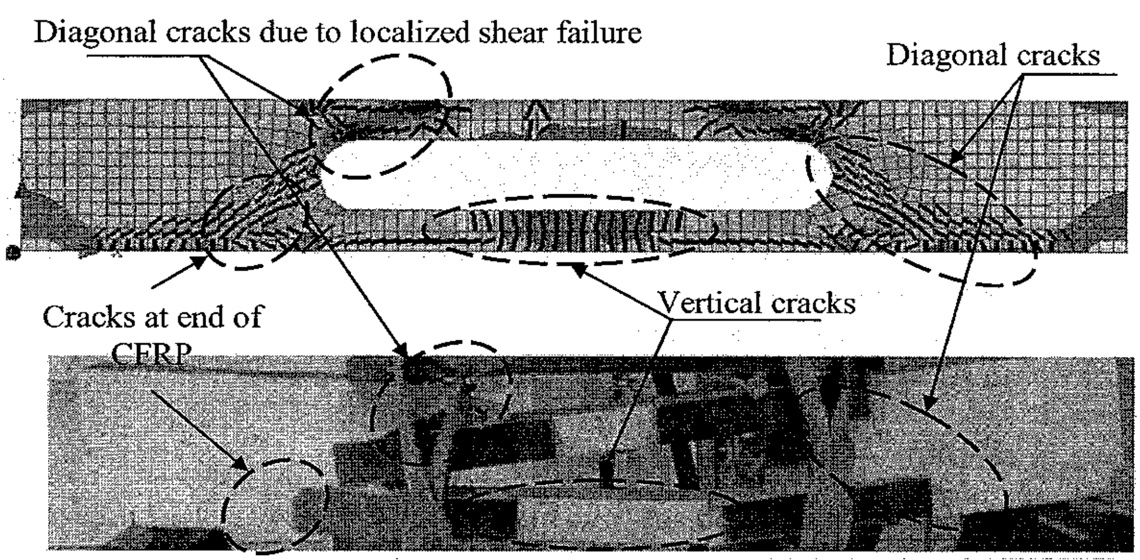

Figure 7.17 Comparison of experimental and FEM crack patterns of beam LEF-S

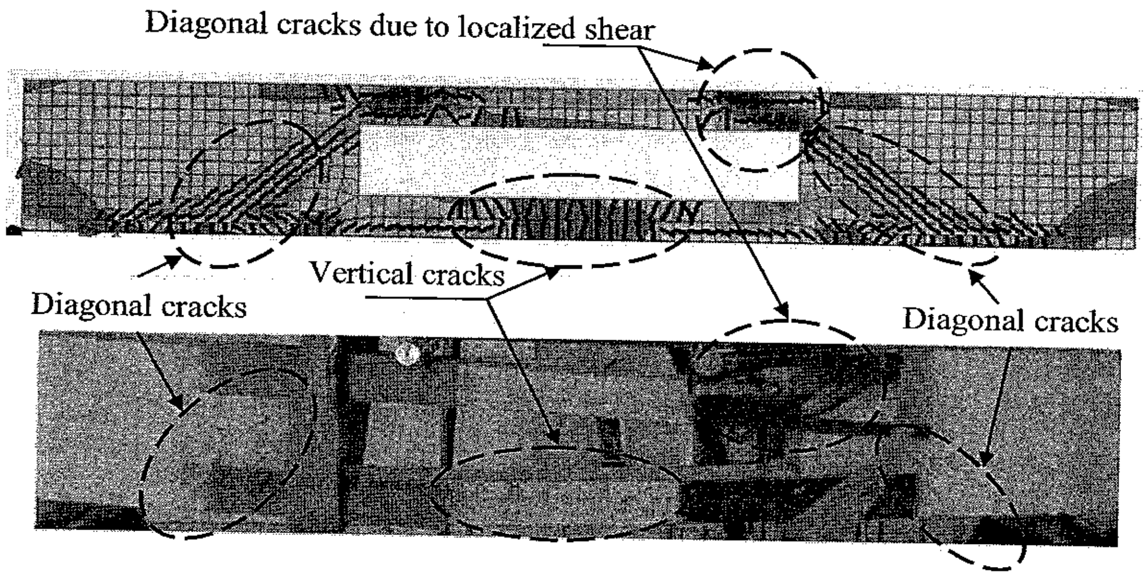

Figure 7.18 Comparison of experimental and FEM crack patterns of beam LRF-S

7.3 Shear Analysis of Un-Strengthened Beams

Comparative analysis of the load-deflection behaviour and crack patterns of beams with openings provided in the shear zone are presented and discussed in the following sub-sections in order to achieve objective no 1(iii). The comparison is divided into two categories, (i) opening at both ends and (ii) opening at one end only.

7.3.1 Load-Deflection Behaviour

The load-deflection behaviour between FE results and experimental beams with openings at both ends and an opening at one end are compared and discussed in this section.

7.3.1.1 Openings at Both Ends

Figures 7.19 – 7.20 present the generalized load-deflection curves for circular and square shaped openings which were placed on the face of support, and at a distance 0.5d and d from the support.

(a) Effects of Circular Opening

Load-deflection curves of beams with circular openings were obtained from FE analysis and experimental testing is compared in Figure 7.19. Both the curves show that at the initial phase of loading, the beam possessed high stiffness due to the high inclination of the slope. The slope of the line declined after the formation of the first crack, both the lines of FE and experimental beam seemed parallel to each other, which was observed until the fully yield condition. After the fully yield condition, both the curve lines exhibited a plastic zone of almost the same ratio parallel to each other. The failure of both experimental and theoretical beams showed a deflection of within 4 – 5 mm. The experimental beam was yielded at 18 kN at 1.8 mm whereas the theoretical analysis predicted the yielding load as 22 kN at 1.6 mm deflection, which in very good agreement.

(b) Effects of Square Opening

Figure 7.20 shows the comparison of load-deflection curves between FE analysis and experimental were found similar. At the early stage of loading, both lines of FE and experimental beam show high inclination which means the beam possessed high stiffness. The stiffness of the beam then reduced after the first crack was formed. Both the curves increase parallel to each other, which was observed until the fully yield condition. After yielding, FE results show a smaller plastic zone before beam failure, which is about 50% of that exhibited by experimental testing, which indicates that the experimental beam has shown slightly higher in ductility because the failure was happened at the deflection of 11 mm as compared to that of the theoretical beam that showed a deflection of 5 mm. There was observed a difference of about 20% in the ultimate load of experimental beam with the theoretical results.

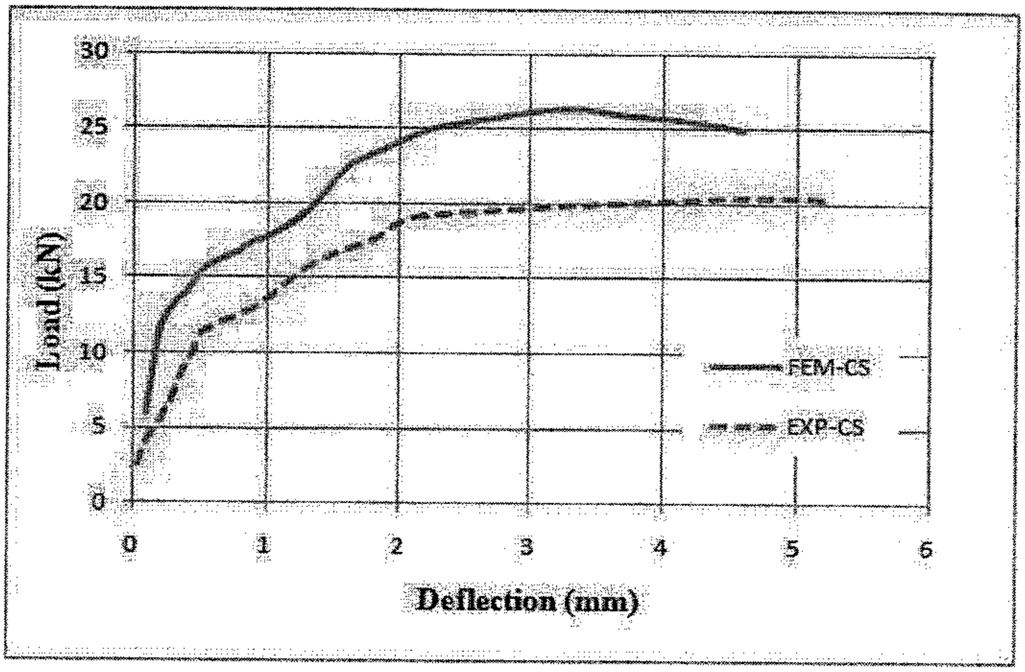

Figure 7.19 Experimental and FEM load-deflection behaviour of beams with circular openings at both ends

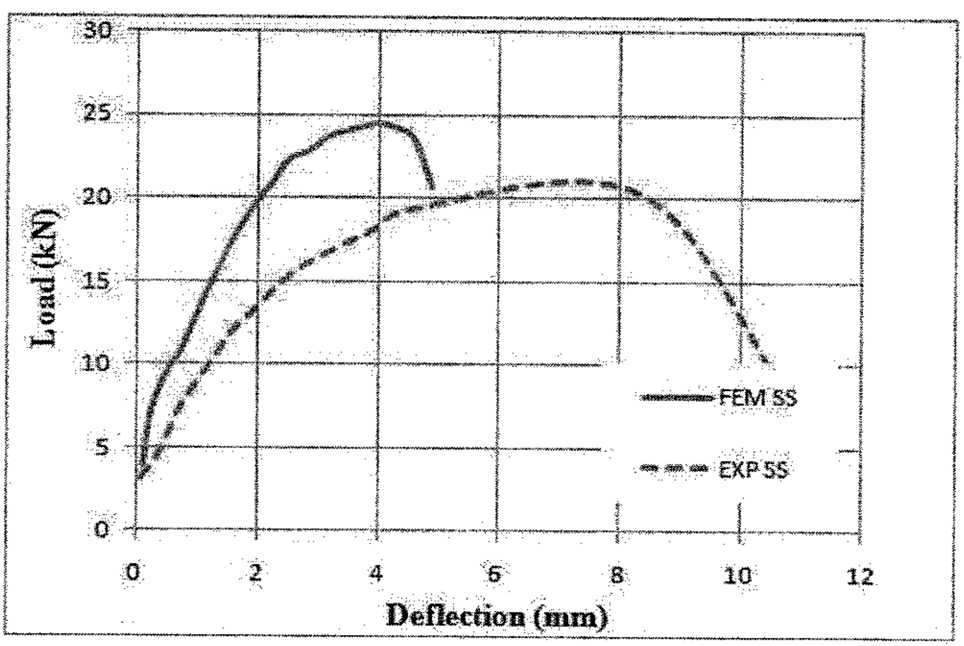

Figure 7.20 Experimental and FEM load-deflection behaviour of beams with square openings at both ends

7.3.1.2 Opening at One End Only

In this section, a circular and square openings was placed at distances 0.5d, d and 1.5d from the support; however, the load-deflection curves of beams S0.5dS1, CdS1, SdS1 and S1.5dS1 showed a very close similarity, within 5%. Therefore, comparison of load-deflection curves of beams with an opening at a distance d is presented and discussed whereas load-deflection curves of beams with an opening at distances 0.5d and 1.5d are illustrated in APPENDIX L. The load-deflection curves of beam with circular and square opening, CdS1 and SdS1, are shown in Figures 7.21 and 7.22, respectively.

(a) Beam with Single Circular Opening (at a distance d from support), CdS1

Load-deflection curves of beam CdS1 which were obtained from FE analysis and experimental testing is plotted in Figure 7.21. Both the curves show that in the early phase of loading, the beams are in high stiffness due to the steepness of slope. After the formation of the first crack, the steepness of the lines declined. Both the lines of FE and experimental seemed in-line with each other, which was observed until the fully yield condition. After the fully yield condition, FE results show an increase in load whereas experimental beam exhibited a small plastic zone, which means experimental beam has shown some ductile behaviour. At the point just before failure, experimental beam failed at the deflection of 1.7 mm at 21 kN as compared to that of the theoretical beam that showed a deflection of 1.3 mm at 24 kN; that indicates both results are comparable to each other.

(b) Beam with Single Square Opening (at distance d from support), SdS1

Figure 7.22 shows the load-deflection curves of beam SdS1 between the theoretical analysis and test results. Both curves exhibited greater stiffness at the initial stage of loading, however the reduction in stiffness was observed after the formation of the first crack. Both the curves increase in load parallel to each other, which was observed until the fully yield condition. After yielding, FE results show a smaller plastic zone, which is about 25% of that exhibited by the tested beam, which means experimental beam possessed higher ductility since the failure was happened at the deflection of 5.7 mm as compared to that of the theoretical beam that showed a deflection of 2.2 mm. There was observed a difference of about 26% in the maximum load of experimental beam with the theoretical results. The comparison shows that the load-deflection curve of FE results is quite comparable to the experimental results.

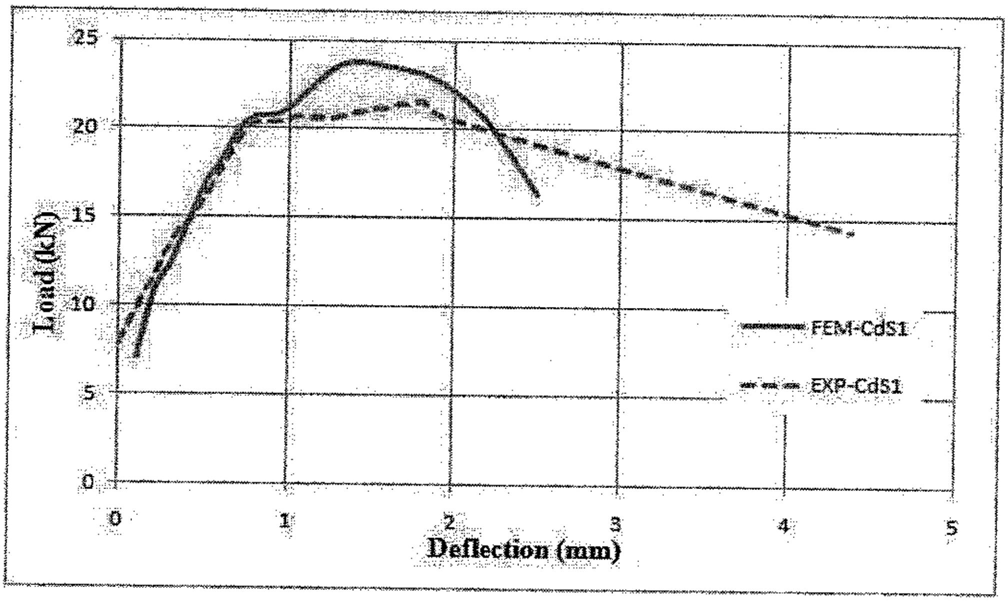

Figure 7.21 Experimental and FEM load-deflection behaviour of beam CdS1

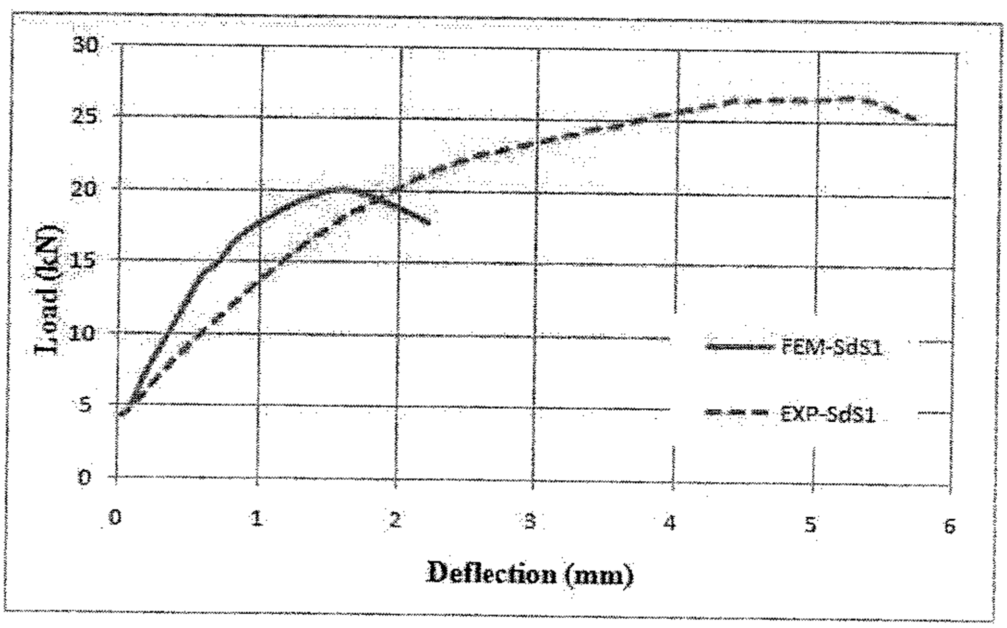

Figure 7.22 Experimental and FEM load-deflection behaviour of beam SdS1

7.3.2 Crack Patterns

Crack patterns obtained from FE analysis and experimental testing of beams with openings at both ends are compared in Figures 7.23 – 7.27 whereas comparative analysis of the crack patterns of beams with an opening at one end only are shown in Figures 7.28 – 7.29.

7.3.2.1 Openings at Both Ends

This section presents the crack patterns comparison of beams with circular and square openings at the face of support and at distances 0.5d and d from the support which obtained from FE analysis and experimental tested beams.

(a) Beam with Circular Openings (zero distance from support), C0S

Beam with circular openings at the face of support, referring to Figure 7.23, theoretical results and tested beam showed the similar crack patterns, which are mainly composed of shear cracks diagonally oriented at the top side and bottom side of opening. The FE analysis cracks which originated at the top side of opening elongated diagonally to the loading points whereas cracks at the bottom side of opening propagated diagonally to the beam support. At the point of failure, the main diagonal cracks were very wide which formed see-through gap in the experimental beam. Hence, it can be concluded that the failure was governed by the shear failure.

(b) Beam with Square Openings (zero distance from support), S0S

Figure 7.24 presents the crack patterns of beam with square openings at the face of support obtained from FE results and experimental testing. The FE analysis predicted diagonal cracks at four corners of the square opening, similar as noticed in the experimental beam. The cracks at the top right corner become horizontally aligned when approaching the loading point whereas cracks at the top left corner were diagonally elongated to the edge of the beam. Both of these phenomena lead to the crushing of concrete cover in the experimental beam. On the other hand, cracks at the bottom left corner was significant as it penetrated to the bottom chord, while observed horizontal cracks at the bottom chord resulted in crushing of concrete cover at the failure of the beam. The comparison shows a good agreement between the crack pattern of observed and theoretical beams.

(c) Beam with Square Openings (zero distance from support), S0.5dS

Crack patterns of beams with openings at distance 0.5d from the support, as shown in Figure 7.25 obtained from theoretical results and beam from experimental testing showed the similar crack patterns, which are consisted of shear and flexural cracks. The FE analysis predicted the shear cracks at the top chord which then elongated diagonally to the applied loads whereas cracks at each corner of the opening in the bottom chord propagated all the way to the bottom edge of the beam and to the solid section near the beam support, respectively. Although vertical aligned flexural cracks were seen in the mid-span of the analyzed beam, however these vertical cracks were not noticeable in the experimental beam. At the point of failure, the diagonal cracks become wide at the top chord of the tested beam, forming a see-through gap. From the crack pattern results, a close match was obtained between FE analysis and experimental results.

(d) Beam with Circular Openings (at distance d from support), CdS

Crack patterns of beam with circular openings at distance d from the support CdS were agreeable between the experimental obtained results and FE analysis as illustrated in Figure 7.26. The FE crack pattern showed cracks at the top side of the opening which oriented diagonally to the load points and upper edge of the beam whereas cracks at the bottom side of opening penetrated diagonally to the beam support as well as the bottom edge of the beam, similar as shown in the tested beam. Flexural cracks that formed vertically from the bottom edge of the beam were noticed along the middle-third span of FE beam; however these cracks were not seen in the beam after testing. The cracks at the top and bottom sides of the circular opening of the experimental beam resulted in crushing of concrete cover with wide cracks spread vertically to the upper edge of the beam and diagonally to the load points whereas wide see-through gap from the bottom side of opening diagonally to the beam support.

(e) Beam with Square Openings (at distance d from support), SdS

Figure 7.27 shows the comparison of crack patterns between the analyzed and tested beam during experimental testing. The trend of crack patterns for this beam was found similar as observed in beams S0S and S0.5dS. From the numerical analysis, cracks were initiated at the four corners of the square openings. At the top chord of opening, cracks at the opening corners were observed penetrating vertically up to the top edge of the beam and diagonally towards the loading points. On the other hand, cracks from the opening corners at the bottom chord stretched to the bottom edge of the beam and all the way to the beam support. At failure, the FE analyzed horizontal aligned cracks near the beam support leads to crushing of concrete cover at the bottom chord exposing the bottom reinforcement as shown in the experimental beam. The crack patterns of FE analysis were found comparable to the crack patterns of the tested beam.

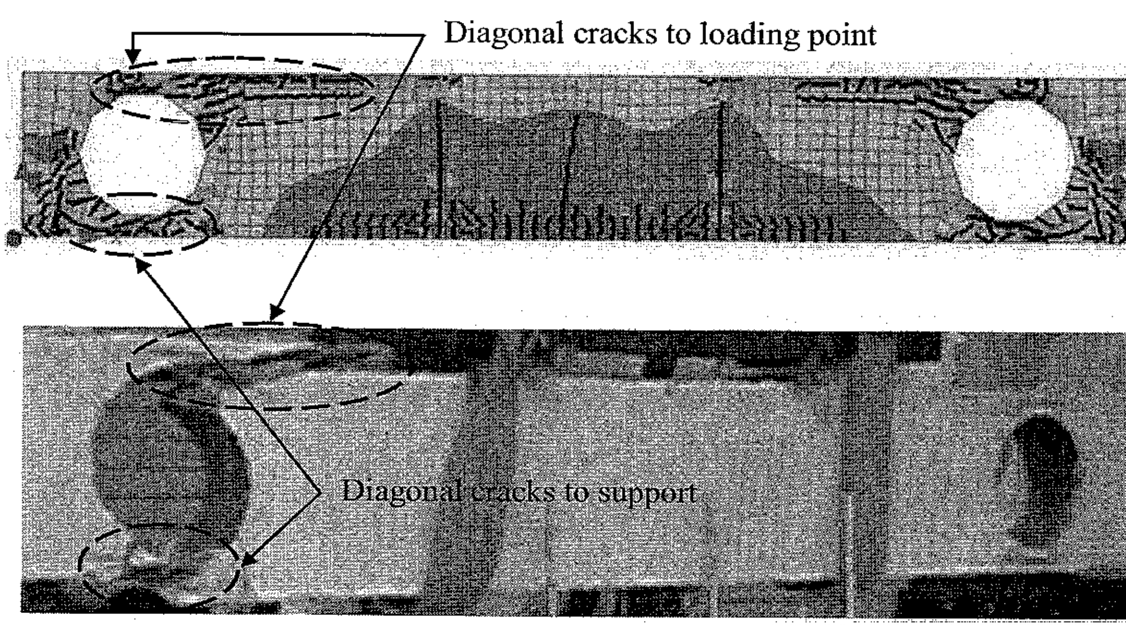

Figure 7.23 Comparison of experimental and FEM crack patterns of beam C0S

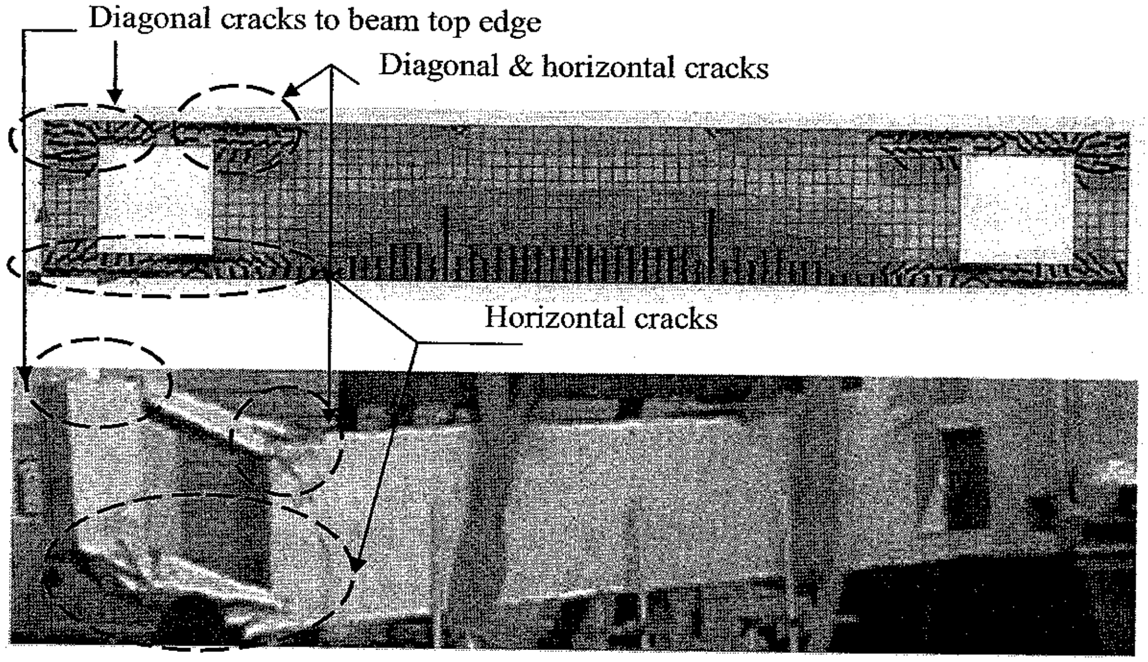

Figure 7.24 Comparison of experimental and FEM crack patterns of beam S0S

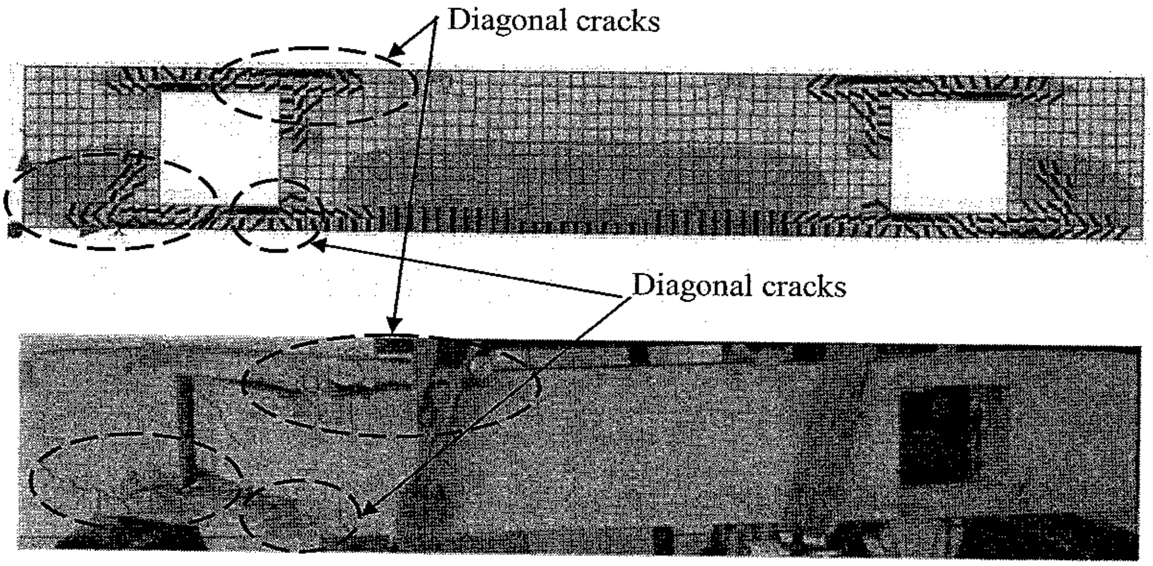

Figure 7.25 Comparison of experimental and FEM crack patterns of beam S0.5dS

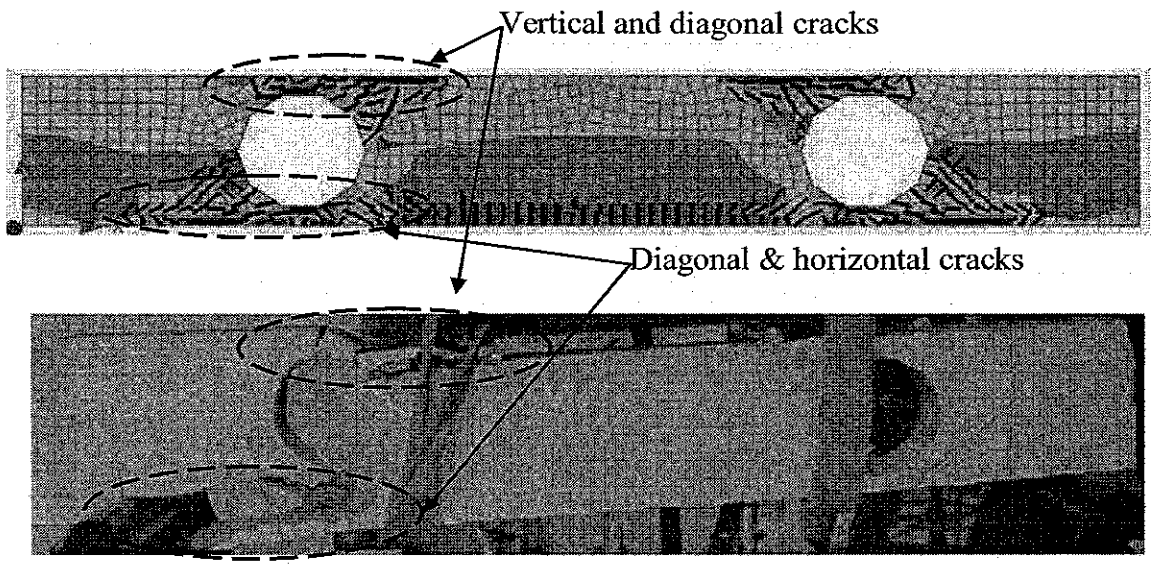

Figure 7.26 Comparison of experimental and FEM crack patterns of beam CdS

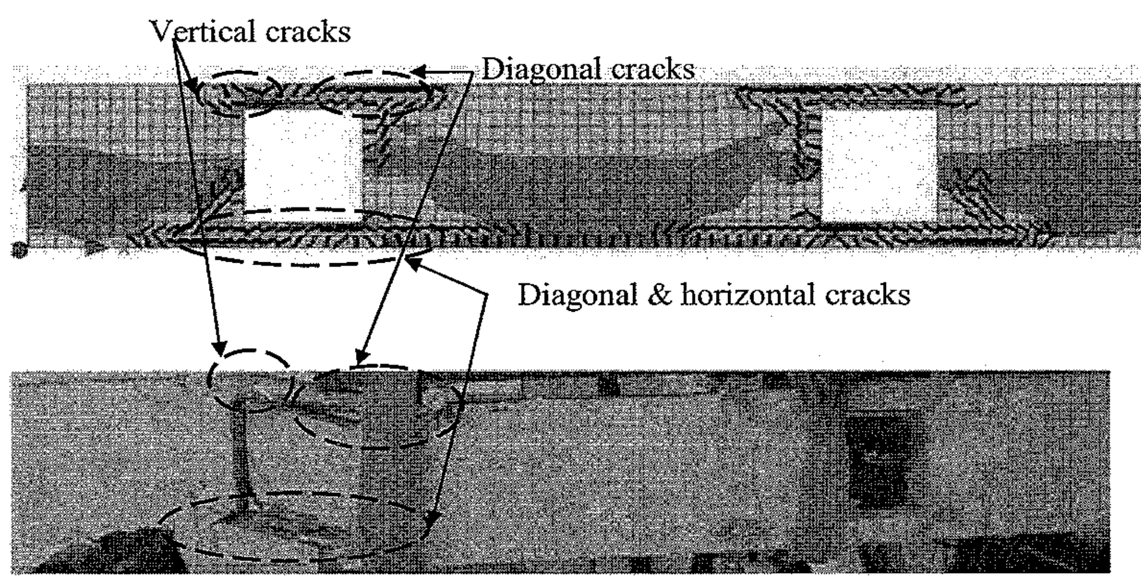

Figure 7.27 Comparison of experimental and FEM crack patterns of beam SdS

7.3.2.2 Opening at One End Only

Comparison of crack patterns from theoretical results and experimental tested beams are presented in Figures 7.28 – 7.29; which consists of beams with circular and square openings at one end at distance d from the support.

(a) Beam with Single Circular Opening (at a distance d from support), CdS1

Crack patterns of beam CdS1 from FE analysis and experimental testing are compared and presented in Figure 7.28. The crack patterns are mainly composed of shear cracks around the opening and flexural cracks in the middle-third span. Shear cracks were observed at the top side and bottom side of circular opening; which oriented diagonally to the loading point at the top chord and elongated diagonally to the beam support, respectively. This trend was found the same as happened in the beam during testing. However, flexural cracks which appeared vertically from the bottom edge within the middle-third span of theoretical beam was unlikely noticeable in the tested beam. Failure of experimental beam showed wide cracks at the top side of opening penetrating to the point load whereas crushing of concrete cover due to the diagonally elongated cracks at the bottom chord as predicted by FE analysis were observed. A good agreement of crack patterns was observed around the openings between the FE and experimental beams.

(b) Beam with Single Square Opening (at distance d from support), SdS1

Figure 7.29 compares the crack patterns of FE analysis and experimental beam and showed good agreement. The analysis results showed that initial cracks at both opening corners at the top chord spread vertically through the top edge of beam and diagonally to the load point. On the other hand, cracks at opening corners at the bottom chord propagated vertically to the bottom edge of beam and diagonally to the beam support, similar as observed in the experimental beam. The FE analysis predicted vertical aligned cracks as flexural cracks which formed from the bottom edge of beam in the middle-third span were found in both theoretical and tested beams. At beam failure, crushing of concrete cover were observed at the top and bottom chords exposing the bottom reinforcements.

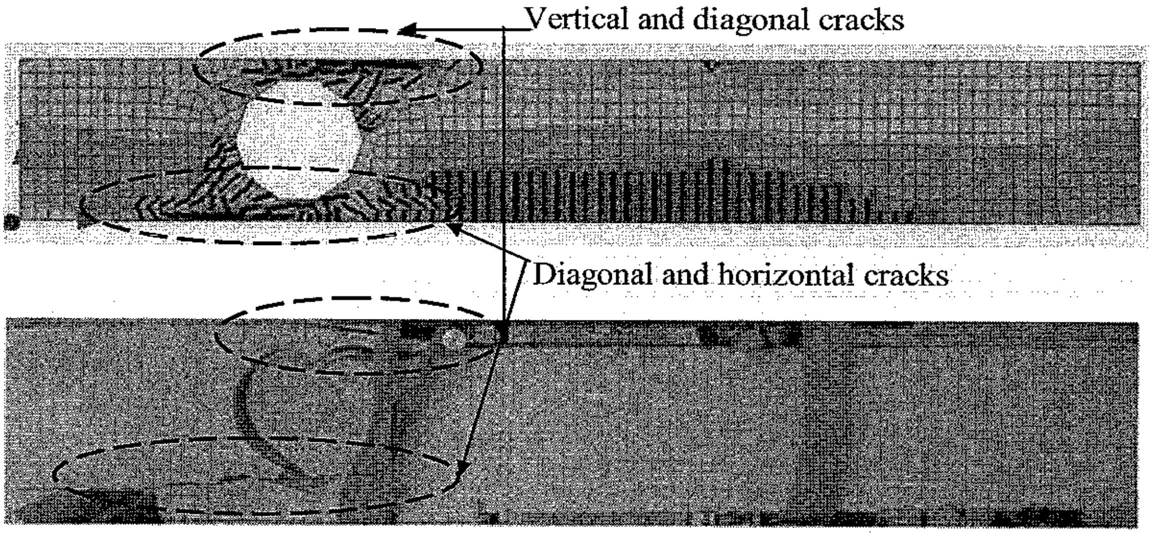

Figure 7.28 Comparison of experimental and FEM crack patterns of beam CdS1

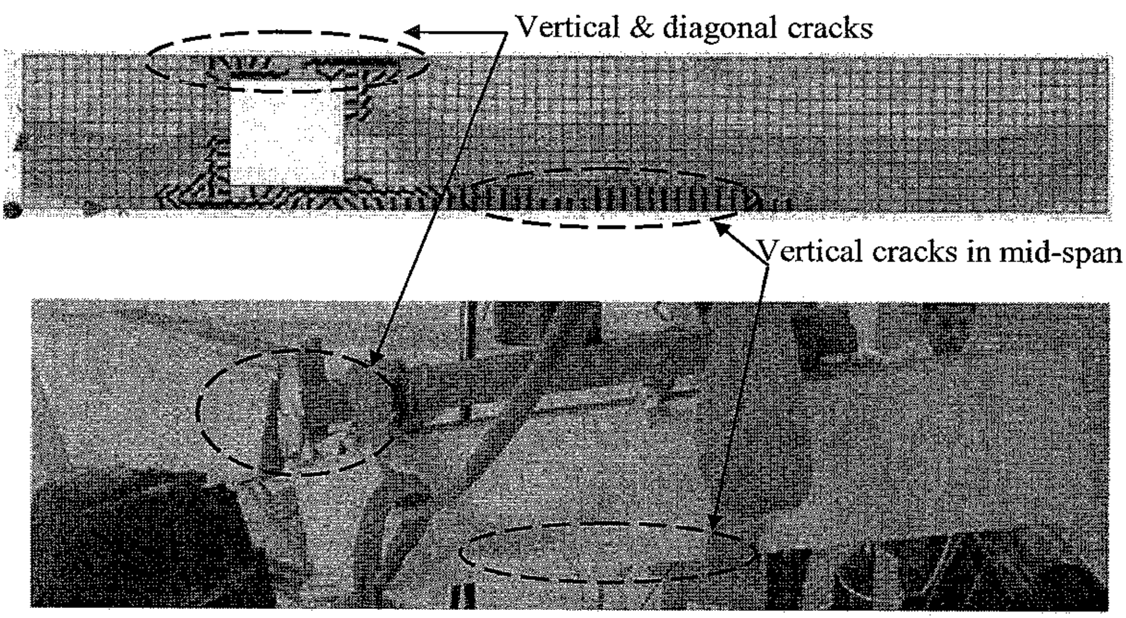

Figure 7.29 Comparison of experimental and FEM crack patterns of beam SdS1

7.3.3 Shear Analysis of Strengthened Beams

Load-deflection behaviour and crack patterns of strengthened beams with openings placed at both ends and at one end only from the support are compared in the following sub-sections to achieve objective no. 2. The comparison was made between the results obtained from FE analysis and experimental tested beams.

7.3.3.1 Load-Deflection Behaviour (Opening at Both Ends)

Comparisons of load-deflection behaviour of strengthened beams with openings at both ends are shown in Figures 7.30 – 7.34, respectively. The load-deflection curves were compared between the results obtained from FE analysis and tested beams from experimental testing. The summarized results of both load-deflection curves are listed in Tables 7.5 and 7.6.

(a) Strengthening for Circular Openings (zero distance from support), C0S-S

Figure 7.30 shows the load-deflection curves of beam C0S-S obtained from theoretical analysis and testing of the beam. Both the curves at the initial stage of loading show that the beam possessed high stiffness due to the high inclination of the slope. Then, the inclination declined after the first crack was formed. The curves of FE and experiment increase parallel to each other, which was observed until the fully yield condition. After the fully yield condition, both the curves of FE and experiment reached their respective maximum load before softening of beams occurred after the failure. The experimental beam achieved a maximum load of 40 kN at 4.4 mm whereas the theoretical beam predicted ultimate load as 50 kN at 2.9 mm deflection.

(b) Strengthening for Square Openings (zero distance from support), S0S-S

Comparison of load-deflection curves of FE analysis and experimental results of beam S0S-S is plotted in Figure 7.31. The trend of the load-deflection curve of theoretical results at the early stage of loading was found slightly different and exhibited higher stiffness as compared to the curve of the experiment. After the formation of the first crack, the steepness of both curves decrease with increasing of load up to the yielding phase of the beam. After yielding, FE beam shows a plastic flow followed by beam failure whereas the experimental beam experienced an abrupt failure recorded by LVDT after the ultimate load was attained. The experimental beam achieved ultimate load at 38 kN at 4.3 mm whereas the theoretical analysis predicted the ultimate load as 37 kN at 3.2 mm deflection, which shows a close match. On the other hand, there was observed a difference of about 5% in the yielding load of experimental beam with the theoretical results. It was observed that both the yielding loads and ultimate loads of FE and experimental results are close to each other.

(c) Strengthening for Square Openings (at distance 0.5d from support), S0.5dS-S

Figure 7.32 compares the load-deflection curves of numerical and experimental results of beam S0.5dS-S. From the trend of load-deflection plots, a good match was observed between the FE and test results. Both the curves show that at the early stage of loading, the beam possessed high stiffness because of the gradient. The gradient declined after the forming of the first crack, both the lines of FE and experimental seemed parallel to each other, which was observed until the fully yield state. After the fully yield state, FE results show a small plastic zone whereas a quick drop in load was observed in the experimental beam upon reaching the ultimate point. The experimental beam failed at the maximum load of 37 kN at 4.1 mm whereas the theoretical beam was at 43 kN and 3.8 mm at ultimate. On the other hand, both the FE and experimental curves yielded at 2.9 mm and 3.2 mm, respectively with a difference of about 20% in the yielding load which in very good agreement.

(d) Strengthening for Circular Openings (at distance d from support), CdS-S

Load-deflection curves of beam CdS-S obtained from FE analysis and experimental tested beam are compared in Figure 7.33. At the early stage of loading, both the curves show that the beam possessed high initial stiffness because of the steepness of the slope. The steepness of the line declined after the first crack was formed. After that, the reduction of the line of steepness was observed with the increase of load until the yielded condition of the beam. Both beams showed softening effects after passing the ultimate point which means the failure of the beam. An abrupt decrease of load after failure of the experimental beam was recorded by LDVT. The experimental beam was yielded at 29 kN at 1.2 mm whereas the FE analysis predicted the yielding load as 49 kN at 1.1 mm deflection. A difference of about 24% was observed in the ultimate load of experimental beam with the theoretical results.

(e) Strengthening for Square Openings (at distance d from support), SdS-S

Figure 7.34 shows the comparison of load-deflection curves between the FE analysis and results from experimental testing of beam SdS-S. Both the curves show that at the initial phase of loading, both beams possessed high stiffness; however the stiffness decreased after the formation of the first crack. Both the loads of FE and experimental results increase parallel to each other, which was observed until the fully yield condition. After the fully yield condition, both the curves still increase in a parallel manner until the ultimate load was achieved. The curve of FE analysis showed a small plastic flow before the failure of the beam whereas an immediate drop in load was observed in the experimental curve after passing the ultimate point. Both the curves of FE and tested beams failed at an ultimate deflection of 3.5 mm and 3.3 mm, with their corresponding ultimate load of 42 kN and 37 kN, respectively. On the other hand, the experimental beam was yielded at 36 kN at 3 mm whereas the theoretical analysis predicted the yielding load as 38 kN at 2.6 mm deflection. This shows a very good agreement between the load-deflection curve of FE analysis and experimental results.

Table 7.6 presents a comparison between the experimental and numerical results of the ultimate loads obtained from numerical analysis and experimental testing. It can be observed that in general the numerical results were in good agreement with the experimental results. Most of the numerical results were found always greater than the experimental ones. The average numerical-to-experiment ultimate capacity ratio and its corresponding standard deviation are calculated as 1.2 and 0.13, respectively. This shows that a good correlation between the numerical and experimental results was obtained.

Table 7.5 Comparison of experimental and FEM results of strengthened beams with openings at both ends

Beam	EXP				FEM			
	Yielding load P_y (kN)	Δ_y (mm)	Ultimate load P_u (kN)	Δ_u (mm)	Yielding load P_y (kN)	Δ_y (mm)	Ultimate load P_u (kN)	Δ_u (mm)
C0S-S	38	4.0	40	4.4	50	2.6	50	2.9
S0S-S	37	4.0	38	4.3	35	1.7	37	3.2
S0.5dS-S	32	3.2	37	4.1	39	2.9	43	3.8
CdS-S	29	1.2	50	3.1	49	1.1	66	2.0
SdS-S	36	3.0	37	3.3	38	2.6	42	3.5

Table 7.6 Comparison of ultimate loads from experimental and FEM results

Beam	Ultimate load, P_u (kN)		FEM/EXP
	EXP	FEM	
C0S-S	40	50	1.26
S0S-S	38	37	0.97
S0.5dS-S	37	43	1.15
CdS-S	50	66	1.32
SdS-S	37	42	1.13

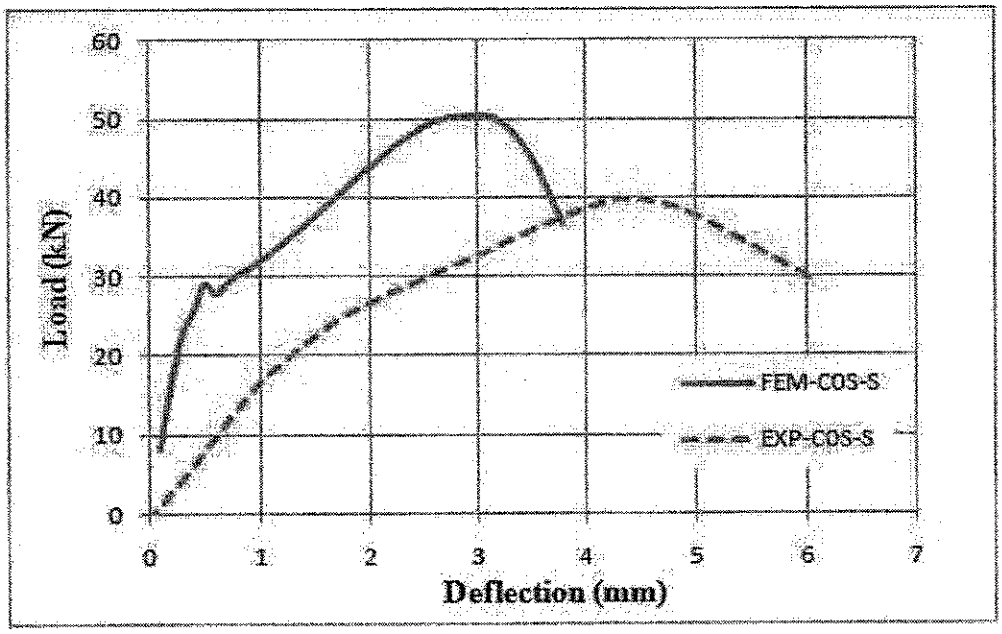

Figure 7.30 Experimental and FEM load-deflection behaviour of beam C0S-S

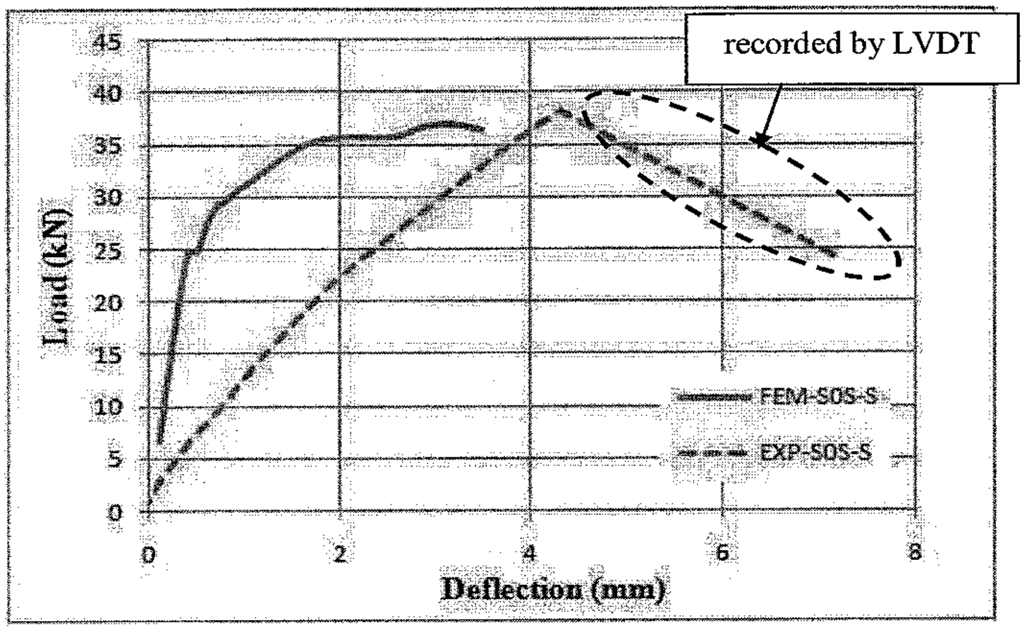

Figure 7.31 Experimental and FEM load-deflection behaviour of beam S0S-S

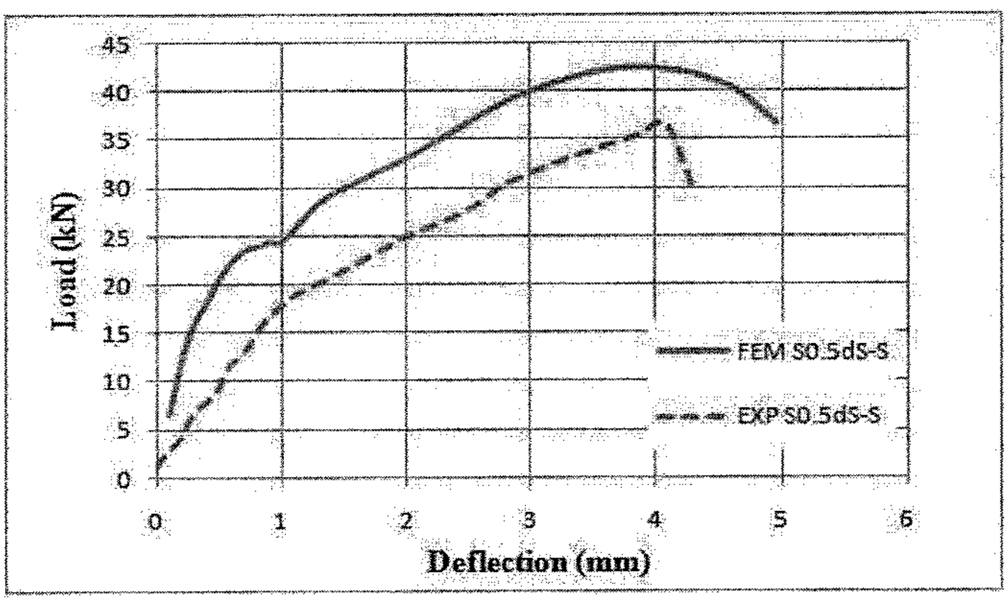

Figure 7.32 Experimental and FEM load-deflection behaviour of beam S0.5dS-S

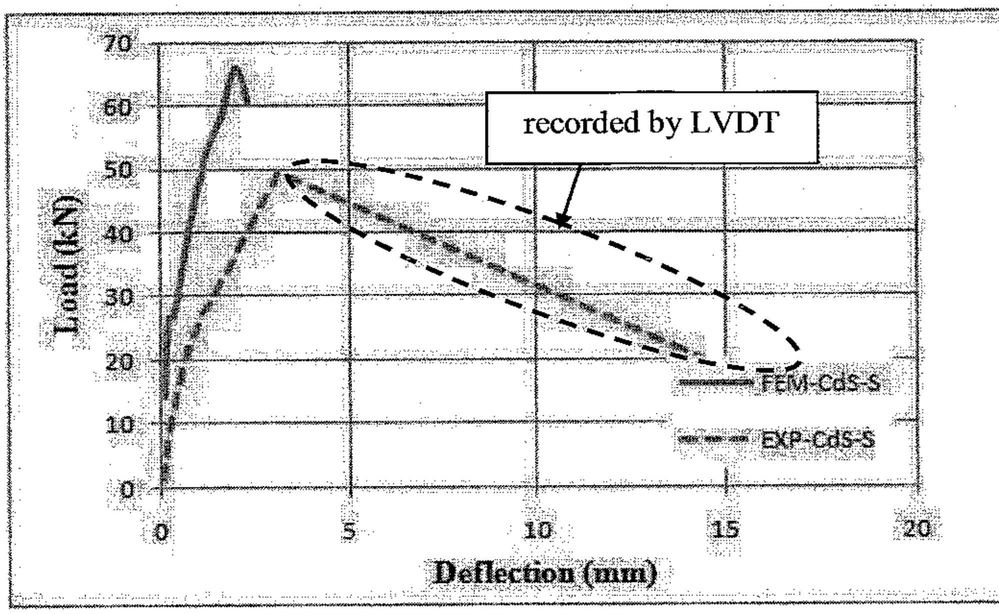

Figure 7.33 Experimental and FEM load-deflection behaviour of beam CdS-S

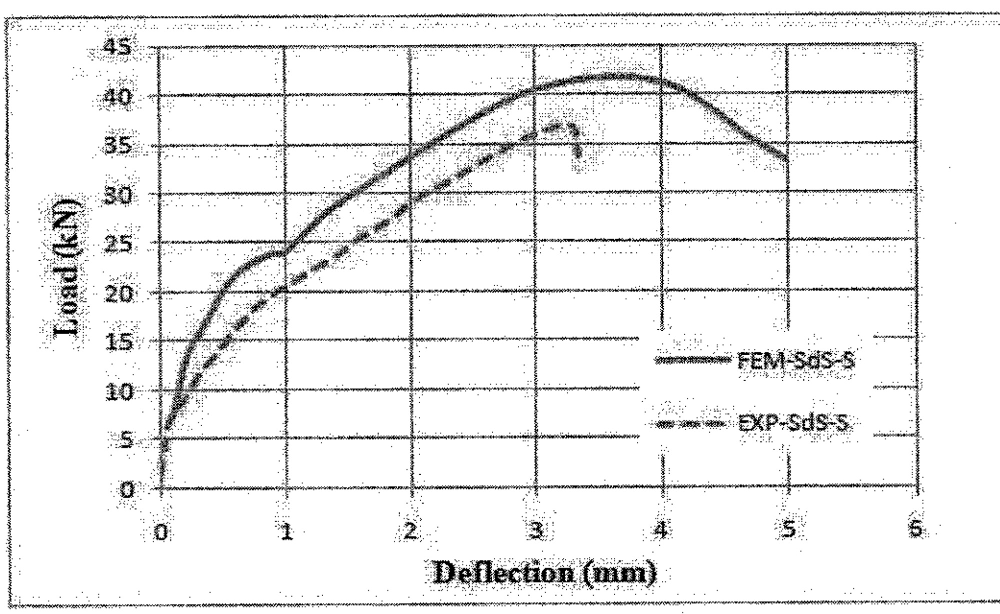

Figure 7.34 Experimental and FEM load-deflection behaviour of beam SdS-S

7.3.3.2 Load-Deflection Behaviour (Opening at One End Only)

Load-deflection plots of experimental and FE results of strengthened beams with a single opening at one end, CdS1-S and SdS1-S are being compared and discussed in Figures 7.35 – 7.36 in the next sub-sections. Tables 7.7 and 7.8 present the summary of both FE and tested beams results.

(a) Strengthening for Single Circular Opening (at a distance d from support), CdS1-S

Comparison of load-deflection curves obtained from numerical analysis and beam testing results is illustrated in Figure 7.35. A similar trend of the load-deflection curve was observed between the plotted numerical and experimental results. Both the curves show that at the initial phase of loading, the beams were in high stiffness. After the first cracking of the beam, the stiffness reduced in both curves which then a parallel increment was observed until the fully yield condition. Beyond the point of yielding, both lines reached their respective maximum points followed by softening effects due to beam failure. The results show that the yielding loads and ultimate loads of both FE and experimental beam were comparable to each other. A difference of yielding loads and ultimate loads between the FE and test results was about 3% and 11%, respectively.

(b) Strengthening for Single Square Opening (at distance d from support), SdS1-S

Figure 7.36 shows the load-deflection curves comparison between the FE and experimental results. It was observed that the load-deflection curve trend of numerical results was quite similar to the curve trend of the experiment. At the early phase of loading, both beams possessed high stiffness in which the two lines seemed close to each other. However, after the first crack was formed, reduction in stiffness had caused both lines to increase part ways. After the yielding of the beam, the experimental curve exhibited a plastic flow followed by softening of the beam after failure. On the other hand, the theoretical beam showed a continual increase of load until the ultimate load was obtained before the beam failed. The yielding loads and deflections of FE and the experiment were found similar in which the loads were obtained as 26 kN and 25 kN at 0.9 mm and 1.2 mm, respectively. Meanwhile, it was calculated than the difference in terms of ultimate load between FE analysis and experimental results was of 20%.

Comparison of ultimate loads between the FE analysis and experimental results is presented in Table 7.8. Both results of the FE-to-experiment ratio were found greater than 1 as most of the numerical results were greater than the experimental ones. The FE-to-experiment ratios of beam CdS1-S and SdS1-S were obtained as 1.13 and 1.25, respectively. Meanwhile, the average ratio and standard deviation of the FE analysis and experiment was calculated as 1.19 and 0.08, respectively. This shows a very good agreement between the FE and experimental result.

Table 7.7 Comparison of experiment and FEM results of strengthened beams with opening at one end only

	EXP				FEM			
Beam	Yielding load P_y (kN)	Δ_y (mm)	Ultimate load P_u (kN)	Δ_u (mm)	Yielding load P_y (kN)	Δ_y (mm)	Ultimate load P_u (kN)	Δ_u (mm)
CdS1-S	29	1.8	31	2.5	30	1.0	35	1.7
SdS1-S	25	1.2	28	3.5	26	0.9	35	2.3

Table 7.8 Comparison of ultimate loads from experiment and FEM results

Beam	Ultimate load, P_u (kN)		FEM/EXP
	EXP	FEM	
CdS1-S	31	35	1.13
SdS1-S	28	35	1.25

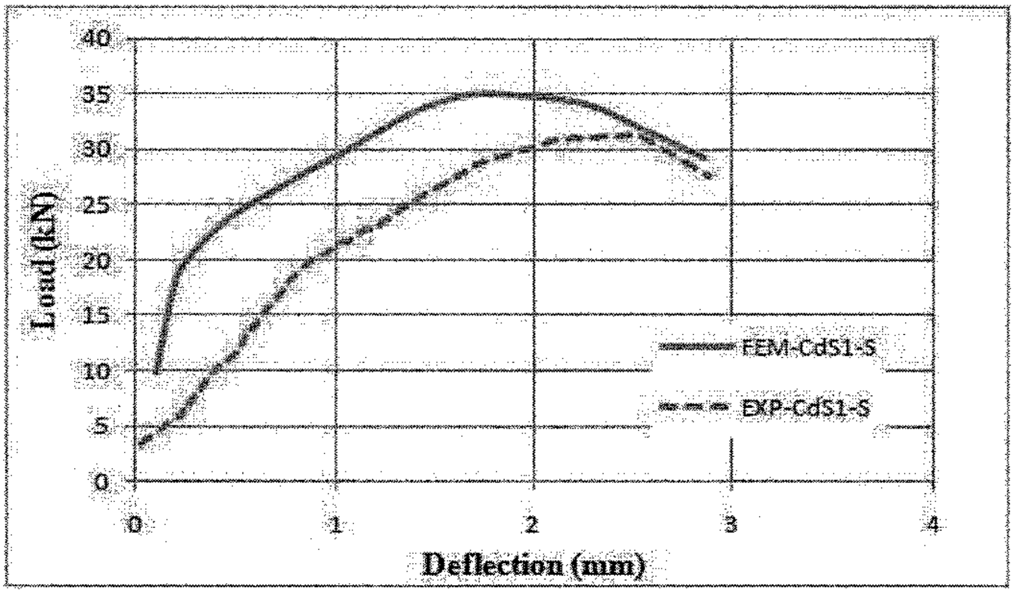

Figure 7.35 Experimental and FEM load-deflection behaviour of beam CdS1-S

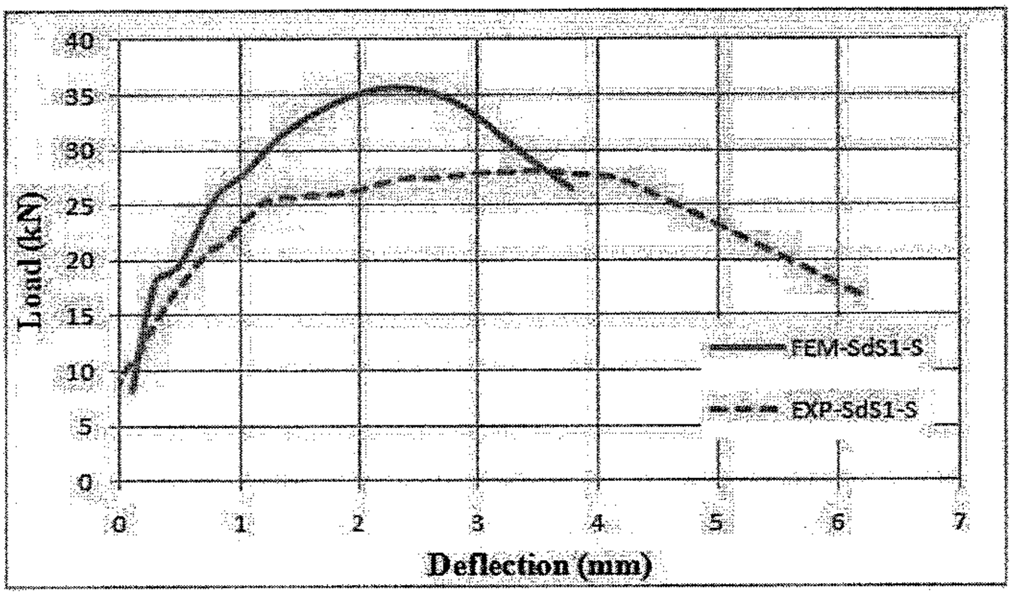

Figure 7.36 Experimental and FEM load-deflection behaviour of beam SdS1-S

7.3.3.3 Crack Patterns

In this section, crack patterns of strengthened beams with openings in the shear zone are compared between the results obtained from FE analysis and experimental testing. The crack patterns of beams with openings at both ends are compared in Figures 7.37 – 7.40 whereas Figures 7.41 – 7.42 shows the comparison of crack patterns of beams with an opening at a single end.

(a) Openings at Both Ends

Figure 7.37 compares the crack patterns of strengthened beam with circular openings at the face of support, COS-S between experimental and FE analysis obtained results. The crack patterns were mainly composed of shear and flexural cracks. The FE analysis shows cracks at the top side of opening; with cracks elongated to the top edge of the beam and diagonally oriented to the loading point. Similar as observed in the tested beam, due to the presence of CFRP along the top chord of the opening, the cracks were formed along the outer edges of CFRP laminates towards the loading point. On the other hand, the FE analysis predicted cracks at the bottom side of the opening which spread diagonally to the beam support. Similarly, cracks were seen diagonally oriented to the beam support causing the peeling of CFRP laminate bonded at the bottom side of opening. CFRP strengthening configuration around the openings had caused the cracks to be diverted into the middle-third span which formed vertically from the bottom edge of beam were observed in both FE and experimental beams. Therefore, the comparisons show a good correlation between the crack patterns of FE analysis and experimental beams.

Comparison of crack patterns of strengthened beam with square openings at both ends, S0S-S is shown in Figure 7.38. In the FE analysis, shear cracks in the form of diagonally oriented cracks were formed at the corners of the opening; causing failure of the beam with a diagonal cracking to the applied load, a wide see-through gap at the corner of the experimental beam was observed at the top chord. On the other hand, FE analysis shows cracks diagonally oriented at the corners of the opening as well as horizontally aligned at the bottom chord. This resulted in crushing of concrete at the bottom chord of opening during laboratory testing exposing bottom steel reinforcements. Flexural cracks were formed vertically aligned from the bottom edge of beam in both experimental and analyzed beams since these cracks were diverted to a different path away from the strengthened area with CFRP into the middle-third span.

Figure 7.39 presents the crack pattern comparison of strengthened beam with circular openings at a distance d from the face of support, CdS-S obtained from FE analysis and experimental testing of the beam. Shear and flexural cracks are mainly observed in the analyzed and tested beams. Due to the presence of CFRP laminates in the strengthening configuration, FE analysis captured vertically aligned flexural cracks formed at the bottom chord of opening in the mid-span, similar as observed in the experimental beam. These cracks then elongated upwards to the bottom edges of the CFRP laminates which bonded diagonally next to the opening. On the other hand, FE analysis predicted cracks at the top side of opening were found similar as the cracks in the tested beam which resulted in crushing of concrete cover at failure. Diagonally oriented shear cracks at the bottom side of opening elongated to the beam support become horizontally aligned as analyzed in FE were found similar to the experimental beam at failure. Due to this, a wide gap of diagonally-horizontal cracking was seen in the tested beam with crushing of bottom concrete cover leaving bottom reinforcement exposed. This comparison clearly shows that the crack patterns were matched between the FE and experimental results.

The crack patterns of strengthened beam with square openings created at a distance d from the face of support, SdS-S between FE analysis and experimental tested beam are illustrated in Figure 7.40. Vertically aligned flexural cracks which appeared at the bottom edge of beam in the middle-third span as predicted in the numerical analysis were found similar to the cracks as shown in the experimental beam during testing. On the other hand, FE analysis captured shear cracks which diagonally oriented at the top edge of the beam which resulted in peeling of concrete cover with CFRP laminates at the top chord, as observed in the tested beam. A diagonal crack at the applied load to the opening corner was predicted in the FE analysis causing a see-through gap and crushing of concrete cover where the top reinforcements were exposed. At the bottom chord, predicted diagonal and horizontal cracks at the bottom side of the opening leads to crushing of concrete cover exposing bottom reinforcements; in which the bottom chord with CFRP laminate was partially dislocated as observed in the experimental beam at failure.

(b) Opening at One End Only

Figure 7.41 shows the comparison of crack patterns obtained from FE analysis and experimental tested strengthened beam with a circular opening at a distance d from the face of support, CdS1-S. FE analysis predicted cracks at the top side of the opening which penetrated to the top edge of the beam and elongated diagonally to the applied load. Similarly as observed in the experimental beam, these cracks caused little crushing of concrete cover with delamination of CFRP laminates bonded at the top side opening. Meanwhile, diagonally oriented cracks at the bottom side of opening to the beam support captured in FE analysis were found similar as observed in the experimental beam, in which a see-through gap were formed at the diagonal cracks causing a displacement of bottom chord from the beam support. On the other hand, flexural cracks which formed vertically from the bottom edge of beam in the mid-span were observed in both numerical and tested beams.

Comparison of crack patterns of strengthened beam with a single square opening at a distance d from the face of support, SdS1-S between theoretical analysis and the experimental beam result is presented in Figure 7.42. During the FE analysis, diagonally oriented and horizontally aligned cracks were formed at the top chord of the opening. This condition caused peeling of concrete cover with CFRP laminates at the top edge of the experimental beam. On the other hand, predicted shear cracks in the form of diagonal and horizontal cracks were found at the bottom chord of the opening. Similarly as observed in the tested beam, a see-through gap of cracking was formed at the corner of the opening and elongated diagonally to the beam support; exposing the bottom steel reinforcements. On the other hand, flexural cracks in the form of vertical aligned cracks were formed at the bottom edge of beam in the middle-third span of the experimental tested beam, similar as predicted in the numerical analysis.

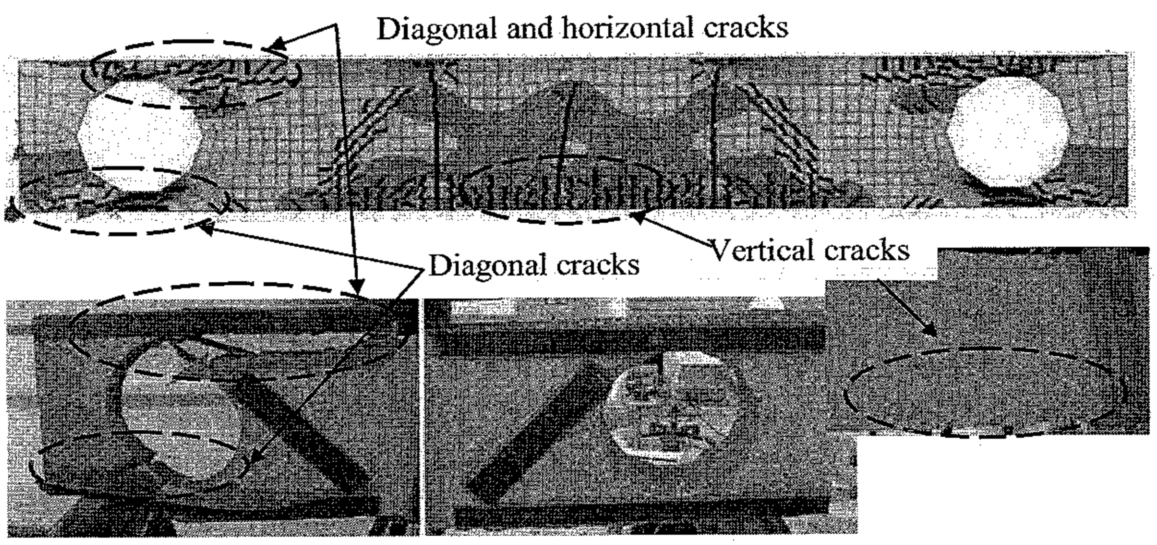

Figure 7.37 Comparison of experimental and FEM crack patterns of beam C0S-S

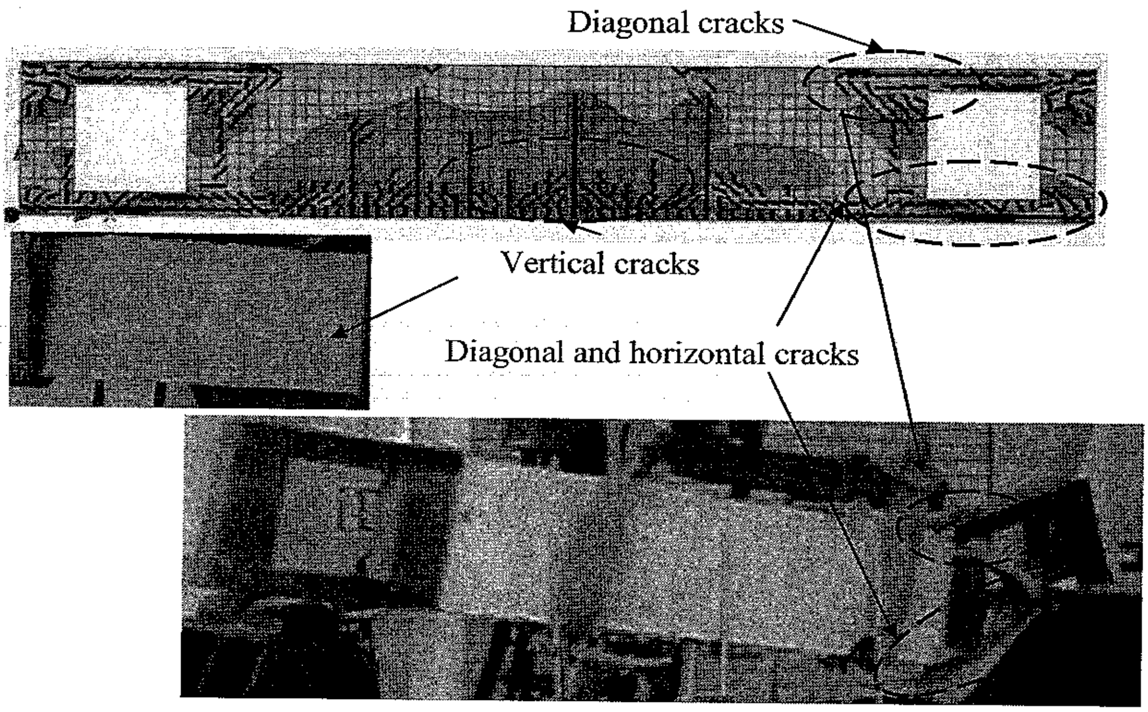

Figure 7.38 Comparison of experimental and FEM crack patterns of beam S0S-S

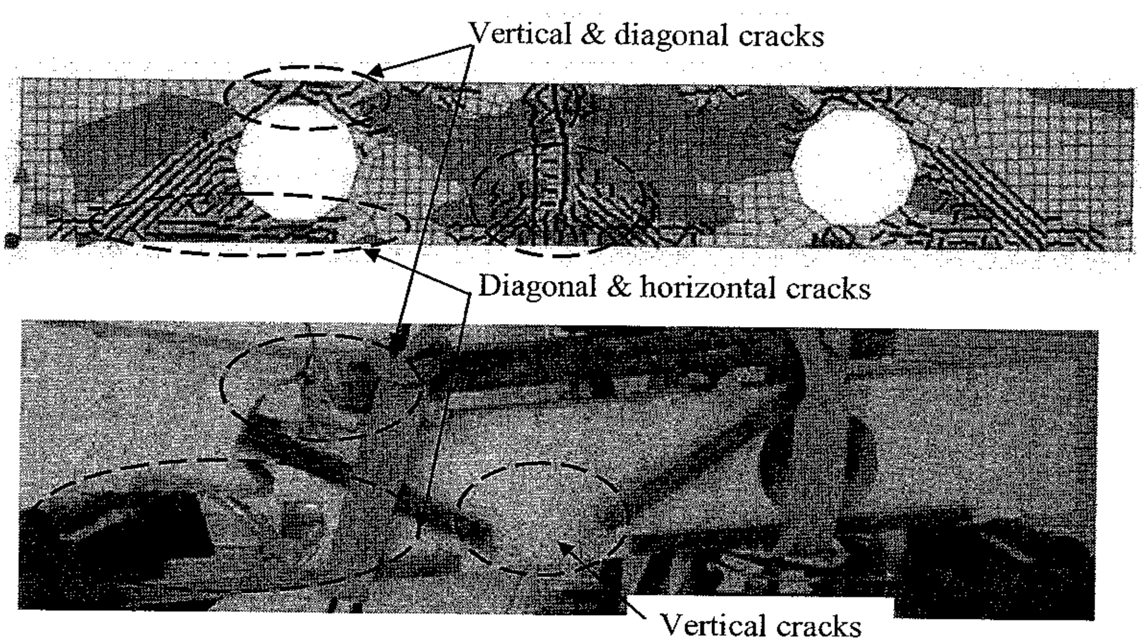

Figure 7.39 Comparison of experimental and FEM crack patterns of beam CdS-S

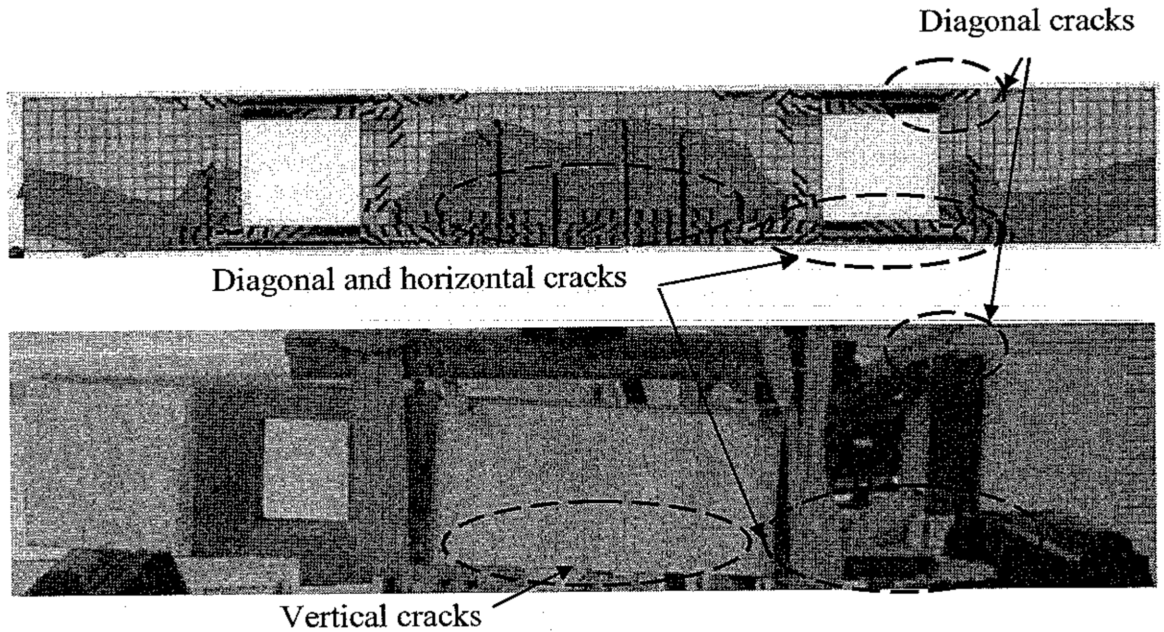

Figure 7.40 Comparison of experimental and FEM crack patterns of beam SdS-S

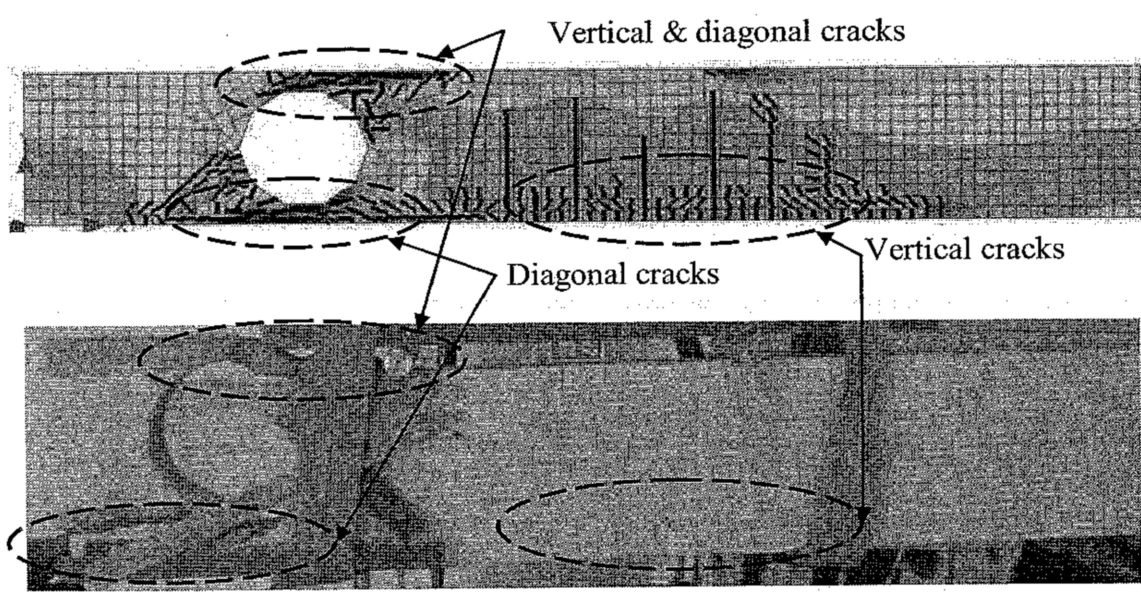

Figure 7.41 Comparison of experimental and FEM crack patterns of beam CdS1-S

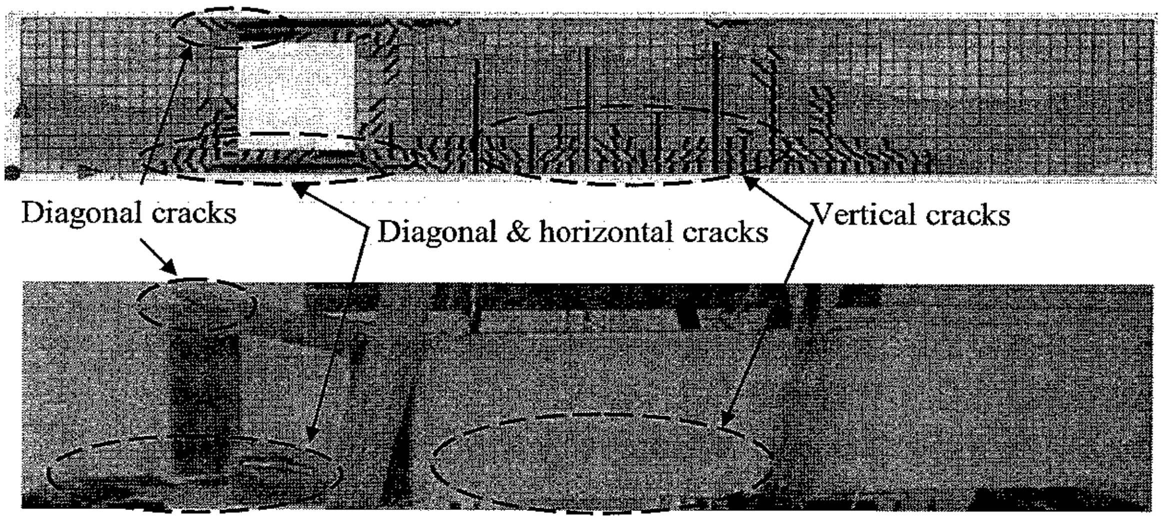

Figure 7.42 Comparison of experimental and FEM crack patterns of beam SdS1-S

7.4 Overall Comparison of Numerical and Experimental Results

In this section, an overall comparison of FE and experimental results is made, which is plotted in Figures 7.43 – 7.46.

(a) Relationship of Experimental vs Numerical Results for Flexural Beams

Here, the flexural beams are referred to those beams contained opening in the flexural zone. In Figure 7.43, the results of the ultimate load of the tested beam are plotted against the corresponding values of ultimate load as obtained from FE analysis. For making a good comparison, a line of equality (at which both x and y axis values are same) is drawn. It can be observed about 50% values are falling very close or almost at the line of equality, which shows a good confidence between the two results. About 25% of experimental results have shown about 20% higher value than the corresponding FE analysis, whereas 20% of the FE results showed 8 – 10% higher values than the experimental results.

Similarly, in Figure 7.44 experimental deflections as observed at ultimate load are drawn against their FE results. It is also observed that about 50 – 60% results are found very close to the line of equality, whereas the rest of the experimental values were found higher (30% - 90%) than the FE results, which means experimental beams showed higher plastic flow than the corresponding theoretical beams. This phenomenon is quite obvious because actual beams experience many factors such as micro-cracking, plastic shrinkage effects of ambient conditions etc., which are not considered in FE analysis.

(b) Relationship of Experimental vs Numerical Results for Shear Beams

The beams contained openings in the shear zone are referred as shear beam. Figure 7.45 shows the results of the ultimate load of the tested beam are plotted against the related values of ultimate load as obtained from FE analysis. A line of equality is drawn in order to have a good comparison between experimental and FE results. It can be observed about 25% values are falling very close to the line of equality which indicates a good confidence between the two results. It is found about 30% of the experimental results have shown about 10 – 30% higher value than the corresponding FE analysis, whereas 70% of the FE results showed 10 – 25% higher values than the experimental results.

On the other hand, experimental deflections as observed at ultimate load are plotted against their respective FE results, as shown in Figure 7.46. It is observed that about 70% results are very close to the line of equality. The experimental values were found higher than the FE results, approximately 20 – 25%. Similar as discussed in flexure beams, the experimental beams showed higher plastic behaviour than the corresponding beams in the analysis. This can be explained that the actual beams in the experiment experienced many factors which cannot be captured in the FE analysis.

From this comparative analysis, it can be concluded that numerical analysis is reliable to incorporate the effects of opening on the structural capacity of beam because about 70% of the results are laid very close to the line of equality and next 20% results were within 20% margin. On the other hand, only 10% results were found between 30-50%. Hence, this fact is valid to justify the application of numerical analysis.

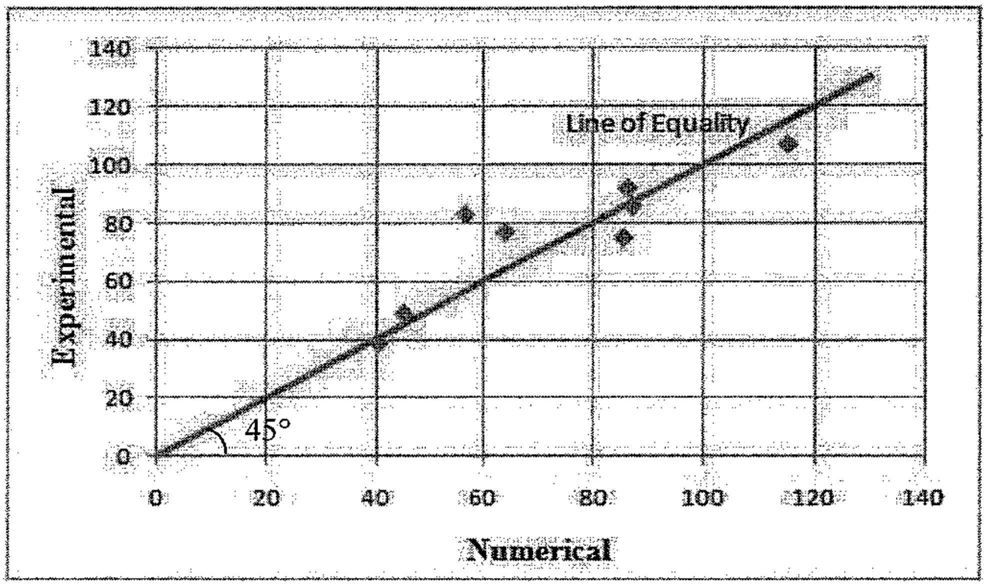

Figure 7.43 Relationship of experimental vs numerical maximum load in flexure

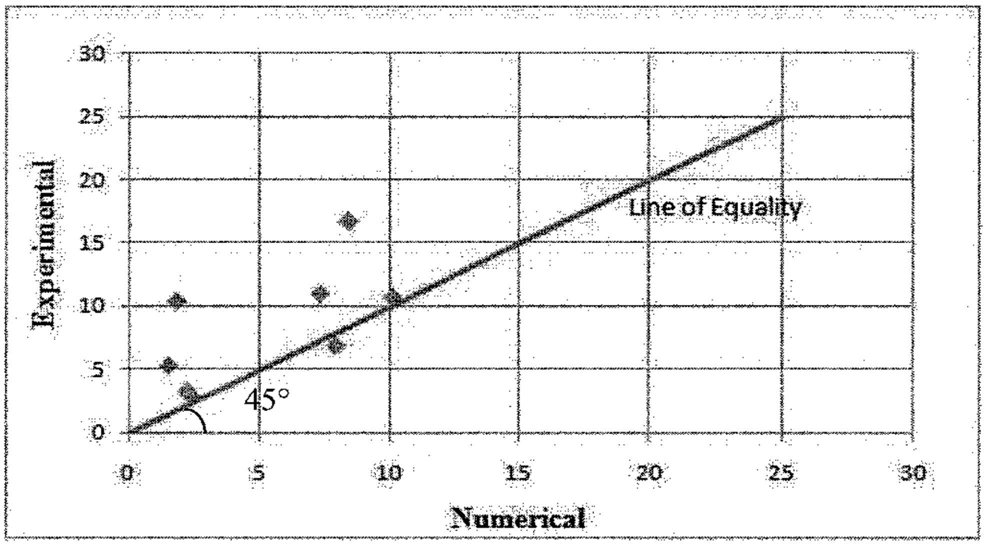

Figure 7.44 Relationship of experimental vs numerical maximum deflections in flexure

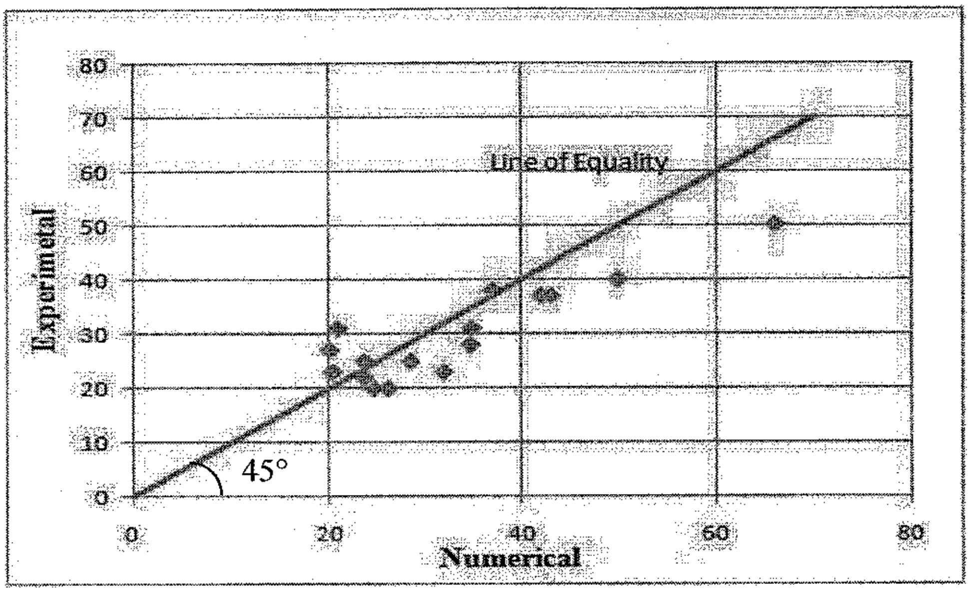

Figure 7.45 Relationship of experimental vs numerical maximum load in shear

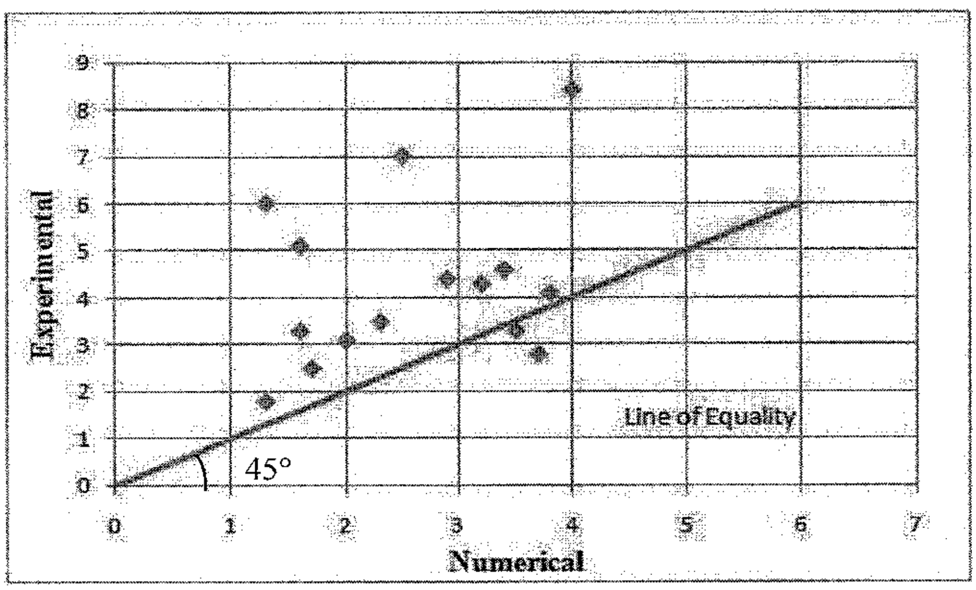

Figure 7.46 Relationship of experimental vs numerical maximum deflection in shear

7.5 Summary

The FE analysis and experimental results are compared and summarized as follows:

In general, results of FE analysis showed higher stiffness as compared to the experimental results. There are many reasons that caused the higher stiffness in the FE models. One of them is the presence of microcracks in the actual concrete. It could be caused by drying shrinkage in the concrete and/or during handling of beams (Özcan et al. 2009) whereas the FE analysis assumed perfect conditions. Therefore, the effects of such microcracks on stiffness are generally not undertaken. Secondly, perfect bond between concrete and steel reinforcing is assumed in the FE analysis; however the assumption may not be perfectly applicable in the experimental beams (Chansawat et al. 2009). Hence, the overall stiffness of the experimental beams is predicted to be lower than the FE models (which also generally impose additional constraints on behaviour) (Kachlakev 2002).

When comparing the results of beams with an opening in flexure, the load-deflection curves of the FE analyzed beams with circular and square openings were in a close agreement with the experimental results while elliptical and rectangular openings (the length of opening extended beyond the load points) did not exhibit softening effects after the peak load was achieved. This is because in large openings, the load was placed on the top chord, which showed the secondary beam action, which was supported on the solid parts at two ends. Therefore, FE analysis could not predict the softening effects, which was recorded by LVDT in the actual testing. On the other hand, the load-deflection curves of FE analyzed beams with openings in the shear zone (at both ends and at one end only) exhibited similarities of trends as compared to the curves of the experimental beams in which a good agreement was obtained. In terms of crack patterns, comparison of beams with openings in flexure and shear zones, a good match of crack patterns was observed between the FE analysis and experimental beams.

The FE results of the most effective strengthening of openings using CFRP laminates are compared with the experiment results and summarized as follows:

In the case of strengthened beams containing openings in the mid-span, the load-deflection curves of FE analysis predicted strengthened beams with circular and square openings, CF-S and SF-S were comparable with their respective load-deflection curves in the experimental testing as the trend of both curves were almost similar. The yield loads and ultimate loads of FE analysis and experimental results were also found in a close agreement. The plotted FE results of beams with large elliptical and rectangular openings (LEF-S and LRF-S) are slightly different compared to the experimental results. A difference of about 40 - 45% was observed in the yielding loads whereas about 20 - 30% in the ultimate loads of experimental beams and FE results was obtained. This could be due to the effects of large openings (the length of opening extended beyond the load points) created in the FE analysis.

In the case of strengthened beams with openings in the shear zone, in general, the load-deflection curves of the FE analysis are in good match with the load-deflection curves of the experimental results, although a slightly higher in stiffness was observed in the curves of FE analysis. One of the reasons may be due to the presence of microcracks in the actual beam for testing in which this is unable to be applied in the FE analysis. Another reason may be due to the perfect bond assumption between the concrete and steel reinforcement in the FE analysis, similarly this assumption is not applicable for beams in the experimental testing. In terms of crack patterns, the comparison between the experimental results and FE analysis for strengthened beams with openings in both flexure and shear shows good agreement.

CHAPTER 8

CONCLUSION AND RECOMMENDATIONS

8.1 Conclusions

Based on the results and discussion of the FE analysis and experimental investigation; the following conclusions were made by conforming to the respective objectives:

1. The effects of opening on the structural behaviour of RC beams by experimental testing and FE analysis were investigated and the following conclusions were drawn.

   i. Using FE analysis to understand the behaviour of beams with opening (that was obtained in terms of load-deflection, crack patterns), the following noteworthy results were observed:

      (a) Circular and square shape openings provided in the beam mid-span did not cause more than 2% reduction in the structural capacity; in fact, it showed quite similar load-deflection curve as that obtained for the control beam, CB. One of the reasons of the effects of the mid-span opening is that the concrete is lost within the low stress zone. This type of openings can be classified as 'small' flexural opening and hence strengthening is not necessary in this case. In this situation, small holes/openings can be drilled in a constructed beam.

      The provision of large rectangular and elliptical openings had caused a reduction of 53% and 48%, respectively in the capacity as compared to the control beam, CB. Elliptical opening showed greater beam stiffness and capacity compared to rectangular because of the stress concentration effects at the opening corners.

(b) The crack patterns of mid-span openings showed that vertical cracks appeared in the middle-third span of the bottom chord and propagated towards the openings. Similarly, diagonal cracks were found at the loading point that encroached until the beam support.

(c) Beams with circular and square openings placed at both ends caused a reduction in capacity of 63 – 70% and 67 – 73%, respectively as compared to the capacity of the beam, CB. The effects of shifting the opening location from a distance of 0, 0.5d and d from the support were not significant, which was obtained within 5% difference.

(d) Similarly, when circular and square openings were provided at one end of the beam (at 0.5d, d and 1.5d distance from the support), about 75% reduction in the structural capacity was obtained.

(e) The crack patterns of beams with openings at both ends showed that minor vertical cracks were formed along the mid-span of the beams. Most cracks appeared at the top and bottom sides of circular shape openings and diagonal cracks at the corners of square shape openings. Similar crack patterns as to that of openings at both ends were traced in beams with openings at one end.

Based on the experimental testing results the following main conclusions were drawn:

(a) Mid-span openings showed a reduction of beam capacity in the range of 21 - 59%; the lowest reduction (21%) caused by the provision of the circular opening while the highest reduction (59%) was obtained due to the rectangular opening. The failure modes observed for all beams were in bending.

(b) When openings provided at both ends, a reduction of 69 - 80% of the beam capacity was obtained. On the other hand, openings assigned at one end only caused a decrease of 68 - 77% of the beam capacity. Location of all types of openings (0, 0.5d, d distance from the support) did not cause any significant effect in terms of capacity loss and the failure mode. The failure modes of these beams were due to shear failure.

ii. In terms of suitable opening shapes and sizes, the overall study showed that the opening with sharp edges and corners caused stress concentration as well as disturbs the load/flow pattern within the beam. Whereas openings with cracks at rounded edges such as circular and elliptical have proved higher capacity with the similar load/flow pattern. Hence, such shapes are more preferable.

iii. In this part of the research, comparison of results showed that the majority of the FE analysis results are agreeable (in terms of crack pattern, load-deflection) with the experimental test results.

In summary, the concluding remarks showed that the first objective was achieved and the results will be helpful to the designers and planners for the selection of appropriate opening(s) in a beam in order to accommodate the requirements for mechanical, electrical and plumbing services.

2. The most effective strengthening of opening using CFRP laminates by FE analysis and experimental validation was determined.

   i. In the first part of the research, where the effects of openings' sizes, shapes and location were investigated. It was found that large size openings in the middle span (rectangular and elliptical shapes) suffered about 50% loss in capacity because such openings went beyond the loading points. FE analysis was used to strengthen the openings with the selected strengthening configurations showed that 65 – 74% of the lost capacity could be restored. The strengthening options from FE analysis was verified using experimental testing and almost similar results were obtained. From this conclusion, openings with length which consists about 30 – 40% of the effective span length is not advisable until and unless the upper and lower chords are properly designed.

ii. In the second part of the research, it was found that the openings (circular and square) provided at both ends (0, 0.5d and d distances from the support) showed about 70% loss in beam capacity. Similarly, when the openings were placed at one end only (0.5d, d and 1.5d distances from the support), the beam capacity loss was about 75%. This is because such openings were created in the critical shear zone that disturbs the load/flow path of the beams. The strengthening of openings (at both ends and at one end only) with the chosen strengthening options showed that a maximum of 40 – 50% of the lost capacity could be restored. The experimental validation for the selected strengthening options proved that almost similar results were obtained. The presence of openings reduces the concrete area in the critical shear zones and this weakens the shear resisting capacity. In general, openings should be avoided from the support up to a distance d.

In summary, this research has achieved all its objectives; the effects of opening shapes, sizes and locations have been investigated in extensive details as well as strengthening options.

8.2 Contribution of Research

This research study can contribute to provide a clear understanding to the structural engineers of creating openings in constructed beams. The understanding of the effects of various types of openings in terms of sizes, shapes and locations in RC beams is very important; especially at the critical locations that can jeopardize the serviceability of the structure. This is to accommodate the changes in the M & E services-line in buildings that usually requested by the M & E engineers to provide and/or relocate the openings to suit the current changes made.

A clear understanding of the effects of openings to the beam behaviour leads to appropriate decision of the structural engineers to select the most suitable type of openings to be provided in the constructed beams which do not affect the beam capacity and serviceability of the structure. However, external strengthening around the openings is always needed in order to ensure the beam behaves similarly as the original beam capacity (before the provision of openings). Hence, various strengthening options can be designed using ATENA and the most effective strengthening system can be adopted in the construction practice.

Experimental work is usually performed to investigate this kind of problems, however it only limits to certain types of opening configuration which can be tested. This may be due to cost implications, manpower and limitation of materials. A better option using the FE tool ATENA can shorten the time taken for experimental testing; reduce the cost of prototype, materials and labor.

8.3 Recommendations for Future Work

In this research, the effects of openings for various shapes, sizes and locations in RC beams subjected to critical shear and bending were investigated, as well as the effective strengthening system using CFRP laminates around the openings were studied. However, the study is limited to 2D FE analysis and static loading condition. The following are the main recommendations for further work of this study:

1. To study the dynamic behaviour of RC beams on the effects of large openings (single or multiple) of various shapes and sizes subjected to critical shear, bending, torsion and combined loading in simply supported beams, T-beams, continuous beams, and deep beams.

2. To investigate the strengthening effects using CFRP laminates on the dynamic behaviour of beams.

3. To study the failure modes of CFRP laminates around the openings of various shapes, sizes and locations in both numerical analysis and experimental investigation.

4. To simulate/validate the beams using 3D FE analyses.

5. To develop models and equations for the prediction of ultimate strength of strengthening beams with CFRP laminate.

REFERENCES

Abdalla, H.A., Torkey, A. M., Haggag, H.A. & Abu-Amira, A.F., 2003. Design Against Cracking at Openings in Reinforced Concrete Beams Strengthened with Composite Sheets. *Composite Structures*, 60(2), pp.197-204.

ACI Committee 318, 1995. Building Code Requirements for Reinforced Concrete (ACI 318-95) and Commentary (ACI 318R-95). *American Concrete Institute,*, (Detroit), pp.369.

ACI Committee 318, 1983. Building Code Requirements for Reinforced Concrete (ACI 318-83). *American Concrete Institute,*, (Detroit), pp.111.

Alagusundaramoorthy, P., Harik, I.E. & Choo, C.C., 2003. Flexural Behavior of R/C Beams Strengthened with Carbon Fiber Reinforced Polymer Sheets or Fabric. *Journal of Composites for Construction*, 7(4), pp.292-301.

Allam, S.M., 2005. Strengthening of RC Beams with Large Openings in the Shear Zone. *Alexandria Engineering Journal*, 44(1), pp.59-78.

Aly, S.A.G., Hammad, Y.H., Abdel-Rahman G.T., Said, M., 2003. Behaviour of RC Beams with Strengthened Openings in D-Region. In *Emerging Technologies in Structural Engineering. In the Proc of the 9th Arab Structural Engineering Conference, Abu Dhabi, UAE.* pp. 163-174.

Aram, M., Czaderski, C. & Motavalli, M., 2008. Debonding Failure Modes of Flexural FRP-Strengthened RC Beams. *Composites Part B: Engineering*, 39(5), pp.826-841.

Arduini, M., Di Tommaso, A. & Nanni, A., 1997. Brittle Failure in FRP Plated and Sheet Bonded Beams. *ACI Structural Journal*, 94(4), pp.363-370.

Ashour, A.F., El-Refaie, S.A. & Garrity, S.W., 2004. Flexural Strengthening of RC Continuous Beams Using CFRP Laminates. *Cement & Concrete Composites*, 26, pp.765-775.

ASTM International, 2008. *ASTM D3039 Standard Test Method for Tensile Properties of Polymer Matrix Composite Materials*, ASTM International.

Badea, C., Bob, C., Balcu, I., Dan, S., Buchman, I., Gruin, A., 2008. The Carbonation Process Influence on Concrete Durability. *Materials Science,* pp. 11-15.

Balaguru, P., Balaguru, P.N., Nanni, A. & Giancaspro, J., 2008. *FRP Composites for Reinforced and Presstressed Concrete Structures: a guide to fundamentals and design for repair and retrofit,* Taylor and Francis.

Barney, G.B., Corley, W.G., Hanson, J.M. & Parmelee, R.A., 1977. Behaviour and Design of Prestressed Concrete Beams with Large Web Openings. *PCI Journal*, 22(6), pp.32-61.

Beushausen, H. & Alexander, M., 2010. Concrete Technology Workshop 2010 Lecture 2-Strength of Concrete- Influencing Factors, Design Principles, Code Requirements.British Standards Institution, 1983. *B.S 1881: Part 116 Method for Determination of Compressive Strength of Concrete*, BSI, London.

British Standards Institution, 1997. *BS 4449: 1997 Carbon Steel Bars for the Reinforcement of Concrete*, BSI, London.

Buyle-Bodin, F., David, E. & Ragneau, E., 2002. Finite Element Modelling of Flexural Behaviour of Externally Bonded CFRP Reinforced Concrete Structures. *Engineering Structures*, 24, pp.1423-1429.

Cervenka, V., 1999. Computer Simulation of Failure of Concrete Structures for Practice. , (E-328), pp.1-16.

Cervenka, V., *Inelastic Finite Element Analysis of Reinforced Concrete Panels under In-Plane Loads*. PhD Thesis,University of Colorado,Boulder,Colorado, 1970.

Cervenka, J. 2001. ATENA Program Documentation Part 4-1 Tutorial for Program ATENA 2D Written by : *Cervenka Consulting, May*, pp.1-61.

Cervenka, V., Cervenka, J. & Pukl, R., 2002. ATENA – A Tool for Engineering Analysis of Fracture in Concrete. *Sadhana*, 27(Part 4), pp.485-492.

Cervenka, V., Jendele, L. & Cervenka, J., 2010. ATENA Program Documentation. *Part 1 Theory*, pp.1-248.

Cervenka, V., Jendele, L. & Cervenka, J., 2003. *ATENA User Manual*, Cervenka Consulting.

Cervenka, V., & Cervenka, J. 2006. *ATENA Program Documentation Part 2-1 User ' s Manual for ATENA 2D*, (November), 1-139.

Chaallal, O., Nollet, M.J. & Pereraton, D., 1998. Shear Strengthening of RC Beams by Externally Bonded Side CFRP Strips. *Journal of Composites for Construction*, 2(2), pp.111-113.

Chajes, M.J., Januzka, T.F., Mertz, D.R., Thomson, T.A. & Finch, W.W., 1995. Shear Strengthening of Reinforced Concrete Beams Using Externally Applied Composite Fabrics. *ACI Structural Journal*, 92(3), pp.295-303.

Chansawat, K., Potisuk, T., Miller, T.H., Yim, S.C. & Kachlakev, D.I., 2009. FE Models of GFRP and CFRP Strengthening of Reinforced Concrete Beams. *Advances in Civil Engineering*, 2009(2009), pp.1-13.

Colomb, F., Tobbi, H., Ferrier, E. & Hamelin, P., 2008. Seismic Retrofit of Reinforced Concrete Short Columns by CFRP Materials. *Journal of Composite Structures*, 82, pp.475-487.

Colotti, V. & Swamy, R.N., 2011. Unified Analytical Approach for Determining Shear Capacity of RC Beams Strengthened with FRP. *Engineering Structures*, 33(3), pp.827-842.

Crisfield, M.A. & Wills, J., 1989. The Analysis of Reinforced Concrete Panels Using Different Concrete Models. *Journal of Engineering Mechanics, ASCE*, 115(3), pp.578-597.

Duthinh, D. & Starnes, M., 2001. Strengthening of Reinforced Concrete Beams with Carbon FRP. *Composites in Construction*, pp.493-498.

El Maaddawy, T. & Sherif, S., 2009. FRP Composites for Shear Strengthening of Reinforced Concrete Deep Beams with Openings. *Composite Structures*, 89(2009), pp.60-69.

Elyasian, I., Abdoli, N. & Ronagh, H.R., 2006. Evaluation of Parameters Effective in FRP Shear Strengthening of RC Beams Using FE Method. *Asian Journal of Civil Engineering (Building and Housing)*, 7(3), pp.249-257.

Emmons, P.H., Vaysburd, V.M. & Thomas, J., 1998. Strengthening Concrete Structures, Part 2. *Concrete International*, pp.56-60.

Engineering Mathematics: *Open Learning Unit Level 1 13.3: Tangents and Normals: The Newton Raphson Method*. (n.d.). pp. 1-18.

Esfahani, M.R., Kianoush, M.R. & Tajari, A.R., 2007. Flexural Behaviour of Reinforced Concrete Beams Strengthened by CFRP Sheets. *Engineering Structures*, 29(2007), pp.2428-2444.

Fanning, P. & Kelly, O., 2000. Smeared Crack Models of RC Beams with Externally Bonded CFRP Plates. *Computational Mechanics*, 26(2000), pp.325-332.

Feldman, D., & Barbalata, A., 1996. *Synthetic Polymers: Technology, Properties, Applications*, Chapman and Hall.

Ferretti, D. & Savoia, M., 2003. Non-linear Model for R/C Tensile Members Strengthened by FRP-Plates. *Engineering Fracture Mechanics*, 70(2003), pp.1069-1083.

Ferrier, E., Avril, S., Hamelin, P. & Vautrin, A., 2003. Mechanical Behavior of RC Beams Reinforced by Externally Bonded CFRP Sheets. *Materials and Structures*, 36(8), pp.522-529.

Franca, P., Costa, A. & Appleton, J., 2007. Prestressed CFRP Laminates for Flexural Strengthening of Reinforced Concrete Beams. *Structural Concrete*, 8(4), pp.175-185.

GangaRao, H.V.S., Taly, N. & Vijay, P.V., 2006. *Reinforced Concrete Design with FRP Composites*, CRC Press, London.

Godat, A., Labossière, P. & Neale, K.W., 2012. Numerical Investigation of the Parameters Influencing the Behaviour of FRP Shear-Strengthened Beams. *Construction and Building Materials*, 32(July), pp.90-98.

Gorji, M.S., 2009. Analysis of FRP Strengthened Reinforced Concrete Beams Using Energy Variation Method. *Applied Sciences*, 6(1), pp.105-111.

Grace, N.F., Sayed, G.A., Soliman, A.K. & Saleh, K.R., 1999. Strengthening Reinforced Concrete Beams Using Fiber Reinforced Polymer (FRP) Laminates. *ACI Structural Journal*, 96(5), pp.865-875.

Graybeal, W. & Pooch, U.W., 1980. *Simulation: Principles and Methods*, Winthrop Publishers, Cambridge, MA.

Hadi, M.N.S., 2007. Behaviour of FRP Strengthened Concrete Columns under Eccentric Compression Loading. *Journal of Composite Structures*, 77(1), pp.92-96.

Hanson, J.M., 1969. Square Openings in Webs of Continuous Joints. *PCA Research and Development Bultetin RD 100.01D*, Portland C(Stokie III), pp.1-14.

Hollaway, L.C. & Head, P.R., 2000. Composite Materials and Structures in Civil Engineering. *in Comprehensive Composite Materials*, 6, pp.490-526.

Hollaway, L.C. & Leeming, M.B., 1999. *Strengthening of Reinforced Concrete Structures Using Externally Bonded FRP Composites in Structural and Civil Engineering*, CRC Press.

Hordijk, D.A. *Local Approach to Fatigue of Concrete*. PhD Thesis, Delft University of Technology, 1991.

Hsu, J.D., Michael, J.W. & Fisk, J.R., 2008. *AAOS Atlas of Orthoses and Assistive Devices* Forth ed., Mosby Elsevier.

Huebner, K.H., Dewhirst, D.L. & Smith, D.E., Byrom, T.G., 2001. *The Finite Element Method for Engineers* Fourth Ed., John, Wiley and Sons.

Hull, D.T. & Clyne, W., 1996. *An Introduction to Composite Materials* Second Ed., Cambridge University Press.

Huston, R. & Josephs, H., 2008. *Stress Concentration (Practical Stress Analysis in Engineering Design)* Third Ed., CRC Press.

Ibrahim, A.M. & Mahmood, M.S., 2009. Finite Element Modeling of Reinforced Concrete Beams Strengthened with FRP Laminates. *European Journal of Scientific Research*, 30(4), pp.526-541.

Jendele, L., & Cervenka, J. 2009. On the Solution of Multi-Point Constraints – Application to FE Analysis of Reinforced Concrete Structures. *Computers and Structures*, *87*, 970-980.

Kabele, P., Cervenka, V. & Cervenka, J., 2010. *ATENA Program Documentation Part 3-1 Example Manual ATENA Engineering*, Cervenka Consulting.

Kachlakev, Damian I., 2002. Finite Element Analysis and Model Validation of Shear Deficient Reinforced Concrete Beams Strengthened with GFRP Laminates. In *Third International Conference on Composites in Infrastructure, San Francisco, California, June 10-12*. pp. 1-11.

Khalifa, A., Tumialan, G. & Nanni, A., Belarbi, A., 1999. Shear Strengthening of Continuous RC Beams Using Externally Bonded CFRP Sheets. In *Proc., 4th International Symposium on FRP for Reinforcement of Concrete Structures (FRPRCS4), Baltimore, MD. Nov.* pp. 995-1008.

Khalifa, A. & Nanni, Antonio, 2000. Improving Shear Capacity of Existing RC T-Section Beams Using CFRP Composites. *Cement & Concrete Composites*, 22(2000), pp.165-174.

Kokcharov, I. (n.d.). Structural Integrity Analysis: Stress Concentration. *Stress: The International Journal on the Biology of Stress*, 1-23.

Kotynia, R., Baky, H.A., Neale, K.W. & Ebead, U.A., 2008. Flexural Strengthening of RC Beams with Externally Bonded CFRP Systems : Test Results and 3D Nonlinear FE Analysis. *Journal of Composites for Construction*, (April), pp.190-201.

Kupfer, H., Hilsdorf, H.K. & Rusch, H., 1969. Behaviour of Concrete under Biaxial Stress. *ACI Journal*, 66(8), pp.656-666.

Larson, D., 1998. Beam Shear Behaviour. *Northen Arizona University*.

Limam, A. & Hamlin, P., 1998. On the Extending Performance of an RC Beam with a CFRP Sheet: Experiments and Simulations. In *Proceedings of the Sixth International Conference on Computer Methods in Composite Materials, CADCOMP'98 , Montreal, Canada*. pp. 569- 578.

Limam, O., Foret, G. & Ehrlacher, A., 2003. RC Two-Way Slabs Strengthened with CFRP Strips : Experimental Study and a Limit Analysis Approach. *Composite Structures*, 60(2003), pp.467-471.

Liu, G.R. & Quek, S.S., 2003. *The Finite Element Method - A Practical Course*, Butterworth Heinemann.

Lorensten, M., 1962. Holes in Reinforced Concrete Girders. *Byggmastaren*, 41(7), pp.141-152.

Lu, X.Z., Teng, J.G., Ye, L.P. & Jiang, J.J., 2005. Bond – Slip Models for FRP Sheets / Plates Bonded to Concrete. *Engineering Structures*, 27(6), pp.920-937.

Madkour, H., 2009. Non-linear Analysis of Strengthened RC Beams with Web Openings. *Proceedings Of The Institution Of Civil Engineers, Structures and Buildings*, 162(2), pp.115-128.

Mansur M.A., 2006. Design of Reinforced Concrete Beams with Web Openings. In *Proceedings of the 6th Asia-Pacific Structural Engineering and Construction Conference (ASPEC 2006), 5-6 September 2006, Kuala Lumpur, Malaysia.* pp. 104-120.

Mansur, M.A., 1983. Combined Bending and Torsion in Reinforced Concrete Beams with Rectangular Openings. *Concrete International*, pp.51-58.

Mansur, M.A., 1998. Effect of Openings on the Behaviour and Strength of R/C Beams in Shear. *Cement and Concrete Composites*, 20(6), pp.477-486.

Mansur M. A., 1999. Design of Reinforced Concrete Beams with Small Openings under Combined Loading. *ACI Structural Journal*, *96*(5), pp.675-682.

Mansur, M.A., Tan, K.H. & Lee, S.L., 1985. Design Method for Reinforced Concrete Beams with Large Openings. *ACI Journal*, 82(4), pp.517-524.

Mansur, M.A., 1988. Ultimate Strength Design of Beams with Large Openings. *International Journal of Structures*, 8(2), pp.107-125.

Mansur, M.A. & Hasnat, A., 1979. Concrete Beams with Small Openings under Torsion. *Journal of the Structural Division, ASCE*, 106(ST11 Nov), pp.2433-2447.

Mansur, M.A., Huang, L.M., Tan, K.H. & Lee, S.L., 1992. Deflections of Reinforced Concrete Beams with Web Openings. *ACI Structural Journal*, 89(4), pp.391-397.

Mansur, M.A., Lee, Y.F., Tan, K. H. & Lee, S.L., 1991. Tests on RC Continuous Beams with Openings. *Journal of Structural Engineering*, 117(6), pp.1593-1606.

Mansur, M.A. & Tan, K.H., 1999. *Concrete Beams with Openings: Analysis and Design*, CRC Press, London.

Mansur, M.A., Tan, K.H. & Lee, S.L., 1984. Collapse Loads of R/C Beams with Large Openings. *Journal of Structural Engineering*, 110(11), pp.2602-2618.

Mansur, M.A., Tan, K.H. & Wei, W., 1999. Effects of Creating an Opening in Existing Beams. *ACI Structural Journal*, 96(6), pp.899-906.

Meier, U., 1996. Advanced Composite for Structural Repair : European Perspective. In *Proc. US- European Workshop on Bridge Engineering*. pp. 491-504.

Meier, U., Deuring, M., Meier, H. & Schwegler, G., 1992. Strengthening of Structures with CFRP Laminates: Research and Applications in Switzerland. In *Proc 1st Int Conf on Advanced Composite Materials in Bridges and Stuctures , Sherbrooke, Canada,*. pp. 243-251.

Mofidi, A. & Chaallal, O., 2011. Shear Strengthening of RC Beams with EB FRP : Influencing Factors and Conceptual Debonding Model. *Journal of Composites for Construction*, (February), pp.62-74.

Moreno, A., 2011. Knovel Solutions in Aerospace Engineering. Available at: librarians.knovelblogs.com/2011/11/04/knovel-solutions-in-aerospace-engineering/.

Mosallam, A.S. & Mossalam, K.M., 2003. Strengthening of Two-Way Concrete Slabs with FRP Composites Laminates. *Construction Building Materials*, 17(1), pp.43-54.

Mosley, B., Bungey, J. & Husle, R., 2007. *Reinforced Concrete Design to Eurocode 2* Sixth Ed., Palgrave Macmillan.

Nasser, K.W., Acavalos, A. & Daniel, H.R., 1967. Behavior and Design of Large Openings in Reinforced Concrete Beams. *ACI Journal, Proceedings*, V.64(1), pp.25-33.

Nazem, M., Rahmani, I., & Rezaee-Pajand, M. 2009. Nonlinear FE Analysis of Reinforced Concrete Structures Using a Tresca-Type Yield Surface. *Scientia Iranica: Civil Engineering*, *16*(6), 512-519.

Ngo, D. & Scordelis, A.C., 1967. Finite Element Analysis of Reinforced Concrete Beams. *ACI Journal*, 64(3), pp.152-163.

Norris, T., Saadatmanesh, H. & Ehsani, M.R., 1997. Shear and Flexural Strengthening of R/C Beams with Carbon Fiber Sheets. *Journal of Structural Engineering*, 123(7), pp.903-911.

Olivia, M. & Mandal, P., 2005. Curvature Ductility of Reinforced Concrete Beam. *Jurnal Teknik Sipil*, 6(1), pp.1-13.

Papadakis, V. G., Vayenas, C. G., & Fardis, M. N., 1989. A Reaction Engineering Approach to the Problem of Concrete Carbonation. *AlChE Journal*, *35*(10), pp.1639-1650.

Pimanmas, A., 2010. Strengthening R/C Beams with Opening by Externally Installed FRP Rods: Behavior and Analysis. *Composite Structures*, 92(8), pp.1957-1976.

Pretzas, E.G., *Behaviour and Reinforcement of Concrete Beams with Large Rectangular Apertures*. PhD Thesis, University of Sheffiled, U.K. 1968.

Ragan, H.S. & Warwaruk, J., 1967. Tee Members with Large Web Openings. *Journal of the Prestressed Concrete Institute*, 12(4), pp.52-65.

Rahimi, H. & Hutchinson, A., 2001. Concrete Beams Strengthened with Externally Bonded FRP Plates. *Journal of Composites for Construction*, 5(1), pp.44-56.

Rai, G. & Indolia, Y., 2011. Fiber Reinforced Polymer Composites: A Novel Way for Strengthening Structures. *NBMCW.*

Rashid Khan, M., & Barron, A. R., 2008. Carbon Fibers: Opportunities and Challenges. *Materials Science and Technology*, (September), pp.47-49.

Reddy, J.N., 1993. *An Introduction to the Finite Element Method* 2nd ed., McGraw Hill, New York.

Ross, C.A., Jerome, D.M., Tedesco, J.W. & Hughes, M.L., 1999. Strengthening of Reinforced Concrete Beams with Externally Bonded Composite Laminates. *ACI Structural Journal*, 96(2), pp.212-221.

Standards Association of Australia, 1974, *SAA Concrete Structures Code,* AS 1480-74, Sydney, pp.101.

Saadatmanesh, H., Ehsani, M. R & Jin, L., 1997. Repair of Earthquake - Damaged RC Columns with FRP Wraps. *ACI Structural Journal*, 94(2), pp.206-214.

Salam, S.A., 1977. Beams with Openings under Different Stress Conditions. In *Proceedings of 3rd Conference on Our World in Concrete and Structures, Cl-Primier, 25- 26 Aug. Singapore.* pp. 259-267.

Shafiq, N., *Durability of Natural Fibers in Mortar Containing Rice Husk Ash.* PhD Thesis, AIT Asian Institute of Technology Bangkok, Thailand, 1987.

Shiskowski, K., & Frinkle, K. 2011. Principles of Linear Algebra With Mathematica: The Newton-Raphson Method, pp.1-36.

Siao, W.B. & Yap, S.F., 1990. Ultimate Behaviour of Un-Strengthened Large Openings Made in Existing Concrete Beams. *Journal of the Institution of Engineers, Singapore*, 30(3), pp.51-57.

Sika, 2010. Sika ® CarboDur ®. , pp.1-4.

Smith, S. T., Hu, S., Kim, S.J. & Seracino, R., 2011. FRP-Strengthened RC Slabs Anchored with FRP Anchors. *Engineering Structures*, 33(4), pp.1075-1087.

Somes, N.F. & Corley, W.G., 1974. Circular Openings in Webs of Continuous Beams. Shear in Reinforced Concrete. *American Concrete Institute, Farmington Hills, Mich,* SP-42(1), pp.359-398.

Spadea, G., Swamy, R.N. & Bencardino, F., 2001. Strength and Ductility of RC Beams Repaired with Bonded CFRP Laminates. *Journal of Bridge Engineering*, (October), pp.349-355.

Supaviriyakit, T., Pornpongsaroj, P. & Pimanmas, A., 2004. Finite Element Analysis of FRP-Strengthened RC Beams. *Songklanakarin J. Sci. Technol.*, 26(4), pp.497-507.

Tan, K. H., Mansur, M.A. & Huang, L.M., 1996. Reinforced Concrete T-Beams with Large Web Openings in Positive and Negative Moment Regions. *ACI Structural Journal*, 93(3), pp.277-289.

Tan, K. H., Mansur, M.A. & Wei, W., 2001. Design of Reinforced Concrete Beams with Circular Openings. *ACI Structural Journal*, 98(3), pp.407-415.

Tarallo, E., & Mastinu, G. (n.d.). FE Analysis with Plane Stress and Plane Strain Elements. *Es-03*.

Triantafillou, T.C., 1998. Shear Strengthening of Reinforced Concrete Beams Using Epoxy-Bonded FRP Composites. *ACI Structural Journal*, 95(2), pp.107-115.

Tuakta, C., *Use of Fiber Reinforced Polymer Composite in Bridge Structures*. PhD Thesis, S.B. Civil Engineering, Massachusetts Institute of Technology, 2004.

Turner, M.J., Clough, R.W., Martin, H.C. & Topp, L.J., 1956. Stiffness and Deflection Analysis of Complex Structures. *Journal of Aeronautical Sciences*, 23(9), pp.805-823.

UCSB College of Engineering. n.d. MODULE for Plane Stress and Plain Strain Analysis. pp.1-12.Available: www.engineering.ucsb.edu/~hpscicom/projects/stress/introge.pdf

Ulaga, T., Vogel, T. & Meier, U., 2003. The Bilinear Stress-Slip Bond Model: Theoretical Background and Significance. In *FRPRCS-8 Conference Singapore, 8 - 10 July*.

Vanmier, J.G.M., 1986. Multi-Axial Strain-Softening of Concrete, Part I: Fracture. *Materials and Structures, RILEM*, 19(111).

Vecchio, F.J. & Collins, M.P., 1986. Modified Compression-Field Theory for Reinforced Concrete Beams Subjected to Shear. *ACI Journal, Proceedings*, 83(2), pp.219-231.

White, T.W., Soudki, K.A. & Erki, M., 2001. Response of RC Beams Strengthened with CFRP Laminates and Subjected to a High Rate of Loading. *Journal of Composites for Construction*, 5(3), pp.153-162.

Yang, K.H. & Ashour, A.F., 2007. Inclined Reinforcement Around Web Opening in Concrete Beams. *Proceedings of The Institution Of Civil Engineers, Structures and Buildings*, 160(SB3), pp.173-182.

Zarnic, R., Gostic, S., Bosiljkov, V. & Bokan-Bosiljkov, V., 1999. Improvement of Bending Load-Bearing Capcaity by Externally Bonded Plates. In *Specialist Techniques and Materials for Concrete Construction,Proceedings of the International Conference "Creating with Concrete", Dundee Scotland, UK*. pp. 433-442.

Zhang, Z. & Thomas Hsu, C.T., 2005. Shear Strengthening of Reinforced Concrete Beams Using Carbon-Fiber-Reinforced Polymer Laminates. *Composites*, 9(2), pp.158-169.

Zienkiewicz, O.C. & Cheung, Y.K., 1967. *The Finite Element Analysis in Structural and Continuum Mechanics*, McGraw Hill, London.

Zienkiewicz, O.C., Taylor, R.L. & Zhu, J.Z., 2005. *The Finite Element Method: Its Basis and Fundamentals* 6th ed., Elsevier Ltd.

Özcan, D. M., Bayraktar, A., Sahin, A., Haktanir, T. & Turker, T., 2009. Experimental and Finite Element Analysis on the Steel Fiber-Reinforced Concrete (SFRC) Beams Ultimate Behavior. *Construction and Building Materials*, 23(2009), pp.1064-1077.

LIST OF PUBLICATIONS

1. **Chin, S.C.** and Shafiq, N. and Nuruddin, M.F. (2012) Strengthening of RC Beams with Large Openings in Shear by CFRP Laminates: Experiment and 2D Nonlinear Finite Element Analysis. *Research Journal of Applied Sciences, Engineering and Technology*, 4 (9). pp. 1172-1180.

2. **Chin, S.C.** and Shafiq, N. and Nuruddin, M.F. (2012) Strengthening of RC Beams with Large Openings in Shear by CFRP Laminates: 2D Nonlinear FE Analysis. *World Academy of Science, Engineering and Technology* 62, pp. 549-554.

3. **Chin, S.C.** and Shafiq, N. and Nuruddin, M.F. (2012) Effects of used Engine Oil in Reinforced Concrete Beams: The Structural Behaviour. *International Journal of Civil and Environmental Engineering*, 6. pp. 83-90.

4. **Chin, S.C.** and Shafiq, N. and Nuruddin, M.F. (2012) Strengthening of RC Beams with Large Openings in Shear by CFRP Laminates: 2D Nonlinear FE Analysis. *International Journal of Civil and Environmental Engineering*, 6. pp. 195-200.

5. Shafiq, N. and Nuruddin, M.F. and **Chin, S.C.** (2012) Durability Study Partially Saturated Fly Ash Blended Cement Concrete. *International Journal of Civil and Environmental Engineering*, 6 . pp. 67-71.

6. **S.C. Chin**, N. Shafiq, M.F. Nuruddin and S.A. Farhan, (2012), Strengthening of RC Beams with Large Openings in Shear by CFRP Laminates: Test Results. *In: International Conference on Civil, Offshore, & Environmental Engineering (ICCOEE 2012), 12^th^-14^th^ June 2012, Kuala Lumpur Convention Centre.*

7. **Chin, S.C.** and Shafiq, N. and Nuruddin, M.F. (2011) CFRP Composites for Strengthening RC Beams with Large Square Opening at Shear: FEM & Experimental. *In: 7th International Conference on Steel & Aluminium Structures, 13th –15th July 2011, Kuching, Sarawak, Malaysia.*

8. **Chin, S.C.** and Shafiq, N. and Nuruddin, M.F. (2011) Optimum Strengthening of R/C Beams with Large Opening at Shear using CFRP Laminates. *In: United Kingdom - Malaysia Ireland Engineering Science Conference 2011 (UMIES 2011), 12-14 July, 2011, Kuala Lumpur.*

9. **Chin, S.C.** and Shafiq, N. and Nuruddin, M.F. (2011) Finite Element Modelling of RC Beams with Large Opening at Critical Flexure and Shear Strengthened with CFRP Laminates. *In: International Building and Infrastructure Technology Conference 2011, (BITECH 2011), June 7-8 2011, Penang.*

10. **Chin, S.C.** and Shafiq, N. and Nuruddin, M.F. (2010) Structural Performance of Reinforced Concrete Beams Containing Used Engine Oil. *In: International Conference on Sustainable Building and Infrastructure (ICSBI 2010), 15-17 June 2010, Kuala Lumpur.*

APPENDIX A: TUTORIAL ON ATENA EXAMPLE MANUAL

(Leonhardt's Shear Beam, LSB)

In this tutorial example, the FE modelling was conducted according to the data given in the manual as listed in Tables A-1 – A4.

Table A-1 Material properties of concrete (Kabele et al. 2010)

Material Type		SBeta Material	
Elastic modulus	E_c	31.72	GPa
Poisson's ratio	ν	0.2	
Compressive strength	f_c	28.48	MPa
Tensile strength	f_t	1.64	MPa
Type of tension softening		Exponential	
Fracture Energy	G_f	100.0	N/m
Crack Model		Fixed	

Table A-2 Material properties of reinforcement (Kabele et al. 2010)

Material Type		Reinforcement	
		bilinear	
Elastic modulus	E	208	GPa
Yield strength	σ_y	560	MPa
Hardening		perfectly plastic	

Table A-3 Solution parameters (Kabele et al. 2010)

Solution Method	Newton-Raphson	
Stiffness/update	Tangent/each iteration	
Number of iterations	40	
Error tolerance	0.010	
Line search	on, with iterations	

Table A-4 Finite element mesh (Kabele et al. 2010)

Finite Element Type	Quadrilateral (CCIsoQuad or CCQ10Sbeta) or Triangular	
Element Shape Smoothing	on	
Optimization	Sloan	

The results obtained were found in good agreement with the results of the example. Comparisons were made in terms of load-deflection behaviour between the results obtained from ATENA user manual and FE analysis results using ATENA. Figure A-1 and Figure A-2 shows the load-displacement curves respectively. The analyzed results were in good agreement with the results in ATENA user manual.

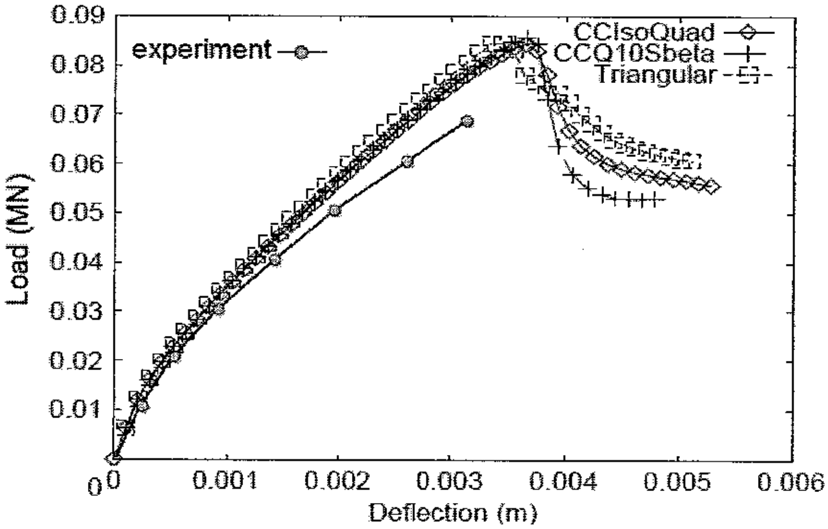

Figure A-1 Load-displacement curves of shear beam (Kabele et al. 2010)

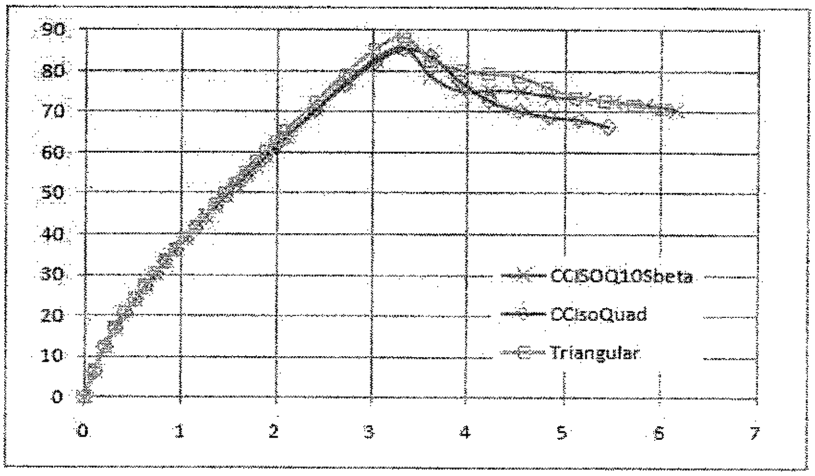

Figure A-2 Load-displacement curves of shear beam analyzed using ATENA

APPENDIX B: STRENGTHENING CONFIGURATIONS OF BEAMS WITH LARGE ELLIPTICAL OPENING IN FLEXURE –BEAM LEF-S

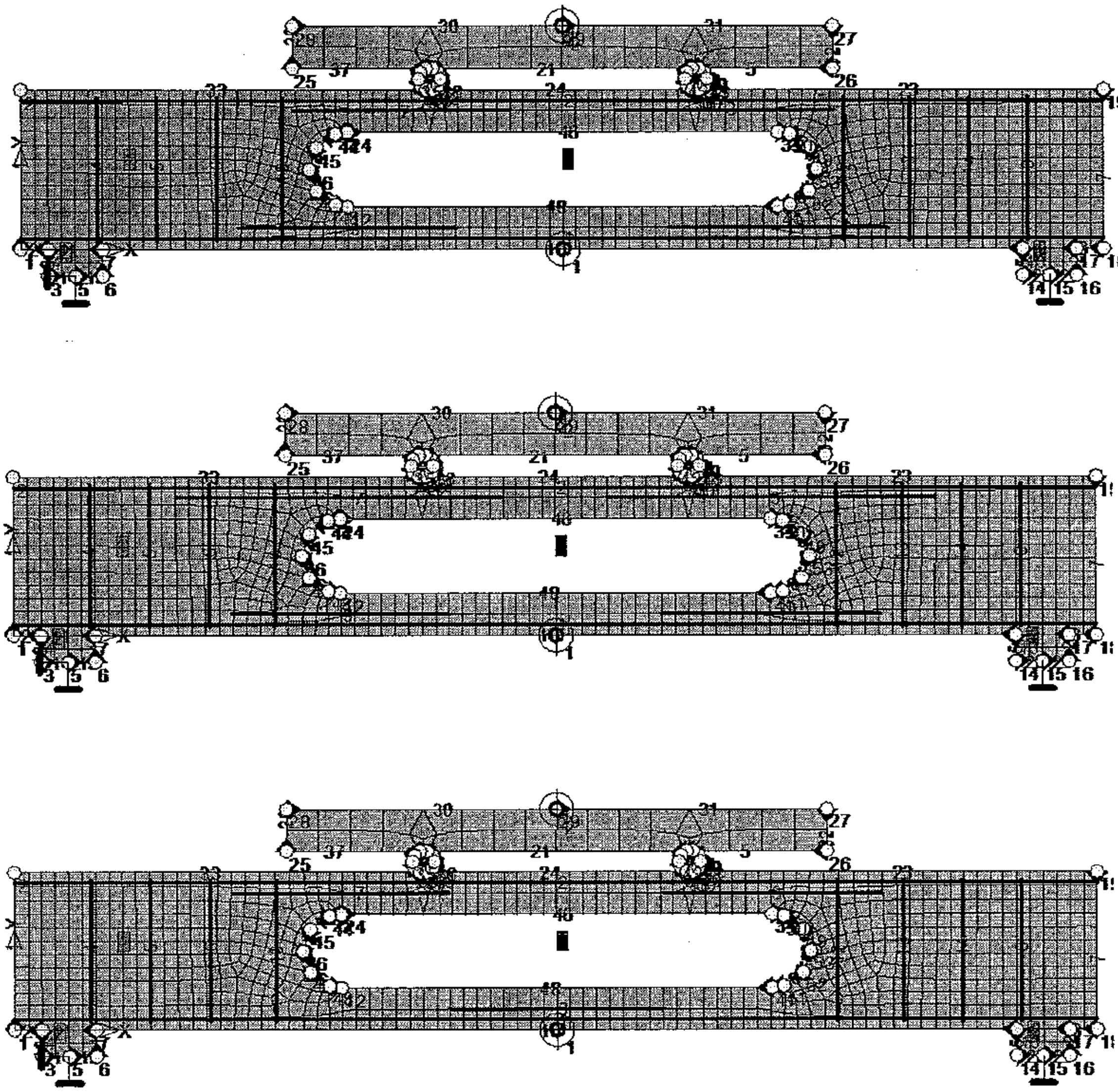

Figure B-1 CFRP strengthening schemes for beams with large elliptical opening in mid-span

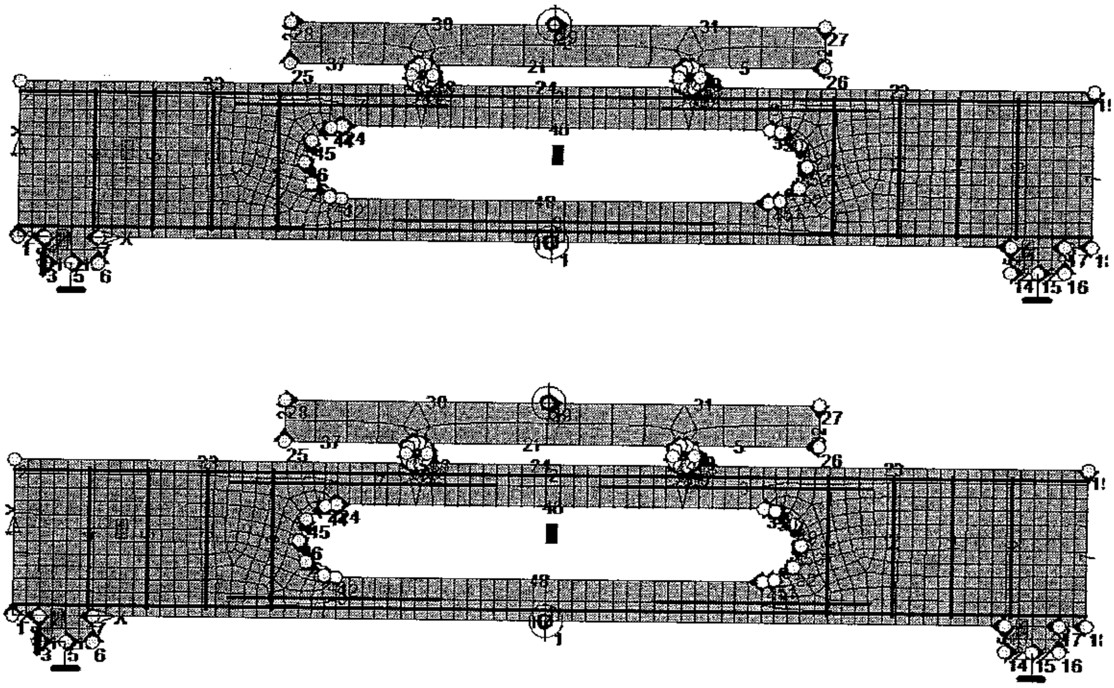

Figure B-2 CFRP strengthening schemes for beams with large elliptical opening in mid-span (Cont')

APPENDIX C: STRENGTHENING CONFIGURATIONS OF BEAMS WITH LARGE RECTANGULAR OPENING IN FLEXURE –BEAM LRF-S

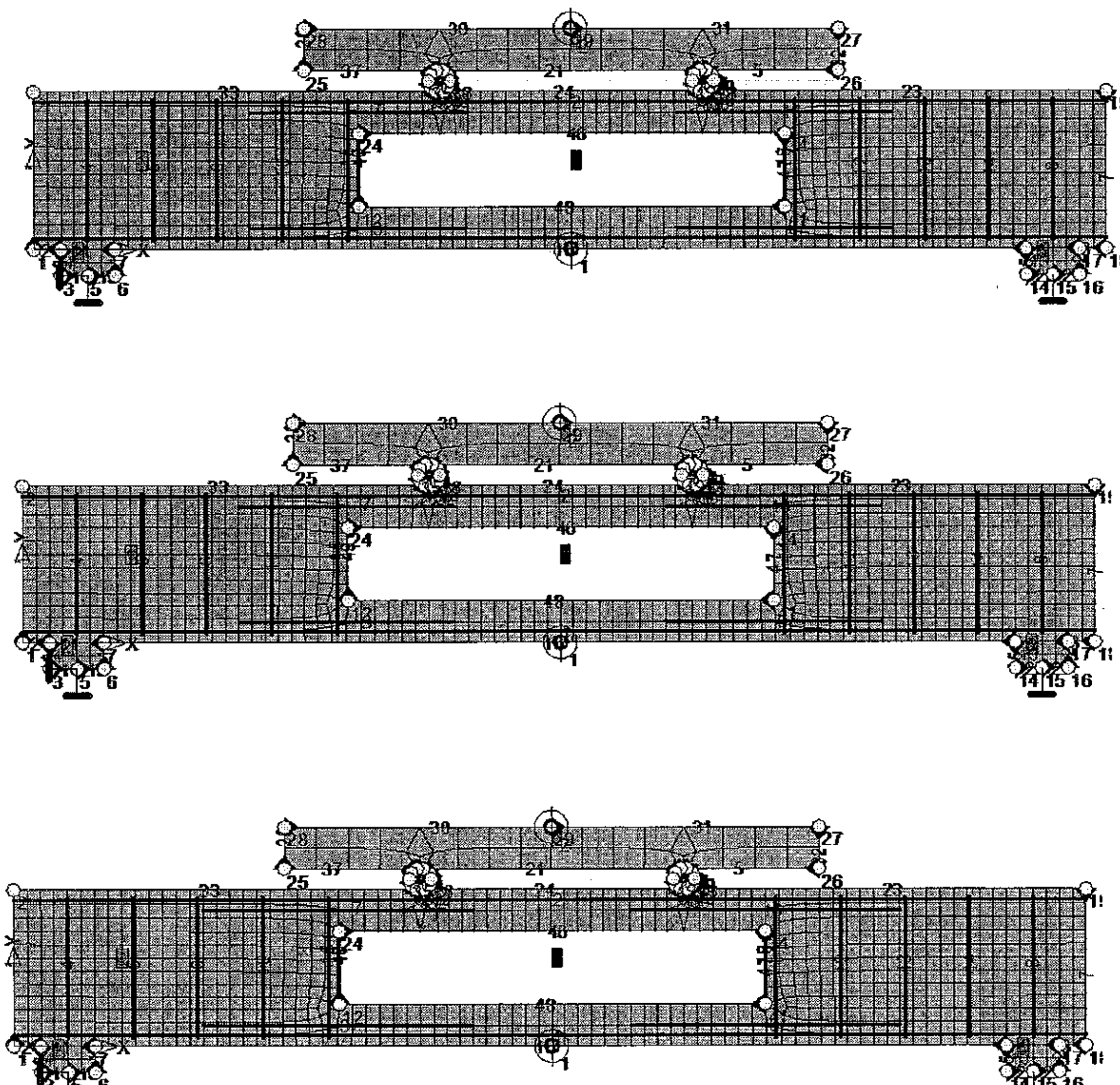

Figure C-1 CFRP strengthening schemes for beams with large rectangular opening in mid-span

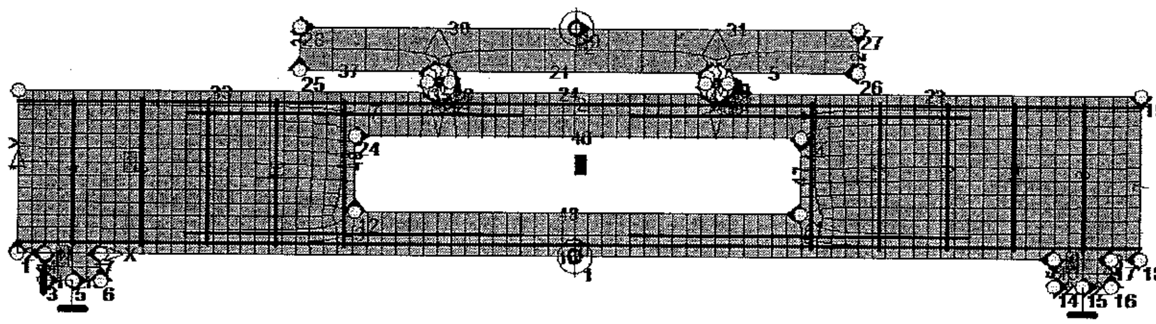

Figure C-2 CFRP strengthening schemes for beams with large rectangular opening in mid-span (Cont')

APPENDIX D: STRENGTHENING CONFIGURATIONS OF BEAMS WITH OPENINGS IN SHEAR (OPENINGS AT BOTH ENDS) –BEAM C0S-S

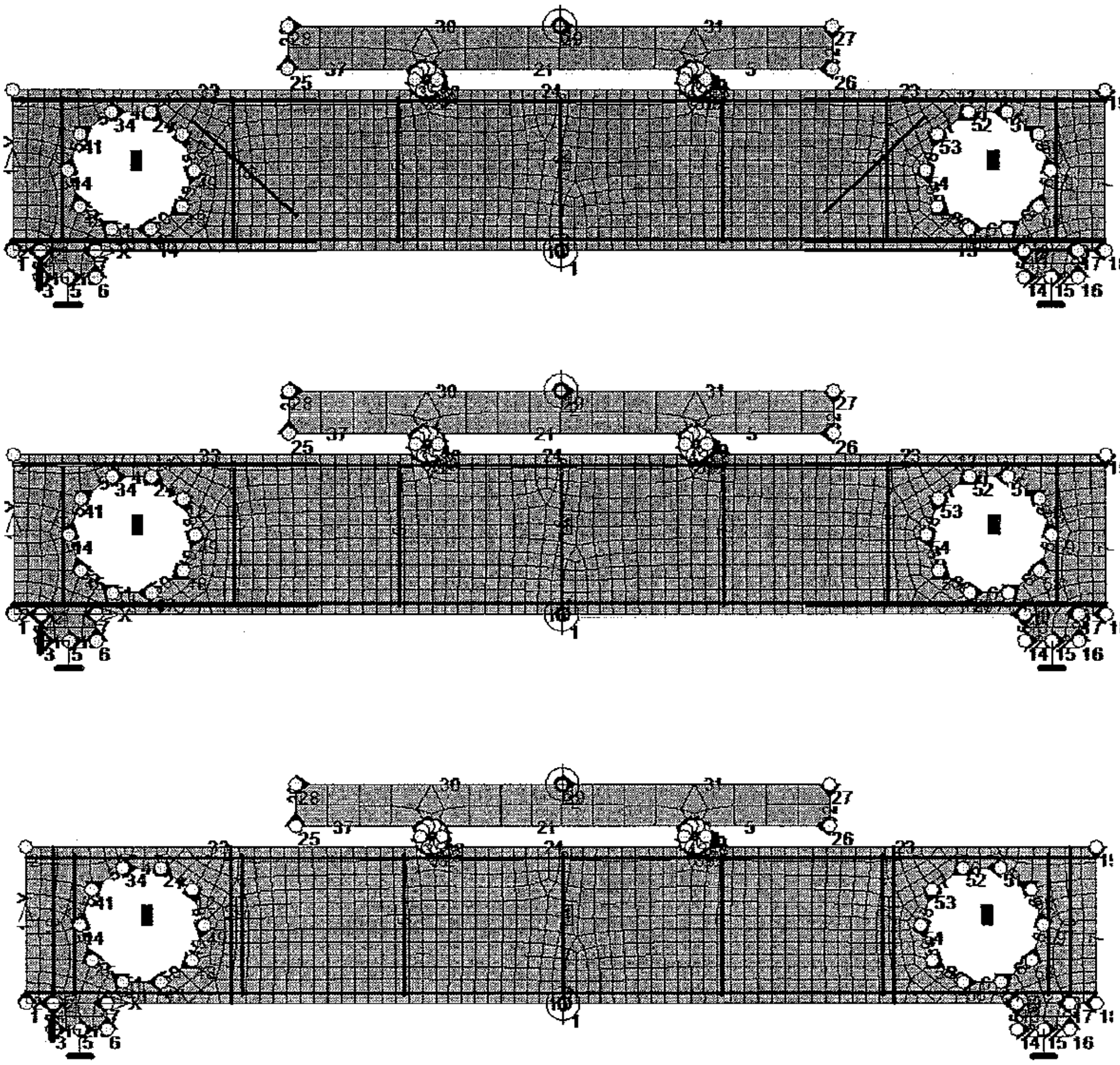

Figure D-1 CFRP strengthening schemes for beams with circular openings at both ends (at the face of support)

APPENDIX E: STRENGTHENING CONFIGURATIONS OF BEAMS WITH OPENINGS IN SHEAR (OPENINGS AT BOTH ENDS) –BEAM S0S-S

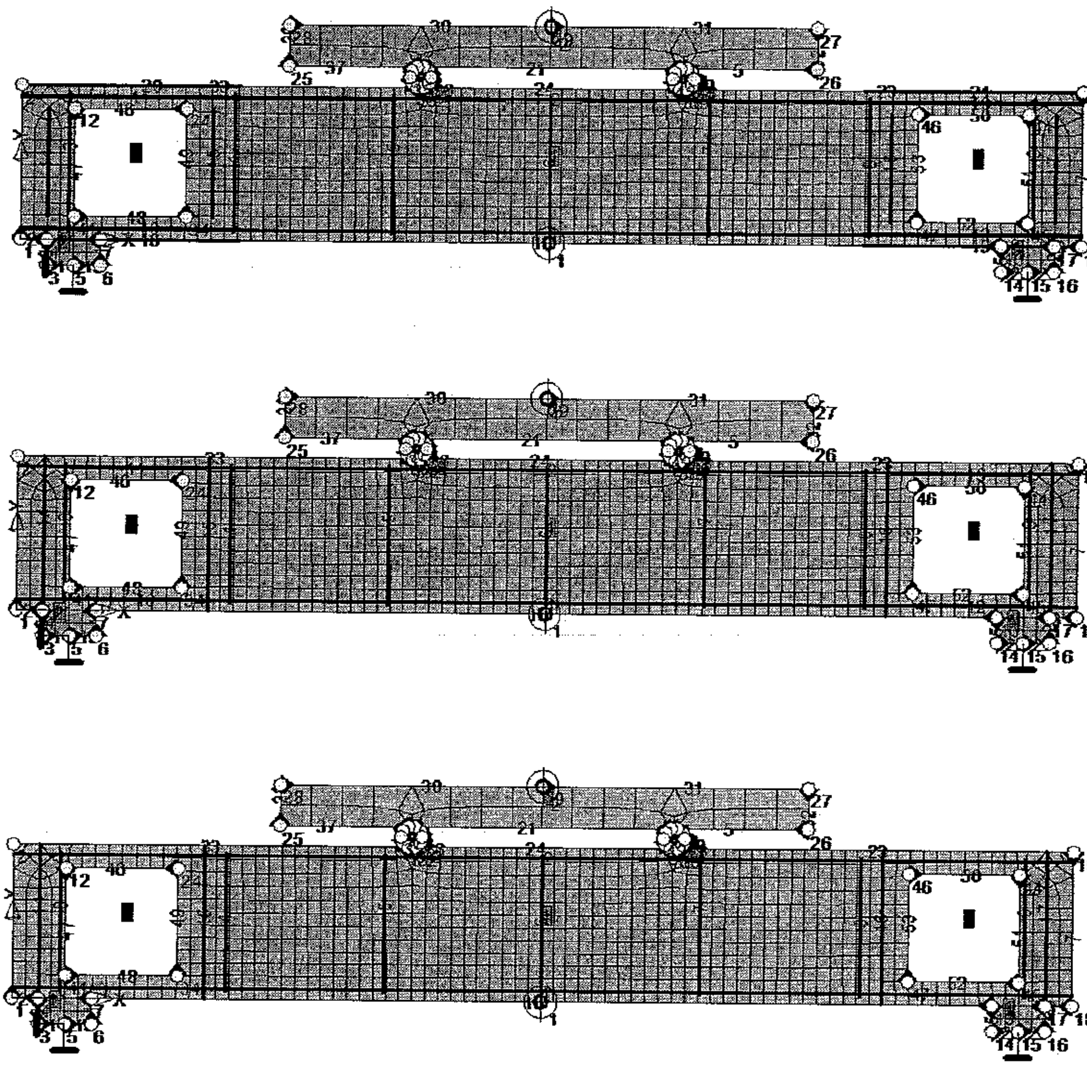

Figure E-1 CFRP strengthening schemes for beams with square openings at both ends (at the face of support)

APPENDIX F: STRENGTHENING CONFIGURATIONS OF BEAMS WITH OPENINGS IN SHEAR (OPENINGS AT BOTH ENDS) –BEAM CdS-S

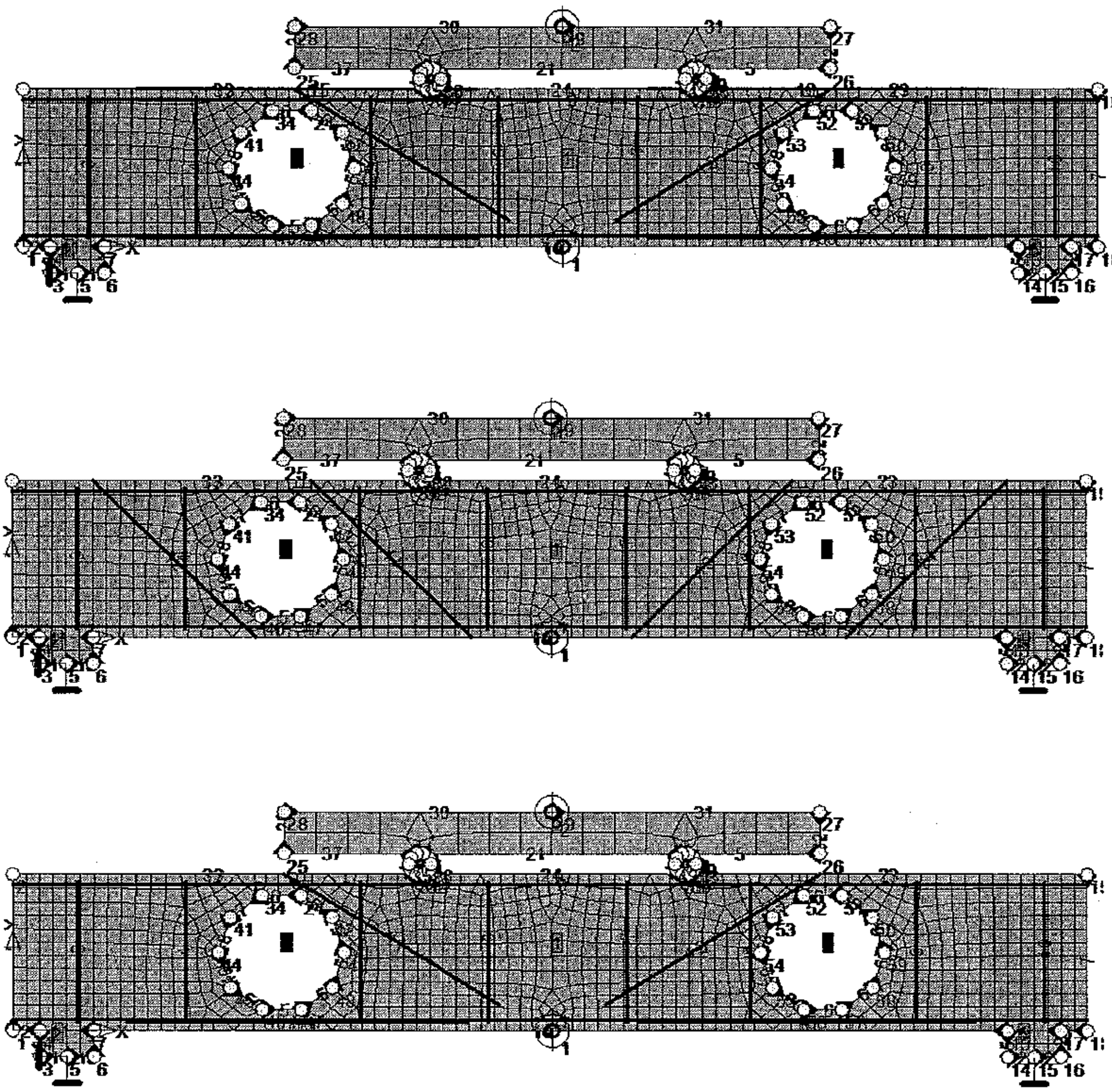

Figure F-1 CFRP strengthening schemes for beams with circular openings at both ends (at distance d from the support)

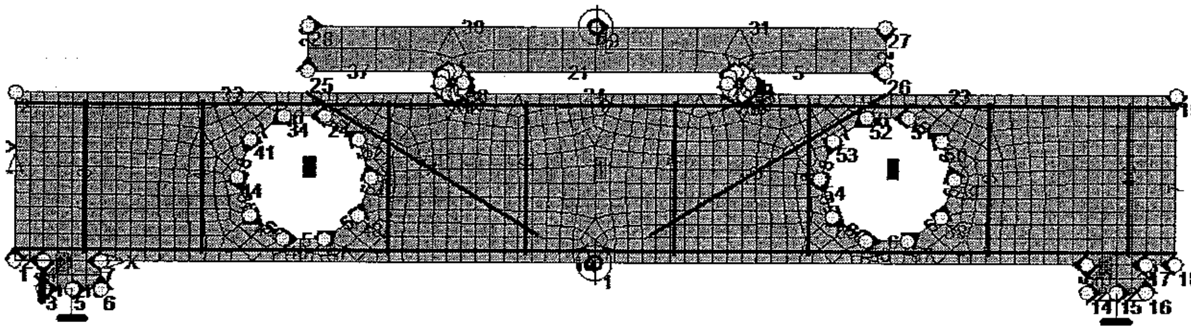

Figure F-2 CFRP strengthening schemes for beams with circular openings at both ends (at distance d from the support) (Cont')

APPENDIX G: STRENGTHENING CONFIGURATIONS OF BEAMS WITH OPENINGS IN SHEAR (OPENINGS AT BOTH ENDS) –BEAM SdS-S

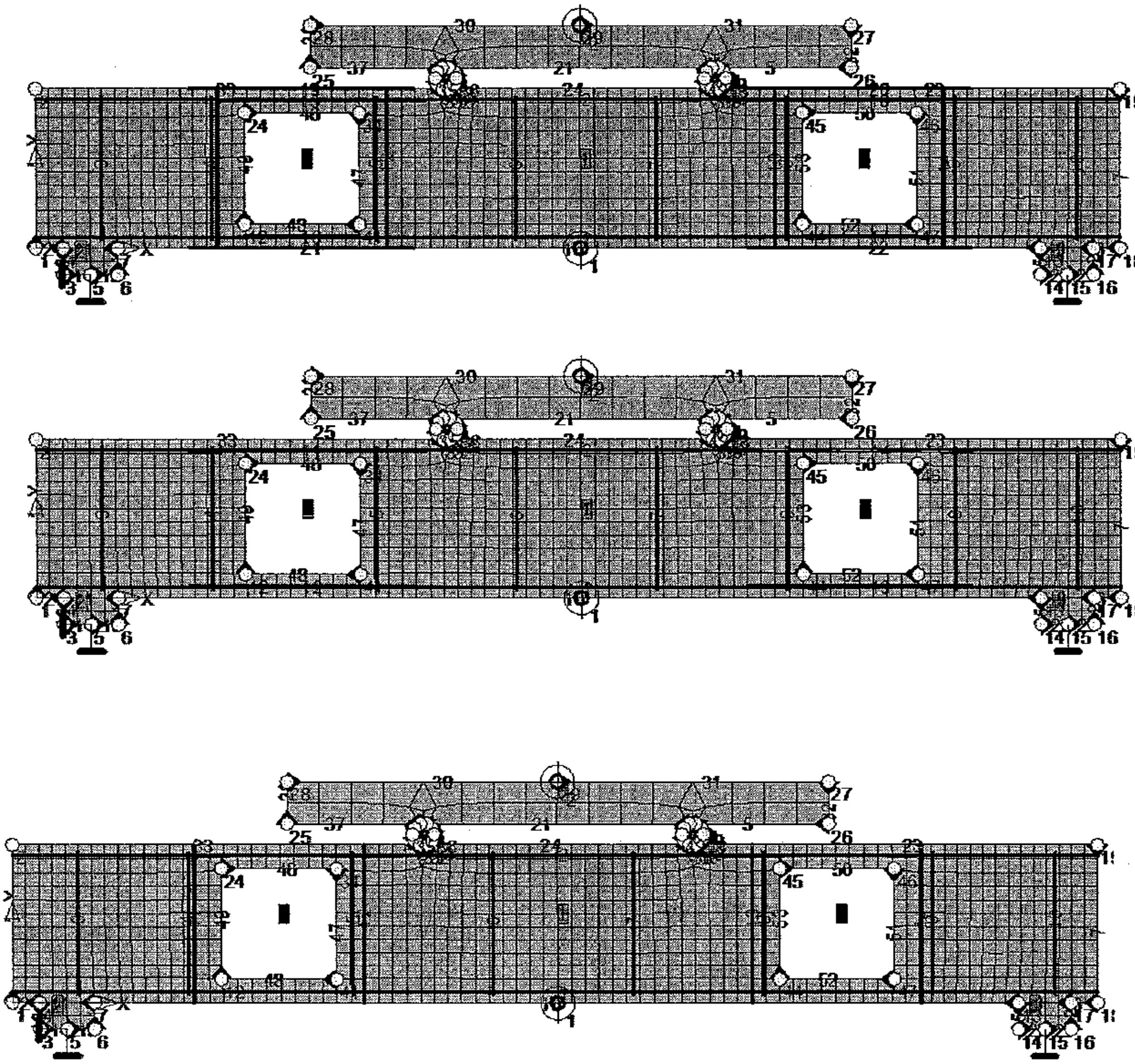

Figure G-1 CFRP strengthening schemes for beams with square openings at both ends (at distance d from the support)

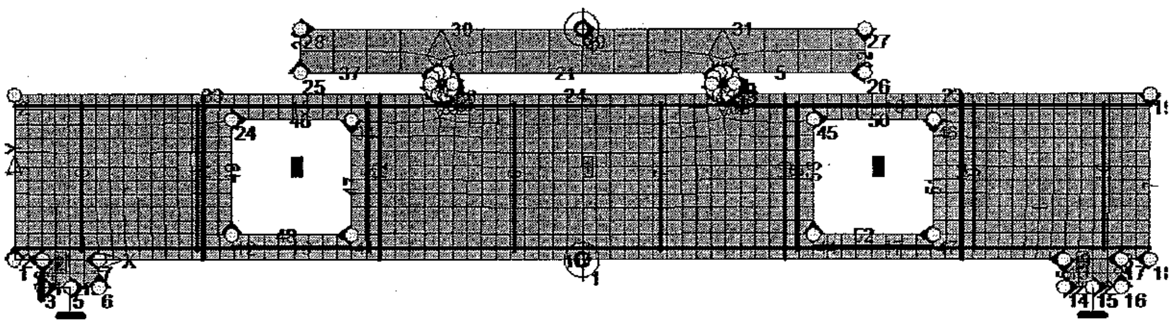

Figure G-2 CFRP strengthening schemes for beams with square openings at both ends (at distance d from the support) (Cont')

APPENDIX H: STRENGTHENING CONFIGURATIONS OF BEAMS WITH OPENING IN SHEAR (OPENING AT ONE END ONLY) --BEAM CdS1-S

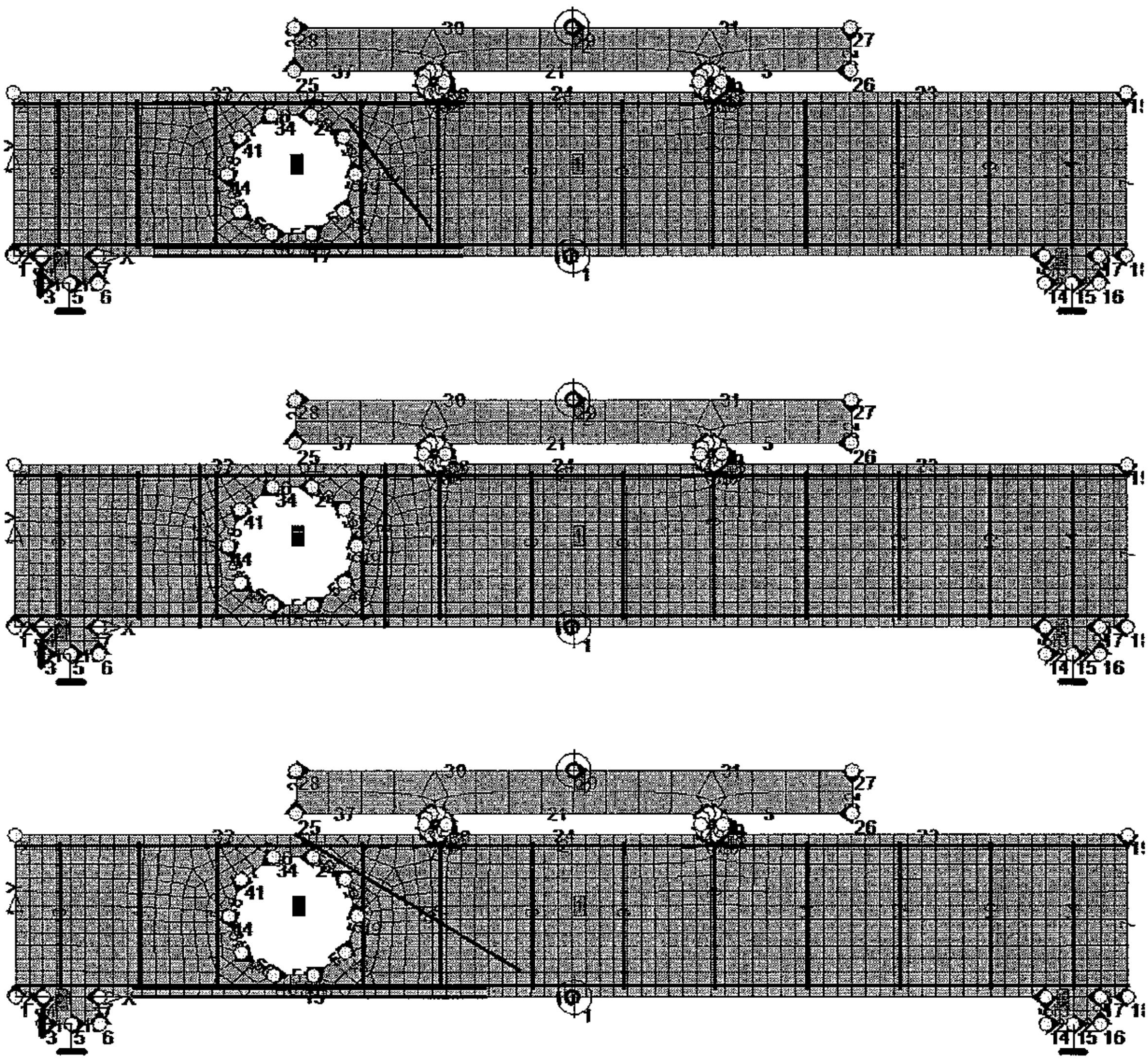

Figure H-1 CFRP strengthening schemes for beams with circular opening at one end Only (at distance d from support)

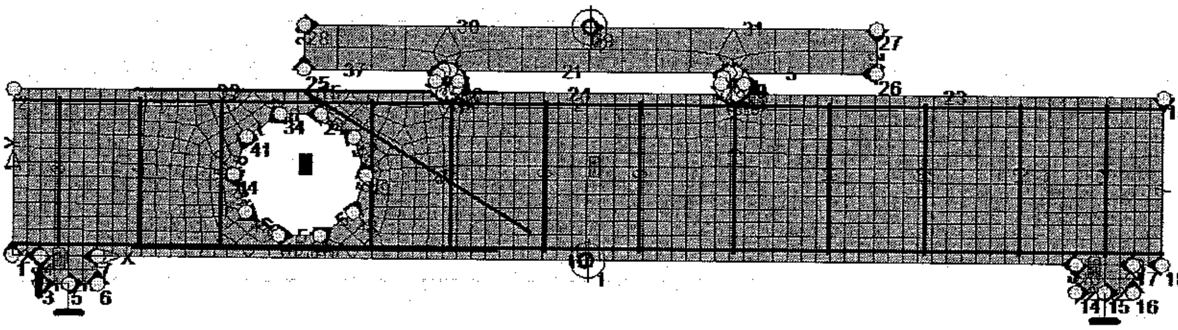

Figure H-2 CFRP strengthening schemes for beams with circular opening at one end only
(at distance d from support) (Cont')

APPENDIX I: STRENGTHENING CONFIGURATIONS OF BEAMS WITH OPENING IN SHEAR (OPENING AT ONE END ONLY) –BEAM SdS1-S

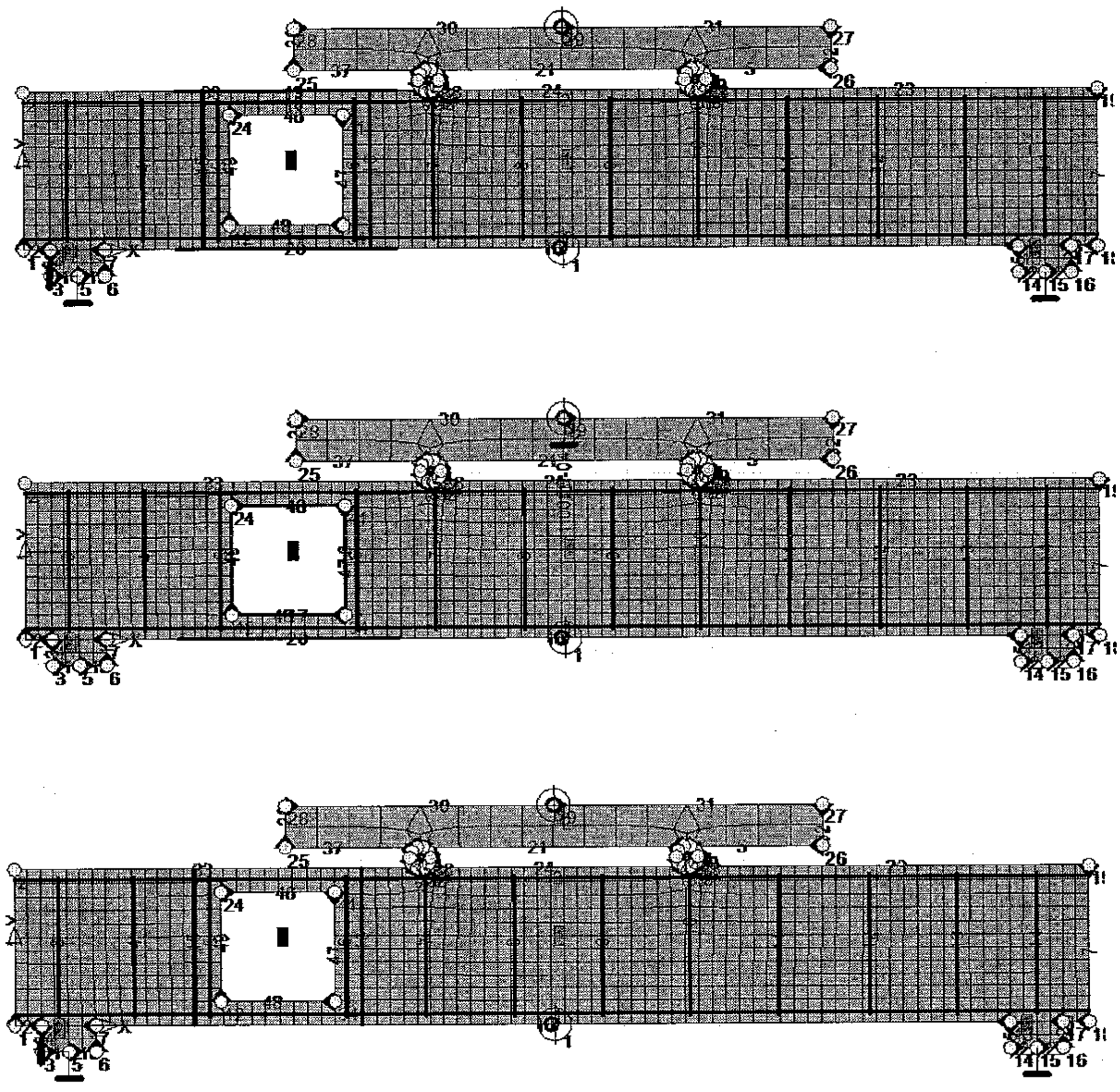

Figure I-1 CFRP strengthening schemes for beams with square opening at one end only (at distance d from support)

APPENDIX J: STRENGTHENING CONFIGURATIONS OF BEAMS WITH OPENING IN FLEXURE –BEAM CF-S

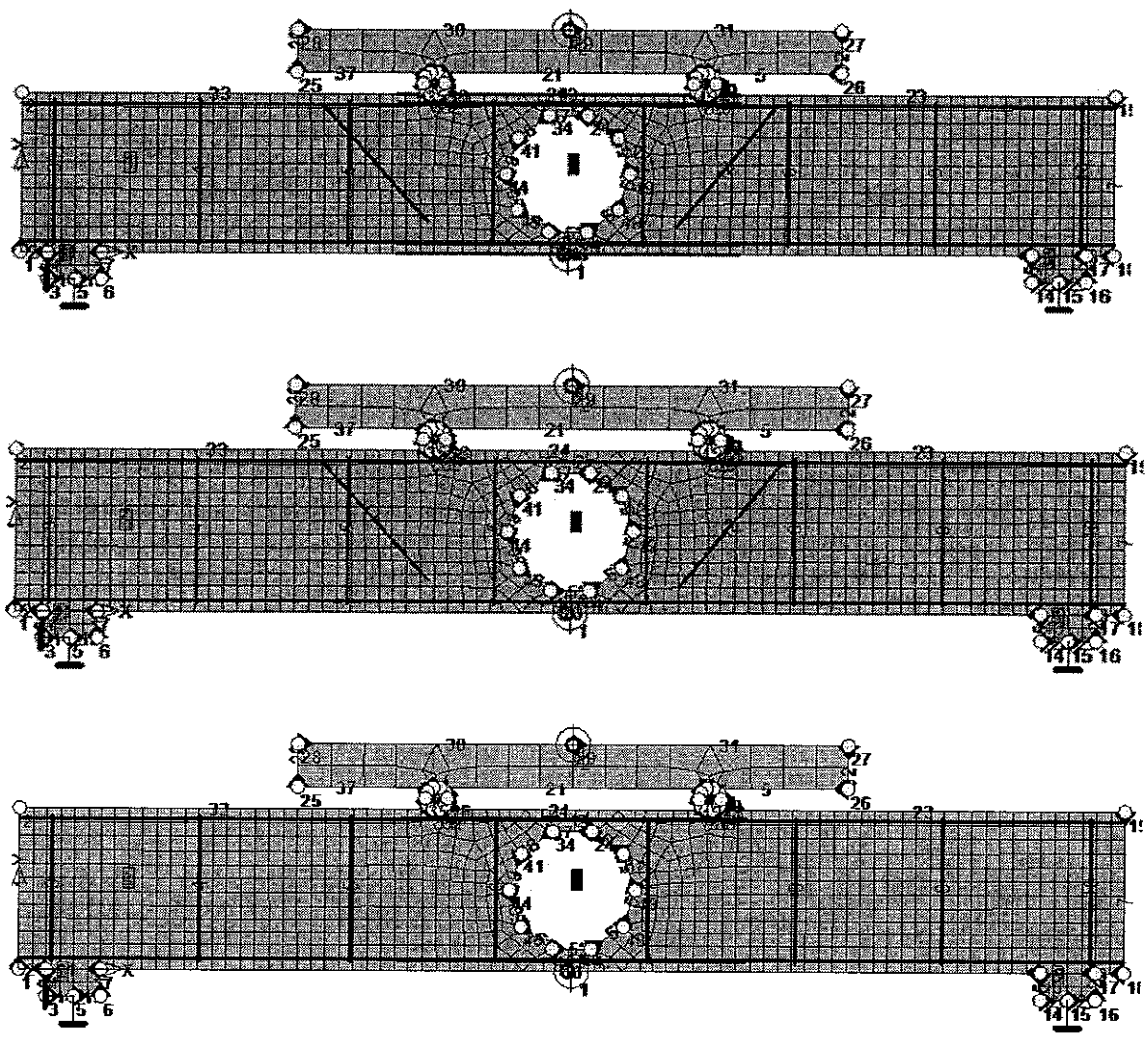

Figure J-1 CFRP strengthening schemes for beams with circular opening in mid-span

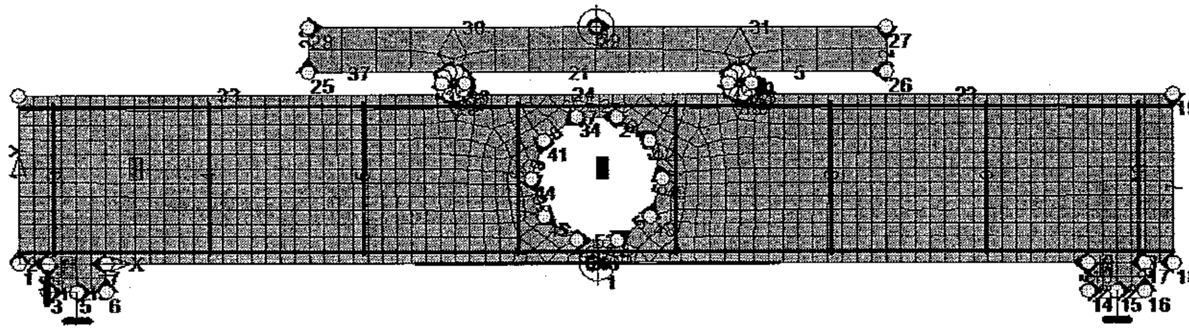

Figure J-2 CFRP strengthening schemes for beams with circular opening in mid-span (Cont')

APPENDIX K: STRENGTHENING CONFIGURATIONS OF BEAMS WITH OPENING IN FLEXURE –BEAM SF-S

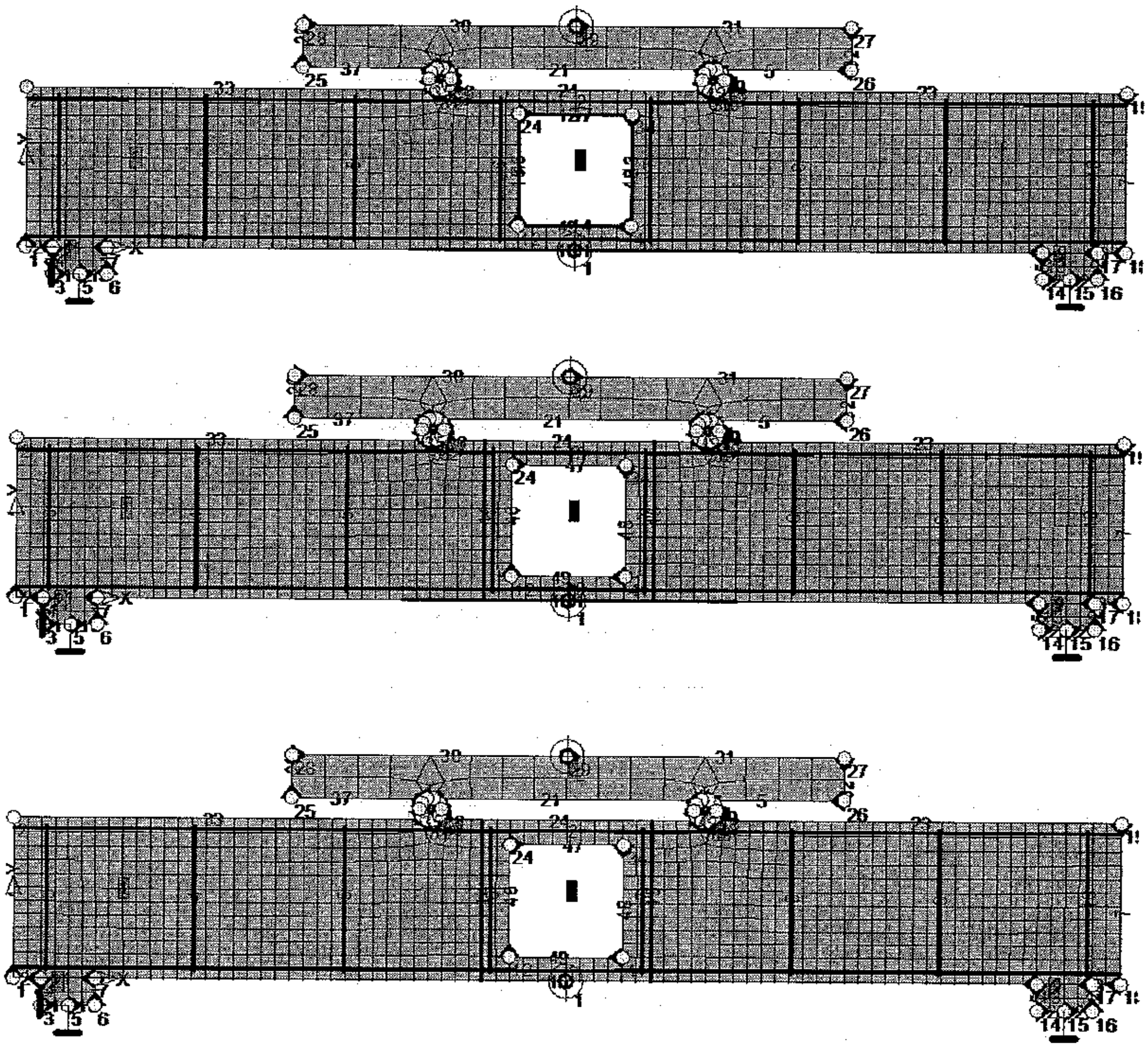

Figure K-1 CFRP strengthening schemes for beams with square opening in mid-span

APPENDIX L: COMPARISON OF LOAD-DEFLECTION CURVES BETWEEN EXPERIMENTAL AND FEM RESULTS

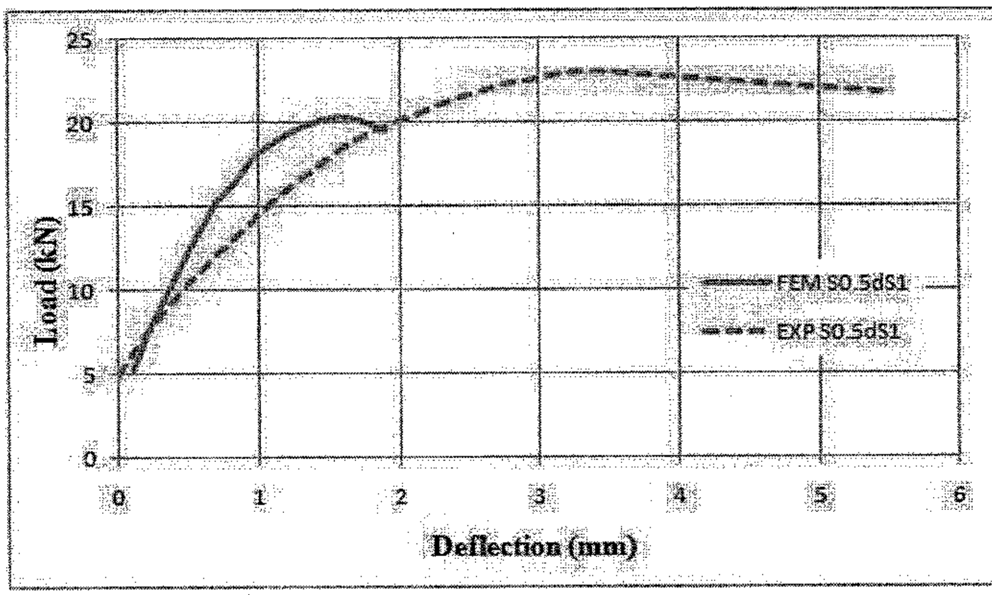

Figure L-1 Experiment and FEM load-deflection curves of beam S0.5dS1

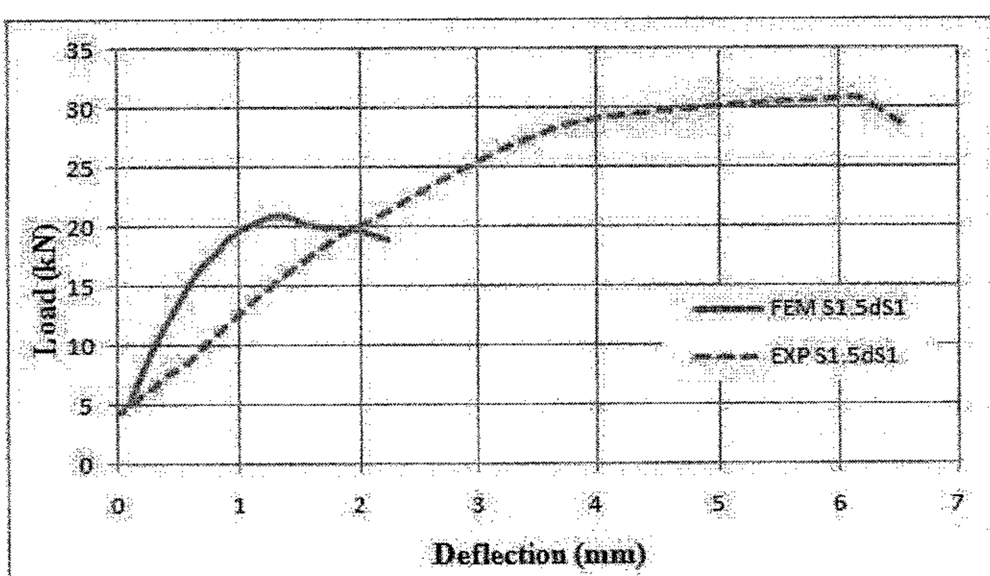

Figure L-2 Experiment and FEM load-deflection curves of beam S1.5dS1